



# Durham E-Theses

---

## *Photo effects in cadmium sulphide*

S.M.A. Salehi Manshadi,

### How to cite:

---

S.M.A. Salehi Manshadi, (1977) *Photo effects in cadmium sulphide*, Durham theses, Durham University. Available at Durham E-Theses Online: <http://etheses.dur.ac.uk/8259/>

### Use policy

---

The full-text may be used and/or reproduced, and given to third parties in any format or medium, without prior permission or charge, for personal research or study, educational, or not-for-profit purposes provided that:

- a full bibliographic reference is made to the original source
- a [link](#) is made to the metadata record in Durham E-Theses
- the full-text is not changed in any way

The full-text must not be sold in any format or medium without the formal permission of the copyright holders.

Please consult the [full Durham E-Theses policy](#) for further details.

The copyright of this thesis rests with the author.  
No quotation from it should be published without  
his prior written consent and information derived  
from it should be acknowledged.

Photo Effects in Cadmium Sulphide

By

S.M.A. Salehi Manshadi

Presented in candidature for the degree of

Doctor of Philosophy

in the

University of Durham

November, 1977



## ACKNOWLEDGEMENTS

It is a pleasure to express my thanks to friends who have helped me during the course of this research project. I am deeply grateful to Dr. J Woods, my supervisor, for his encouragement and guidance. Thanks are due to Dr. G J Russell for valuable discussions on electron diffraction.

I would like to thank Professor G G Roberts and Professor D A Wright for allowing me to use the departmental research facilities and I am grateful to workshop staff, headed by Mr. F Spence, for their technical help and advice. Thanks are due to Mr. N Thompson for growing the crystals studied in this project.

I would also like to thank The British Council and the Iranian Ministry of Science and Higher Education for the award of a grant.

Finally, I would like to express my gratitude to my mother for her many sacrifices and constant encouragement over the years.

## ABSTRACT

The work described in this thesis is mainly concerned with the electrical and optical properties of three types of CdS device namely :

1. Photoconductive cells with two ohmic contacts
2. Schottky diodes with one ohmic contact, and
3. P-n heterojunctions made by the heat treatment of CdS crystals carrying deposited layers of copper.

Since a high stability in use is essential for successful application of CdS photoconductors and solar cells, one of the main aims of the research has been to investigate the optically induced processes which lead to the degradation of the efficiency of CdS photosensitive devices. Using the technique of thermally stimulated currents on CdS : Cl crystals doped with monovalent and bivalent copper ions, we have shown that optically induced degradation of photoconductivity in CdS : Cl rods doped with  $\text{Cu}^{++}$  ions occurs in conjunction with a reduction in the density of shallow traps, and the simultaneous formation of deep traps. In contrast, optical illumination does not have any deleterious effect on CdS : Cl samples doped with  $\text{Cu}^+$  ions.

With the Schottky diodes, the resistivity of the sample was found to play a significant role. The effects of ageing on such properties as the short circuit photoresponse, the C-V characteristics and the I-V characteristics of the diodes were investigated. It is shown that during ageing an increase in the thickness of the interfacial layer occurs in conjunction with a decrease in the uncompensated donor density.

Devices of the third type, i.e. p-n heterojunctions were produced by heating crystals of CdS carrying layers of copper metal. Optical and electrical measurements showed that the heat treatment of a Cu-CdS contact leads to the formation of a layer  $\text{Cu}_{2-x}\text{S}$  which is a mixture of djurleite and chalcocite.

## CONTENTS

### ACKNOWLEDGEMENTS

### ABSTRACT

#### CHAPTER ONE :

Page Nos

1.1	PHOTOELECTRICITY	1.
1.2	OTHER PHOTOELECTRIC EFFECTS	3.
	1.2.1 The Dember Effect	3.
	1.2.2 The Photomagnetolectric Effect	3.
	1.2.3 Anomalous Photovoltaic Effect	4.
	1.2.4 The Photoangular Effect	4.
	1.2.5 Lateral Photoeffect	5.
1.3	PHOTOELECTRIC APPLICATIONS	5.
1.4	REASONS FOR THE PRESENT WORK	7.
1.5	BRIEF HISTORY OF THE DEVELOPMENT OF THE CdS:Cu <sub>2</sub> S SOLAR CELL	10.
	1.5.1 The Clevite Model for Solar Cell	14.
	1.5.2 Instability and Degradation	17.

#### CHAPTER TWO :

2.1	PHOTOCONDUCTIVITY	20.
2.2	SUPERLINEARITY	24.
2.3	OPTICAL AND THERMAL QUENCHING	30.
2.4	THERMALLY STIMULATED CURRENT TECHNIQUES	32.
2.5	THE PHOTOVOLTAIC EFFECT	38.
2.6	METAL-SEMICONDUCTOR CONTACT	39.
2.7	CONDUCTION MECHANISM IN SCHOTTKY BARRIERS	42.
2.8	MEASUREMENT OF SCHOTTKY BARRIER HEIGHT	46.
2.9	VOLTAGE-CAPACITANCE MEASUREMENTS	47.
2.10	CURRENT-VOLTAGE MEASUREMENTS	52.
2.11	METAL-INSULATOR-SEMICONDUCTOR (MIS) DIODES	54.
2.12	EQUIVALENT CIRCUIT OF MIS CAPACITOR	55.

#### CHAPTER THREE :

3.1	VAPOUR PHASE GROWTH	59.
3.2	CADMIUM TREATMENT	62.
3.3	SULPHUR TREATMENT	63.

#### CHAPTER FOUR :

4.1	PHOTOCONDUCTIVITY MEASUREMENTS	65.
	4.1.1 Mounting the Crystals	65.
	4.1.2 Temperature Variation and Measurement	66.
	4.1.3 Thermally Stimulated Currents	67.
	4.1.4 Spectral Response of Photoconductivity	68.
4.2	SCHOTTKY BARRIER FORMATION	68.
	4.2.1 The Vacuum System and Metal Film Deposition	69.
	4.2.2 Measurement of Current-Voltage Characteristics of the Diodes	70.
	4.2.3 Capacitance-Voltage Measurements	71.
	4.2.4 Photoresponse Measurements	71.
	4.2.5 Photo-capacitance Measurements	72.
4.3	X-RAY POWDER PHOTOGRAPHY	72.

CHAPTER FIVE :

5.1	INTRODUCTION	74.
5.2	SAMPLE PREPARATIONS	74.
5.3	DOPING WITH DIVALENT COPPER IONS	75.
5.4	IDENTIFICATION OF THE FORMATION OF A COVELLITE LAYER ON THE CdS BARS	76.
5.5	COPPER DIFFUSION	78.
5.6	DOPING WITH MONOVALENT COPPER IONS	79.
5.7	OHMIC CONTACTS	80.
5.8	PHOTOCONDUCTIVITY OF FLOW RUN CRYSTALS	81.
5.9	THE EFFECTS OF VARYING THE COPPER IMPURITY CONCENTRATION	82.
5.10	THE EFFECT OF SULPHUR COMPENSATION	84.
5.11	THE EFFECT OF PROLONGED ILLUMINATION ON SAMPLES DOPED WITH $Cu^{++}$ IONS	84.
5.12	THERMALLY STIMULATED CURRENTS IN SAMPLES DOPED WITH CUPRIC IONS	87.
5.13	PHOTOCONDUCTIVITY OF BOULE CRYSTALS	88.
5.14	THE EVALUATION OF THE IONIZATION ENERGIES OF THE TRAPS	91.
5.15	DISCUSSION	92.

CHAPTER SIX :

6.1	INTRODUCTION	98.
6.2	DEVICE PREPARATION	98.
6.3	PHOTORESPONSE MEASUREMENTS	99.
6.4	PHOTORESPONSE OF THE HIGH RESISTIVITY SAMPLES	99.
6.5	THE EFFECT OF ILLUMINATION	100.
6.6	IMPORTANCE OF SAMPLE RESISTIVITY	100.
6.7	PHOTORESPONSE OF Au-Cds	101.
6.8	CAPACITANCE-VOLTAGE MEASUREMENTS	104.
6.9	C-V MEASUREMENTS ON Au-Cds DIODES CONTAINING DOPANTS	104.
6.10	VARIATION OF CAPACITANCE WITH FREQUENCY	105.
6.11	G-V MEASUREMENTS	107.
6.12	THE EFFECT OF THE INTERFACIAL LAYER ON C-V MEASUREMENTS	108.
6.13	THE DIFFUSION POTENTIAL $V_{bi}$	109.
6.14	THE DEPLETION LAYER WIDTH, $w$	110.
6.15	THE IMAGE FORCE BARRIER LOWERING $\Delta\phi_n$ AND THE MAXIMUM ELECTRIC FIELD STRENGTH $\epsilon_{max}$ AT THE JUNCTION	110.
6.16	THE EVALUATION OF THE INTERFACIAL LAYER THICKNESS	111.
6.17	CHANGES IN C-V CHARACTERISTICS OF A DIODE WITH TIME (AGEING)	112.
6.18	CURRENT-VOLTAGE CHARACTERISTICS	113.
6.19	FORWARD BIAS I-V CHARACTERISTICS	114.
6.20	REVERSE BIAS CHARACTERISTICS	115.
6.21	EFFECTS OF AGEING ON CURRENT-VOLTAGE CHARACTERISTICS OF Au-Cds DIODES	117.
6.22	PHOTOCAPACITANCE MEASUREMENTS ON Au-Cds DIODES	118.
6.23	PHOTOCAPACITANCE RESULTS ON Au-Cds DIODES CONTAINING DONORS AND ACCEPTORS	118.
6.24	SOME ELECTRONIC PROCESSES IN THE PHOTOCAPACITANCE EFFECT	119.

CHAPTER SEVEN :

7.1	INTRODUCTION	122.
7.2	SAMPLE PREPARATION	122.
7.3	PHOTORESPONSE MEASUREMENTS	123.
7.4	CAPACITANCE-VOLTAGE MEASUREMENTS	124.
7.5	THE EFFECT OF HEAT TREATMENT ON THE CURRENT-VOLTAGE CHARACTERISTICS OF Cu-CdS DIODES	124.
7.6	CONCLUSION	125.

CHAPTER EIGHT :

8.1	SUMMARY OF THE RESULTS	127.
8.2	SUGGESTIONS FOR FUTURE WORK	132.

REFERENCES :

133.

CHAPTER ONEPHOTO EFFECTS AND THE DEVELOPMENT OF THECu<sub>2</sub>S-CdS SOLAR CELL1.1 PHOTOELECTRICITY

Although the three photo-electric phenomena of photoconductivity, the photovoltaic effect, and photoemission were discovered in the 19th Century, no major development and application took place until substantial progress had been made in the technology of producing pure and doped materials.

Photoconductivity is the phenomenon in which the electrical conductivity of a photoconductor increases when it is illuminated with light of the correct wavelength. It was first observed in selenium by W. Smith (1873). The process usually involves the excitation of electrons either from the valence band or impurity levels to the conduction band, i.e. to energy states where the electrons are free to move. A photoexcited electron leaves behind a free hole in the valence band. Since the capture cross section of defects in photo-sensitive cadmium sulphide is higher for holes., the holes are captured in these imperfection sites, and immobilised, Consequently the major contribution to the photoconductivity is made by the electrons.

Imperfections and impurities, depending on the location of their energy levels, play important roles in determining the characteristics of a photoconductor. Such characteristics include the dependence of the photocurrent on light intensity, the temperature dependence of the photosensitivity, susceptibility to optical quenching and speed of response.

The photovoltaic effect which is the generation of an e.m.f. under



illumination was also originally observed in selenium: its discovery is ascribed to Adams and Day (1876). In 1927 Crondahl and subsequently Lange (1930) observed the generation of an e.m.f. at a contact between  $\text{Cu}_2\text{O}$  and Cu; the basic aspects of this phenomenon which is called the photovoltaic barrier effect, were clarified by Schottky et al (1930, 1931).

The search for an explanation of the photovoltaic effect continued and Landau and Lifshitz (1936), Dabydov (1938) and Mott (1939) came to the right conclusion that the photo-emf arose from a non-equilibrium concentration of minority carriers. The high efficiency solar cell was first developed by Chapin, Fuller and Pearson in 1954, using a diffused silicon p-n junction. Since then, efforts to fabricate highly efficient solar cells have been continued. It is worth mentioning that nowadays silicon solar cells with efficiencies up to 18% are used as the means of power production in communication satellites. The first cadmium sulphide photovoltaic cell was described by Reynolds et al (1954) who made a photo cell by applying a Cu contact to single crystal CdS. They attributed erroneously the photovoltaic effect of their cell to p-type conduction in a copper impurity band. Later Williams and Bube (1960) suggested that the observed facts can be better explained by the assumption of the emission of electrons from the metal contact into the semiconductor, but current ideas favour the production of a p-n heterojunction in which the p-type material is copper sulphide.

The third photoelectric effect, i.e. photoemission was discovered by Hertz during his experiments on electrical induction circuits (1887). He realized that a spark passed with greater ease when the gap was illuminated with the spark from the primary coil. Further experiment showed that it was the u.v. component of the spark which had the effect on the negative terminal of the secondary gap. Hallwachs (1888) confirmed these results and concluded that negative electrical carriers, later identified

as electrons, were emitted from the cathode under u-v illumination. The work of Elster and Geitel on more sensitive materials like Na and K led to the achievement of the high yield photocathodes by preparation of composite surface films, leading to caesium antimonide films, and the multialkali cathodes which are used in photomultipliers, scintillation counters, and the television pick up tubes of today.

## 1.2 OTHER PHOTOELECTRIC EFFECTS

### 1.2.1 The Dember Effect

Strongly absorbed radiation can generate a high density of electron hole pairs at the surface of a semiconductor. Electrons having the higher mobility say, diffuse away from the surface more quickly than holes. In the absence of any other effect, the differential diffusion will tend to make the surface more positive than the bulk. The direction of the resulting electric field is such as to accelerate the lower mobility carriers and to slow down the more mobile carriers, so that the net current is nil, Dember (1931) and (1932).

### 1.2.2 The Photomagnetolectric Effect

Illumination with strongly absorbed light causes a concentration gradient of electron-hole pairs diffusing away from the illuminated surface in a direction parallel to the direction of the incident light. If a magnetic field is applied transversely to this diffusion current, the electrons and holes will be deflected in opposite directions (as in the Hall effect), with the result that a voltage in the third orthogonal direction will appear across the ends of the specimen.

Unlike the Dember effect, for a photomagnetolectric effect to be observed the mobilities of electrons and holes need not be different.

For a given illumination, the P.M.E. voltage depends on the surface recombination velocity,  $s$ , and the lifetime,  $\tau$ , of the carriers in the bulk. The P.M.E. effect has been used to find these quantities  $s$  and  $\tau$  which are important in the performance of the semiconductor devices, T.S. Moss et al (1953) and H. Bulliard (1954).

### 1.2.3 Anomalous Photovoltaic Effect

Some semiconductors in the form of thin layers exhibit a high voltage photovoltaic effect. Voltages as high as 5000 V have been reported (Adirovich et al 1966) which are many times larger than the semiconductor band gap. The anomalous photovoltage effect has been observed in a large number of obliquely deposited semiconductor films and in single crystals of ZnS (W.J. Mertz 1958) and ZnSe (B. Goldstein 1959). Several models have been proposed to explain the effect and they are all based on a summation of the elementary photovoltages generated in an array of small photo cells. These photovoltages, it is suggested, are generated either from the Dember effect in micro-cells or from photovoltaic effect at p-n junctions or at grain boundaries. The high resistance of the material involved such as ZnS has precluded any useful applications being made.

### 1.2.4 The Photoangular Effect

This effect has been observed in relatively thick films (2 - 50  $\mu\text{m}$ ) of polycrystalline GaAs and Si. The films were deposited by vapour-phase transport across a small gap between the source crystal and the substrate. (F.H. Nicoll 1963). Unlike the films which display an anomalous photovoltaic effect, the deposition direction was normal to the substrate and, therefore, the structure of the film was different from that of the angularly grown films. When the film was illuminated at normal incidence, no

voltage appeared. As the light beam was tilted from a normal to the substrate, a photo-voltage developed and grew with further inclination of the beam. The spectral response cut off abruptly at photon energies less than the band gap, and extended undiminished to 4 eV. This confirms that the photo-angular effect occurred at the free surface of the polycrystalline layer.

#### 1.2.5 Lateral Photoeffect

The Lateral photoeffect is the generation of a photovoltage parallel to the p-n junction, Wallmark (1957) and J.I. Alferov et al (1970). The device consists of an n-type semiconductor substrate which is strongly doped by acceptors to form a p-n junction. Due to the high conductivity of p-region holes generated by the light spot on the left side of the junction leak out of the right side of the junction, making the right side more positive than the left side. Electrons in the n-type region instantly redistribute themselves to preserve local space charge neutrality. This charge redistribution generates a voltage across the two ohmic contacts. The polarity of the lateral photovoltage reverses when the light spot illuminates the right side of the junction.

### 1.3 PHOTOELECTRIC APPLICATIONS

As their technology has developed, photoelectric devices have found extensive applications. Photoconductive and photovoltaic devices were originally used as radiation detectors and flux meters. Nowadays, because of the fabrication of devices from semiconductor materials with different energy gaps, photoconductors can be used to detect energies ranging from those of infra-red photons to atomic particles. Semiconductor detectors (counters) for nuclear particles are in effect solid-state

ionization chambers in which the carriers produced by the absorption of the radiation are collected on the electrodes. Semiconductor detectors can record any radiation capable of producing sufficient ionization in the sensitive layer. The higher the resistance of the sensitive layer, the smaller the ionization energy that can be detected, so that to detect radiation one uses high resistance homogeneous crystals and reverse biased p-n junctions. As light-detectors, photoresistors can be competitors to photomultipliers when their small size and low cost are more important than their sensitivity. Probably the most common application is as a light-operated switch for street lamps, lift doors, industrial control, or intruder alarms etc. More complex uses of photoconducting layers are in image converters, and vidicon type television pick-up tubes for example.

The photoemissive effect is mostly used in photomultiplier tubes which find various applications. Photocathodes are also used in television camera tubes such as the image orthicon and in image intensifiers. In addition to these applications of photoelectric effects, there are varieties of light measuring devices using photocells, such as pyrometers, micro-densitometers, and photometers. Use is also made of photo cells in film production for sound recording, in industry for smoke and flame detection, and in intruder alarms.

In recent years the rate of consumption of fossil fuel in industrialised countries has increased enormously, so that the problem of the depletion of the resources of these fuels (especially oil) has attracted attention as attempts are made to find different means of providing energy. The possible exploitation of the earth's thermal energy, the use of nuclear energy and the development of electric cars are examples of this effort. The sun is a very important source of energy. On a cloudless summer day at a latitude of  $55^{\circ}\text{N}$ , the rate of receiving solar energy at sea level is  $800 \text{ watt m}^{-2}$ . The maximum efficiency of conversion of solar energy to

electrical energy in a silicon p-n junction with a band gap of 1.1 eV was calculated theoretically by Shockley and Quiesser (1960, 1961). Their calculation puts a limit at 24% for the power conversion efficiency. Although in practice the maximum attainable efficiency of 14% is much less than the theoretical one, it is still higher than the efficiency of a nuclear power reactor.

Beyond the earth's atmosphere (air mass zero amo) where solar radiation energy is incident at a rate of  $1400 \text{ watt m}^{-2}$ , the low conversion efficiency of a solar cell can still provide power for a communication satellite. In addition, photovoltaic cells can be used as detectors for  $\gamma$  radiation,  $\beta$  radioactive elements,  $\alpha$  particles protons, neutrons, or any other means of creating electron-hole pairs without changing the properties of the junction appreciably.

#### 1.4 REASONS FOR THE PRESENT WORK

Before discussing the reasons for the present work, it is pertinent to describe some of the advantages and disadvantages of the materials that are used for the fabrication of solar cells. The predicted efficiencies of various semiconductors (Wysocki and Rappaport, 1960) show that semiconductors like GaAs, AlSb, InP, should have the highest conversion efficiencies. In practice, however, because of the highly developed state of silicon technology, silicon solar cells have been exploited for a long time as unequalled photovoltaic converters. Nevertheless, particular disadvantages led to an extensive search for alternative materials that might offer greater efficiency, cheapness of manufacture, and maintenance.

Some of the disadvantages of the silicon solar cell can be summarized as follows. Beyond the earth's atmosphere where the solar cells

are used as power sources for satellites and space vehicles; the performance of a cell is affected by the radiation damage caused by high energy particles. These particles introduce recombination centres in the cell in addition to the centres already present. The net result is to decrease the minority carrier life-time and likewise the minority carrier diffusion length, which gives rise to a decrease in the short-circuit current of the cell. Experimentally, the deterioration of the efficiency of Si solar cells under electron bombardment has been measured for three kinds of cell. It has been shown that the radiation resistance of n-on-p cells is higher than that of p-on-n cells (Rosenzwaig et al, 1963). Similar effects have been observed with solar cells subject to proton bombardment (R L Statler, 1967 and R.V. Tanke and B.J. Faraday, 1967). Efforts to prevent such irreversible radiation damage by doping cells with Cu and Li have been only partially successful (Loferski, 1963, Usami, 1970; Berman 1972).

Since the mass production of solar energy converters is highly desirable, the difficulties of preparing large area Si solar cells and the high cost involved have led to a search for an alternative material to meet the requirements of relative cheapness and relative ease of mass production.

Considering the factor of efficiency, the spectral response of the power source should be matched with the spectral emission of the sun, and with silicon that is not so. Theoretical calculations of efficiency as a function of energy gap (J.J. Loferski 1956, Wysocki and Rappaport 1960 and Wolf 1960) show a broad optimum favouring semiconductors with gaps in the range 1.25 to 1.5 eV. with a maximum conversion efficiency of 23.6 per cent. Silicon with  $E_g$  1.1 eV is not an ideal material. Several semiconducting compounds such as indium phosphide (1.27 eV), gallium

arsenide (1.34 eV) and aluminium antimonide (1.63), have gaps in the required energy range. Gallium arsenide would appear to be the most promising material for solar energy conversion for two reasons: firstly, its energy gap is the closest to the optimum value, and secondly, its electron mobility of  $5-8000 \text{ cm}^2 \text{ v}^{-1} \text{ sec}^{-1}$  is higher than that of silicon of  $1350 \text{ cm}^2 \text{ v}^{-1} \text{ sec}^{-1}$ . Another high mobility material of interest is indium phosphide, but in practice the difficulties of its preparation are even greater than with gallium arsenide, which is undesirable. CdS with a band gap of 2.4 eV seems a poor material for the purpose of solar energy conversion, but the effective energy gap of 1.2 eV which is attributable to the copper sulphide layer of the heterojunction makes the materials attractive as a solar cell .

For optimum performance, some general conditions should be fulfilled. For example:

- (1) Reflection losses should be a minimum.
- (2) The material should have a high coefficient of absorption in order to absorb a large proportion of the sun's radiated energy.
- (3) The whole spectral range of photon energy should be utilized for the creation of electron-hole pairs.
- (4) Collection of the electron-hole pairs should be complete. Incomplete collection occurs when electron-hole pairs are created far from the junction, i.e. their distance from the junction is greater than their diffusion length.
- (5) The voltage factor which is defined as the ratio of the open circuit voltage to the energy gap should be a maximum. By proper choice of material and the selection of proper doping levels, it is possible to increase the voltage factor.

- (6) The curve factor given by the ratio of the maximum power point voltage times maximum power point current to open-circuit voltage times short-circuit current should be a maximum.
- (7) Additional degradation of the curve due to internal series resistance should be reduced to a minimum (this has been partly solved by better grid design).
- (8) The cell should be radiation resistant, especially for space use.

Although the efficiencies of solar cells made of some other materials such as gallium arsenide and CdS/InP (Wagner and Shay 1975 and Shay and Wagner 1976) are higher than that of CdS:Cu<sub>2</sub>S solar cells, in practice, the difficulties of their preparation and their expense, rule out these materials for the purpose of mass production of solar cells.

#### 1.5 BRIEF HISTORY OF THE DEVELOPMENT OF THE CdS:Cu<sub>2</sub>S SOLAR CELL

Since the original observation of a photovoltaic effect associated with a Cu contact on CdS by Reynold et al in 1954, many investigations have been carried out to improve the performance of the cell and to help understand the physical mechanisms which control the operation of the cell. In 1960 Williams and Bube observed the photovoltaic effect in cells where the Cu was electrolytically deposited on to the CdS. They attributed the effect to electron emission from the metal (Cu) to the semiconductor (CdS). Woods and Champion on the other hand, suggested that the diffusing-in of a high concentration of copper produced a p-type conduction in CdS, and that the phenomenon could therefore be interpreted as a p-n junction effect. Measuring the hole conductivity in CdS, Woods and Champion indicated that the p-conductivity in CdS could not be

explained by normal hole conductivity, because the number of free holes decreased with an increase in the temperature and that the Hall mobility of the holes was connected with an admittedly small energy of activation. Grimmeiss and Memming (1962) likewise found that the concentration of the added metal was much greater on the p-side than the concentration of holes, as found from Hall measurements. All these results were taken to indicate that the hole conductivity in CdS was an impurity band effect, but later it was demonstrated the solubility of copper impurity in CdS is limited and that the hole conductivity must have been associated with a separate phase of copper sulphide.

In 1963 Cusano reported the fabrication of a CdTe solar cell which consisted of a heterojunction between a p-type copper telluride and n-type cadmium telluride. The comparison of this heterojunction with those in other II-VI compounds including CdS, gave rise to the identification of cuprous telluride and cuprous sulphide, generally with a departure towards excess sulphur ( $\text{Cu}_{2-x}\text{S}$ ), and tellurium ( $\text{Cu}_{2-x}\text{Te}$ ). These layers were identified by electron diffraction techniques. Hall measurements of the  $\text{Cu}_{2-x}\text{S}$  films showed that they were p-type with a hole mobility at room temperature of about  $2 \text{ cm}^2 \text{ v}^{-1} \text{ sec}^{-1}$  with carrier concentrations around  $10^{20} \text{ cm}^{-3}$  or greater.

The impurity photovoltaic effect in cadmium sulphide was investigated by (N. Duc Cunong and J Blair 1966). They fabricated a photovoltaic cell by evaporating a thin copper layer on to a low-resistivity single-crystal n-type cadmium sulphide. They found that the spectral response of a cell in the infra-red was enhanced by as much as two hundred fold when it was illuminated by radiation with energy corresponding to the energy gap. (Green light). The enhancement of the infra-red photovoltaic response was attributed to creation of additional minority carriers by transition of electrons from the valence band to impurity

levels. Chamberlain and Skarman (1966) prepared thin film photovoltaic cells by a chemical spray technique.  $\text{CdS-Cu}_{2-x}\text{S}$  cells with an active film thickness of  $1 \mu$  gave efficiencies as high as 4% from areas of  $1 \text{ cm}^2$ . These cells were prepared by the chemical spray deposition of two distinct layers. The first layer was n-type CdS and the second layer was p-type copper sulphide of the diginite form. The photovoltaic operation of this type of cell was attributed to the formation of a distinct heterojunction between the cadmium sulphide and the copper sulphide. The photovoltaic characteristics of CdS solar cells fabricated by electroplating copper on to CdS single crystals have been described by Tokao Shitaya and Hisanao Sato (1968). From the resemblance of the spectral response of the cells to that of Cu doped CdS single crystals and the fact that the capacitance of the cells did not depend on the bias voltage, Shitaya and Sato concluded that the barrier near the electroplated surface consisted of an insulating layer of CdS which could be described as a Mott barrier. Measurements of the spectral response of the  $\text{Cu}_2\text{S-CdS}$  solar cells, prepared by the chemiplating technique, as a function of the plating solution concentration and the plating time were made by Mytton (1968). He showed that the intrinsic response of the cell was dependent on the concentration of the plating solution and the plating time. In contrast the extrinsic CdS response, within certain limits was independent of the dip time and was only a function of the concentration of the solution. After reviewing the previous models of  $\text{CdS-Cu}_2\text{S}$  solar cells, Mytton proposed an energy band structure for the cell in which the junction region consists of a transition from p-type  $\text{Cu}_2\text{S}$ , through photoconducting (insulating) CdS doped with Cu acceptors lying about 1.0 eV above the valence band, to n-type CdS where the Fermi level is very close to the conduction band. This is the model suggested as a possibility by Keating (1965) and is

similar to that of Bockemuehl et al (1961). A more precise model based on the  $\text{Cu}_2\text{S-i-CdS-n-CdS}$  double junction has been proposed by Shiozawa and Co. workers (1967). (The Clevite Model). They have considered in great detail the structure of copper-doped high-resistivity CdS, and pointed out that photoconductivity is to be expected in the i-CdS region, resulting in the observed reduction in the cell series resistance when illuminated.

Several other models that have been suggested by other workers such as Lewis Model by Potter and Schalla, 1967; Harshaw Model by Hill and Keramidas, 1966; E.S.R.O. Model by Van Aershodt et al, 1968, all contain common features, but differ in the details of the proposed energy band structures at the  $\text{Cu}_2\text{S-CdS}$  interface. To account for the optical quenching and enhancement of photocurrent due to secondary illumination in  $\text{Cu}_2\text{-CdS}$  cells, Grill and Bube, 1970, proposed a model in which the hole trapping in the deep imperfection centres in the CdS near the junction was considered to be the key mechanism. In their proposed model, electrons diffusing across the junction from  $\text{Cu}_2\text{S}$  must tunnel through a conduction band spike at the interface in the postheat-treatment cells. The tunnelling probability is controlled by the occupancy of deep lying imperfection levels in the CdS depletion region. This model was supported and extended by Lindquist and Bube (1972) who measured the influence of trapped charge on the photovoltaic properties of an efficient  $\text{Cu}_2\text{S-CdS}$  single crystal heterojunction by the photocapacitance technique. After rejecting the possibility that the deep acceptor levels originate from native defects or defects introduced into the CdS during the formation of heterojunction, they then attributed the major part of the hole trapping to the copper centres diffused into the CdS during the formation of the junction. Similar effects were observed by Shiozawa et al in thin film solar cells (1969). In their proposed model (the Clevite model) Shiozawa et al consider an interfacial layer which is formed by the diffusion of Cu into the CdS during the

formation of copper sulphide layers on the CdS and the heat treatment of the cell afterwards. In addition, they modify the model by including the interface states at the  $\text{Cu}_2\text{S}$ -CdS junction which act as recombination centres when the cells are forward biased. In view of the wide range of experiments supporting it in detail, this model has been accepted by many to be the most satisfactory one to date.

#### 1.5.1 The Clevite model for solar cell

The model presents an energy band diagram for the p- $\text{Cu}_2\text{S}$ -i-CdS n-CdS heterojunction. Since the impurity levels in n-CdS and the optical and electrical properties of the i-CdS region play important roles in the performance of the cell it seems relevant to discuss the pertinent features of the model. These are:

- (1) Gold makes an ohmic contact to p- $\text{Cu}_2\text{S}$  and the ZnAg substrate electrode makes an ohmic contact to the n-CdS.
- (2) Almost all the light absorption occurs in the thin layer of p- $\text{Cu}_2\text{S}$ . The spectral response of the cell corresponds to the intrinsic absorption spectrum of  $\text{Cu}_2\text{S}$  modified by the photoconductive properties of the i-CdS layer.
- (3) The i-CdS layer results from Cu diffusion during the cell fabrication. This layer which is insulating in the dark becomes photoconductive when the cell is illuminated by sunlight. The quasi-Fermi level for electrons moves upward during illumination and the layer becomes weakly n-type. The layer has all the photoconductive properties of Cu-compensated CdS.
- (4) When the cell is illuminated the main junction occurs between  $\text{Cu}_2\text{S}$  and i-CdS. The barrier height in this case is about 0.85 eV.



(5) In the dark, the principal junction occurs between the i-CdS and n-CdS. The barrier height is then about 1.2 eV. A small junction of reversed polarity with a barrier height of 0.35 eV occurs between the p-Cu<sub>2</sub>S and i-CdS. This barrier disappears when the cell is illuminated.

(6) The interface states at the p-Cu<sub>2</sub>S:i-CdS junction are mainly responsible for the recombination which occurs under forward bias conditions.

When photons with energies less than 1.2 eV fall on the cell there is no appreciable absorption in the Cu<sub>2</sub>S layer. The photons pass through the i-CdS layer and n-CdS and are absorbed or reflected by the AgZn electrode. Strong but not complete absorption occurs for photons with energies between 1.2 and 2.4 eV. The reason for this is that the indirect band gap of Cu<sub>2</sub>S requires the absorption coefficient for photon energies in this range to rise slowly with increasing photon energy. This coupled with the small thickness of the Cu<sub>2</sub>S layer, allows some photons with energies between 1.2 and 2.4 eV to pass into the i-CdS layer where their absorption gives rise to photoconductivity, making it weakly n-type. Photons with energies greater than 2.4 eV are absorbed in the Cu<sub>2</sub>S layer. The more energetic the photons, the closer is their absorption to the illuminated surface.

The absorption of photons of appropriate energy generates electron-hole pairs in the Cu<sub>2</sub>S layer. The electrons are the minority carriers in the p<sup>+</sup>-Cu<sub>2</sub>S and have a relatively large lifetime because of the indirect band gap of the Cu<sub>2</sub>S. The electrons diffuse to the Cu<sub>2</sub>S:i-CdS interface, then they are collected by the electric field in the i-CdS region. After reaching the n-type CdS, they pass eventually to the ZnAg electrodes.

As a photoexcited electron leaves the Cu<sub>2</sub>S layer and proceeds towards the ZnAg ohmic contact, the corresponding photogenerated hole moves

towards the ohmic gold contact, where it is annihilated by an incoming electron.

Recombination occurs in the bulk and the interfaces of the  $\text{Cu}_2\text{S}$  layer. For energies higher than 2.4 eV absorption occurs near the illuminated  $\text{Cu}_2\text{S}$  surface. The higher recombination rate at the surface resulting from (a) the higher density of free carriers in excess of equilibrium value, and (b) the surface recombination centres, results in the diminished photoresponse of the cell for these energies.

Many experimental observations demonstrate the dependence of the optical and electrical properties of the cell as a whole on the optical and electrical properties of i-CdS layer. For example:

- (1) the enhancement of the red portion of the spectral response due to the illumination of the cell by green light.
- (2) the decrement of the green portion of the spectral response by infrared light bias (quenching of photoconductivity).
- (3) the appearance of the effects (1) and (2) only after the heat treatment of the cells which indicates that the i-CdS layer is formed by Cu diffusion.
- (4) the decrease in the cell capacitance by additional heat treatment which is due to further growth of the i-layer.
- (5) enhancement of the spectral response at longer wavelengths by doping the n-CdS layer with indium. The photoconductive response of Cu compensated In-doped CdS extends to much longer wavelengths.
- (6) the cross-over of the dark I-V curve and light I-V curve which is associated with the photoconductive effect in the i-CdS layer.
- (7) the growth of the i-layer with heat treatment with consequent loss of tunnelling and shunting paths improves the squareness of the

I-V characteristics.

(8) The series resistance of cells heated in vacuum or inert gas at temperatures above  $150^{\circ}\text{C}$  increases irreversibly. This is due to the growth of the i-layer by copper diffusion. The effect can be reduced by donor doping of the CdS layer.

### 1.5.2 Instability and degradation

Obviously the stability and durability of a solar cell are very important parameters affecting its practical use. In recent years a great deal of attention has been devoted to attempts to understand the mechanisms which result in the failure of the efficient functioning of the solar cells. Knowledge about these mechanisms provides an insight into a better approach to the problem and its solution. The  $\text{Cu}_2\text{S}$ -CdS cell is subject to a number of degradation mechanisms (W. Palz et al 1970, 1973; Mytton et al 1972 and Shiozawa et al, 1969).

- (1) The polycrystalline surface area is reactive with the ambient atmosphere,
- (2) The existence of phases other than chalcocite  $\text{Cu}_2\text{S}$  in the Cu-S system present possibilities for degradation.
- (3) The ionic mobility of Cu in  $\text{Cu}_2\text{S}$  provides a mechanism for ionic segregation when a marked potential drop can be developed across the  $\text{Cu}_2\text{S}$ .
- (4) Cu diffusion into CdS also provides a mechanism for degradation.

As mentioned earlier, the  $\text{Cu}_2\text{S}$ -CdS cell degrades if it is heated above  $150^{\circ}\text{C}$  in vacuum or in an inert gas. This degradation which consists of loss of fill factor, followed by a reduced short-circuit current, is due to copper diffusion. This leads to the growth of the i-layer and consequently to an irreversible increase in the series resistance of the cell.

The introduction of a small concentration of donors into the CdS layer causes substantial changes in the magnitude of this mode of degradation.

The short circuit current is found to be dependent on the composition of the cuprous sulphide layer (Palz et al, 1972). A quantum efficiency equal to that of standard silicon cells can be obtained in cells with the orthorhombic chalcocite phase of  $\text{Cu}_2\text{S}$ , but this decreases when the composition of the cuprous sulphide changes by chemical reaction with the ambient atmosphere. It is well known that copper sulphide can have distinctive compositions such as  $\text{Cu}_2\text{S}$  (orthorhombic chalcocite),  $\text{Cu}_{1.96}\text{S}$  (orthorhombic djurleite) and  $\text{Cu}_{1.8}\text{S}$  (digenite). X-ray studies on copper sulphide by Shiozawa et al (1969) show that the copper sulphides tend to change with time from those with higher to lower copper content:  $\text{Cu}_2\text{S} \rightarrow \text{Cu}_{1.96}\text{S} \rightarrow \text{Cu}_x\text{S}$  (with  $1.96 < x < 1.8$ ). These changes which are due to the reaction with oxygen in the atmosphere, would result in a decrease of this short circuit current of the cell. Likewise studies of Palz et al (1973) showed that cells with different  $\text{Cu}_2\text{S}$  compositions behave like cells at different stages of degradation. Measurements of the short circuit photocurrent of these cells as a function of  $x$  in  $\text{Cu}_2\text{S}$  indicates that the short circuit current decreases with  $x$  and optimum values are obtained with the  $\text{Cu}_2\text{S}$  phase. (Figure 2).

The conversion of chalcocite ( $\text{Cu}_2\text{S}$ ) to phases of lower copper content takes place faster at high temperatures in air. Cu whiskers on the surface of the  $\text{Cu}_2\text{S}$  layer would be oxidized to  $\text{Cu}_2\text{O}$  or  $\text{CuO}$  (depending on the temperature and the oxygen pressure) and the process would then be irreversible. Degradation resulting from the oxidation of the cells at  $150^\circ\text{C}$  in air is different from vacuum degradation. Air degradation has no effect on the series resistance but decreases the short circuit current, while vacuum degradation causes an increase in series resistance.

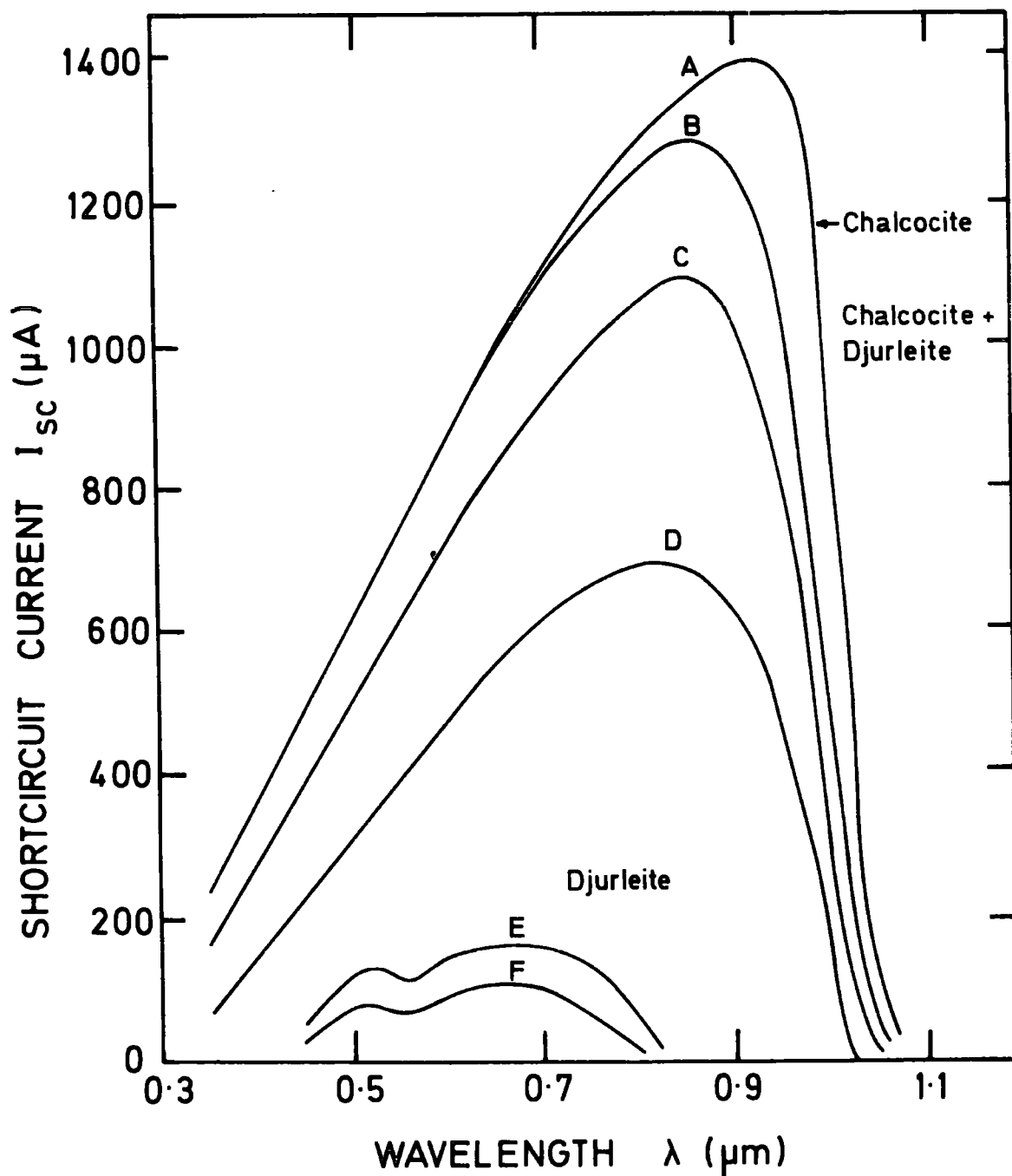


FIG.1:2 SPECTRAL RESPONSES OF  $\text{CdS-Cu}_x\text{S}$  AS A FUNCTION OF  $x$

A $x = 1.995$	B $x = 1.994$	C $x = 1.988$
D $x = 1.972$	E $x = 1.955$	F $x = 1.923$

W. PALZ et al (1973)

Although several degradation mechanisms are involved in the performance of the  $\text{Cu}_2\text{S-CdS}$  cells, none of the associated processes seem to be so basic that it cannot be avoided to a degree sufficient to allow for a life expectancy in excess of 20 years in terrestrial deployment. As a result efforts are continuing to improve the stability of  $\text{Cu}_2\text{S-CdS}$  solar cells. Several expedients for example, the inclusion of dopants (Palz et al, 1973) in the CdS, the use of a special etch solution (Mytton et al, 1972) and the deposition of excess Cu on the  $\text{Cu}_2\text{S}$  surface (K. Bogus and S. Mattes, 1972) have been reported by one author or another to improve the performance and stability of their cells.

In the work presented in this thesis, attention will be drawn to the importance of the role of Cu in CdS and its charge state, i.e. that the monovalent  $\text{Cu}^+$  ion provides a more stable situation than the bivalent  $\text{Cu}^{2+}$  ion. In addition some other photoeffects in CdS such as photoconductivity, photocapacitance, and the role of interface states in the CdS Schottky barrier system, will be discussed.

## CHAPTER TWO

### PHOTOEFFECTS IN CADMIUM SULPHIDE

#### 2.1 Photoconductivity

The phenomenon of absorption of light by a semiconductor or semi-insulator which results in increased electrical conductivity of the material, is known as photoconductivity. Although the phenomenon was discovered late in the 19th Century, its development was closely related to the post war advancement in the technology of producing pure and doped crystals. With II-VI compounds the preparation of large crystals and single crystal thin films has been greatly hindered by the tendency of these compounds to form various intrinsic defects, to deviate from stoichiometry and also to have high melting temperatures. Nonetheless, the great interest in these materials, together with the development of modern technological methods such as crystal growth by vapour transport, crystal growth from the melt under high pressures of inert gas, and preparation of thin films by electron beam evaporation and ion implantation, has led to significant progress in the preparation of semiconducting materials based on these compounds.

There are many reasons for the continued interest in the photoconductivity of II-VI compounds. The widths of the forbidden bands of these compounds and their solid solutions span the total spectrum of visible light and in part to the ultraviolet region, Table (1). This makes it possible to use them in principle as semiconducting sources and detectors of visible and ultraviolet light.

The photoconductivity characteristics of the II-VI compounds can be summarized as follows.

TABLE (1)

Material	Energy gap $300^{\circ}\text{K}$ (ev)	Gap Transition	Mobility $300^{\circ}\text{K}$ ( $\text{cm}^2\text{V}^{-1}\text{sec}^{-1}$ ) Electron Hole	Dielectric Constant (relative)	Electron affinity (ev)
ZnS (hex)	3.58	Direct	120 -	8.3	3.9
ZnSe	2.67	Direct	530 -	9.1	4.09
ZnTe	2.26	Direct	530 130	10.1	3.5
CdS (hex)	2.42	Direct	340 -	9.0-10.3	4.5
CdTe	1.44	Direct	700 65	9.6	4.28
CdSe (hex)	1.7	Direct	600	9.3-10.6	4.95

Reference : A.L.MILNES & D.L. FEUCHT, Heterojunctions and Metal-semiconductor junctions

Academic Press, N.Y. 1972.

When light of appropriate energy falls on a photoconductor, electrons from the valence band are excited to the conduction band where they can move freely. The excited electrons leave behind holes in the valence band. The holes have lower values of mobility, but in any event are rapidly captured in recombination centres and, therefore, the major contribution to photoconductivity is made by electrons. The photoexcited electrons whose density depends on the rate of excitation, recombine with the immobilised hole, but some may be trapped in trapping centres. When steady state conditions are reached the rate of photoexcitation equals the rate of recombination. The factors determining the number of carriers in the conduction band are (1) the rate of photoexcitation  $F$ , and (2) the lifetime of electrons

$$n = F \tau \quad (2.1)$$

$\tau$ , the time during which electrons remain in the conduction band is determined mainly by the density and location of the recombination centres in the forbidden gap. When an electric field is applied to a photoconductor with ohmic contacts, the photoexcited electrons move toward the anode and charge moves round the external circuit. The photocurrent thus generated is given by

$$I = \frac{ne}{T_r} \quad (2.2)$$

where  $T_r$  is the electron transit time between the two ohmic contacts. If the spacing between the two ohmic contacts is  $d$ , then

$$T_r = \frac{d}{v_d} = \frac{d}{\mu \epsilon} = \frac{d^2}{\mu V} \quad (2.3)$$

$v_d$  is the drift velocity of electrons,  $\epsilon$  the electric field,  $\mu$  the mobility and  $V$  is the voltage applied to the device.

Substituting for  $n$  in equation (2.2) from equation (2.1) we have

$$I = eF \frac{\tau}{T_r} = eFG, \text{ or } G = \frac{I}{eF} = \frac{1}{T_r} \quad (2.4)$$

where  $G$  is the photoconductive gain and is defined as the number of charge carriers which pass between the electrodes for each photon absorbed.

Substituting for  $T_r$  in equation (2.4) from equation (2.3), we have:

$$G = \frac{\mu \tau V}{d^2} \quad (2.5)$$

i.e. the photoconductivity gain is directly proportional to the product of  $\mu$  and the voltage applied to the device. It is inversely proportional to the square of spacing between the electrodes. For higher gain, therefore, it is necessary to increase the voltage applied to the device and to decrease  $d$  the distance between the contacts. It is possible to change  $\tau$  by the introduction of suitable dopants. In fact the lifetime of the free carrier is determined mainly by the location of the energy levels associated with the recombination centres in the forbidden gap, rather than by the density of these centres (Grimeiss, 1974).

Another determining parameter for the performance of a photoconductor is the response time, i.e. the time required for the photocurrent to reach a steady state (or some appropriate fraction of the steady state, say 0.5). This is also the time required for the photocurrent to decay to the same fraction of its steady-state value after the light is interrupted. In the absence of traps the response time is equal to the lifetime, but in general, the response time is controlled by both recombination and trapping centres. For definiteness assume that an illuminated conductor is in the steady state and that the illumination is then switched off at  $t = t_0$ . The initial response time of an n-type photoconductor will be

$$\left. \frac{dn}{dt} \right|_{t = t_0} = \frac{-n(t_0)}{\tau_{\text{resp}}} \quad (2.6)$$

where  $n(t_0)$  is the steady state electron concentration,  $n = F\tau$ . It is possible to prove that the initial response time of a photoconductor equals the steady state lifetime  $\tau^*$  of the excited state (see, for example, F. Stockmann, 1975).

It is worth noting that there is a maximum value for the gain of a photoconductor. This value corresponds to the maximum voltage that can be applied to the photoconductor before the injection of carriers from cathode dominates the conductivity of the crystal (Rose, 1959) and space charge limitations occur. The maximum gain is given by

$$G_{\text{max}} = \frac{\tau_{\text{resp.}}}{\tau_{\text{rel.}}} M \quad (2.7)$$

where  $\tau_{\text{resp.}}$  is the response time and  $\tau_{\text{rel.}}$  is the ohmic relaxation time. For a trap free device  $M$  equals unity but in general,  $M$  is the ratio of shallow traps to deep traps or is the ratio of total charge required to fill the deep traps to the total charge in thermal equilibrium or therm contact with the conduction band. The performance of a photoconductor is determined by the product of its gain and the reciprocal of its response time. Traps play a dual role in this,

- (1) they give rise to long response times and hence decrease the product  $\frac{G_{\text{max}}}{\tau_{\text{resp.}}}$ , and
- (2) they permit higher values of voltage to be applied before injected carriers dominate the conductivity and hence increase the gain.

Homogeneous II-VI photoconductors are capable of high gain and high speed of response for high intensity excitation. With low intensity excitation,

however, the effects of traps dominate the response time and the speed of response is low.

Experimentally photocurrents corresponding to unit gain, called primary photocurrents, were identified in CdS by Van Heerden (1957). The requirement for unit gain is that the lifetime of majority carriers should almost be the same as their transit time. If the majority-carrier lifetime is longer than the transit time, the gain exceeds unity, and the corresponding photocurrents are called "secondary photocurrents". Gains of the order of  $10^4$  have been observed by Lappe (1959) for evaporated CdS layers under electron excitation, and factors up to values of 500 have been reported for CdS single crystals by Bube and Barton (1959).

## 2.2 Superlinearity

The photocurrent of a photoconductor depends on the intensity of the incident light and temperature in many different ways. Experimental evidence shows that the photocurrent may vary superlinearly, linearly or sub-linearly with light intensity. Similarly the photocurrent may be insensitive to temperature or increase or decrease with increasing temperature. Analytically, the process of illuminating a photoconducting device with light of increasing intensity gives rise to the separation of the electron and hole steady state Fermi levels. As a result, some centres change their status and become recombination centres instead of trapping centres. The capture cross sections of these centres for free carriers determine whether they behave as sensitizing or desensitizing centres, when they are electronically added to the existing recombination centres. This concept which is called "electronic doping" provides a simple and wide ranging mechanism to account for the dependence of photocurrent on light intensity.

(A. Rose, 1963).

If the photocurrent varies with a power of excitation intensity greater than unity, this is the phenomenon of superlinearity. Such an effect requires an increase in the free-electron lifetime with increasing excitation intensity. Different authors (R.H. Bube 1957, H.A. Klasens 1958 and J. Voigt 1962,1964), have proposed models to explain the phenomenon in CdS. A simple model was generalized by Cardon and Bube (1964) to include the effects of a quasi continuous trap distribution. This model was then extended by G.A. Dussel et al, 1966, to cover the effect of a high density of shallow traps. In their model which contains two types of recombination centres, together with shallow and deep traps, the authors show that three processes are essential for the onset of superlinearity with increasing excitation intensity. These three conditions are: (1) holes must reside primarily in the sensitizing centres rather than in the fast recombination centres, (2) deep traps must be filled, and (3) the occupancy of fast recombination centres must be determined by recombination kinetics rather than by thermal equilibrium with the valence band. To be clear, let us consider the important features of the model proposed by G.A. Dussel et al, 1966, (Fig. 1), and briefly discuss why it is essential for example for the onset of superlinearity that the occupancy of fast recombination centres be determined by recombination kinetics rather than by thermal equilibrium with the valence band.

In the steady state the kinetic equations describing the transitions illustrated in Fig. 1 are the following:-

For free electrons ,

$$\frac{dn}{dt} = 0, \quad 0 = F - \beta_{e1} n (N_1 - n_1) - \beta_{e2} n (N_2 - n_2) - \beta_{e3} n (N_3 - n_3) + P_{e3} n_3 - \beta_{e4} n (N_4 - n_4) + P_{e4} n_4 \quad (2.8)$$

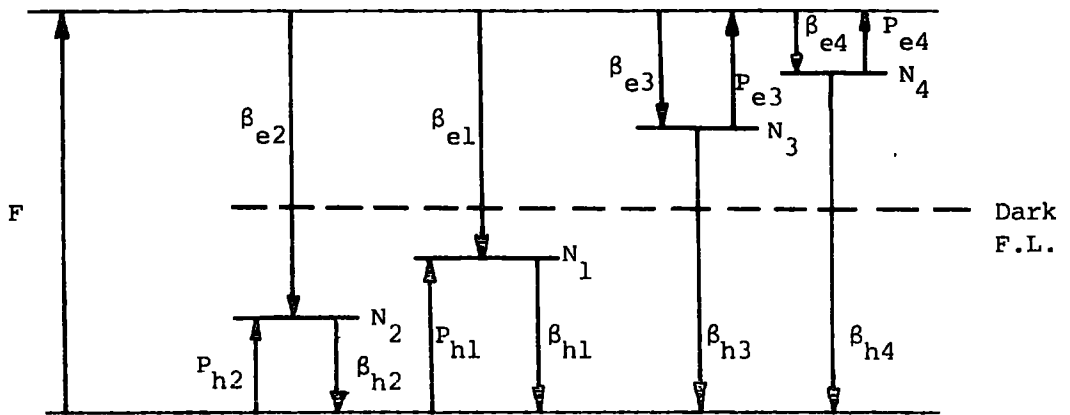


Figure 2.1: Important transitions are shown in the diagrams.

The directions of the arrows show the directions of electron motion.

With the notation used:

$F$  = density of free electron-hole pairs created per second.

$N_i$  = total density of states ( $i = 1, 2, 3, 4$ ).

$n_i$  = density of states occupied by electrons ( $i = 1, 2, 3, 4$ ).

$\beta_{ei}$  = capture probability for electrons at empty centres  $i$ .

$\beta_{hi}$  = capture probability for holes at occupied centres  $i$ .

$n$  = density of free electrons.

$p$  = density of free holes.

$E_i$  = electron ionization energy to the conduction band from centres  $i$  for  $i = 3, 4$ , or hole ionization energy to the valence band from centres  $i$  for  $i = 1, 2$ .

$p_{ei}$  = probability for thermal excitation of electrons from centres  $i$  to the conduction band for  $i = 3, 4$ ,  $p_{ei} = N_c \beta_{ei} \exp\left(\frac{-E_i}{kT}\right)$ .

$N_c$  = effective density of states in the conduction band.

$P_{hi}$  = probability of thermal excitation of holes from centres  $i$  to the valence band for  $i = 1, 2$ ;  $P_{hi} = N_v \beta_{hi} \exp\left(\frac{-E_i}{kT}\right)$ .

$N_v$  = effective density of states in valence band.

For the unoccupied centres 1 ,

$$0 = \beta_{e1} n(N_1 - n_1) - \beta_{h1} p n_1 + P_{h1} (N_1 - n_1) \quad (2.9)$$

For the unoccupied centres 2 ,

$$0 = \beta_{e2} n(N_2 - n_2) - \beta_{h2} p n_2 + P_{h2} (N_2 - n_2) \quad (2.10)$$

For the occupied centres 3 ,

$$0 = \beta_{e3} n(N_3 - n_3) - n_3 p_{e3} - \beta_{h3} n_3 p \quad (2.11)$$

For the occupied centres 4 ,

$$0 = \beta_{e4} n(N_4 - n_4) - n_4 p_{e4} - \beta_{h4} n_4 p \quad (2.12)$$

and for charge conservation ,

$$p + (N_1 - n_1) + (N_2 - n_2) = n + n_3 + n_4 \quad (2.13)$$

Equations (2.9) to (2.12) can be solved to give  $(N_1 - n_1)$ ,  $(N_2 - n_2)$ ,  $n_3$  and  $n_4$  as functions of  $n$  and  $p$ .

By substituting these values in equation (2.8), one gets ,

$$F = \sum_i R_i = np \sum_i \left[ \frac{\beta_{ei} \beta_{hi} N_i}{\beta_{hi} p + \beta_{ei} n + P_i} \right] \quad (2.14)$$

where,  $p_i = p_{ei}$  for  $i = 3,4$  and  $p_i = p_{hi}$  for  $i = 1,2$ . The quantity  $R_i$  has been introduced to express the recombination through centres  $i$ .

Similarly equation (2.13) becomes:

$$\begin{aligned}
 p \left[ 1 + \frac{\beta_{h1} N_1}{\beta_{h1} p + \beta_{ei} n + P_{h1}} + \frac{\beta_{h2} N_2}{\beta_{h2} p + \beta_{e2} n + P_{h2}} \right] = \\
 n \left[ 1 + \frac{\beta_{e3} N_3}{\beta_{h3} p + \beta_{e3} n + P_{e3}} + \frac{\beta_{e4} N_4}{\beta_{h4} p + \beta_{e4} n + P_{e4}} \right]
 \end{aligned} \tag{2.15}$$

By considering the dominant terms in equations (2.14) and (2.15) it is possible to recognize the type of the centre through which the recombination takes place. Since the model has been proposed for an n-type photoconductors (CdS) and specifically for the superlinear behaviour of such material, only those cases that give rise to superlinearity are considered. Centres 1 and 2 are called "recombination centres" and centres 3 and 4 "electron traps", even though their role can change from one to the other in different ranges of excitation. Centres 2 are identified as sensitizing centres, i.e.  $\beta_{e1} \gg \beta_{e2}$ . Centres 3 are deep traps and centres 4 shallow ones.

To acquire a better insight into the nature of the processes involved let us consider, for example, the occupancy of centres 1. This is given by

$$N_1 - n_1 = \frac{\beta_{h1} N_1 p}{(\beta_{h1} p + \beta_{ei} n + P_{n1})} \tag{2.16}$$

Three possibilities for the dominant term may arise from the three terms in the denominator of equation (2.16). Since we are dealing with n-type crystals, the term involving  $p$  may in general be neglected. (Exceptions are for the case:  $\beta_{h1} \gg \beta_{e1}$ , or for very high excitation where  $p = n$ ). Eliminating the term involving  $p$  leaves two possibilities, one where  $P_{h1}$  is dominant, and the other where  $\beta_{ei} n$  is dominant.

When  $P_{h1}$  is dominant ,

$$N_1 - n_1 = \frac{\beta_{h1} N_1 p}{P_{h1}} \quad (2.17)$$

In this case, centres 1 are in thermal equilibrium with the valence band.  $p$ , the density of free holes is dependent on the density of trapped holes.

With increasing excitation, the term containing  $n$  becomes dominant.

$$N_1 - n_1 = \frac{\beta_{h1} N_1 p}{\beta_{e1} n} \quad (2.18)$$

The density of unoccupied 1 centres depends now on  $p$  as well as  $n$ . In other words, the variation of  $p$  with  $n$  determines the occupancy of 1 centres. If  $p$  increases more rapidly than  $n$ ,  $(N_1 - n_1)$  increases; if  $p$  increases at the same rate as  $n$ ,  $(N_1 - n_1)$  remains constant; and if  $p$  increases more slowly than  $n$ ,  $(N_1 - n_1)$  decreases. The variation of  $p$  with  $n$  as given in equation (2.15) depends on whether the trapped holes are primarily in centres 1 or 2, and whether the centres 3 are empty or filled.

As far as recombination is concerned, when centres 1 are in thermal equilibrium with the valence band, the capture rate of holes from the valence band is equal to the hole excitation rate from these centres to the valence band. In this case, the role of centres 1 in recombination is limited by the capture of electrons from the conduction band ,

$$R_1 = \left( \frac{\beta_{e1} \beta_{h1} N_1}{P_{h1}} \right) pn \quad (2.19)$$

When the hole capture from the valence band equals the hole excitation to the valence band, the recombination is given by:

$$R_1 = \beta_{h1} N_1 p \quad (2.20)$$

i.e. the role of centres 1 in recombination depends only on  $p$  the density of free holes.

In general a certain recombination path will remain dominant only if it can preserve the equality of the recombination rate  $R$ , and the excitation rate  $F$ . This means that the terms on the right side of the equation (2.20) should give a linear dependence with  $F$ . So when  $p$  starts to vary sublinearly with  $F$ , then  $R_1$  can no longer be the dominant recombination path. This is the essential condition for the occurrence of superlinearity.

### 2.3 Optical and Thermal Quenching

The photocurrent of a II-VI compound excited by light in the visible part of the spectrum can be considerably reduced by simultaneous illumination with infrared light.

The photocurrent may also be reduced by increasing the device temperature while maintaining the light intensity fixed. This will cause the photoconductor to revert to the insensitive state by moving the steady state Fermi levels further from the band edges so that the sensitizing centres become traps instead of recombination centres. (Rose 1963). Exploitation of thermal techniques is limited as far as the determination of capture cross-sections is concerned, because a plot of the  $\ln$  of the electron density at the break-point (i.e. the electron density at the temperature at which the photosensitivity of the photoconductor starts to fall) as a function of  $1/T$  does not give the absolute value of the electron or hole cross section of the sensitizing centres (see for example, Aven and Prener, 1967).

Optical quenching techniques can be used to obtain information about the energy levels and capture cross-sections of sensitizing centres. The optical hole ionization energy of a sensitizing centre is obtained directly by the measurement of the quenching efficiency as a function of the energy of the quenching radiation.

Measurements of optical quenching spectra for crystals of CdS:I, CdS:Cu and pure CdS have shown that the threshold of quenching occurs at an energy of about 1.1 eV in all three crystals. This implies that the sensitizing centre lies 1.1 eV. above the valence band (Bube et al, 1964).

Similar measurements in CdSe have yielded a value of 0.66 eV for the hole ionization energy of the sensitizing centres in this material. Quenching experiments carried out on CdS crystals grown in various atmospheres of excess sulphur and cadmium all showed two broad bands at room temperature which were centred at approximately 0.82  $\mu\text{m}$  and 1.35  $\mu\text{m}$ . (Carter and Woods, 1973). However, at 90 K, quenching occurred in the shorter wavelength band only. No differences in the quenching spectra were observed with either the Cd rich or S rich samples when the measurements were repeated at 90 K after cooling the samples from 388 K under illumination. However, with the specimens which had been grown at  $T_s = 50^\circ\text{C}$  ( $T_s$  is the temperature of sulphur tail of the growth tube), the shape of the quenching spectrum depended on whether the sample was illuminated or not during cooling. The resemblance of the quenching spectrum of this particular sample with those of Cd rich samples led to the conclusion that the illumination of the sample had caused an effective chemical reduction of the crystal.

Infrared quenching has been also observed by a number of workers in other II-VI compounds, e.g. CdSe, (Lashkazev and Sheinkman, 1965), ZnSe (Reinberg et al, 1971, and Gobrecht et al, 1971) and ZnS (Burget

and Lin, 1970). For optoelectronics problems, interest attaches to the infrared extinction of photoconductivity. The point is that the dielectric constant, and consequently also the refractive index, depends essentially on the concentration of the electrons in the conduction band. Infrared extinction of photoconductivity makes it possible to vary the number of electrons in the conduction band and to control the refractive index of the semiconductor. (Maev et al, 1973). It is worth noting that infrared extinction of photoconductivity is observed most frequently in crystals with high photosensitivity, so that in the preparation of the corresponding material one should bear in mind the joint occurrence of these phenomena.

#### 2.4 Thermally stimulated current Techniques

Trapping is a fundamental process of energy storage in almost all the electronically active solids. This energy storage takes place in the form of electrons or holes captured in the defects and imperfection sites, where an electron or a hole is prohibited from moving freely through the crystal unless supplied with thermal or optical energy. When the trapped electron or hole is released, it is free to move until captured by a recombination centre or by another trap.

Since the performance of photoconductors as well as phosphors depends on the trap parameters and their distribution, numerous investigations have taken place to determine these parameters using different methods and techniques. All the early investigations were concerned with thermoluminescence. Several investigators such as Randall and Wilkins, 1945, Garlick and Gibson, 1948, and Grossweiner, 1953, proposed different methods of analysing glow curves. In recent years similar techniques have been used for the study of the energy levels of

traps in photoconductors. Instead of the luminescent intensity, the thermally stimulated conductivity is measured as a function of temperature. A plot of the conductivity versus temperature usually contains several peaks which are associated with the release of trapped electrons, when the thermal energy supplied to the crystal reaches an adequate value.

In determining the trap parameters, most workers have only used one or two special features of the T.S.C. curve, such as the value of conductivity at the maximum  $\sigma^*$ , and the corresponding temperature,  $T^*$ , or the two temperatures at which the conductivity equals to  $\frac{1}{2}\sigma^*$ , (see for example Nicholas and Woods, 1964). This leads to experimental inaccuracy because of the difficulty of locating  $T^*$  with sufficient accuracy or of determining temperatures which are close together. To avoid this, we describe a method which has been developed by Cowell and Woods (1967). The method which is based on the work of Haering and Adams (1960), utilizes all the measured values of conductivity and temperature and, therefore, is more accurate.

For a single set of traps with energy  $E_t$ , at equilibrium, the rate of change of electron concentration in the conduction band is equal to the net rate of thermal excitation of the trapped electrons to the conduction band minus the rate of electron recombination with holes ,

$$\frac{dn_c}{dt} = -\frac{n_c}{\tau} - \frac{dn_t}{dt} \quad (2.21)$$

where

$$\frac{dn_t}{dt} = -n_t N_c s v e^{\frac{-E}{kT}} + n_c (N_t - n_t) s v \quad (2.22)$$

i.e. the rate of change of the concentration of trapped electrons is equal to the rate of retrapping of excited electrons minus the rate of thermal excitation of trapped electrons to the conduction band.

The notation is as follows,  $N_t, N_c$  = concentration and effective concentration of trapping and conduction states, respectively,  $n_t, n_c$  = concentrations of electrons in traps and in the conduction band,  $s$  = cross section of a trap for an electron,  $v$  = thermal velocity of electrons in the conduction band,  $E = E_c - E_t$ ,  $k$  = Boltzmann's constant, and  $T$  = temperature in degrees K. The resulting conductivity is given by :

$$\sigma = n_c e \mu \quad (2.23)$$

In the limits of slow and fast retrapping the solution of equations (2.21) and (2.22) is straightforward and provides the value of  $n_c$ . In the case of slow retrapping, the probability of retrapping is much less than the probability of recombination, i.e.  $(N_t - n_t) s v \ll \frac{1}{\tau}$ . In this case, the second term in the right side of equation (2.22) is negligible and therefore, the solution with the assumption that the temperature is a linear function of time becomes:

$$n_t = n_{t_0} \exp \left[ -\frac{1}{\beta} \int_{T_0}^T N_c s v e^{\frac{-E}{kT}} dT \right] \quad (2.24)$$

where  $T = T_0 + \beta t$

Equation (2.21) is a linear differential equation of the form  $y' + p(T)y = Q(T)$  with the integrating factor of  $e^{\int P(T) dT}$ . The solution to equation (2.21) is ,

$$n_c = -\beta \tau \frac{dn_t}{dT} \quad (2.25)$$

and the conductivity is therefore :

$$= n_c e \mu = n_{t_0} e \mu v \exp \left\{ -\frac{E}{kT} - \int_{T_0}^T \frac{v}{\beta} \exp \left( -\frac{E}{kT} \right) dT \right\} \quad (2.26)$$

where  $n_{t_0}$  is the initial density of filled traps,  $\tau$  is the lifetime of

a free electron and  $\mu$  the electron mobility.  $\beta$  is the heating rate and  $T_0$  the temperature from which heating begins following the filling of the traps.  $\nu$  is the attempt-to-escape frequency of a trapped electron:  $\nu = N_c \nu_s$ . If it is assumed that  $\nu$  is independent of  $T$  and that over the temperature span of a T.S.C. curve the variation of  $\mu$  and  $\tau$  with  $T$  can be ignored, equation (2.26) can be rewritten as :

$$\sigma = A \exp \left\{ -t + B \int_{t_0}^t \exp(-t) t^{-2} dt \right\} \quad (2.27)$$

where  $t = \frac{E}{kT}$  and  $A$  and  $B$  are constants:  $A = n_{t_0} \tau e \mu \nu$  and  $B = \frac{\nu E}{\beta K}$ .

Repeated integration by parts of the integral (2.27) leads to a convergent infinite series of the form:

$$\sigma = A \exp \left[ -t - B \left\{ \exp(-t)t^{-2} - 2 \exp(-t)t^{-3} + 3 \times 2 \exp(-t)t^{-4} + \dots \right\} \right]_{t_0}^t \quad (2.28)$$

Since  $t$  is large in practice, in the range 15-40, an approximate value of  $\sigma$  can be obtained by considering only the first term of the series; then

$$\sigma \approx A \exp \left\{ -t - B \exp(-t)t^{-2} \right\} \Big|_{t_0}^t \quad (2.29)$$

The bottom limit in (2.29) can be ignored provided  $t_0 \geq 1.5 t^*$  and

$$\sigma \approx A \exp \left\{ -t - B \exp(-t)t^{-2} \right\} \quad (2.30)$$

If (2.30) is differentiated and equated to zero, one can find the maximum of the curve which occurs at  $t = t^* = \frac{E}{kT^*}$ , then

$$B' = \exp(t^*) \frac{t^{*3}}{t^* + 2} \quad (2.31)$$

where  $\hat{B}$  is the approximate value of B obtained by replacing the approximation sign of (2.30) by an equality. The true value of B can be found by differentiating (2.27) and equating the result to zero:

$$B = \exp(t^*) t^{*2} \quad (2.32)$$

For the determination of trap parameters the values of A and B should be determined. In the curve fitting technique (Cowell and Woods, 1967) A is determined by its use as an adjustable parameter to normalize the theoretical curve with the experimental one at the maximum. The approximate value for B, i.e.  $B'$ , is determined by the following procedure. An isolated peak of the measured T.S.C. curve yields the value of  $T^*$ . This can be used to determine the approximate value of the trap depth E. (See for example Nicholas and Woods, 1964).  $T^*$  with E give an approximate value for  $t^*$  which can be inserted in (2.31) to yield  $B'$ . The value of  $\sigma$  is then calculated from (2.30) with the use of  $B'$  instead of B.

Once the curves were fitted, the determination of the final value of E leads to the calculation of B from (2.32) and hence the capture cross section S. The trap density  $n_{t_0}$  can be estimated from the value of A. Since  $A = n_{t_0} \tau e \mu v$ , this requires a knowledge of  $\tau$ , the free electron lifetime and  $\mu$  the electron mobility. The values of  $\mu$  can be chosen from the tabulated Hall mobility data and the value of  $\tau$  can be measured by determining the photoconductive gain.

In the case of fast retrapping, it is much more probable for the thermally excited electrons to be retrapped than to recombine with holes, i.e.  $(N_t - n_t) s v \gg \tau^{-1}$ . In other words, the time required for thermal equilibrium to be established between the trapped electrons and electrons in the conduction band is much shorter than the recombination lifetime.

If the total number of electrons is denoted by  $n = n_c + n_t$ , then equation (2.21) can be written as:

$$\frac{dn}{dt} = -\frac{n_c}{\tau} \quad (2.33)$$

where,  $n_c$  is the electron concentration in the conduction band, and can be written in terms of  $n$  as:  $n_c = n \left( \frac{N_c}{N_t} \right) e^{-E/kT}$  therefore

$$\frac{dn}{dt} = -\frac{n}{\tau} \left( \frac{N_c}{N_t} \right) e^{-E/kT} \quad (2.34)$$

The solution of equation (2.34) is

$$n = n_{t_0} \exp \left[ -\frac{1}{\beta} \int_{T_0}^T \left( \frac{N_c}{N_t} \right) \frac{1}{\tau} e^{-E/kT} dT \right] \quad (2.35)$$

and the resulting conductivity is:

$$\sigma(T) = n_c e \mu = \frac{N_c \mu e n_{t_0}}{N_t} \exp \left[ \frac{-E}{kT} - \frac{1}{\beta N_t \tau} \int_{T_0}^T N_c e^{-E/kT} dT \right] \quad (2.36)$$

putting  $t = E/kT$  as before, equation (2.36) becomes:

$$\sigma = c \exp \left\{ -t + D \int_{t_0}^t \exp(-t) t^{-7/2} dt \right\} \quad (2.37)$$

where  $c = \frac{N_c \mu e n_{t_0}}{N_t}$  and  $D = \frac{N_c E^{5/2}}{N_t \beta T^{*3/2} K^{5/2} \tau}$

Since the term  $N_c$  contains  $T^{*3/2}$ , then  $D$ , like  $C$ , is a constant. Repeated integration by parts of the equation (2.37) leads to a convergent series which its first term gives the following expression for  $\sigma$ :

$$\sigma \approx C \exp \left\{ -t - D \exp(-t) t^{-7/2} \right\} \quad (2.38)$$

If (2.38) is differentiated and equated to zero, one can find the value of  $t$  at the maximum (i.e.  $t^*$ ) by the following expression:

$$D' = \frac{\exp(t^*) t^{*9/2}}{t^* + 3.5} \quad (2.39)$$

where  $D'$  is the value of  $D$  to the limits of the approximation used.

In this case the curve fitting procedure is done by the use of (2.38) and (2.39). Values of  $S$  cannot be found since equation (2.38) does not contain  $v$ . The value of  $C$  gives a measure of the fraction of traps originally filled since  $C = \frac{N_c e \mu n_{t0}}{N_t}$ , and the value of  $D = N_c E^{5/2} / N_t \beta \tau T^{*3/2} K^{5/2}$  gives an estimate of  $N_t$ , provided  $\tau$  is determined from the photoconductive gain.

## 2.5 The Photovoltaic Effect

The photovoltaic effect is defined as the creation of an electromotive force by the absorption of light in an inhomogeneous solid. The purpose of the inhomogeneity is to separate electrons and holes which have been generated by the absorption of light. This non-uniformity can occur in a metal-semiconductor contact, or at a junction between two regions of a semiconductor with different types of conductivity, such as p-n junctions. The p-n junction can be a homojunction which has the same semiconductor on both sides of the junction, or a heterojunction composed of two different semiconductors. Although the great majority of solar cells are made with p-n junctions, there are some advantages exhibited by other kinds of photovoltaic cells such as Schottky barriers, and heterojunctions that make them attractive. The Schottky barrier cells in particular are very simple and economical to fabricate, and have improved spectral response at short wavelengths, but their expected efficiencies may be

somewhat lower than conventional cells because of lower open circuit voltage.

## 2.6 Metal-semiconductor Contact

When a metal of work function  $\phi_m$  is brought into an intimate contact with a semiconductor of work function  $\phi_s$ , a readjustment of charge takes place to establish thermal equilibrium. For a metal contact to an n-type semiconductor with  $\phi_m > \phi_s$ , flow of electrons from the semiconductor to the metal continues until the Fermi level in the semiconductor lines up with that of the metal. In association with this readjustment of charge, an energy band bending occurs at the interface, on the semiconductor side of the contact. The amount of band bending is essentially the difference between the two work functions. This potential difference  $q\phi_m - q(\chi + V_n)$ , is called the contact potential where  $q\chi$  is the electron affinity measured from the bottom of conduction band to the vacuum level, and  $qV_n$  is the energy difference between the conduction band and the Fermi level of the semiconductor (Fig.2). Neglecting Schottky barrier lowering, the effects of any interfacial layer and those of surface states, the barrier height is given by:

$$q\phi_{Bn} = q(\phi_m - \chi) \quad (2.40)$$

i.e. the barrier height is simply the difference between the metal work function and the electron affinity of the semiconductor. In the limiting case where a large density of surface states is present, depending on the thickness of the interfacial layer, surface states are either in equilibrium with the metal or with the bulk of the semiconductor. For interfacial thicknesses roughly less than  $30 \text{ \AA}$  most of the states are in equilibrium with the metal and they tend to lock the top of the

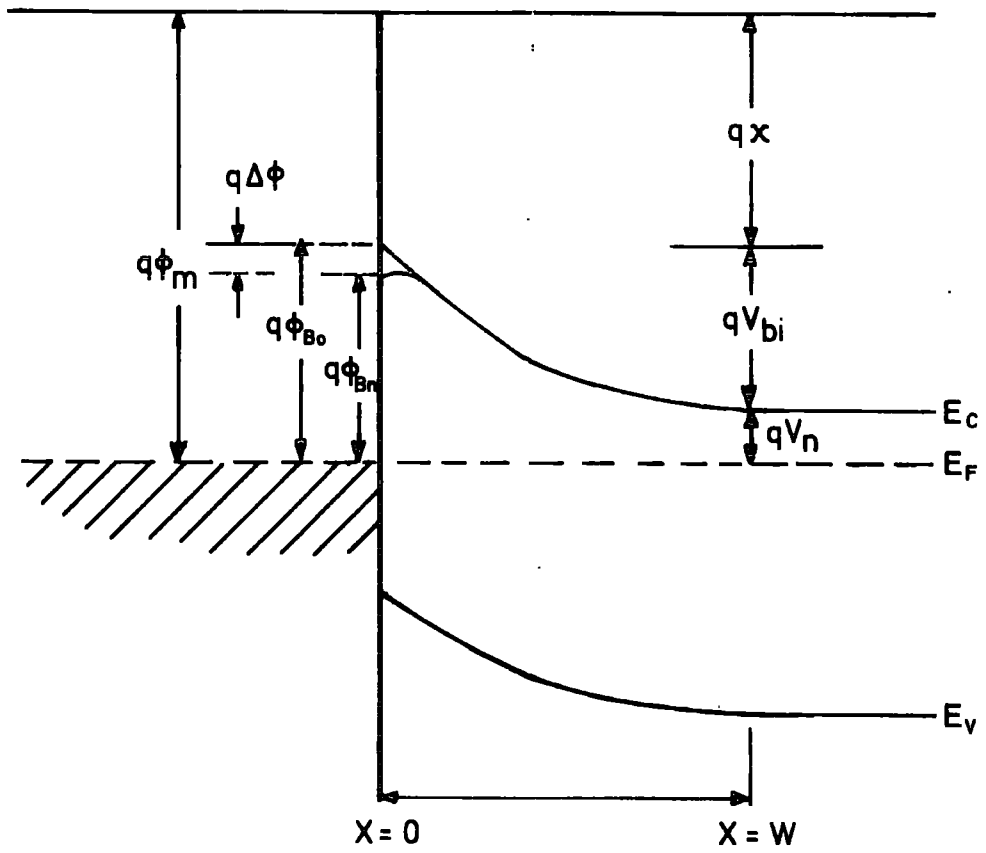


FIG. 2-2 ENERGY BAND DIAGRAM OF A METAL- $n$ -TYPE SEMICONDUCTOR CONTACT

barrier relative to the Fermi level in the metal while for the thicknesses greater than about  $30 \text{ \AA}$  the surface states are in equilibrium with the semiconductor and tend to lock the top of the barrier to the Fermi level in the semiconductor (Card and Rhoderick, 1971a). It is obvious that as the interfacial layer gets thicker, the more the device fails to behave as an ideal metal-semiconductor diode. We later on discuss how the results of measurements of the barrier height are affected by the presence of an interfacial layer and surface states. For the moment, however, we consider the metal-semiconductor barrier under the abrupt approximation that  $\rho \approx q N_D$  for  $x < w$ , and  $\rho \approx 0$  for  $x > w$  when  $w$  is the depletion width. The solution to Poisson's equation under the above boundary conditions is:

$$v(x) = \frac{q N_D}{\epsilon_s} \left( Wx - \frac{1}{2} x^2 \right) - \phi_{Bn} \quad (2.41)$$

$$|\epsilon(x)| = \frac{q N_D}{\epsilon_s} (W - x) = \epsilon_m - \frac{q N_D x}{\epsilon_s} \quad (2.42)$$

and

$$w(\text{depletion width}) = \sqrt{\frac{2 \epsilon_s}{q N_D} \left( v_{bi} - v - \frac{kT}{q} \right)} \quad (2.43)$$

where  $N_D$  is the donor concentration,  $\epsilon_s$  the permittivity of the semiconductor and  $\frac{kT}{q}$  arises from the contribution of the kinetic energy of the mobile carriers. The electric field maximum occurs at  $x = 0$  :

$$\epsilon_m = \epsilon(x=0) = \sqrt{\frac{2 q N_D}{\epsilon_s} \left( v_{bi} - v - \frac{kT}{q} \right)} = 2 \left( v_{bi} - v - \frac{kT}{q} \right) / w \quad (2.44)$$

Assuming total ionization of the donors, the space charge  $Q_{SC}$  per unit area of the semiconductor can be written as:

$$Q_{SC} = q N_d w = \sqrt{2 q \epsilon_s N_d \left( V_{bi} - V - \frac{kT}{q} \right)} \text{ Coul./cm}^2 \quad (2.45)$$

and the depletion layer capacitance  $c$  per unit area as:

$$c = \frac{\partial Q_{SC}}{\partial V} = \sqrt{\frac{q \epsilon_s N_d}{\left( V_{bi} - V - \frac{kT}{q} \right)}} = \frac{\epsilon_s}{w} \text{ farad/cm}^2 \quad (2.46)$$

i.e. The depletion layer capacitance is voltage dependent, and is inversely proportional to the depletion width. At a fixed bias voltage when  $w$  remains constant, the depletion layer capacitance resembles a parallel plate capacitance. Equation (2.46) can be written in the form:

$$\frac{1}{c^2} = \frac{2 \left( V_{bi} - V - \frac{kT}{q} \right)}{q \epsilon_s N_d}$$

$$\frac{d\left(\frac{1}{c^2}\right)}{(-dV)} = \frac{2}{q \epsilon_s N_d}$$

or

$$N_d = \frac{2}{q \epsilon_s \frac{d\left(\frac{1}{c^2}\right)}{(-dV)}} \quad (2.47)$$

If  $N_d$ , the uncompensated donor density of the semiconductor is constant throughout the depletion region, a plot of  $\frac{1}{c^2}$  versus bias voltage is a straight line, the slope of which yields  $N_d$ , while the intercept on the abscissa gives the contact potential. When a large negative bias is applied to the device, the semiconductor Fermi level is lowered and the electron traps empty down to a certain level below the conduction band. Depending whether the density of donors is large compared to the density of traps or not, the plot of  $\frac{1}{c^2}$  versus  $V$  is either a straight line or has a concave downward curvature. (A.M. Goodman, 1963).

## 2.7 Conduction mechanism in Schottky barriers

Mechanisms which may occur when conduction takes place in a Schottky junction from an n-type semiconductor to the metal are as follows:

- (a) transport of electrons from the conduction band of the semiconductor over the top of the barrier into the metal,
- (b) injection of holes into the neutral region of the semiconductor,
- (c) recombination of electrons and holes in the depletion region of the semiconductor, and
- (d) quantum mechanical tunnelling through the barrier.

The major contribution to the current conduction is provided by the first mechanism, and in fact the other processes, i.e. (b), (c) and (d) are the causes of the non-ideal behaviour of some diodes.

For emission over the barrier into the metal, an electron must be transported first through the depletion region of the semiconductor. The conduction in this region takes place by the drift and diffusion mechanisms. That is why the first theory of conduction in Schottky diodes was the diffusion theory proposed by Wagner (1931) and Schottky and Mott (1939). Later in 1942 the thermionic emission theory was proposed by Bethe. According to this theory, the current flowing in a metal-semiconductor barrier is determined by the emission of electrons from the semiconductor over the top of the barrier into the metal. The difference between the two theories can be more clearly understood in terms of the quasi-Fermi level for electrons (Rhoderick, 1972). The quasi-Fermi level is a hypothetical energy level which gives the correct concentration of the electrons, if inserted into the Fermi-Dirac distribution function, even though the system is not in true thermal equilibrium. Far from the junction the quasi-Fermi level must coincide with the Fermi levels in the metal and in the semiconductor respectively.

The assumption made in the diffusion theory is that the quasi-Fermi level coincides with the Fermi level in the metal at the junction. This means that the conduction electrons in the semiconductor adjacent to the metal are in equilibrium with those in the metal, i.e. that the concentration of electrons at the top of the barrier does not change when a bias is applied. The assumption that the quasi-Fermi level coincides with the Fermi-level in the metal at the junction is in sharp contrast with the assumption made in the case of p-n junctions that the quasi-Fermi level remains flat through the junction. This contradiction was resolved by Gossick (1963) by considering the fact that the electrons which cross over the barrier from the semiconductor to the metal are not in thermal equilibrium with the electrons in the metal, i.e. that they have a quasi-Fermi level which differs from the Fermi level of the conduction electrons in the metal. Because of electron-electron collisions the electrons emitted from the semiconductor lose energy and their quasi-Fermi level falls to that of electrons in the metal. At the other extreme, the assumption is that the quasi-Fermi level remains constant throughout the barrier region as in a p-n junction. This is the approximation made in the thermionic emission theory. It is equivalent to saying that the concentration of electrons at the top of the barrier changes with a factor of  $e^{qV/kT}$  if a forward bias voltage  $V$  is applied. According to the thermionic emission theory, the current-voltage dependence can be expressed by:

$$J = J_s \left( e^{\frac{qV}{kT}} - 1 \right) \quad (2.48)$$

Where  $J_s$  is the saturation current density,

$$J_s = A^* T^2 \exp \left( \frac{-\phi_{Bn}}{kT} \right) \quad (2.49)$$

Here  $A^* = \frac{4 n m^* q K^2}{h^3} = 120 \frac{m^*}{m_o} \text{ amp/cm}^2/\text{oK}^2$  is the effective Richardson constant corresponding to the electron effective mass in the semiconductor.

For the diffusion theory, on the other hand, the j-V relation is given (Spence, 1958) by:

$$J = q N_c \mu \epsilon_{\max} \exp\left(-\frac{q \phi_{Bn}}{kT}\right) \left[ \exp \frac{qV}{kT} - 1 \right] \quad (2.50)$$

where  $\epsilon_{\max}$  is the maximum electric field strength in the barrier and  $\mu$  is the electron mobility. The difference between equation (2.50) and (2.48) arises from the fact that the term before the bracket in equation (2.50) is voltage dependent, while  $J_s$ , neglecting the dependence of Schottky barrier lowering on voltage, is considered to be voltage dependent.

Crowell and Sze (1966) have combined the thermionic and diffusion theories. In their approach Crowell and Sze assume that the potential energy developed in the metal-semiconductor junction is due to the superimposed effects of the electric field associated with the ionized donors and the attractive image force experienced by an electron when it approaches the metal. According to Crowell and Sze, in the region of maximum potential barrier and the interface, the distribution of the carriers cannot be expressed by the quasi-Fermi level for electrons, because the potential energy changes rapidly in distances comparable to the electron mean free path, (i.e. the current in this region is not determined by the collision process which is associated with diffusion). Considering the metal to act as a sink for the electrons the current can be described in terms of a recombination velocity  $v_R$  at the potential energy maximum:

$$J = q (n_m - n_o) v_R \quad (2.51)$$

where,  $q n_m v_R$  represents the current from the semiconductor to the metal and the term  $q n_o v_R$  gives the current from the metal to the semiconductor, i.e. the current in the equilibrium situation. The J-V relation in this case is given by:

$$J = \frac{q N_c v_R}{(1 + v_R/v_D)} \exp\left(-\frac{\phi_{Bn}}{kT}\right) \left[ \exp \frac{qV}{kT} - 1 \right] \quad (2.52)$$

which takes diffusion and drift in the depletion region into account. The term  $v_D$  is an effective diffusion velocity associated with the transport of electrons from the edge of the depletion region to the top of the barrier, and is expressed by:

$$v_D = \left\{ \int_{x_m}^W \frac{q}{\mu kT} \exp \left[ - (\phi_{Bn} - E_c)/kT \right] dx \right\}^{-1} \quad (2.53)$$

where  $E_c$  is the energy of the bottom of the conduction band,  $\mu$  is the electron mobility,  $x_m$  is the position of the maximum of the potential barrier and  $w$  is the depletion width. If  $v_D \ll v_R$ , the pre-exponential term in equation (2.52) reduces to  $q N_c v_D$  and the diffusion theory applies. If, however,  $v_D \gg v_R$  the thermionic emission process is dominant. The condition that  $v_D \gg v_R$  is equivalent to:

$$\begin{aligned} \mu \epsilon_{\max} &\gg \frac{\bar{v}}{4} , \\ q \epsilon_{\max} &\gg \frac{q \bar{v}}{4 \mu} , \quad \mu = \frac{q \tau}{m^*} , \\ q \epsilon_{\max} &\gg \frac{m^* \bar{v}}{4} , \quad \lambda = \bar{v} \times \tau , \quad \bar{v} = \left( \frac{8 kT}{\pi m^*} \right)^{1/2} \\ \lambda q \epsilon_{\max} &\gg \frac{m^* \bar{v}^2}{4} \quad \text{or} \quad \lambda q \epsilon_{\max} \gg \frac{2kT}{\pi} \end{aligned} \quad (2.54)$$

where  $\lambda$  is the mean free path of the electrons in the semiconductor and  $\tau$  their mean free time. This condition for the validity of the thermionic

emission theory is equivalent to Bethe's criterion that the mean free path must exceed the distance in which the barrier decreases by an amount  $kT$ . A check on the flatness of the electron quasi-Fermi level throughout the junction provides yet another way of determining whether the thermionic emission theory is applicable to a particular device or not. (Rhoderick, 1972). Using the data published by Goodman (1964) on Au-CdS Schottky diodes, Rhoderick has tested the applicability of thermionic emission theory using Bethe's criterion as well as the above mentioned technique. On the basis of Bethe's criterion the diodes do not satisfy the thermionic emission theory, whereas the flatness of the quasi-Fermi level confirms the validity of this theory. Rhoderick has then concluded that criterion (2.54) is unduly severe as a condition for the validity of thermionic emission theory.

## 2.8 Measurement of Schottky barrier height

Different techniques involving the measurement of C-V and I-V characteristics, and finding photoelectric thresholds have been used for determining the barrier height of a metal-semiconductor diode. Among these methods, the photoelectric measurement is the most accurate and most direct (Crowell et al, 1962). The reason is that for the photoelectric measurement the device need not be biased. This leaves the barrier free from the effect of an external field.

When monochromatic light of energy  $h\nu$  falls on the surface of the metal in a metal-semiconductor junction, if  $h\nu > q\phi_{Bn}$  the photon energy can excite electrons to cross over the barrier and if the metal layer is thin enough and  $h\nu > E_g$ , it can generate electron and hole pairs also. With back illumination, i.e. when the semiconductor side of the junction is illuminated, the photoelectric emission occurs when

$h\nu > q\phi_{Bn}$ . Photons with energy  $h\nu > E_g$  are strongly absorbed at the back semiconductor surface, and the photogenerated electron-hole pairs have a low probability of reaching the metal-semiconductor interface.

According to the theory developed by Fowler (1931), the photocurrent per absorbed photon can be expressed by:

$$R \sim \frac{T^2}{\sqrt{E_s - h\nu}} \left[ \frac{\chi^2}{2} + \frac{\pi^2}{6} - \left( e^{-\chi} - \frac{e^{-2\chi}}{4} + \frac{e^{-3\chi}}{9} - \dots \right) \right] \text{ for } \chi > 0 \quad (2.55)$$

where  $h\nu_0$  is the barrier height ( $q\phi_{Bn}$ ),  $E_s$  the sum of  $h\nu_0$  and the Fermi energy measured from the bottom of the metal conduction band, and

$\chi \equiv \frac{(h\nu - h\nu_0)}{kT}$ . When  $E_s \gg h\nu$  and  $\chi > 3$  equation (2.55) reduces to:

$$R \sim (h\nu - h\nu_0)^2$$

or

$$\sqrt{R} \sim (h\nu - h\nu_0) \quad (2.56)$$

i.e. the square root of photoresponse is linearly dependent on photon energy. The intercept of the line with the energy axis gives directly the barrier height.

## 2.9 Voltage-Capacitance measurements

Since the capacitance associated with the depletion region of the metal-semiconductor contact is voltage dependent, it is possible to obtain the barrier height as well as the charge density in the depletion region from the C-V measurement under certain conditions.

If the effect of any interfacial layer is not taken into account the actual circuit of the contact may be represented by a fixed resistance  $r$  (the semiconductor bulk resistance) in series with the parallel combination of a voltage dependent capacitance  $C$  and a voltage dependent

conductance  $G$ . Most bridges used for such measurements characterize the circuit in terms of only two parameters,  $C'$  and  $G'$ . Obviously  $C'$  and  $G'$  are not the actual values of the capacitance and the conductance of the barrier. It can be shown (Goodman 1963) that under the conditions that  $rG \ll 1$  and  $\omega^2 r^2 C^2 \ll 1$ , the measured values of capacitance and conductance give the actual values of these parameters ( $\omega$  is the frequency of a.c. component of the bias). Both  $C$  and  $G$  are frequency dependent and to exclude the effects of trapped carriers it is necessary for the a.c. component of the bias to have a relatively high frequency. In certain cases when  $\omega^2 r^2 C^2$  is relatively small and  $rG \approx 0$  and equivalent to the relation (2.47) can be written as:

$$\left(\frac{1}{C'}\right)^2 = 2 (V_{bi} - V)/q \epsilon_s Nd + 2\omega^2 r^2 \quad (2.57)$$

The slope of the plot of  $\left(\frac{1}{C'}\right)^2$  versus  $V$  will not differ from that of  $\left(\frac{1}{C}\right)^2$ , but the intercept on the voltage axis will. The actual diffusion potential  $V_{bi}$  can be obtained from  $V'_{bi}$  the intercept of  $\left(\frac{1}{C'}\right)^2$  versus  $V$ , since

$$V_{bi} = V'_{bi} - 2 r^2 \omega^2 \left[ d\left(\frac{1}{C'}\right)^2 / dV \right]^{-1} \quad (2.58)$$

Crowell et al (1965) have shown that an effective interfacial layer of non-zero thickness must exist between the metal and the semiconductor even when both are in intimate atomic contact. The thickness of this interfacial layer affects the measurement of the barrier height from C-V plots. (Cowley, 1966). According to the model proposed by Cowley for the metal-interface layer - semiconductor contact without surface states the magnitude of the intercept  $V_o$  of the  $\frac{1}{C^2}$  versus  $V$  line is given by:

$$V_o = V_{bi} - \frac{kT}{q} + \frac{V_1}{4} + (V_1 V_{bi})^{1/2} \quad (2.59)$$

where  $V_{bi}$  is the diffusion potential, and  $V_1 = \frac{2 q \epsilon_s N_d \lambda_i^2}{\epsilon_i^2}$ ,  $\lambda_i$  is the thickness of the interfacial layer and  $\epsilon_i$  is the permittivity of the interfacial layer.

To consider the effect of surface states as well as the interfacial layer on the capacitance-voltage relationship, use is made of the model developed by Crowell and Roberts, 1969. Consider an n-type semiconductor with a donor density of  $N_d$  and a surface density per unit area per unit energy of  $n_{ss}$ . The thickness of the interfacial layer is  $\lambda_i$  and its permittivity  $\epsilon_i$ . The charge due to ionized donors in the depletion region produces an electric field  $E$  at the surface of the semiconductor. A change in the applied bias or in the doping concentration of the semiconductor will cause a change in the amount of charge in the depletion region. This in turn causes a change of charge  $\epsilon \Delta E$  in the surface states and in the metal ,

$$\epsilon \Delta E = \Delta\sigma_{\text{surface states}} + \Delta\sigma_{\text{metal surfaces}} \quad (2.60)$$

where  $\Delta\sigma$ , with appropriate subscripts, is the change in the surface charge density.

Since the semiconductor bandgap and the electron affinity  $\chi$  are independent of electric field, the change will appear in the field in the interface and density of filled surface states which gives rise to a change in the barrier height by an amount  $\Delta\phi_{Bn}$ . Equation (2.60) then becomes

$$\epsilon \Delta E = -q n_{ss} \Delta\phi_{Bn} - \left(\frac{\epsilon_i}{\lambda_i}\right) \Delta\phi_{Bn} \quad (2.61)$$

or

$$\frac{d\phi_{Bn}(E)}{dE} = -\epsilon \left[ q n_{ss} + \left(\frac{\epsilon_i}{\lambda_i}\right) \right]^{-1} \quad (2.61)$$

It is assumed here that the interfacial layer is sufficiently transparent to the electron flow that the occupation of surface states is determined by the Fermi level in the metal. It is worth noting that when  $n_{ss}$  is large or  $\lambda_i$  is small, the barrier height is no longer dependent on  $E$ .

The capacitance-voltage relationship is affected by the quantity  $\frac{d\phi_{Bn}}{dE}$  which is related to the surface states density and the thickness of the interfacial layer. Applying Poisson's equation to the semiconductor depletion region with a uniform doping concentration  $N_d$ , we have:

$$E^2 = \left( \frac{2qN_d}{\epsilon_s} \right) (\phi_{Bn} - U - V) \quad (2.62)$$

where  $U \equiv \frac{kT}{q} \left[ 1 + \ln \left( \frac{N_c}{N_d} \right) \right]$  and  $N_c$  is the effective density of states in the conduction band of the semiconductor. The quantity  $(qU - kT) \equiv q\phi_n$  is the difference in energy between the conduction band and the Fermi level in the semiconductor bulk. The barrier capacitance per unit area  $c$ , can be written as

$$c = \frac{d\sigma}{dV} = \epsilon_s \left( \frac{dE}{dV} \right) \quad (2.63)$$

where  $\sigma$  is the stored charge per unit area in the depletion region of the semiconductor.

Differentiation of equation (2.62) with respect to  $E$  gives:

$$\frac{dV}{dE} = - \left( \frac{\epsilon_s E}{q N_d} \right) + \frac{d\phi_{Bn}}{dE} \quad (2.64)$$

Then from equations (2.62), (2.63) and (2.64),

$$\frac{1}{c^2} = \left( \frac{2}{\epsilon_s q N_d} \right) \left[ \phi_{Bn} - V - U - E \left( \frac{d\phi_{Bn}}{dE} \right) + \left( \frac{q N_d}{2 \epsilon_s} \right) \left( \frac{d\phi_{Bn}}{dE} \right)^2 \right] \quad (2.65)$$

From equation (2.65),  $\frac{d\left(\frac{1}{C^2}\right)}{dV}$  gives the doping concentration if :

$$\left[ \left( \frac{q N_d}{\epsilon_s} \right) \left( \frac{d\phi_{Bn}}{dE} \right) - E \right] \left( \frac{d^2\phi_{Bn}}{dE^2} \right) \left( \frac{dE}{dV} \right) \ll 1$$

The voltage intercept  $V_i$  of the plot  $\frac{1}{C^2}$  versus  $V$  gives the apparent barrier height  $\phi_a$ ,

$$\phi_a \equiv V_i + U = \phi_{Bn} - E \left\{ \frac{d\phi_{Bn}}{dE} \right\} + \left\{ \frac{q N_d}{2 \epsilon_s} \right\} \left\{ \frac{d\phi_{Bn}}{dE} \right\}^2 \quad (2.66)$$

Since the term  $\frac{d\phi_{Bn}}{dE}$  is always negative, the true barrier height is always less than the measured barrier height.

From equations (2.62) and (2.66) we get :

$$\frac{d\phi_{Bn}}{dE} = \left\{ \frac{\phi_{Bn} - V - U}{q N_d / 2 \epsilon_s} \right\}^{\frac{1}{2}} \left[ 1 - \left\{ \frac{\phi_a - V - U}{\phi_{Bn} - V - U} \right\}^{\frac{1}{2}} \right] \quad (2.67)$$

This gives  $\frac{d\phi_{Bn}}{dE}$  in terms of  $\phi_a$ , the apparent barrier height,  $\phi_{Bn}$  the true barrier height and  $N_d$ , the semiconductor donor concentration.

Since  $\left. \frac{d\phi_{Bn}}{dN_d} \right|_V = \left\{ \frac{d\phi_{Bn}}{dE} \right\} \left\{ \frac{dE}{dN_d} \right\} \left|_V \right. \left\{ \frac{dU}{dN_d} \right\}$ ,

$\left. \frac{d\phi_{Bn}}{dN_d} \right|_V$  may be calculated by obtaining  $\left. \frac{dE}{dU} \right|_V$  from equation (2.62),  $\frac{d\phi_{Bn}}{dE}$  from equation (2.67) and the fact that  $\frac{dU}{dN_d} = -kT/qN_d$  then,

$$\left. \frac{d\phi_{Bn}}{dN_d} \right|_V = -\frac{kT}{qN_d} \left[ 1 + \frac{q}{kT} \left\{ \phi_{Bn} - V - U \right\} \right] \left[ 1 - \left\{ \frac{\phi_{Bn} - V - U}{\phi_a - V - U} \right\}^{\frac{1}{2}} \right] \quad (2.68)$$

Thus given  $\phi_{Bn}$  at one value of  $N_d$  and a measurement of  $\phi_a$  as a function

of  $N_d$ , we can obtain  $\phi_{Bn}$  as a function of  $N_d$  by integration of equation (2.68).

It is possible to calculate  $\frac{d\phi_{Bn}}{dE}$  from (2.67) by inserting the true value of the barrier height determined from phototreshold measurements, and the apparent barrier height from the C-V plot. Knowing the density of surface states equation (2.61) then gives the thickness of the interfacial layer.

### 2.10 Current-Voltage Measurements

In the theory developed by Crowell and Sze (1966) for carrier transport in the Schottky barrier, these authors have also taken into account the effects of optical phonon scattering in the region between the top of the barrier and the metal interface, and the quantum mechanical reflection of electrons with sufficient energy to surmount the barrier. Their combined effect is to replace the Richardson constant  $\bar{A}^*$  in equation (2.49) by :

$$A^{**} = f_p f_Q \bar{A}^* / \left\{ 1 + f_p f_Q \frac{v_R}{v_D} \right\}, \quad (2.69)$$

where  $f_p$  is the probability of an electron reaching the metal without being scattered back, and  $f_Q$  is the average transition coefficient.  $f_p$  and  $f_Q$  depend on the maximum electric field in the barrier, on the temperature, and on the effective mass. The field at which  $f_Q$  starts to rise rapidly marks the transition between thermionic and thermionic-field (T.F.) emission, since at this point tunnelling becomes the dominant mechanism.

Replacing  $\bar{A}^*$  in equation (2.49) by  $A^{**}$ , gives :

$$J = A^{**} T^2 \exp \left\{ -\frac{q\phi_{Bn}}{kT} \right\} \left[ \exp \left\{ \frac{qV}{kT} \right\} - 1 \right] \quad (2.70)$$

For forward biases  $V > \frac{3kT}{q}$ , equation (2.70) can be rewritten as :

$$J = A^{**} T^2 \exp \left\{ - \frac{q \phi_{Bo}}{kT} \right\} \exp \left[ \frac{q(\Delta\phi + V)}{kT} \right] \quad (2.71)$$

where  $\phi_{Bo} = \phi_{Bn} + \Delta\phi$ , is the barrier height when the Schottky barrier lowering  $\Delta\phi$  is not taken into account. Since both  $A^{**}$  and  $\Delta\phi$  are voltage dependent which leads to departures from ideal behaviour even in practically perfect diodes, the experimental forward characteristic is written in the following form to include this non-ideal behaviour :

$$J = J_s \left[ \exp \left\{ \frac{qV}{nkT} \right\} \right] \quad \text{for } V > \frac{3kT}{q}$$

where,

$$n = \frac{q}{kT} \left[ \frac{d(\ln J)}{dV} \right]^{-1} \\ = \left[ 1 + \frac{\partial \Delta\phi}{\partial V} + \frac{kT}{q} \frac{\partial \{ \ln A^{**} \}}{\partial V} \right]^{-1} \quad (2.72)$$

which means that  $n$  is not independent of  $V$ .

In equation (2.71), if  $V$  tends to zero,  $J$  approaches the saturation current density  $J_s$ , and the barrier height can be obtained from the following equation :

$$\phi_{Bn} = \frac{kT}{q} \ln \left\{ \frac{A^{**} T^2}{J_s} \right\} \quad (2.73)$$

when  $f_p f_Q = 1$  and  $V_D \gg V_R$ , it can be concluded from equation (2.69) that  $A^{**} = A^*$  and then thermionic emission is the dominant mechanism.

### 2.11 Metal-Insulator-Semiconductor (MIS) Diodes

The (MIS) diode which is characterized by having an insulating layer between the metal and the semiconductor, is a most useful device in the study of semiconductor surfaces. Since the stability of all semiconductor devices is closely related to their surface conditions, an understanding of the surface physics with the help of MIS diodes is of great importance to device operations. A comprehensive treatment of the theory of semiconductor surfaces and the techniques used to measure their properties can be found in the books on 'Semiconductor Surfaces' by Many et al (1965) and 'Surface Physics of Phosphors and Semiconductors' edited by Scott and Reed (1975). What we consider in this section is a brief account of the conductance mechanism which is associated with an energy loss and occurs in the semiconductor-insulator interface of an MIS diode. When the equilibrium between the surface states and the semiconductor is disturbed by the application of a small a.c. signal, a conductance is observed due to the capture and emission of the majority carriers by the interface states. The measurement of this conductance leads to the evaluation of the density of these states and their capacitance. By considering the MIS capacitance in a depletion region, Fig. (3), i.e. when the semiconductor (n-type) is reverse biased, it is possible to describe phenomenologically the conductance mechanism associated with the interface states. (Nicollian & Goetzburger, 1967).

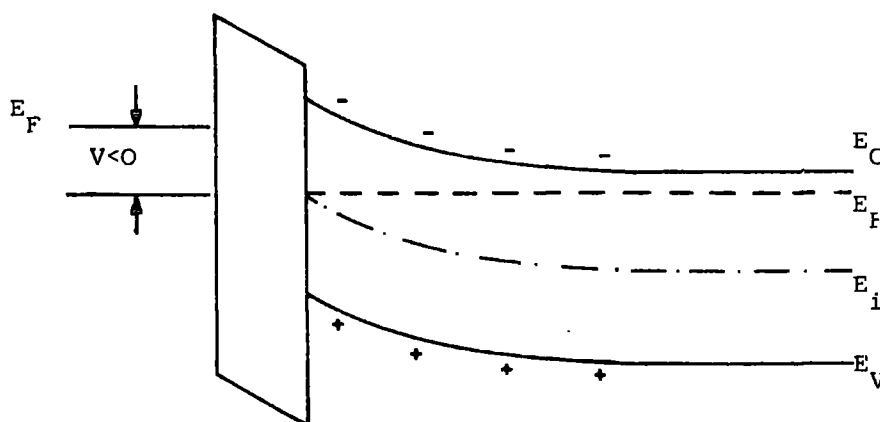


Fig. 2.3 The energy band diagram of an MIS diode in the depletion region.

The first half of the cycle of the applied a.c. signal moves the conduction band towards the Fermi-level. This increases the average energy of the free electrons in the semiconductor. Since the interface states do not respond immediately to this change of energy, their energy is lower than that of the electrons in the semiconductor. Therefore, the electrons in the semiconductor are captured by the surface states at a lower average energy. This results in an energy loss. On the other half of the cycle, the signal moves the valence band towards the Fermi level. Electrons in the filled surface states now will be at a higher energy than the average energy of the electrons in the semiconductor. The emission of the electrons from the surface states to the semiconductor takes place with an energy loss again. Thus there will be an energy loss on both halves of the cycle which is supplied by the signal source.

The interface states disturbed from the equilibrium will reach equilibrium with the semiconductor exponentially with a time constant  $\tau$ . Since they are capable of storing charge, there will be a capacitance  $C_s$  associated with them which is proportional to their density. The conductance related to the process of capture and emission of electrons by the interface states is  $G_s = \frac{C_s}{\tau}$ , where both  $\tau$  and  $C_s$  can be extracted directly from a measurement of equivalent parallel conductance.

### 2.12 Equivalent Circuit of MIS Capacitor

By considering the charge in each component of the MIS diode and its change due to a proper bias voltage on which has been superimposed a small a.c. signal, it is possible to work out the equivalent circuit of the MIS capacitor.

The total charge density  $Q_T$  at a given bias can be written as :

$$Q_T = Q_{sc} + Q_s + Q_f, \quad (2.74)$$

where  $Q_{sc}$  is the semiconductor space charge density,  $Q_s$ , the interface charge density and  $Q_f$  is the fixed charge density in the insulator. By differentiating both sides of the equation (2.74) with respect to time, one obtains :

$$i_T(t) = i_{sc}(t) + i_s(t), \quad (2.75)$$

where,  $i_{sc}(t)$  and  $i_s(t)$  are the a.c. current densities which charge the semiconductor space-charge layer and the interface states respectively.

Since the semiconductor band bending is dependent on time  $t$ , one can write :

$$i_{sc}(t) = \left\{ \frac{dQ_{sc}}{d\psi_s} \right\} \left\{ \frac{d\psi_s}{dt} \right\} \quad (2.76)$$

where  $\psi_s(t) = \psi_{s0} + \delta\psi_s$  is the semiconductor band bending which consists of two terms ;  $\psi_{s0}$  the band bending established by the bias, and  $\delta\psi_s = a \exp(j\omega t)$  which is due to the a.c. signal. From this,  $\frac{d\psi_s}{dt} = j\omega\delta\psi_s$ .

Since  $\frac{dQ_{sc}}{d\psi_s} = C_D$  the depletion capacitance per  $\text{cm}^2$ , (2.76)

becomes :

$$i_{sc}(t) = j\omega C_D \delta\psi_s \quad (2.77)$$

Assuming a single-level of interface states, it can be shown that :

$$i_s(t) = Y_s \delta\psi_s \quad (2.78)$$

where  $Y_s$  is the admittance of a single level interface state (see Nicollian & Goetzberger 1967).

Substituting (2.78) and (2.77) into (2.75), we have :

$$i_T(t) = \left\{ j\omega C_D + Y_S \right\} \delta\psi_s \quad (2.79)$$

Equation (2.79) shows that  $C_D$  appears in parallel with the series RC network of the interface states.

It can be easily shown that the insulator (oxide) capacitance appears in series with the parallel combination of the depletion layer capacitance and the RC network of the interface states. This is shown in Figure 2.4.

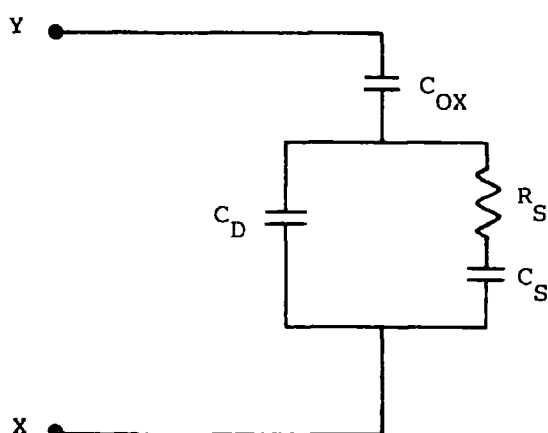


Fig. 2.4 The equivalent circuit of MIS capacitor.

Comparing the admittance of a series RC combination,

$$Y = \frac{1}{R_S - j \frac{1}{C_S \omega}} = \frac{j C_S \omega}{1 + R_S^2 C_S^2 \omega^2} + \frac{R_S C_S^2 \omega^2}{1 + R_S^2 C_S^2 \omega^2} \quad \text{where, } R_S C_S = \tau$$

with the admittance of the single-level interface states worked out on the basis of the Schottky and Reed theory (1952), by Nicollian and Goetzberger (1967), one obtains the equivalent parallel capacitance as :

$$C = \frac{C_S}{1 + \omega^2 \tau^2} \quad (2.80)$$

and the equivalent parallel conductance as :

$$G_P = \frac{C_S \omega^2 \tau}{1 + \omega^2 \tau^2} \quad (2.81)$$

since  $C_D$  is in parallel with RC network, then

$$C_P = C_D + \frac{C_S}{1 + \omega^2 \tau^2} \quad (2.82)$$

From (2.81)  $\frac{G_P}{\omega}$  is given by :

$$\frac{G_P}{\omega} = \frac{C_S \omega \tau}{1 + \omega^2 \tau^2} \quad (2.83)$$

$\frac{G_P}{\omega}$  goes through a maximum when  $\omega \tau = 1$ ; the value of  $\frac{G_P}{\omega}$  at the maximum is  $C_S/2$ . Thus, the equivalent parallel conductance corrected for  $C_{ox}$  gives  $C_S$  and  $\tau$  directly from the measured conductance. Once  $C_S$  is known, the surface state density is obtained by using the relation  $N_{SS} = \frac{C_S}{qA}$  where  $A$  is the area of the metal contact.

## CHAPTER THREE

### CRYSTAL GROWTH

#### 3.1 Vapour Phase Growth

Although the melting points of the elemental components of II-V compounds are relatively low, the compounds usually have high melting points. For example, while Cd melts at  $321^{\circ}\text{C}$  and S at  $119^{\circ}\text{C}$ , the compound (CdS) has a melting point of  $1475^{\circ}\text{C}$  at a minimum pressure of 3.8 atm. This places CdS outside the safe limits for sealed unsupported quartz containers. It is, therefore, of little surprise to find more of the reported work in the area of vapour growth. There are three ways in which crystals can be grown from the vapour phase. Namely :

- 1) By the sublimation of the substance itself.
- 2) By reaction in the vapour phase and,
- 3) By chemical transport.

Since CdS is sufficiently volatile and can be evaporated without decomposing, its crystals can be grown by sublimation. In practice various experimental conditions have been employed namely open systems using an inert carrier gas, and closed systems (often sealed glass tubes) either evacuated or containing gas.

The simplest method of sublimation growth (Reynolds & Czyzack, 1950) relies on the interchange of material between charge and vapour to produce crystal growth on the charge itself. The crystals produced by this method are usually small. The method suffers also from the severe disadvantages that any impurity in the charge is likely to be present in the crystals. This difficulty can be overcome by maintaining a proper temperature gradient along the growth ampoule so that the material is transported from the hot to the cooler end of the tube. By moving the growth tube relative to the

furnace, Piper and Polich (1961) were able to produce single crystal boules of considerable size. A modified version of the Piper and Polich method was developed by Clark and Woods (1966) in which the growth tube was positioned inside a long mullite tube containing argon at a pressure slightly above atmospheric. The growth ampoule could communicate with the argon filled outer jacket via an orifice to allow any non-stoichiometric excess of either element of the charge to diffuse out from the ampoule before substantial growth began. This was necessary because the evaporation rate of cadmium sulphide can be reduced by two orders of magnitude by slight deviation from the stoichiometry (Somorjai & Jepsen, 1964). Investigation of the properties of the boules grown by this method indicated that the boules usually had non-uniform resistance. In addition, the radial temperature gradient which resulted from the practical difficulty of aligning the growth tube along the axis of the furnace, sometimes led to the poly-crystallinity of the resulting boule. In order to control the properties of a crystal during growth and improve its homogeneity, it was found desirable (Clark & Woods, 1966) to use a completely sealed system. Work with sealed tubes also allowed a vertical pulling arrangement to be adopted, which assisted the elimination of the radial temperature gradient.

To allow excess cadmium or sulphur to diffuse away from the growth region, a more convenient arrangement was adopted by Demeis & Fischer (1967) in which the sealed growth ampoule was provided with a long tail extending to a lower temperature.

Although this method lends itself to growth of reproducible crystals, the conditions are not under complete control in the sense that the partial pressure of the elements during growth are determined by the experimental arrangements and the composition of the starting material.

To overcome this difficulty, Clark & Woods (1968) provided growth

ampoules with a tail which contained a reservoir of cadmium or sulphur which could be held at a fixed temperature throughout the growth cycle. Thus rather than allowing the system to establish the partial pressure conditions determined largely by the nature of the charge, a known partial pressure could be obtained.

Another advantage of providing the growth ampoule with the tail is that the partial pressure produced from the elemental constituent of the charge in the tail can limit the transfer of the cadmium sulphide from the charge to the crystal growing region. This is because in growth ampoules without an inert gas, the whole charge is transferred from one end of the capsule to the other in a few hours and a very polycrystalline lump of material results. (Fochs, et al 1968).

In the present work, boules of CdS were grown using the method developed by Clark and Woods (1968). The purity of the starting material is considered to be the most important factor involved in establishing a reproducible process for growing CdS boule crystals from the vapour phase. To remove the volatile impurities, the charge used in growth ampoules was taken from the CdS rods and platelets already grown by the flow run technique (Clark and Woods, 1966). The starting material for the growth of the flow run crystals was usually B.D.H. optran grade lumps.

In the following table some of the parameters of the various growth runs and the physical appearances of the crystals produced for the present work have been summarized.

To prepare a proper Schottky diode, the sample should contain a suitable donor density ( $10^{15} - 10^{16}$ ) and therefore a proper resistivity ( $3 - 30 \Omega \text{ cm}$ ). Since it was not possible to obtain a precise control of the electrical properties of the grown crystals, it was found necessary to heat the sample in either liquid cadmium or cadmium vapour in order to reduce its resistivity. To increase the resistivity of the sample, on the other

Boule No.	(Cd ) Charge Quantity	Dopant Quantity	Excess in Tail & Quantity	Dopant in Tail	Temperature of the upper Furnace (°C)	Temperature of the Lower furnace	Remarks about the boules
611	20 g	2% Cd Cl <sub>2</sub>	0.4 g Cd	-	1150	600	4½ Cm, red, single crystal
613	20 g	-	0.4 g Cd	-	1150	550	4½ Cm, light brown
619	20 g	4% Cd Cl <sub>2</sub>	0.4 g S	Cu (100ppm)	1150	300	1.8 Cm, black
623	20 g	Cu (50 ppm)	0.2 g Cd	-	1150	600	3.5 Cm, dark brown, with cracks
626	20 g	2% Cd Cl <sub>2</sub>	0.2 g S	-	1150	300	3 Cm, dark brown, cracked, highly stressed
630	20 g	-	0.2 g Cd	-	1150	600	4.5 Cm, light brown cracked due to fast temperature drop
631	20 g	-	0.2 g S	-	1150	300	3.3 Cm, Transparent, orange.

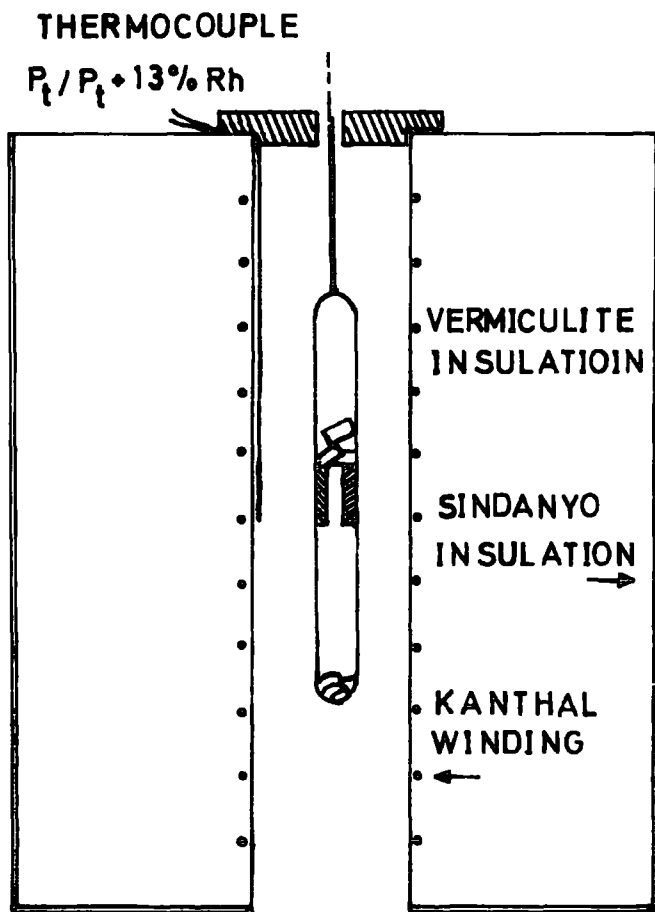
hand, a treatment in sulphur vapour was desirable.

### 3.2 Cadmium Treatment

Crystals of high resistivity such as the samples from the boule 623 which had resistivities of the order of  $10^9 \Omega \text{ cm}$ , were heated in molten cadmium at  $600^\circ \text{ C}$  for three days. As a result of this treatment, the resistivity of the samples dropped to about  $0.1 \Omega \text{ cm}$ . Heating the samples in cadmium for as little as 3 hours produced samples of similar low resistivity. Since the depletion width  $W$  of a Schottky diode is inversely proportional to the square root of the donor density  $N_d$ , the sample should contain a proper donor density to give a reasonable depletion width. A donor density of  $10^{16} \text{ cm}^{-3}$  gives a depletion width of about  $0.25 \mu\text{m}$ . To obtain a better control of the resistivity of the samples, therefore, it was decided to bake them in cadmium vapour. Treatments of this kind produced less extreme changes in the electrical conductivity of the samples, for example, baking the samples in cadmium vapour at  $600^\circ \text{ C}$  for 1.5 hours reduced the resistivity of a sample to  $\sim 10^6 \Omega \text{ cm}$  and even after an additional baking time of 20 hours the samples had a high resistivity of  $\sim 10^5 \Omega \text{ cm}$ . Cadmium has a vapour pressure of about 80 torr at  $600^\circ \text{ C}$ .

To carry out the heat treatment in molten cadmium, a silica tube of 6 mm inner diameter and 15 cm long was used, see Figure (1a). A slice from a capillary tube was sealed in the middle of the tube to facilitate the removal and separation of the crystals from the melt after treatment.

The tube was washed with distilled water after it had been cleaned in aqua regia for several hours. Finally it was heated at  $150^\circ \text{ C}$  for 2 hours in an oven. Crystal cubes with dimensions of  $2 \times 2 \times 2 \text{ cm}^{-3}$  were cut from the boule using a diamond wheel, polished with 1200 grade Carborundum and etched in conc. HCl to remove the surface damage caused by the mechanical polishing procedures. The CdS cubes were placed at one end of the silica



(a)

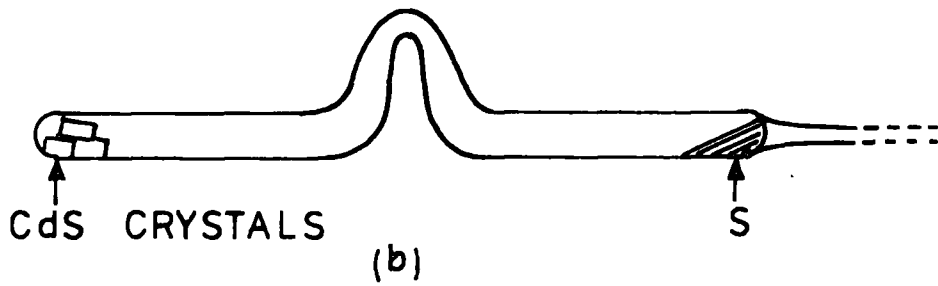


FIG. 3.1

tube. To avoid oxidation special care was taken in order not to heat up the crystals. To the other end of the tube 5N cadmium metal from Metal Research Ltd., was added. The tube was evacuated and flushed with high purity argon several times and sealed at a pressure of  $4 \times 10^{-6}$  torr. It was then suspended in a vertical furnace which was kept at a temperature of  $600^{\circ}$  C for different periods of time as mentioned earlier. On completion of the heating the tube was removed from the furnace and inverted. The molten cadmium ran to the bottom of the capsule while the crystals were held on the ledge formed by the slice of the capillary tube.

### 3.3 Sulphur Treatment

The resistivity of the CdS samples which had been doped with donor materials or grown in excess pressures of cadmium could be increased by annealing them in sulphur vapour. Highly photosensitive samples were prepared from flow run CdS : Cl crystals by heating them at  $700^{\circ}$  C in 2 atmospheres of sulphur vapour for a period of 2 hours. Since sulphur has a high vapour pressure, special care was taken not to work at higher temperatures. The quantity of the material used was also small. Sulphur boils at  $444^{\circ}$  C and has a vapour pressure of about two atmospheres at  $600^{\circ}$  C. Rods cut from boule 619 which had resistivities of the order of  $0.1 \Omega$  cm were baked in sulphur vapour. After measuring the temperature profile of the furnace, the proper length of the silica tube (14 cm) to maintain a temperature difference of  $100^{\circ}$  C between its ends was determined. To keep the crystals separate from the sulphur at the end of the heat treatment and the removal of the tube from the furnace a bend was made in the middle of the tube, as shown in Figure (1b). After the tube was sealed at one end it was washed and dried according to the schedule mentioned earlier. 0.5 gm of 6N grade sulphur was placed at one end of the tube and at the other end, rods cut from the boule 619 were added. The tube was then flushed three times with high purity argon

and sealed at a pressure of  $2 \times 10^{-6}$  torr. It was positioned in the furnace in such a way that the end of the tube containing the crystals was at the centre of the furnace at a temperature of  $700^{\circ}$  C. Thus the other end of the tube containing sulphur was at  $600^{\circ}$  C.

Although the resistivities of the crystals which were heated in this way for 4 hours increased by about two orders of magnitude, the result of the subsequent heating period of 24 hours showed that the change in the resistivity of the sample was relatively limited. In contrast to the CdS:Cl rods grown by the flow run technique which had a high photo-sensitivity (see Chapter 5), the boule samples had a very poor photoconductivity. This was probably because the higher donor density of the doped boules required a larger quantity of sulphur to be diffused in for compensation.

Another method which was adopted as an alternative to sulphur treatment to increase the sample resistivity was to heat the crystal in vacuum at  $1000^{\circ}$  C for varying periods of time from 1-72 hours. Inspection of the tube after the heat treatment confirmed the precipitation of black coloured particles which was indicative of the out-diffusion of cadmium from the crystals.

## CHAPTER FOUR

### EXPERIMENTAL TECHNIQUES AND SPECIMEN PREPARATION

#### 4.1 Photoconductivity Measurements

Measurements were carried out on two types of device :

- 1) Photoconductive samples which were supplied with ohmic contacts and,
- 2) Schottky barrier diodes with a blocking contact.

Several measurements such as thermally stimulated currents, spectral response of photoconductivity and variation of photocurrent with temperature etc, were carried out on the photoconductive samples. Prior to these measurements, the samples with dimensions of  $2 \times 2 \times 8 \text{ mm}^3$  were etched in conc. HCl for  $\frac{1}{2}$  - 1 minute to remove the surface damage caused by the mechanical polishing of the bars. Ohmic contacts to the samples were provided by pure indium metal wire which was obtained from Johnson Matthey Chemicals Ltd. The indium wire was either vacuum evaporated or pressed on to the chemically etched surface of a crystal. The evaporation was done at a pressure of  $10^{-5}$  torr, obtained with a mercury diffusion pumping system and a cold trap. To obtain an ohmic contact on Cds it was necessary to heat the sample for five minutes at about  $200\text{--}220^\circ \text{C}$  in an argon atmosphere. The temperature was raised to the required temperature rather slowly, i.e. within 15 minutes, and a similar period of time was used to cool the bar to room temperature.

##### 4.1.1 Mounting the crystals

As measurements were made over a temperature range of  $90^\circ \text{K}$  to  $400^\circ \text{K}$ , it was necessary to mount the crystals in a crystal. The crystals were first fixed on to thin microscopic slides (dimensions  $\frac{1}{8} \times \frac{1}{8}$  inch  $\times$  0.5 mm) by melting strips of indium onto the evaporated contacts and the slides.

Prior to this, the slides were cleaned by ultrasonic agitation in a detergent type solvent (quadralene) which was followed by degreasing in propan 2-ol (isopropyl alcohol) vapour. The slides provided electrical insulation from the cryostat block while still allowing reasonable thermal conduction. Thin copper leads were attached to the ends of the indium strips using a miniature soldering iron. Care was taken not to melt that part of the indium attached to the crystal. The slides were held on the cryostat block by small clips. A thin layer of silicone grease was introduced between the slide and the block to improve thermal conduction.

Great care was taken during both contacting and mounting the crystals to ensure that no contamination occurred, which would give rise to significant leakage currents. This was necessary because of the high resistances of the crystals.

The technique described above resulted in good electrical contacts which were also mechanically strong. After mounting a crystal a V-I curve was measured under illumination. A linear relationship was generally found and reversing the polarity of the applied voltage did not cause any change in the characteristic. Although not conclusive, these checks suggested that the contacts were ohmic.

#### 4.1.2 Temperature variation and measurement

The vacuum jacket of the cryostat was usually evacuated using a rotary pump which produced a pressure of approximately  $10^{-1}$  torr. Cooling of the cryostat block (made of copper) was achieved by the introduction of liquid nitrogen into an attached reservoir. To heat the crystal a wire coil, insulated by a silica tube, was inserted into a hole in the centre of the block. The heater was supplied from a 12 volt transformer and adjusted with a 'variac' control.

The temperature of a crystal was measured using a copper-constantan thermocouple in conjunction with a potentiometer (Tinsley Model 3387B).

The cold junction was immersed in liquid nitrogen. The cryostat was provided with a thermocouple which was indium soldered on to the microscopic slide close to the crystal during the mounting procedure. It was not possible to attach the thermocouple to the crystal because the resultant pick up of electrical noise interfered with the measurement of small currents.

All the electrical measurements (i.e. of thermally stimulated currents and photoconductivity) were made under d.c. conditions. The circuit used for the T.S.C. measurements is shown schematically in Fig.(4.1). The applied voltage was derived from a stabilised d.c. power supply, which could be varied between 0 and 100 volts.

Currents in the range  $10^{-12}$  -  $10^{-6}$  A were measured using a vibron electrometer (Model 33B). The vibron output was displayed on a chart recorder. This enabled currents to be continuously monitored against temperature, time or wavelength of illumination. The recorder input could be shorted out by means of a switch. This produced a blip on the trace so that the point corresponding to a particular temperature, for example, could be marked.

Non-microphonic co-axial cable and B.N.C. sockets and plugs were used for the external connections in order to minimise both noise and leakage currents.

#### 4.1.3 Thermally stimulated currents

A diagram of the cryostat used in the measurement of thermally stimulated currents is shown in Figure (4.2). Monochromatic illumination, was provided from a 240 watt (24 volt) quartz halogen lamp, via a Hilger and Watts D.330 grating monochromator. The cryostat was fixed to the exit slit of the monochromator by a brass tube. It was supported by a stand and could be moved up and down as well as from left to right and vice versa. This was necessary in order to align the crystal with the

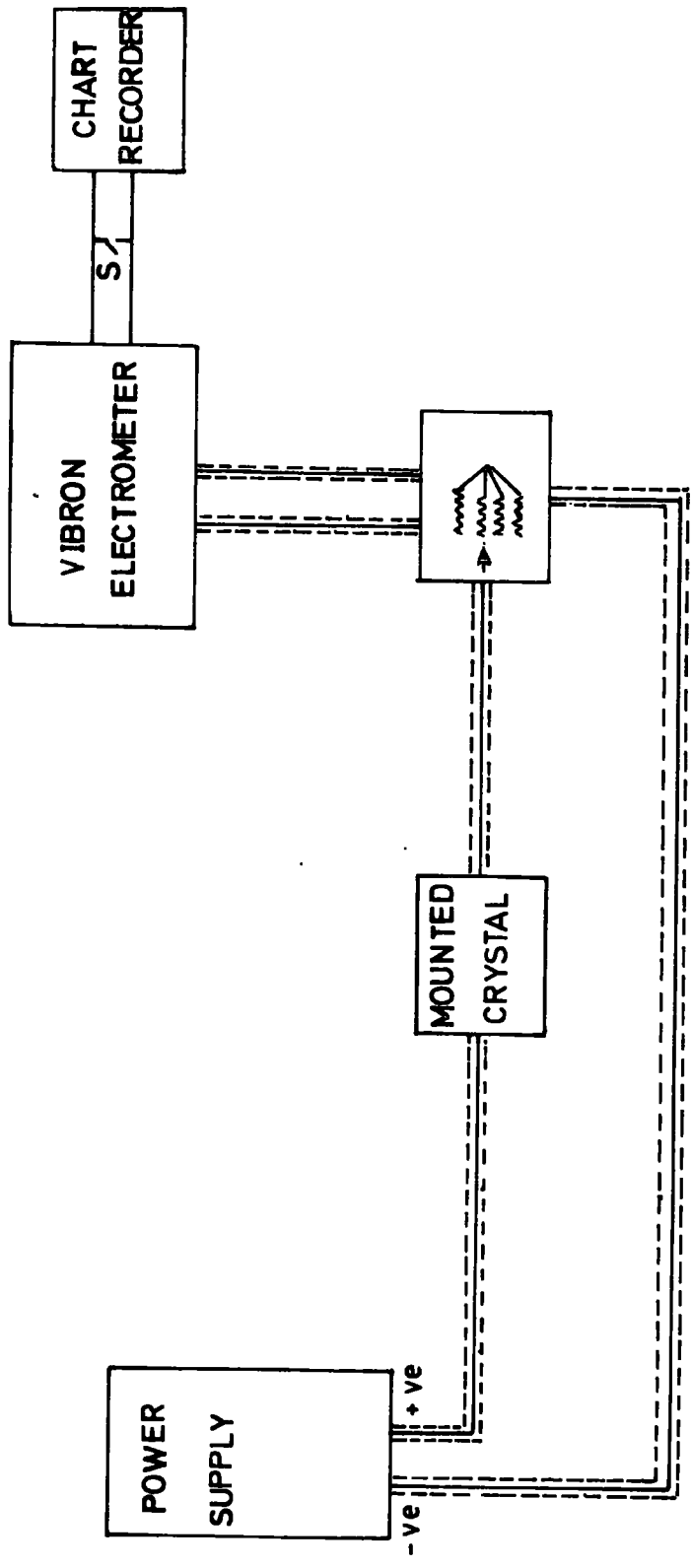


FIG. 4.1 CIRCUIT FOR T.S.C. MEASUREMENTS.

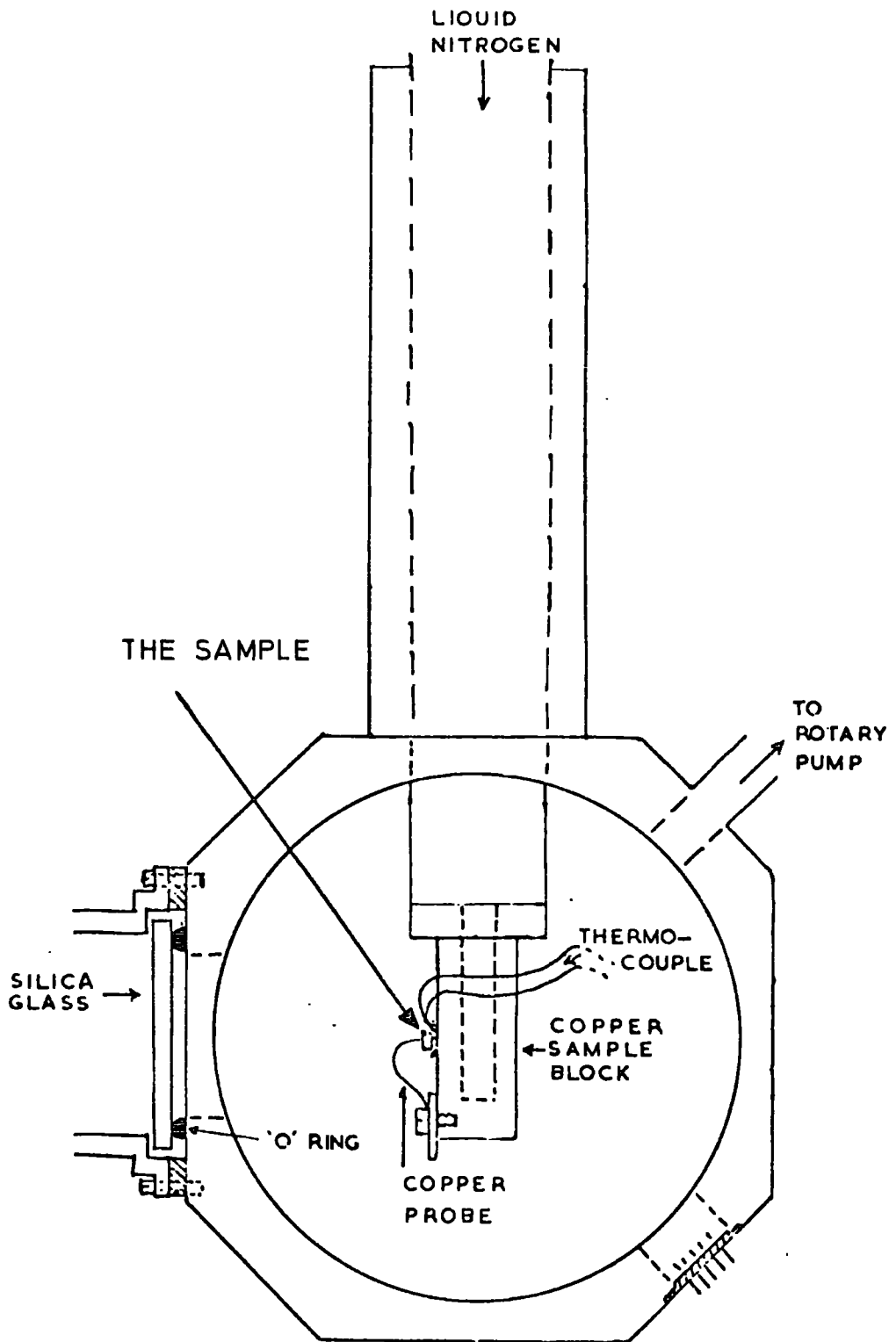


FIG. 4-2 CRYOSTAT USED FOR T.S.C.  
ELECTRICAL & OPTICAL MEASUREMENTS

exit slit of the monochromator.

Thermocouple and electrical leads were introduced into the cryostat by means of glass to metal seals.

Ideally the measurement of thermally stimulated currents requires a constant heating rate. However, this is not simple to achieve. In practice, as the cryostat was heated up from  $90^{\circ}$  K TO  $400^{\circ}$  K, the heater current was increased four times to counteract the decrease in heating rate. This did not produce a uniform rate of heating, for the purpose of comparability, therefore the same heater current was used for most of the T.S.C. experiments. The procedure adopted in the measurement of thermally stimulated current is described in Chapter 5.

#### 4.1.4 Spectral response of photoconductivity

For the measurement of spectral response of photoconductivity, monochromatic light from the exit slit of the Hilger and Watts D.330 grating monochromator was aligned to fall on to the crystal.

With the grating used the wavelength could be changed from  $.4\mu$  to  $1\mu$  either manually or by an automatic derive. Illumination, was originally supplied by a 500 W tungsten lamp. This was later replaced by a 240 W (24 volt) quartz halogen projector lamp, the spectral emission of which contained a much smaller proportion of infra red radiation. During the course of measurements the width of inlet and exit slits of the monochromator was kept unchanged in order to be able to compare the photoconductive responses of different samples which had been treated under different conditions.

#### 4.2 Schottky Barrier Formation

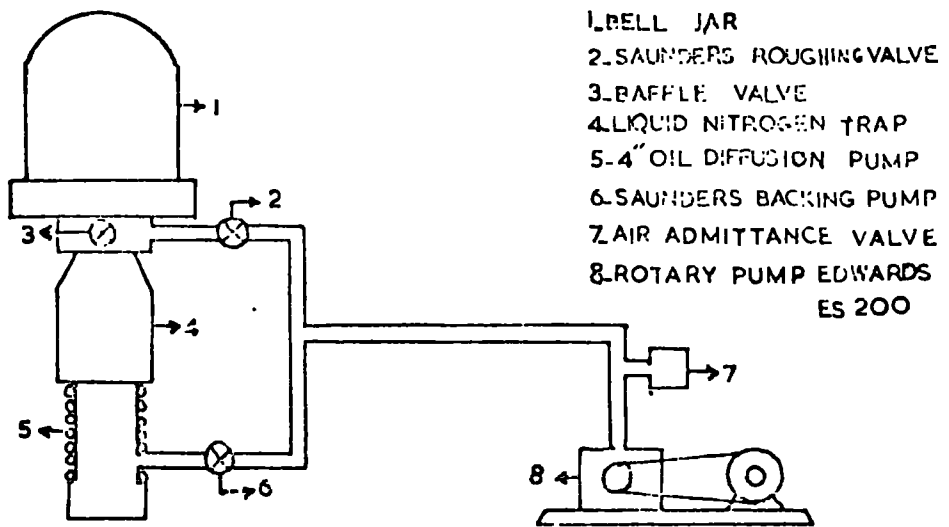
The Schottky barrier diodes were prepared by vacuum deposition of rectifying contacts. The rectifying contact was formed on the face of a die opposite that to which the indium contact had been applied.

Pure gold, obtained from Johnson Matthey Chemicals, was used almost exclusively to provide the rectifying contact. The face to receive the thin layer of gold was again etched in conc.HCl and washed in distilled water after alloying the indium contact on to the opposite face. During the etching process the indium contact was covered with a protective layer of "lacomit " which the chemical etchants did not affect. The thin protective layer was dissolved in acetone later on. Finally gold films,  $1.77 \times 10^{-2} \text{ cm}^2$  in area were deposited on the freshly cleaned surfaces.

#### 4.2.1 The vacuum system and metal film deposition

The schematic diagram of the vacuum system used is shown in Figure 4.3. The 4" oil diffusion pump and the backing rotary pump were both obtained from Edwards High Vacuum Ltd. An Edwards 70 series unit was employed to measure the pressure in the vacuum chamber, i.e. a pirani 11 gauge for pressures higher than  $10^{-3}$  torr, and a 1 G5 ionisation gauge for pressures below  $10^{-3}$  torr. With liquid nitrogen in the cold trap and silicone fluid 705 in the diffusion pump, the lowest pressure attained in the chamber was  $1 \times 10^{-6}$  torr. The pressure was maintained below  $6.0 \times 10^{-6}$  torr during most of the depositions.

The vacuum chamber used to deposit thin metal film layers on the single crystal dice is illustrated diagrammatically in Figure 4.3. The dice were placed on top of the stainless steel mask over a small hole through which the thin metal film would be deposited. The stainless steel mask was mounted on an 8 mm thick stainless steel disc, which was placed 3 cm above the source. Resistively heated molybdenum boats containing small pieces of gold metal were used as sources. The source was supplied by a L.T. transformer enabling 30 amps at 30 volts to be drawn if required. A silica cylinder, 5 cm in diameter, was located in the volume between the source and the stainless steel masks and a magnetic



SCHMATIC DIAGRAM OF PUMPS AND VALVES  
 OF EVAPORATOR

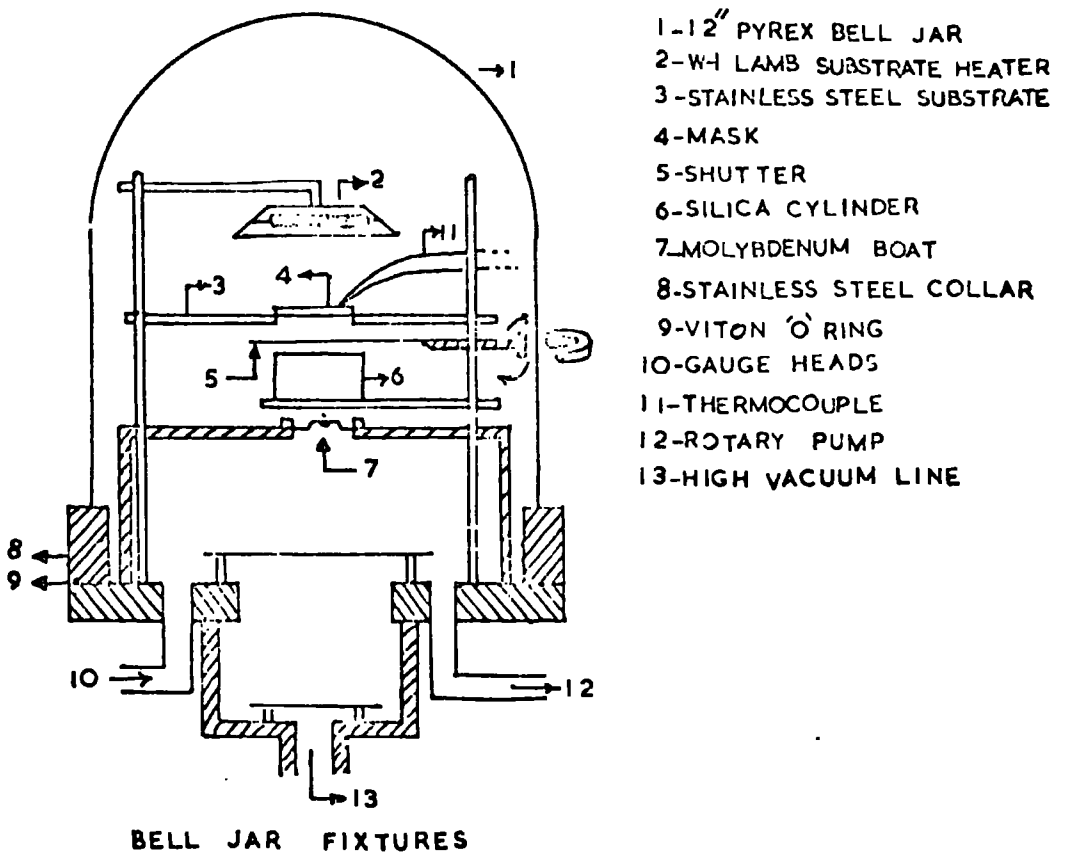


FIG. 4.3 SCHEMATIC DIAGRAM OF VACUUM  
 SYSTEM & BELL JAR FIXTURES

shutter was situated just below the stainless steel disc.

Before insertion in the vacuum system both the stainless steel mask and the pure gold metal were cleaned in chromic acid and washed with absolute alcohol. The initial step, before any metallic evaporation was undertaken, was to outgas the system. For this, the work chamber was evacuated to  $1.0 \times 10^{-6}$  torr and power was applied to an empty molybdenum boat. When this outgassing procedure was completed the work chamber was let down to air for a short period, during which the dice was quickly mounted on the stainless steel mask, and the small gold pieces were placed in the molybdenum boat.

The work chamber was then re-evacuated to  $1.0 \times 10^{-6}$  torr when the gold evaporation was carried out. Initially the shutter was kept closed so that the dice would not be exposed to metallic vapours until a steady evaporation rate has been attained, and minor outgassing was completed. The estimated film thicknesses prepared in this way were usually around a few thousand angstroms. The diodes produced were not encapsulated.

#### 4.2.2 Measurement of current-voltage characteristics of the diodes

The diodes were mounted on a copper sheet which was screwed to the copper finger of the cryostat by a p.v.c. screw. For the purpose of electrical insulation a thin layer of mica was placed between the copper sheet and copper finger of the cryostat. All electrical connections were made via a 6-way glass-to-metal seal.

A soft copper wire was used to hold the sample vertically on the copper sheet. The pressure inside the cryostat was reduced to  $10^{-1}$  torr with a rotary pump.

Current voltage characteristics were measured in the dark. A digital multimeter type DMM2 and sometimes an avometer were used to measure

the applied biases.

#### 4.2.3 Capacitance-Voltage measurements

The differential capacitance ( $c$ ) of the Schottky diodes was measured as a function of applied voltage ( $v$ ). For this purpose a C-G-V plotter, designed and built in this laboratory by P.G.Martin, was used. It operated accurately in the frequency range from 10 Hz to 300 kHz. An external oscillator provided the signal voltage 25 mV (p-p). The instrument included a low frequency sweep generator capable of biasing the device under test over the range of -20 to 20 volts. Most of the C-V plots were taken with biases between 2 volts (reverse) to .2 volt (forward). For some devices the C-V measurement was carried out for higher forward voltages up to 1 volt. A "Bryans" X-Y Autoplotter, Model 21005, was connected to the output of the C-G-V plotter to obtain an automatic record.

The C-V measurements were made on diodes mounted in the cryostat. The pressure was reduced to  $10^{-1}$  torr and most of the C-V plots were made in the dark at the room temperature.

#### 4.2.4 Photoresponse measurements

In addition to electrical measurements, some photoelectric studies were also made on most of the devices. A Barr and Stroud double monochromator type VL.2 with Quartz prisms (spectrosil 'A' quality) was used which enabled measurements to be made out to  $4 \mu$  if necessary. The light source used was a 240 watt (24 volt) quartz halogen projector lamp. Prior to the short circuit photocurrent measurements, the monochromator was calibrated using the light from a sodium lamp. The schematic diagram of the apparatus used to measure the photoresponse of the diodes is shown in Figure (4.4). The diode photocurrent was amplified by taking the signal from the 10 K.ohm load resistor to the input terminal of a Brookdeal lock-in

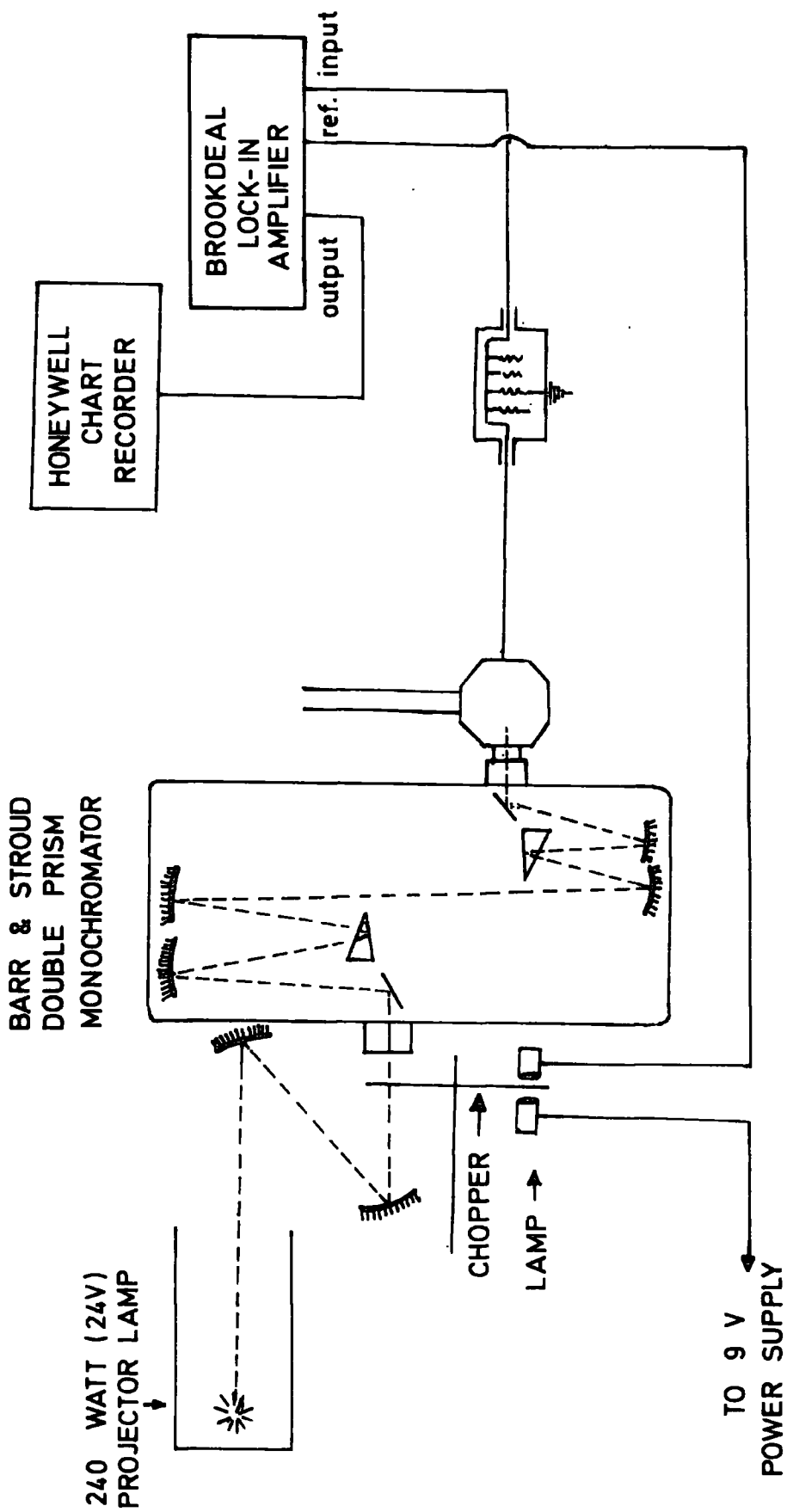


FIG. 4.4 ARRANGEMENT FOR SHORTCIRCUIT PHOTOCURRENT MEASUREMENTS

amplifier, type 401. The reference signal to the lock-in amplifier was obtained from light falling on the photodiode which was fed from the internal 9 volt supply of the amplifier. Both the light incident on the inlet slit of the monochromator and the light falling on the photodiode were chopped with a multi-bladed chopper which was driven by a synchronous motor via a flexible drive. This motor allowed a chopping frequency of 200 cps to be obtained with the help of a 40 bladed chopper.

The output of Brook deal lock-in amplifier was displayed on a Honeywell chart recorder.

#### 4.2.5 Photo-capacitance measurements

The GCV plotter mentioned earlier in Section 4.2.3 was used for photo-capacitance measurements. The cryostat was aligned with the exit slit of the Barr and Stroud double monochromator so that monochromatic light fell on to the device. The sweep voltage was maintained at zero. In this case a fixed value for the depletion layer capacitance could be read from the meter. As the wavelength of the light was changed manually the corresponding changes in the photo-capacitance were read from the meter. All the measurements were carried out at room temperature.

#### 4.3 X-Ray Powder Photography

Some photoelectric properties of CdS crystals doped with copper are reported in Chapter 5. Two methods have been employed to incorporate copper into CdS samples. In the first method, CdS crystals were dipped in a copper sulphate solution, the preparation of which has been described in Chapter 5. In the second method, the incorporation of copper was achieved by dipping the CdS samples in a solution of cuprous chloride, (see also Chapter 5). The technique of reflection electron diffraction has been used previously in this laboratory (Caswell et al, 1975) to demonstrate that

dipping CdS in a solution of CuCl leads to the formation of a surface layer of chalcocite,  $\text{Cu}_2\text{S}$ . This work has now been extended to show that dipping in a solution of  $\text{CuSO}_4$  leads to the production of a layer of covellite,  $\text{CuS}$ . The technique of X-Ray diffraction has also been employed to confirm these findings.

To obtain samples suitable for X-Ray photography, the CdS crystals were dipped in an  $\frac{N}{10}$  copper sulphate solution at a temperature of  $80^\circ\text{C}$  for 7 hours. This produced a thick enough layer of copper sulphide which was removed by a razor blade and crushed and ground to a fine powder of about 250 mesh size. The powder then was stuck on a cylindrical glass fibre of 0.2 mm diameter using flexible collodion as a binder. The fibre was then mounted at the centre of the Debye-Scherrer camera. The camera was loaded asymmetrically with the 'Kodirex' X-Ray film from Kodak Ltd., and mounted on the fast arm of a Philips "smoothed D.C. X-Ray Generator", type PW.1009/30. An X-Ray diffraction tube containing a copper target was used as the X-Ray source. This was filtered with a nickel filter to remove the background white X-Rays. The tube itself was operated at 40 kV, 20 mA. The specimens were exposed to copper  $K_a$  radiations ( $\lambda_{K_{a1}} = 1.5405 \text{ \AA}$  and  $\lambda_{K_{a2}} = 1.54434 \text{ \AA}$ ) for 1-2 hours. This produced an X-Ray pattern which contained lines with different intensities. The values of diffraction angle  $\theta$  (Bragg angle) were measured using a film measuring rule obtained from "Rigaku Denki Ltd". The  $\theta$  values and the intensity of these lines were compared with the corresponding A.S.T.M. values of different phases of copper-sulphide, the results are described in Chapter 5.

## CHAPTER FIVE

### PHOTOCONDUCTIVITY IN COPPER-DOPED CdS

#### 5.1 Introduction

Impurities and imperfections play important roles in the performance of CdS photo devices. Copper is particularly important because a highly photosensitive photoconductor can be prepared by counter-doping n-type CdS with copper, (Bube, et al, 1962 a, 1964 b) and the well known CdS solar cell is prepared by converting a thin surface layer of CdS to p-type  $\text{Cu}_2\text{S}$ , (A.G. Stanley, 1975). For high efficiency of the solar cell, it is essential to administer a short bake at  $200\text{--}250^\circ\text{C}$  following the deposition of the  $\text{Cu}_2\text{S}$  layer. One result of this treatment is the formation of a photoconducting i-layer between the n-type CdS and the p-type  $\text{Cu}_2\text{S}$  (Shiozawa, et al, 1969).

With both types of device a high stability in use is essential for the successful application, and indeed the processes which lead to the degradation of the efficiency of the CdS solar cell have attracted considerable attention in recent years, (Shiozawa, et al, 1970), (Palz, et al, 1973, 1974), and (Mytton, et al, 1973). However, the possibility that the photoconductive properties of the i-layer may change during operation appears to have been overlooked. The purpose of this chapter, therefore, is to describe the results of an investigation into the stability of the photoconductive sensitivity of rods of CdS doped with chlorine and counter-doped with  $\text{Cu}^+$  or  $\text{Cu}^{++}$  ions, (Salehi-Manshadi & Woods, 1977). The reason for studying cuprous and cupric ions is that no attention has been given hitherto to the possibility that the charge state of the copper may have an appreciable effect on the maintenance of photoconductive sensitivity.

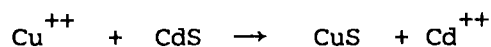
#### 5.2 Sample Preparations

Photoconductivity experiments were carried out on two types of

crystals prepared in the crystal growth laboratory of the department. The first series of experiments were done on the CdS crystals prepared by the flow run technique from the original B.D.H. Optran grade lumps. These crystals were doped with chlorine during their growth and were rods of thickness  $\sim 1$  mm and with resistivity  $\rho$  ranging from 0.1 to 1  $\Omega$  cm. The variation in the conductivity of these crystals arises from the fact that in a dynamical technique of crystal growth such as gas transport, it is very difficult to maintain the uniformity of the electrical properties of the crystals. The other crystals used were cut from the boules grown in sealed ampoules using the vapour phase technique of Clark & Woods (1968). The CdS:Cl rods produced from the argon flow technique were then used as a starting charge in the growth ampoules. Since the details of the growth of the crystals used have been discussed in Chapter 3, we describe here the method used for the preparation and the counter doping of the CdS:Cl crystals with copper.

### 5.3 Doping with Divalent Copper Ions

$\text{Cu}^{++}$  ions were introduced by dipping the CdS:Cl rods in an aqueous solution of copper sulphate. Different concentrations ranging from  $\frac{1}{10}$  N to  $\frac{N}{3}$  were employed. After dipping for 20 minutes in the solution, the colour of the rods changed from light orange to dark brown. The reaction responsible for this change is :



i.e. a topotaxial layer of CuS (covellite) is formed on CdS rods by an exchange mechanism in which  $\text{Cd}^{++}$  ions are replaced by  $\text{Cu}^{++}$  ions (see below). To diffuse Cu into the CdS bulk, the samples were baked in sealed ampoules containing argon gas at 700<sup>o</sup> C for various lengths of time, e.g.  $\frac{1}{2}$  to  $2\frac{1}{2}$  hours.

#### 5.4 Identification of the Formation of a Covellite Layer on the CdS Bars

For the purpose of structural investigations, samples which had been cut and mechanically polished on their basal planes were plated in a cupric sulphate bath at  $80^{\circ}\text{C}$  for a period of 1 hr. Non-destructive reflection electron diffraction (RED) observations were made of these plated  $\text{Cu}_x\text{S}$  layers in a JEM 120 electron microscope using electrons of energy 100 KeV. For further support of the electron diffraction measurements, X-ray powder photographs were obtained using a Debye sherer camera and material scraped from the surface of the plated sample.

RED patterns like that shown in Figure 5.1 were obtained from several samples plated on different occasions. While the pattern clearly does not arise from a single crystal, it is comprised of "arced spots" that are characteristic of diffraction from a set of crystallites having one or more fibre axes of a preferred orientation. By comparing measurements taken from this diffraction pattern with ASTM Index Values of interplanar spacings of the phases of copper sulphide, it was found that all of the reflections present could be best explained by the identification of the phase of copper sulphide as covellite ( $\text{CuS}$ ). However, since patterns, such as those in Figure 5.1, may not contain certain reflections which are otherwise allowed for the particular crystal structure of the material being examined, it was considered necessary to employ the X-ray powder technique to obtain diffraction from all the "allowed" reflecting planes and thereby to make the identifications more substantial. The measurements taken from the X-ray powder photograph are given in Table 1 together with the A.S.T.M. Index Values of interplanar spacings for covellite ( $\text{CuS}$ ). From this it can be seen that there is good agreement between the experimental and A.S.T.M. Index Values of both interplanar spacings and intensities, and so it can be firmly concluded that the

phase of copper sulphide formed under the conditions described above was that of covellite.

EXPERIMENTAL VALUES		A.S.T.M. INDEX VALUES		
Interplanar Spacings Å	Intensity	Interplanar Spacings Å	Intensity	Index of reflecting planes
3.220	strong	3.285 } 3.220 }	14 } 28 }	(100) } (101) }
3.045	very strong	3.048	67	(102)
2.810	very strong	2.813	100	(103)
2.715	strong	2.724	56	(006)
2.320	very weak	2.317	10	(105)
2.080	very weak	2.097 } 2.043 }	6 } 7 }	(106) } (008) }
1.900	very strong	1.902 } 1.896 }	25 } 75 }	(107) } (110) }
1.730	strong	1.735	34	(108)
1.560	strong	1.572 } 1.556 }	15 } 37 }	(203) } (116) }

TABLE 1

In addition to providing supporting evidence for the identification of the phase of copper sulphide, the (RED) pattern shown in Figure 5.1 also gives an indication of the form in which CuS is present. As mentioned above, the fibrous pattern arises from a set of crystallites having a common or preferred orientation. The fact that the arced spots in Figure 5.1 do not form a single two-dimensional array can be explained with reference to Figure 5.2 in which the RED pattern of Figure 5.1 is indexed. This shows that the diffraction pattern arises from two sets of crystallites each having a  $[10\bar{1}2]$  fibre axis where reflections from one set of crystallites are mirror images of those from the other set across the fibre axis. That is to say,

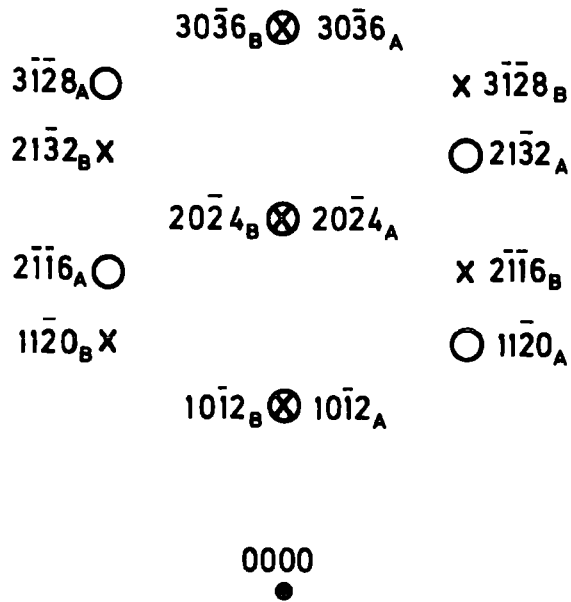


FIG. 5.2 Indexing of RED pattern shown in Fig. 5.1

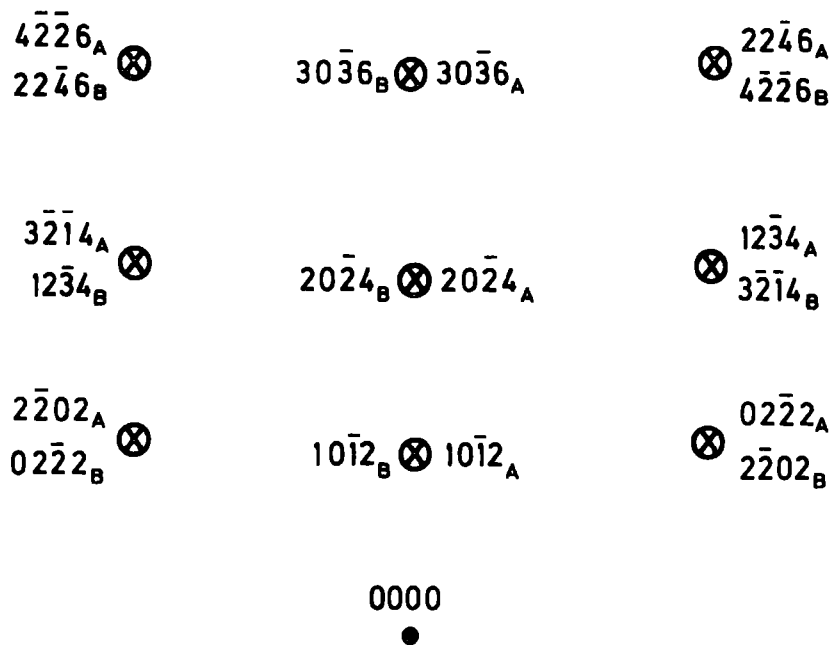


FIG. 5.4 Indexing of RED pattern shown in Fig. 5.3

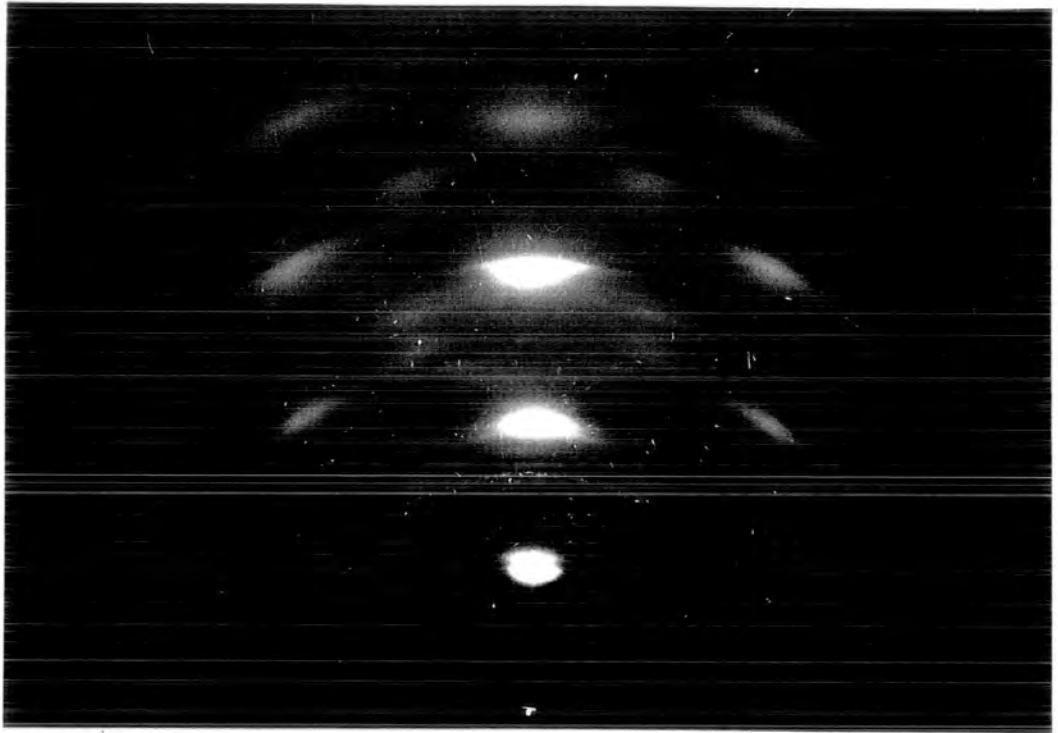


Figure 5.1 : RED pattern from CuS

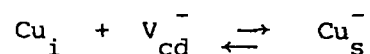


Figure 5.3 : Another low index RED pattern obtained from CuS after rotating the sample about the C-axis of the CdS

one set is in a twin orientation with respect to the other. That the fibre axis of the crystallites was the  $[10\bar{1}2]$  direction was confirmed by rotating the plated CdS sample to another low index orientation of CuS crystallites and establishing that the  $(10\bar{1}2)$  planes of these crystallites still gave rise to diffraction. This second orientation is shown in Figure 5.3 and the arced spots are indexed in Figure 5.4. As the sample was rotated about the  $[0001]$  axis of the CdS substrate, it follows that the orientational relationship between the CuS crystallites and CdS substrate is  $(10\bar{1}2) \text{ CuS} \parallel (0001) \text{ CdS}$ .

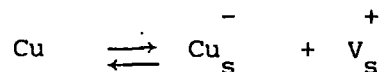
### 5.5 Copper Diffusion

We have not been concerned with experiments on the diffusion and solubility of Cu in CdS crystals. However, because of the important consequences of doping of CdS semiconductor devices with copper, it is interesting to enquire how Cu diffuses in CdS and what is the compensation mechanism of Cu in CdS. In recent years, a number of investigations have been carried out to answer these questions (see for example, G.A.Sullivan, 1969, W. Szeto and G. A. Somarjai, 1966, Woodbury, 1965, Clarke, 1959). An acceptable model for copper diffusion in CdS is that copper diffuses interstitially into CdS with an interstitial-substitutional equilibrium superimposed on the diffusion process. The copper impurities diffusing interstitially react with ionized cadmium vacancies  $V_{\text{cd}}^-$  according to the reaction :



In this way copper ions substitute the acceptor cadmium vacancies. This process does not account for the Cu compensation in CdS because a single acceptor has been replaced by another single acceptor. For compensation it is necessary that the total concentration of Cd vacancies is maintained constant during the diffusion process by thermal regeneration. (Sullivan 1969).

Since the solubility of the substitutional copper ions is higher than that of cadmium vacancies in the undoped crystal, copper dissolves in the lattice by the self-compensation mechanism, (G. Mandel, 1964).



This means that the exchange between copper and substitutional cadmium ions takes place in the presence of sulphur vacancies. This process is responsible for the fact that CdS cannot be made p-type.

#### 5.6 Doping with Monovalent Copper Ions

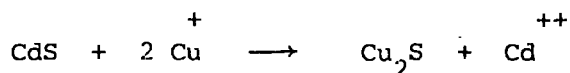
Cuprous ( $\text{Cu}^+$ ) ions were introduced into CdS:Cl crystals by dipping them in an aqueous solution of cuprous ions after which they were baked in sealed ampoules containing argon gas at  $700^\circ\text{C}$  for  $2\frac{1}{2}$  hrs.

The cuprous ( $\text{Cu}^+$ ) ion solution was prepared in the following way :-

- (a) 75 ml of distilled water was heated in a closed reaction vessel and then oxygen-free nitrogen gas was bubbled through the liquid to remove any dissolved oxygen.
- (b) 12 ml of concentrated hydrochloric acid was added to the water and the heating and nitrogen gas flow was continued.
- (c) 1 gm of cuprous chloride was added when the temperature was approximately  $60^\circ\text{C}$ .
- (d) Approximately 7.5 ml of hydrazine hydrate solution was added to the solution to produce a resultant pH of 2 to 3 as measured by indicator papers.
- (e) After heating the solution to  $90^\circ\text{C}$ , the pH was measured again and corrected to 2.5 using a small amount of hydrochloric acid or hydrazine hydrate. The solution was made up to 100 ml by the addition of a little deoxygenated distilled water. During preparation

and while using the bath, a constant flow of oxygen-free nitrogen was maintained through the solution. The purpose of this was to keep as much oxygen away from the solution as possible and to keep the solution fully mixed.

A layer of  $\text{Cu}_2\text{S}$  (chalcocite) was formed on the  $\text{CdS}:\text{Cl}$  rods by dipping them in the solution, for the short period of about 10 seconds. The layer was formed according to the reaction :



This is a topotaxial reaction in which  $\text{Cd}^{++}$  ions are replaced by  $\text{Cu}^+$  ions. After the formation of the first film of  $\text{Cu}_2\text{S}$ , the growth rate of the layer depends on the rate at which  $\text{Cu}^+$  ions diffuse in and  $\text{Cd}^{++}$  ions diffuse out of the  $\text{Cu}_2\text{S}$  layer.

Since there is a mismatch between the lattice structures of  $\text{CdS}$  and the  $\text{Cu}_2\text{S}$ , a tension develops which causes fine cracks in the  $\text{Cu}_2\text{S}$  layer. Using the reflection electron diffraction technique, (Caswell, et al, 1975) have identified the formation of a  $\text{Cu}_2\text{S}$  layer (chalcocite) on  $\text{CdS}$  single crystals by comparing the RED pattern with the A.S.T.M. index for copper sulphides.

It is worth mentioning that the formation of the  $\text{Cu}_2\text{S}$  (chalcocite) layer on  $\text{CdS}$  single crystals takes place much quicker than that of the  $\text{CuS}$  (covellite) layer. This is probably because the activation energy of reaction for the formation of  $\text{Cu}_2\text{S}$  layer is less than that of the  $\text{CuS}$  layer.

### 5.7 Ohmic Contacts

An ohmic contact is defined as a contact which will not add parasitic impedance to the structure on which it is applied. In other words, the contact between a metal and a semiconductor is ohmic when the following criteria are fulfilled.

- (1) The current-voltage characteristics are linear and,
- (2) There is no photovoltaic effect. That is to say, an ohmic contact is characterized by having no potential barrier (hence no asymmetry) and an infinite surface recombination velocity (hence linearity).

In recent years numerous investigations have been made to find the best metal as well as the technique for applying ohmic contacts to CdS. Smith (1955) used In and Ga for making ohmic contacts to CdS. Indium amalgam has been successfully used for electrical contact on II-VI semiconductors by Hill, et al (1972). A low resistance ohmic contact to CdS has been achieved by vacuum annealing of crystals before deposition of indium, (Thompson and Cornwall, 1972). This process was adopted in order to outgas the absorbed oxygen from the crystal surfaces which otherwise would give rise to a surface barrier (Reed and Scott, 1965). Diffusion of high purity indium into the CdS samples (Zold, 1973) has provided yet another technique to make ohmic contact to CdS crystals by indium. In our experiments we have made ohmic contacts to CdS crystals by melting and diffusing indium into the samples by heating them at 200-220°C in an inert (Argon) atmosphere for 10-15 minutes. Prior to this the CdS rods were etched in the concentrated hydrochloric acid for 1-2 minutes and then washed in distilled water. The purpose of the etch was to remove oxidised and work damaged surface layers which otherwise produce non-ohmic contacts.

#### 5.8 Photoconductivity of Flow Run Crystals

Photoconductivity measurements were carried out on flow run CdS:Cl rods doped with Cu<sup>++</sup> ions. The rods were illuminated with light from the exit slit of a Hilger and Watts D.330 grating monochromator described in Chapter 4. The source employed was a 500 watt tungsten lamp. The photocurrent was measured over the wavelength range of 7600 Å to 4400 Å at room and liquid nitrogen temperatures. The effect of concentration of Cu impurity

on the photocurrent of CdS:Cl:Cu rods was also measured.

To compare the compensation effects of copper with that of sulphur in CdS, sulphur was diffused into the CdS:Cl bars, (see Chapter 3) and the spectral response of the photoconductivity of the resultant samples was determined. In an attempt to understand the degradation mechanism and the well known photochemical changes (see Tscholl, 1967) in CdS crystals, the samples were illuminated by either monochromatic or white light for different periods of time and the variation of photocurrent as well as the variation of the spectral response of the samples with time and temperature was measured. Such measurements were either followed or preceded by thermally stimulated current measurements in order to determine the corresponding changes in the shape and the magnitude of the T.S.C. curves due to these optical treatments.

#### 5.9 The Effects of Varying the Copper Impurity Concentration

Photoconductive samples with different dark resistivities ranging from  $10^8$  -  $10^{12}$   $\Omega\text{cm}$  were prepared by dipping the conductive CdS:Cl rods with resistivities of the order of  $\rho \sim 10^{-1}$   $\Omega\text{cm}$  into copper sulphate solutions of different concentrations. The same dipping time and the same heat treatment for diffusing Cu into the samples were adopted to ensure that the copper content of the samples was the only changing factor. A typical graph of the measured spectral response of photoconductivity of the samples, prepared in this way, is shown in Figure 5.5. The power supplied to the light source and the slit width of the monochromator were kept unchanged to ensure the reproducibility of the conditions under which the experiments were carried out. As is clear from Figure 5.5 a change in the concentration of the Cu impurity has had a considerable effect on the shape and the magnitude of the spectral response of the samples. Although both curves exhibit the extrinsic excitation of the compensated Cu impurities as a broad band, there are several aspects in

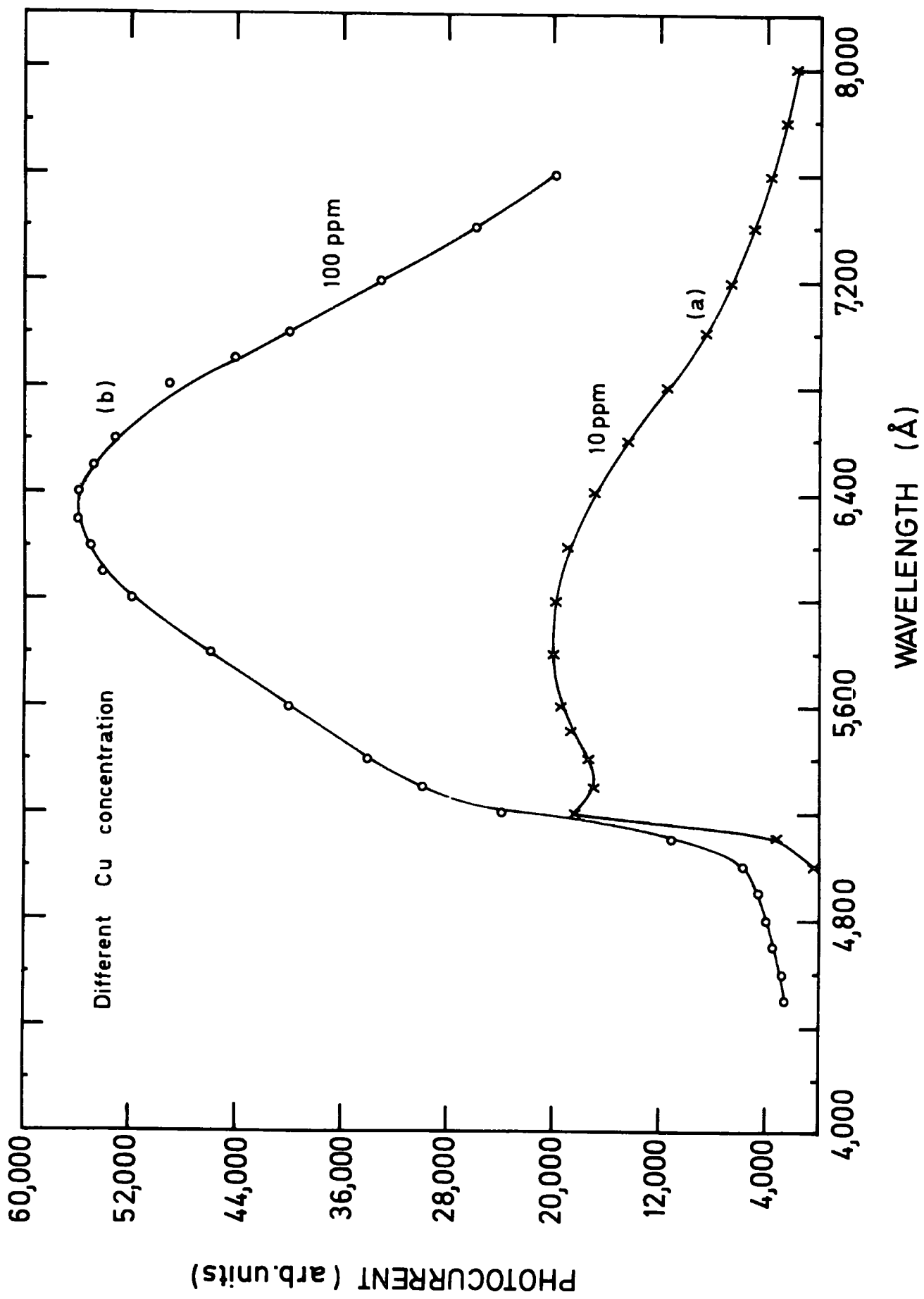


FIG. 5.5

which the two curves differ,

(1) the curve (a) shows a prominent peak near  $5200 \text{ \AA}$  associated with excitation across the band gap, whereas in curve (b) this feature is suppressed by the greater magnitude of the extrinsic excitation due to the higher Cu content of the sample from which the curve (b) was obtained.

(2) Maximum extrinsic excitation in curve (a) occurs around  $\lambda = 5800 \text{ \AA}$ , i.e. a photon energy of 2.13 eV. For the sample with higher copper impurity content, there is a shift in the position of the impurity peak to larger wavelengths. This peak occurs at about  $\lambda = 6400 \text{ \AA}$ , i.e. a photon energy of 1.93 eV.

(3) The long wavelength threshold is more pronounced in sample (b) than in (a). The ratio of the photocurrents of the two samples at different wavelengths is increased from about 1.5 at  $\lambda = 5200 \text{ \AA}$  to a value greater than 5 at  $\lambda = 7600 \text{ \AA}$ .

(4) The short wavelength threshold is also more pronounced in the sample (b) than in (a). This denotes that the surface recombination velocity is changed.

The spectral response of the photoconductivity of the samples (a) and (b) was also measured at temperatures close to that of liquid nitrogen, i.e. at  $93.5^\circ\text{K}$  and  $85^\circ\text{K}$  respectively. It is obvious from the curves in Figure 5.6 that the extrinsic excitation peak occurs at  $\lambda = 6700 \text{ \AA}$  (1.85 eV) in both samples. Comparison of the curves of Figure 5.5 with those of Figure 5.6 reveals that the peaks at  $\lambda = 5800 \text{ \AA}$  and  $\lambda = 6400 \text{ \AA}$  associated with the Cu impurities at room temperature both shifted to  $\lambda = 6700 \text{ \AA}$  at liquid nitrogen temperature.

According to these measurements, the band gap excitation occurred at  $\lambda = 5200 \text{ \AA}$  at room temperature which gives the band gap energy as  $E_g = 2.384 \text{ eV}$ . The measured energy gap at  $85^\circ\text{K}$ , is  $E_g = 2.523 \text{ eV}$ . These measurements give the temperature coefficient of forbidden band width as  $\alpha = 6.62 \times 10^{-4} \text{ eV/deg}$ .

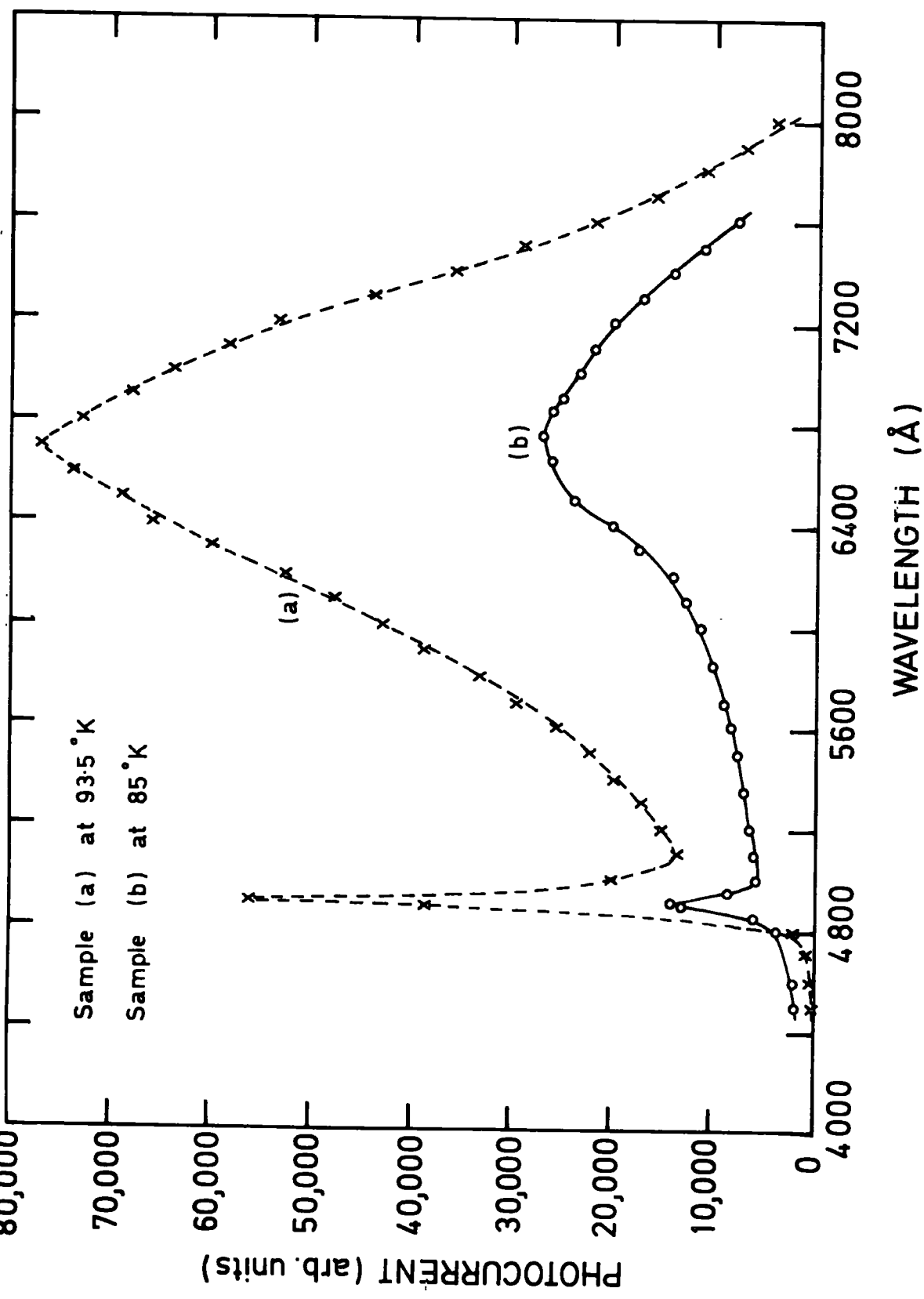


FIG. 5-6

Substituting the value of  $\alpha$  in the expression  $E_g = E_{g_0} + \alpha T$ , the energy gap of the sample at  $T = 0$  is obtained to be  $E_{g_0} = 2.579$  eV. Whereas the substitution of the temperature coefficient  $\alpha = 5.2 \times 10^{-4}$  eV/deg, (Bube, 1960) gives the energy gap at  $T = 0$  of  $E_{g_0} = 2.567$  eV.

#### 5.10 The Effect of Sulphur Compensation

It is well known that sulphur vacancies behave as donors in CdS crystals, i.e. the non-stoichiometric crystals with a sulphur deficiency are fairly conductive. This type of crystal, together with CdS:Cl rods, can also be compensated by annealing in sulphur vapour, (A. G. Sullivan, 1969). To observe the effects of sulphur compensation, CdS:Cl rods were baked in sealed ampoules containing sulphur, (Chapter 3) at  $700^\circ\text{C}$  for 2 hours. Following this treatment, photoconductive samples were obtained from the original conductive ( $\rho \sim 10^{-2}$   $\Omega\text{cm}$ ) rods. The measured spectral response of photoconductivity of a CdS:Cl:S sample is shown in Figure 5.7. The particular features of the curve can be described as follows :-

- (1) Maximum band gap excitation occurs at  $\lambda = 5350 \text{ \AA}$  which corresponds to  $E_g = 2.317$  eV.
- (2) The extrinsic photoconductivity occurs over a wide range of wavelengths and the corresponding broad band is centred at  $\lambda = 6400 \text{ \AA}$ .
- (3) The height of the peak corresponding to the band gap excitation is greater than that of the extrinsic excitation peak in contrast with the situation obtained with copper compensated samples.

#### 5.11 The Effect of Prolonged Illumination on Samples Doped with $\text{Cu}^{++}$ ions

As mentioned previously in Chapter 1, degradation in CdS photo devices can be attributed to various mechanisms ; for example, CdS- $\text{Cu}_2\text{S}$  cells are subject to a number of degradation processes such as : (1) the reactivity of the polycrystalline surface area with the ambient atmosphere, (2) the existence of the other oxidised phases in the  $\text{Cu}_2\text{S}$  systems with compositions near  $\text{Cu}_2\text{S}$ ,

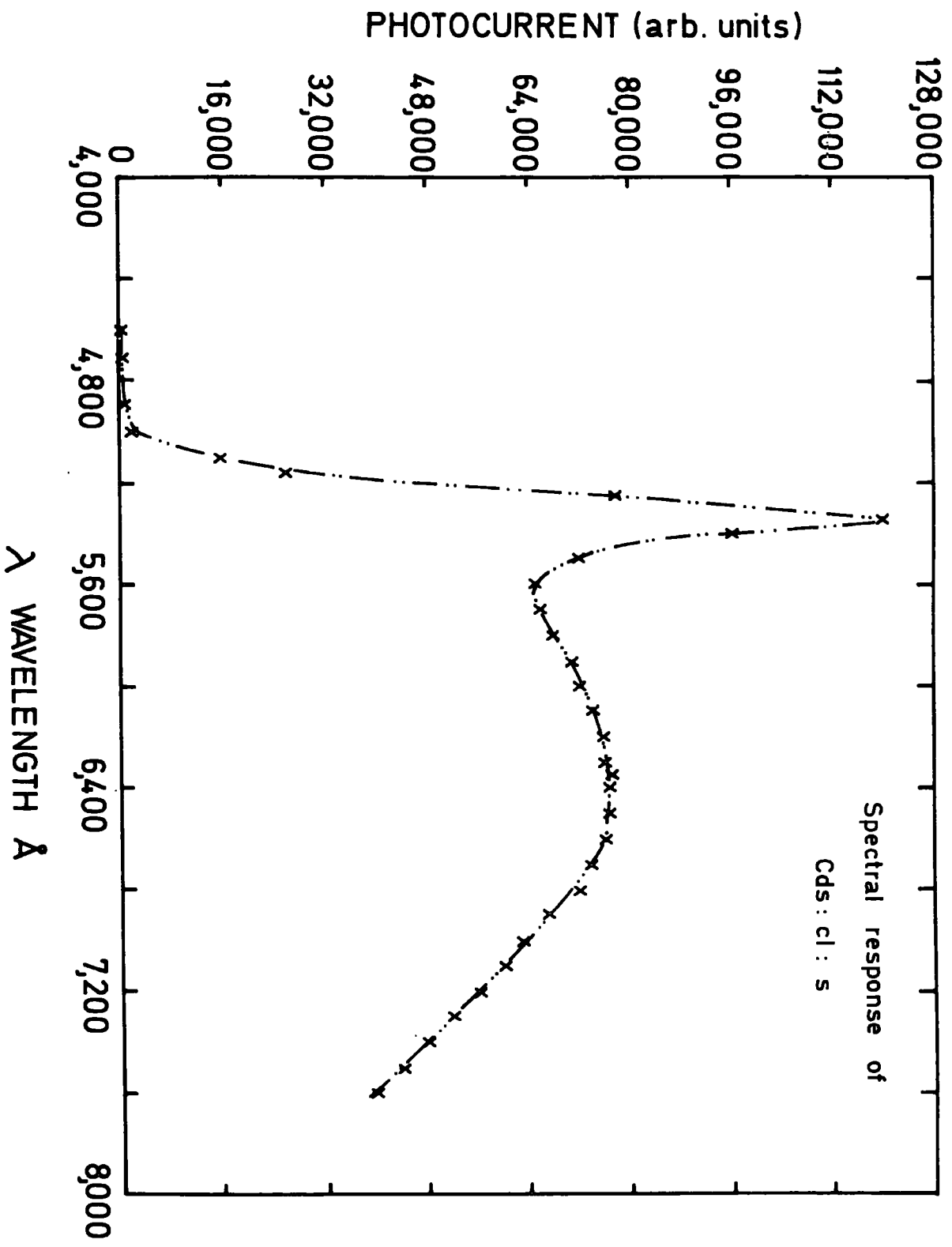


FIG. E7

(3) ionic segregation due to the ionic mobility of Cu in  $\text{Cu}_2\text{S}$  when a marked potential drop can be developed across the  $\text{Cu}_2\text{S}$ , (4) Cu diffusion into CdS provides still another degradation mechanism. CdS photoconductive devices are mainly subject to two degradation mechanisms :- (a) The reactivity of the device surface area with ambient atmosphere and (b) photochemical changes in the crystals.

In our investigations we have been mainly concerned with the second type of degradation mechanism, i.e. the effect of illumination on the photoconductive properties of the chlorine doped crystals compensated with either copper or sulphur.

The procedure which was adopted for this investigation was as follows :-

(1) Immediately after the preparation and mounting of the sample in the cryostat, the spectral response of the photoconductivity was measured;

(2) the sample was then cooled to a temperature close to liquid nitrogen temperature when the measurement of the spectral response of photoconductivity was again carried out;

(3) the variation of photocurrent with temperature was measured, This was followed by :

(4) the measurement of the thermally stimulated current during which the sample was heated up in the dark at a rate of  $0.5^\circ \text{K/sec}$  while the current was monitored over the range of  $85$  to  $390^\circ \text{K}$ ;

(5) steps (1) to (4) were repeated after the sample had been illuminated with white light from the source for a certain length of time at room temperature.

The degradation effect of light on the rods of  $\text{CdS:Cl:Cu}^{++}$  was tested by measuring the variation of the photocurrent with time at room temperature. This measurement was carried out while the samples were constantly illuminated by an ordinary (100 W) Tungsten lamp for a period of 382 hours in a special test box. It is obvious from the curves in Figure 5.8 that the degradation

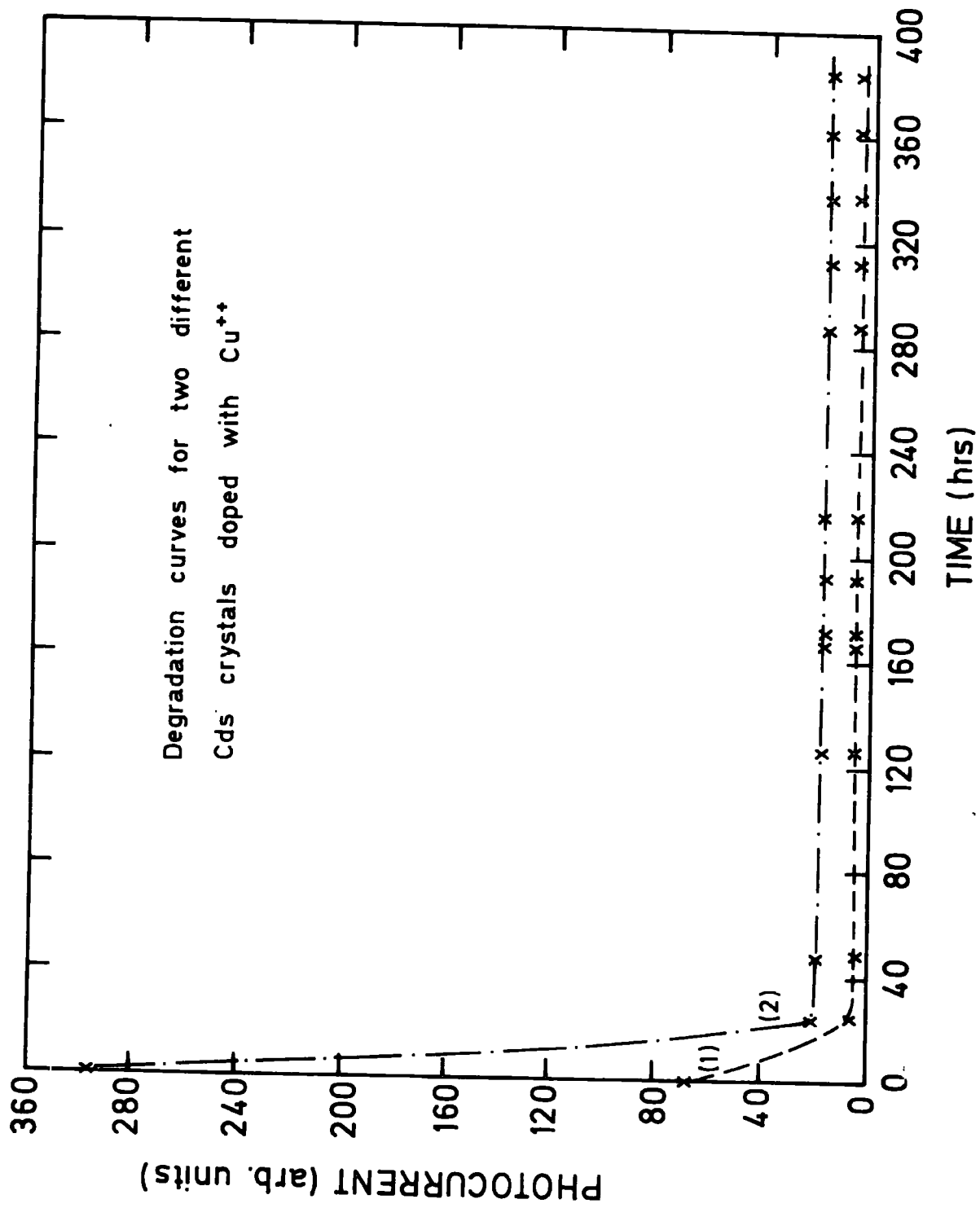


FIG. 5.8

mainly occurs over the first 20 hours of the illumination during which the photocurrent decays nearly two orders of magnitude. It then remains fairly constant over the remaining period of the experiment.

As a further step towards the understanding of the effect of light on CdS:Cl:Cu<sup>++</sup> crystals, the spectral response of photoconductivity of the rod ( $F_B$ ) was measured at room temperature before and after an intervening period of two hours during which the sample was illuminated directly with the light source. Following this illumination an appreciable change in the spectral response of photoconductivity of the sample was observed, see Fig.5.9. Thus, there is an appreciable shift of the photoresponse to larger wavelengths. In particular, there is a shift in the maximum extrinsic photoconductivity from 6100 Å to 6400 Å which corresponds to an energy shift from  $E = 2.03$  eV to  $E = 1.939$  eV.

During the course of these experiments, it became clear that the photo-induced changes in CdS:Cl:Cu<sup>++</sup> samples were responsible for the degradation of the photoconductivity. This was further supported by the results of measuring the spectral response of photoconductivity of the device ( $F_A$ ) at intervals over a period of time without exposing it to continuous illumination from the source. Although the successive measurements of the spectral response (Fig. 5.10) illustrates that there is a contribution to the degradation from the reactivity of the device surface with the ambient atmosphere, it is easily recognizable that the extent to which this degradation affects the photoresponse is not comparable with that of the photoinduced degradation. In contrast with the above observations, direct illumination does not cause any degradation at all in the performance of the CdS:Cl rods which have been heat treated in sulphur vapour. The spectral response of a CdS:Cl:S rod which was measured before and after an intervening period of 2 hours during which the sample was illuminated with monochromatic light of wavelength  $\lambda = 5350$  Å is shown in Figure 5.11. An increase is observed both in the intrinsic and extrinsic

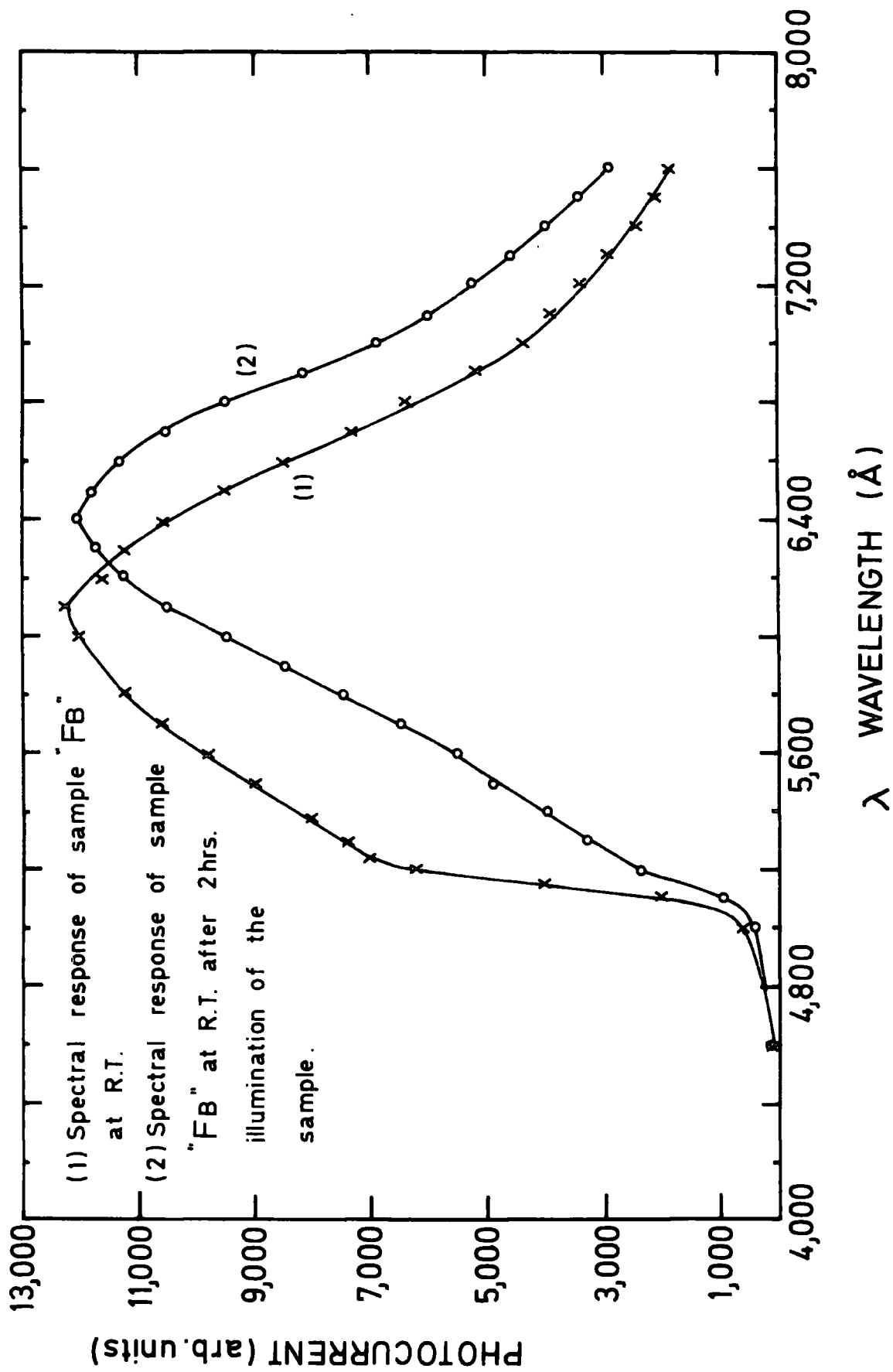


FIG. 5.9

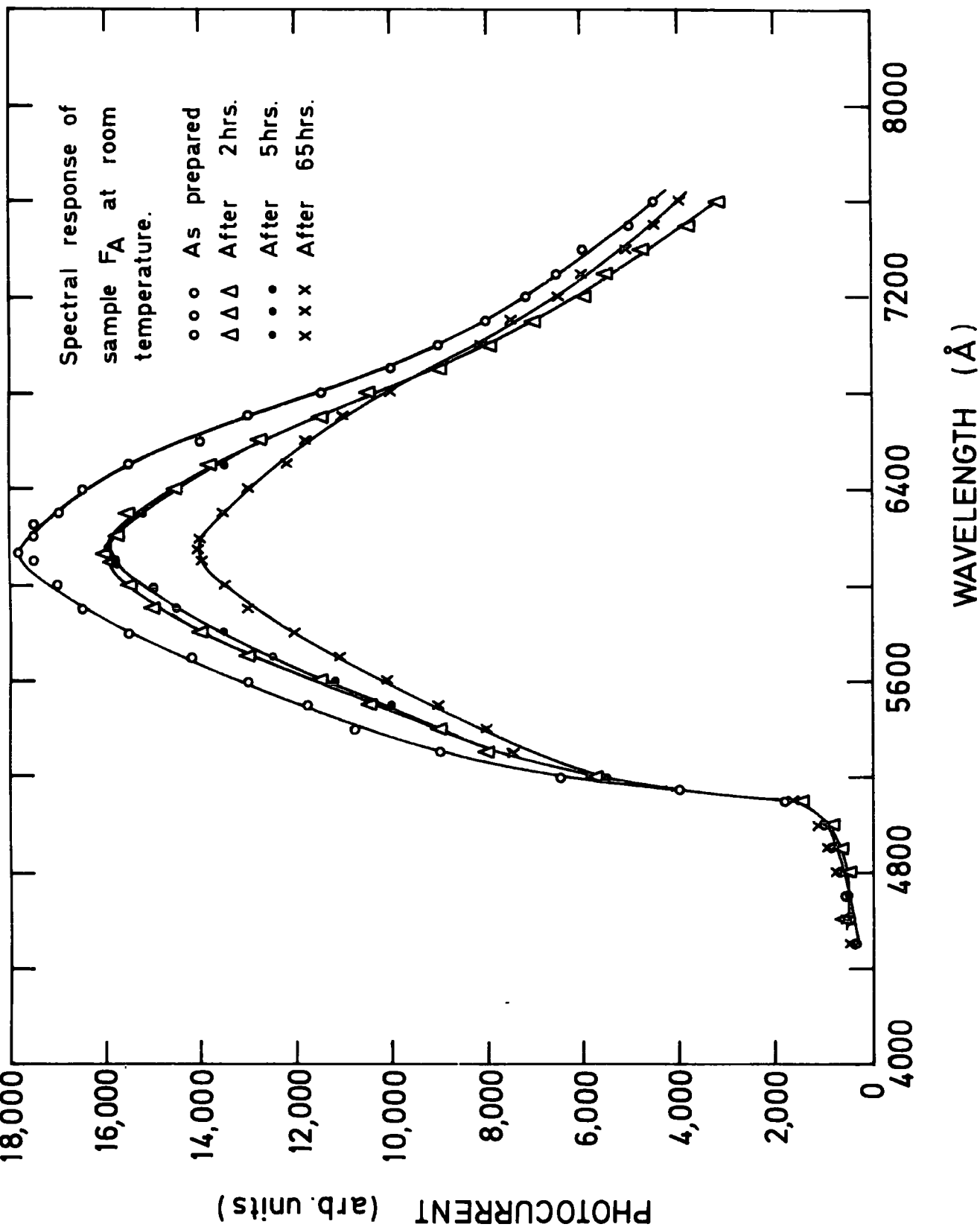


FIG. 5-10

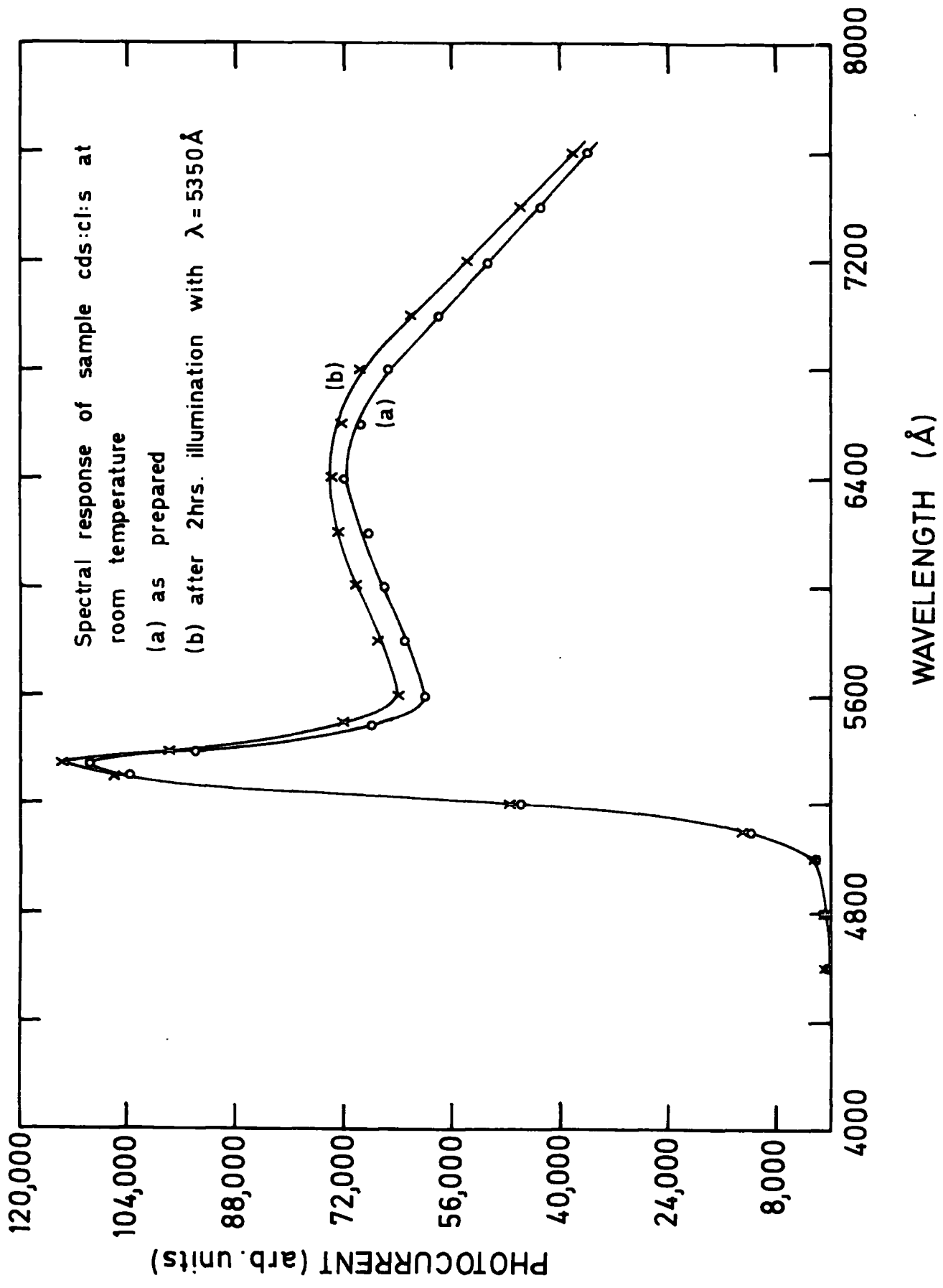


FIG. 5-11

regions of the photoresponse as a result of the illumination.

#### 5.12 Thermally Stimulated Currents in Samples Doped with Cupric Ions

Previous studies of the stability of the photoconductivity of CdS:Cl:Cu crystals showed that a substantial decay occurs in the magnitude of the photocurrent which is due to the effects of illumination. Since the deterioration may be associated with changes in the trap distribution of the samples, thermally stimulated current measurements were made to investigate this possibility.

In previous work on the photochemical effect in CdS crystals (Cowell and Woods 1969), the sample was heated to  $393^{\circ}$  K in the dark prior to each T.S.C. measurement to establish a reproducible state. It was then cooled to  $85^{\circ}$  K. Since such a heat treatment might have affected the diffused state of the copper in the sample, this procedure was only used with curves 1 and 2 in Figure 5.12. The usual procedure which was adopted throughout this set of measurements was as follows:-

After the sample ( $F_A$ ) was cooled to  $85^{\circ}$  K, it was illuminated with band gap light of  $\lambda = 4900 \text{ \AA}$  for 20 minutes. The illumination was then extinguished and the sample was heated in the dark at a linear rate of  $0.5^{\circ}$  K/sec. The conductivity was monitored and its variation with temperature is plotted as curve (1) in Figure 5.12. Curve (2) represents T.S.C. of the sample after it had been illuminated with green light with  $\lambda = 5200 \text{ \AA}$  for 1.5 hours at room temperature. For the T.S.C. curves (3) and (4) the step of heating up of the sample to  $377^{\circ}$  K in the dark was eliminated. The difference between the curves (3) and (4) lies in the fact that prior to the measurement of curve (4), the sample was subjected to one hour's direct illumination at room temperature from a 240 watt quartz halogen lamp. As can be seen from Figure 5.12, the direct illumination has a substantial effect on the trap distribution. The curves indicate that there are two groups of electron traps, i.e. shallow traps with trap depths in the range of 0.15 - 0.30 eV which empty over the range of

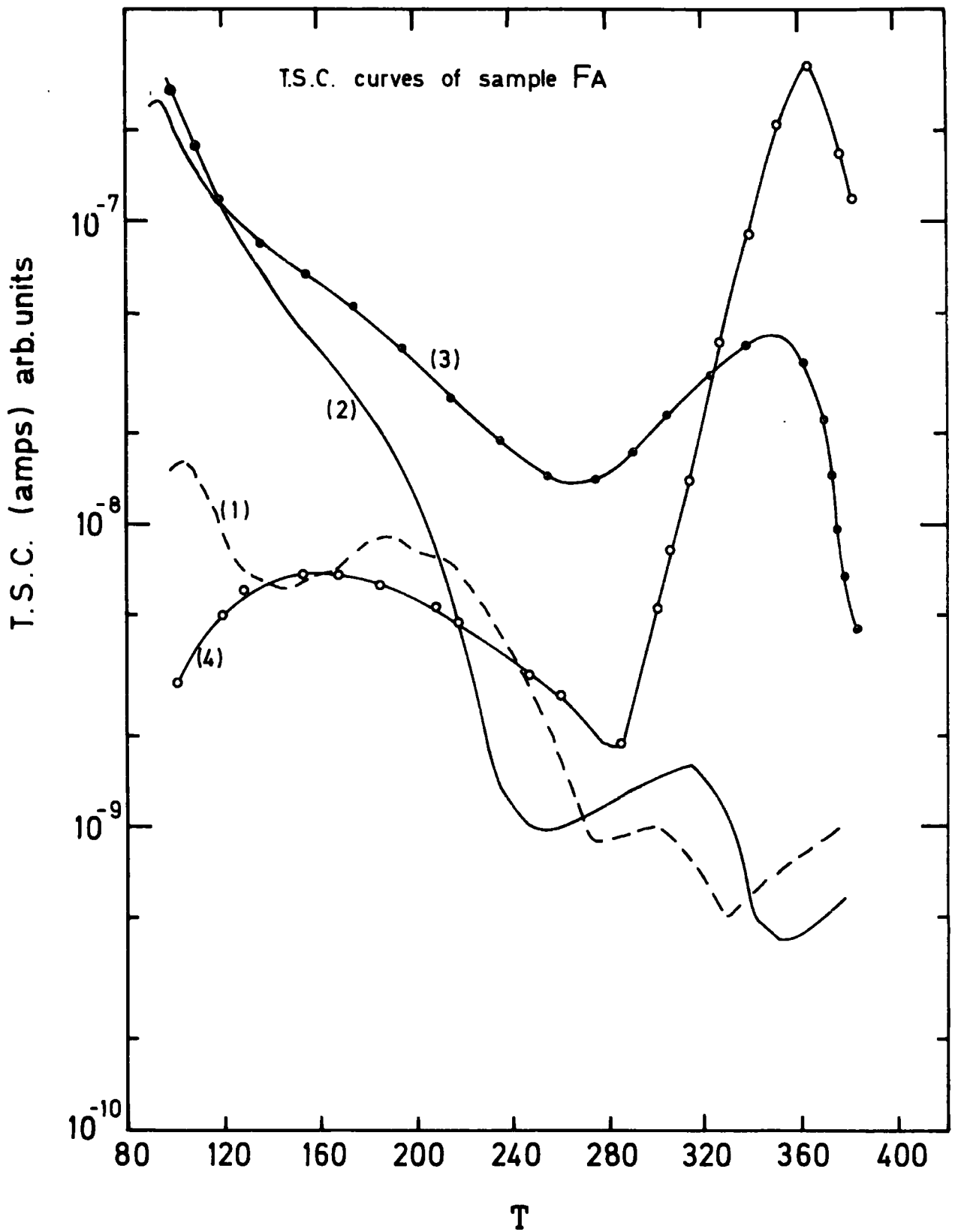
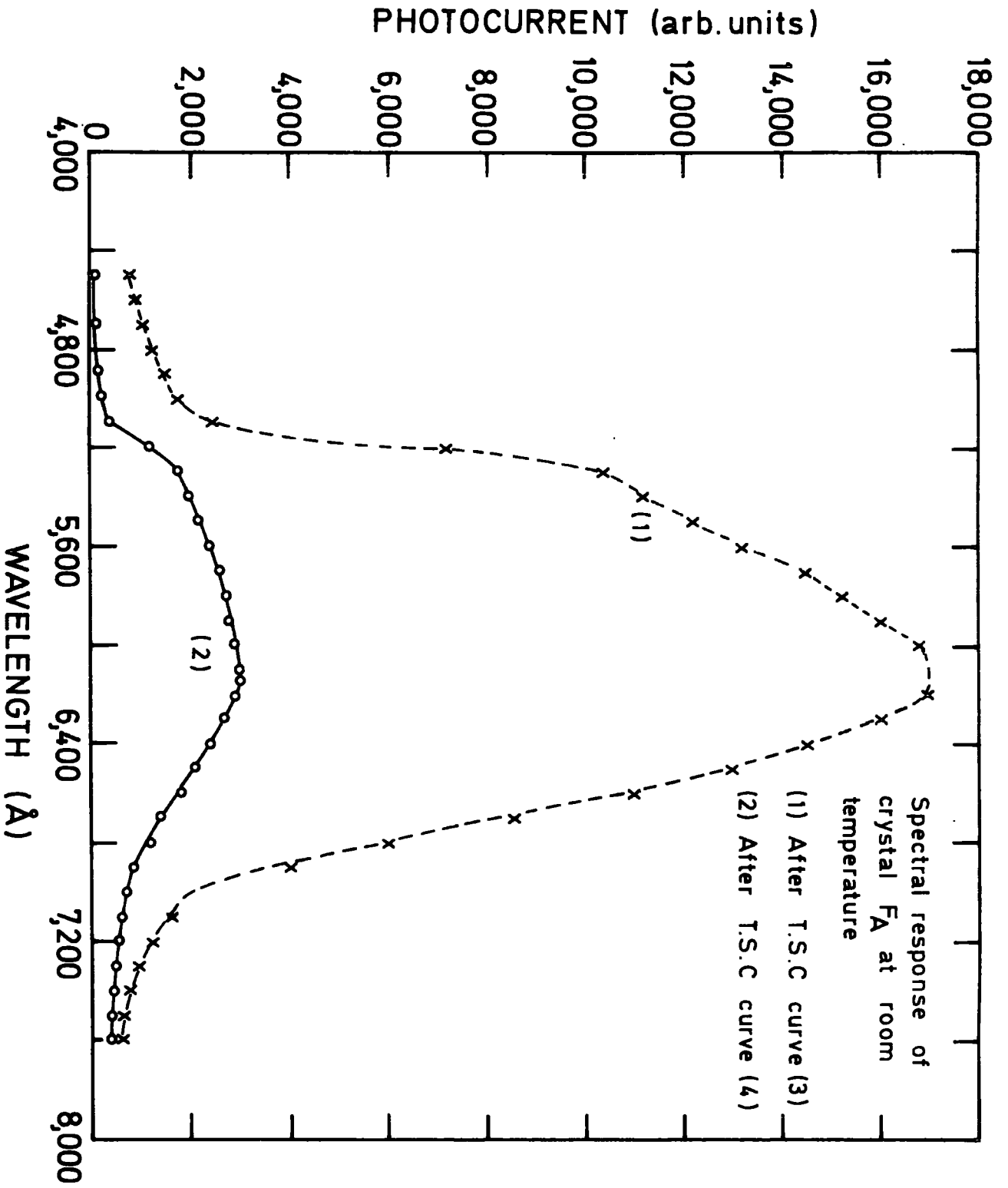


FIG. 5-12



100 - 200<sup>o</sup> K, and deep traps with depths of the order of 0.6 to 0.8 eV, which empty between 280 and 400<sup>o</sup> K. The one hour illumination produces a decrease of over one order of magnitude in the concentration of the shallow traps and a corresponding increase in the density of deep traps. It is worth mentioning that since the thermally stimulated current also depends on the product  $\mu\tau$ , where  $\mu$  is the electron mobility and  $\tau$  is the lifetime, any conclusion about the change in the trap distribution must be drawn after determining that  $\mu\tau$  remains fairly constant and does not play any role in the change in the T.S.C. One way to assess this is to measure the variation of photocurrent, which is also a function of  $\mu\tau$ , with temperature.

It will be shown later that the measurements of the variation of photocurrent with temperature support the conclusion that direct illumination of the sample leads to the change in the distribution of the traps described above. This change is accompanied by a substantial decrease in the magnitude of the photocurrent as shown in Figure 5.13. Curve (1) was measured after the T.S.C. curve (3) and curve (2) after the T.S.C. curve (4) of Figure 5.12.

It is worth mentioning that the T.S.C. curves obtained from the CdS:Cl rods treated in sulphur vapour at 700<sup>o</sup>C for 2 hours did not contain peaks corresponding to deep traps. The effect of light on these samples was to enhance the magnitude of the current associated with the release of electrons from the shallow traps.

### 5.13 Photoconductivity of Boule Crystals

After preliminary investigations of the photoconductivity and photochemical effects in CdS: Cl flow run crystals counter doped with cupric ions, experiments were continued on the CdS:Cl single crystals grown in sealed ampoules. Photoconducting samples were prepared by diffusing cuprous and cupric ions into rectangular bars (5 x 1 x 1 mm<sup>3</sup>) of single crystal CdS containing sufficient chlorine to reduce the resistivity to 1 ohm cm. Bivalent copper was introduced by dipping the bars into an aqueous solution of copper sulphate so

that a surface layer of CuS was formed. The formation of this layer, however, did not take place with the same ease as in the case of the flow run crystals and in fact it was necessary to heat up the solution in order to speed up the reaction. The cupric ions were then diffused into the CdS by heating the samples in sealed ampoules containing argon at  $700^{\circ}\text{C}$  for  $2\frac{1}{2}$  hours. After this treatment the dark resistivity of the bars had risen to about  $10^8$  ohm-cm and a high photoconductive sensitivity had been produced. A similar procedure was used to introduce the cuprous ions, when a layer of  $\text{Cu}_2\text{S}$  was formed on the surface of each bar by dipping it in the solution of cuprous chloride described earlier in this chapter. An identical heating schedule was used to drive the cuprous ions into the bulk of the CdS. The technique of reflection electron diffraction has been used previously in this laboratory (Caswell, et al, 1975) to demonstrate that dipping CdS in a solution of CuCl leads to the formation of a surface layer of chalcocite  $\text{Cu}_2\text{S}$ . We have also described earlier in this chapter that dipping in a solution of  $\text{CuSO}_4$  leads to the production of a layer of covellite CuS.

Ohmic indium contacts were applied to the ends of the bars and the spectral response of photoconductivity was measured by illuminating the bars with light from the exit slit of a Hilger and Watts D.330 grating monochromator. The source employed was a 240 watt quartz halogen projector lamp. The photoconductive properties of CdS:Cl single crystals cut from the boule (611) and doped with bivalent copper ions were similar to those of flow run crystals mentioned earlier. The spectral response of the photoconductivity of a typical sample (103) is shown in curve (a), Figure 5.14. Curve (b) shows the spectral response of the photoconductivity after an intervening period of one hour during which time the sample was illuminated directly with light from the projector lamp. The most obvious feature of the curves in Figure 5.14 is that photosensitivity has fallen by 50 to 60% after as little as one hour's intense illumination. Thermally stimulated curves were also measured over the range

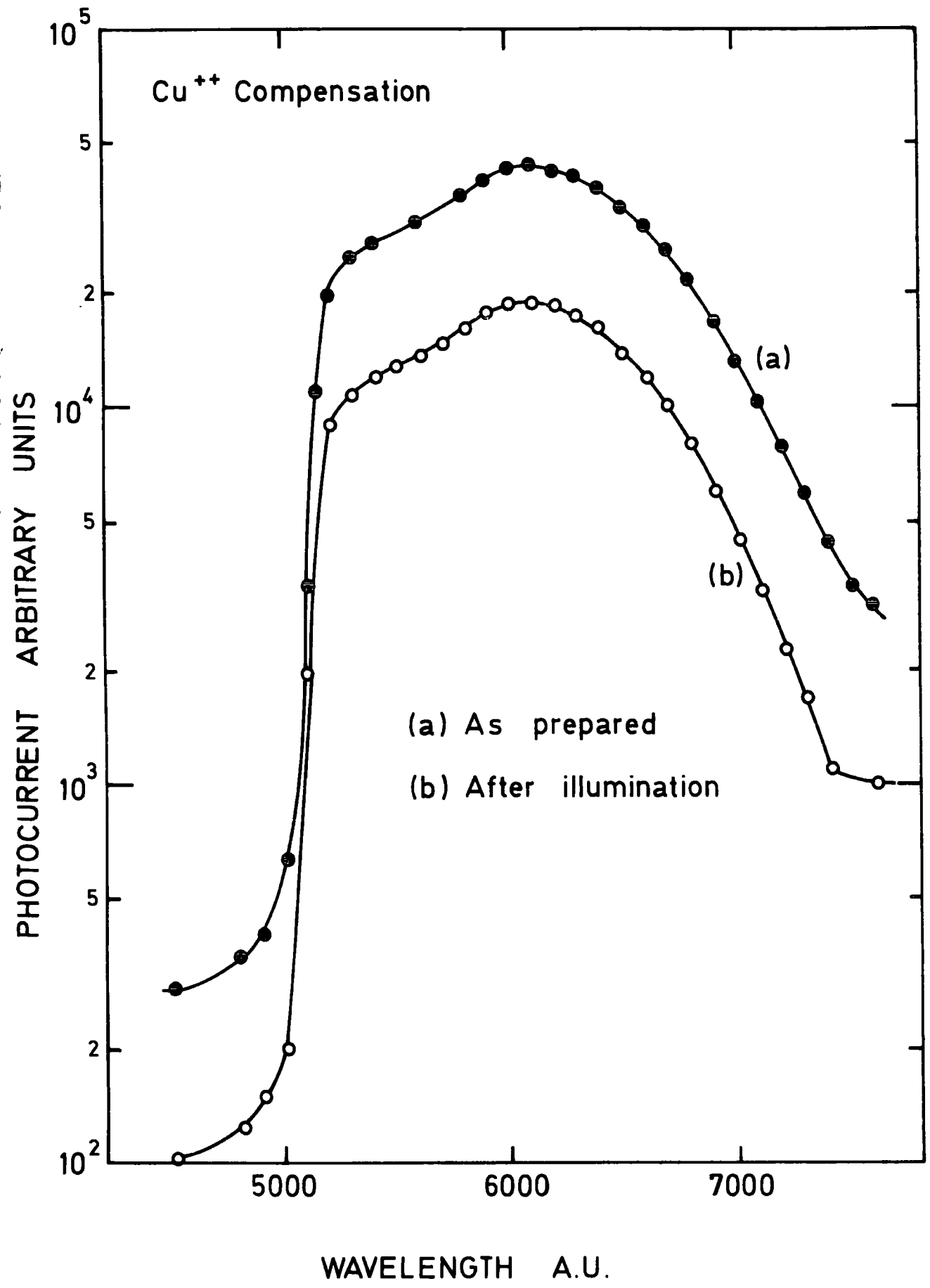


FIG. 5-14

of temperature from 85 to 390° K. The T.S.C. curves for the sample (103) doped with cupric ions are shown in Fig. (5.15). Curve (a) was measured immediately after diffusing in the copper, while curve (b) was measured after one hour's intense illumination. The interesting feature of these curves is that the high initial concentration of shallow traps is reduced by at least three orders of magnitude by the one hour illumination. At the same time the concentration of deep traps is greatly increased.

In contrast to the above observations, the photosensitivity of the samples doped with cuprous ions was increased due to the direct illumination. The spectral response of the photoconductivity of a typical sample (105) counter-doped with monovalent copper is illustrated by curve (a) in Figure (5.16). Curve (b) shows the spectral response of the photoconductivity measured after an intervening period of 6 hours, during which time the sample was illuminated directly with light from the projector lamp. Comparison of curves (a) and (b) shows that the effect of the prolonged intense illumination was to enhance the photosensitivity by roughly 50%. The shapes of the two curves are substantially similar, although it is obvious that the long wavelength threshold became more pronounced after the 6 hour illumination.

Thermally stimulated current curves for the sample (105) doped with cuprous ions are shown in Figure (5.17). Curve (a) was measured immediately after the diffusion process had been completed, and curve (b) after the sample had been illuminated with the intense light for 6 hours.

Since the thermally stimulated conductivity depends on  $n_t$ , the density of the filled traps,  $\mu$  the electron mobility and the majority lifetime  $\tau$ ; any changes in the shape and magnitude of the T.S.C. curves may be attributed to the changes in the trap distribution or in the magnitude of  $\mu\tau$  or both. Fortunately the steady-state photocurrent is proportional to the product  $\mu\tau$ . We have measured the photocurrent of our crystals as a function of temperature,

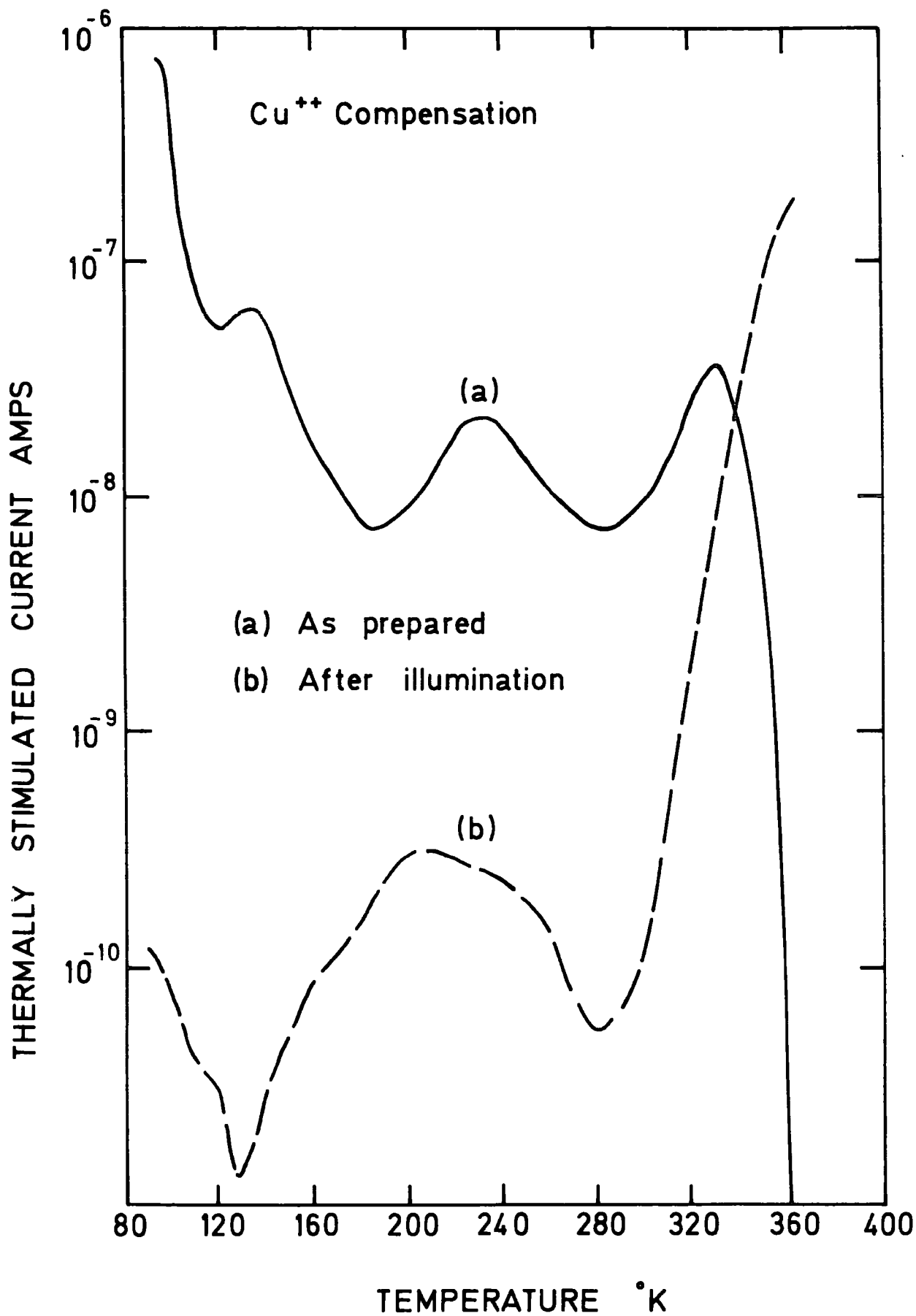


FIG. 5-15

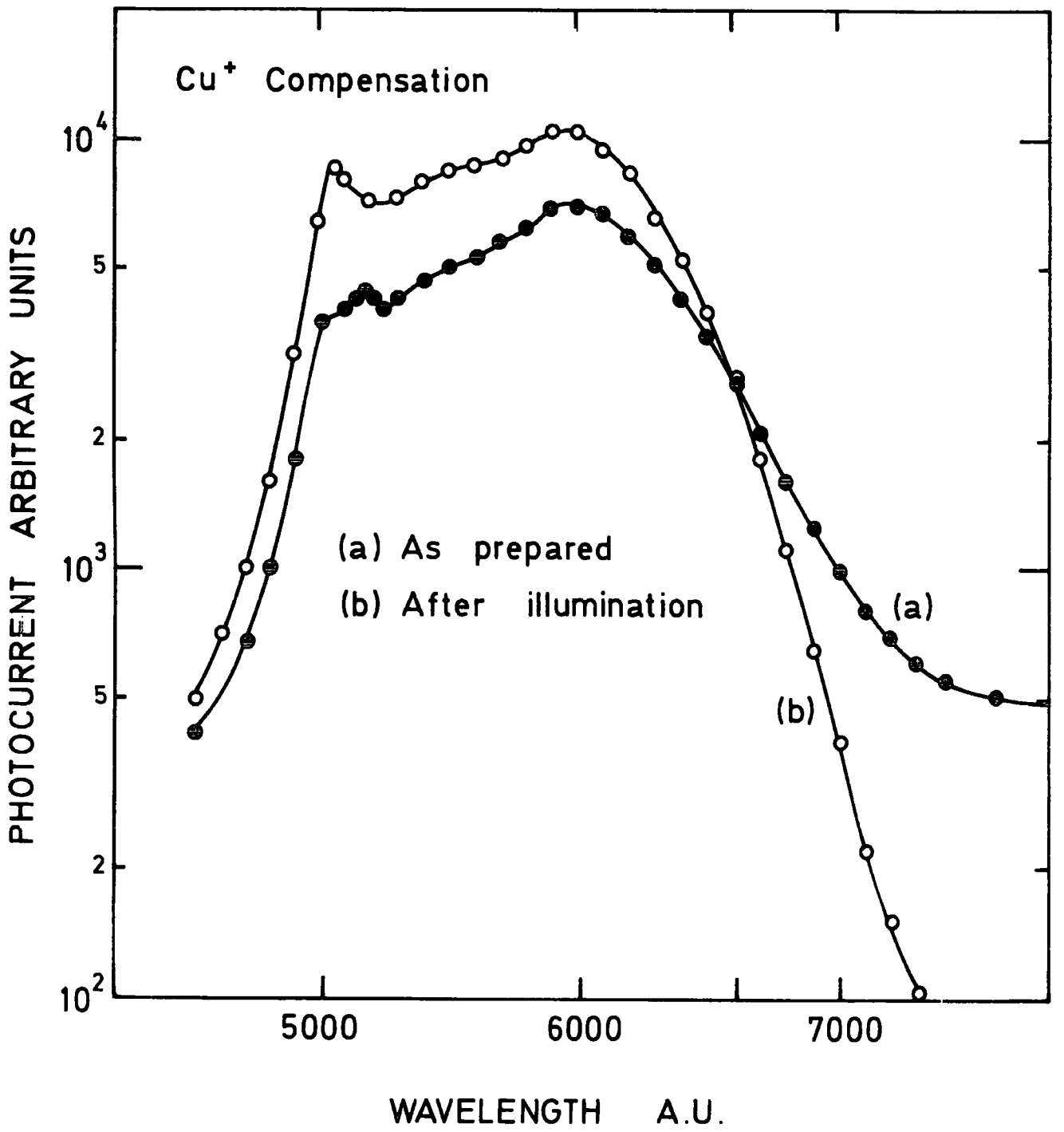


FIG. 5.16

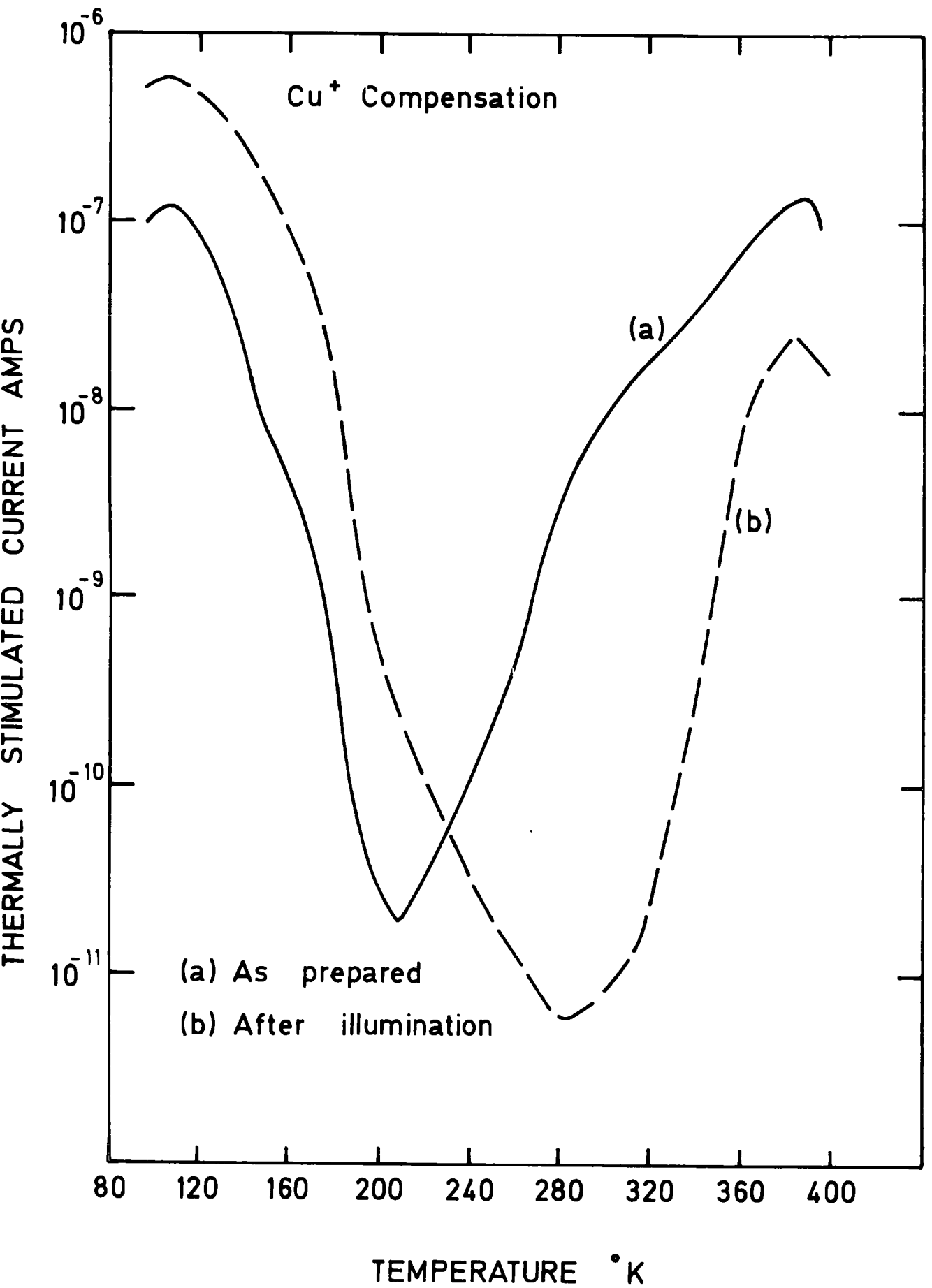


FIG. 5-17

PHOTOCURRENT 100

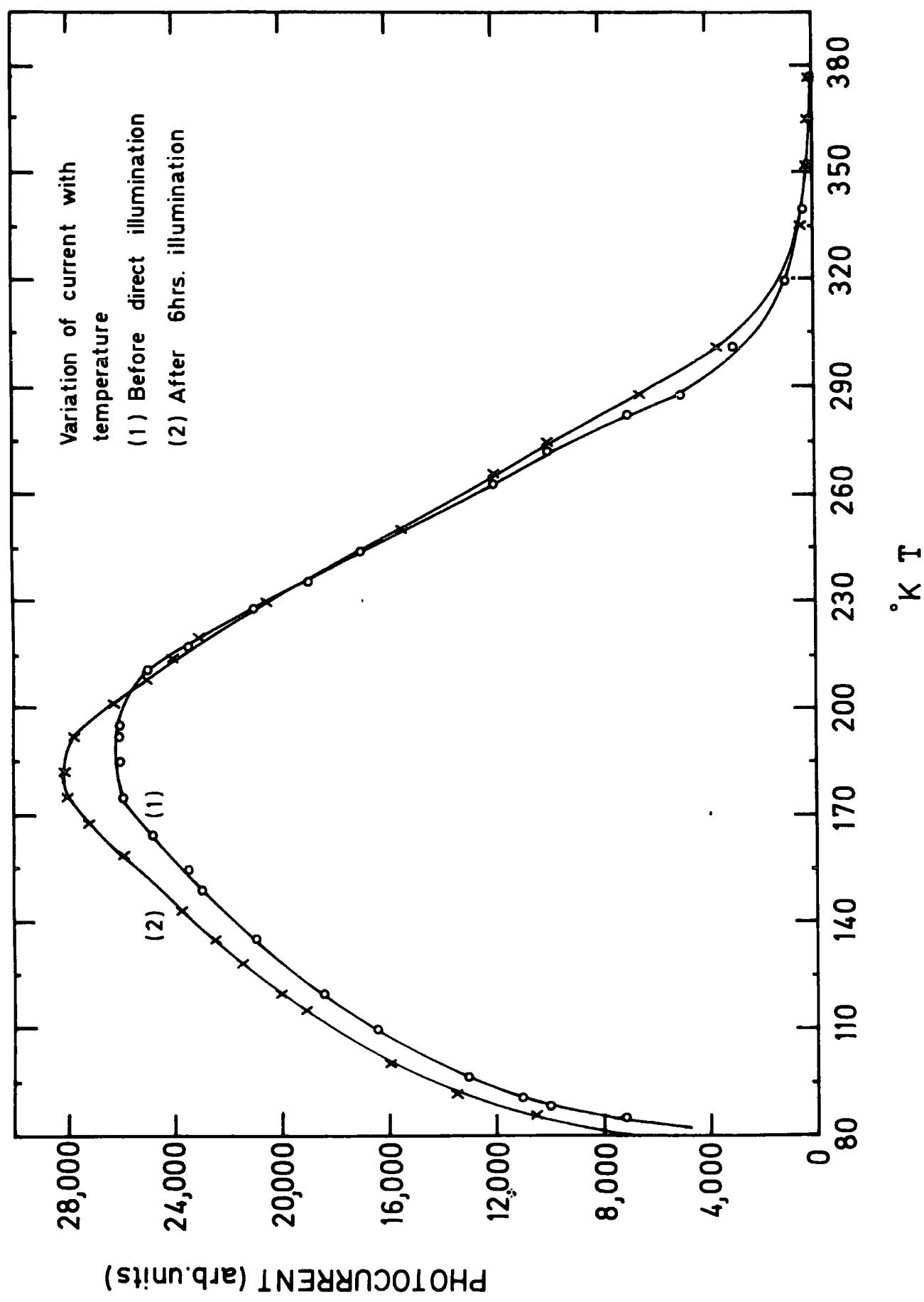


FIG. 5-18

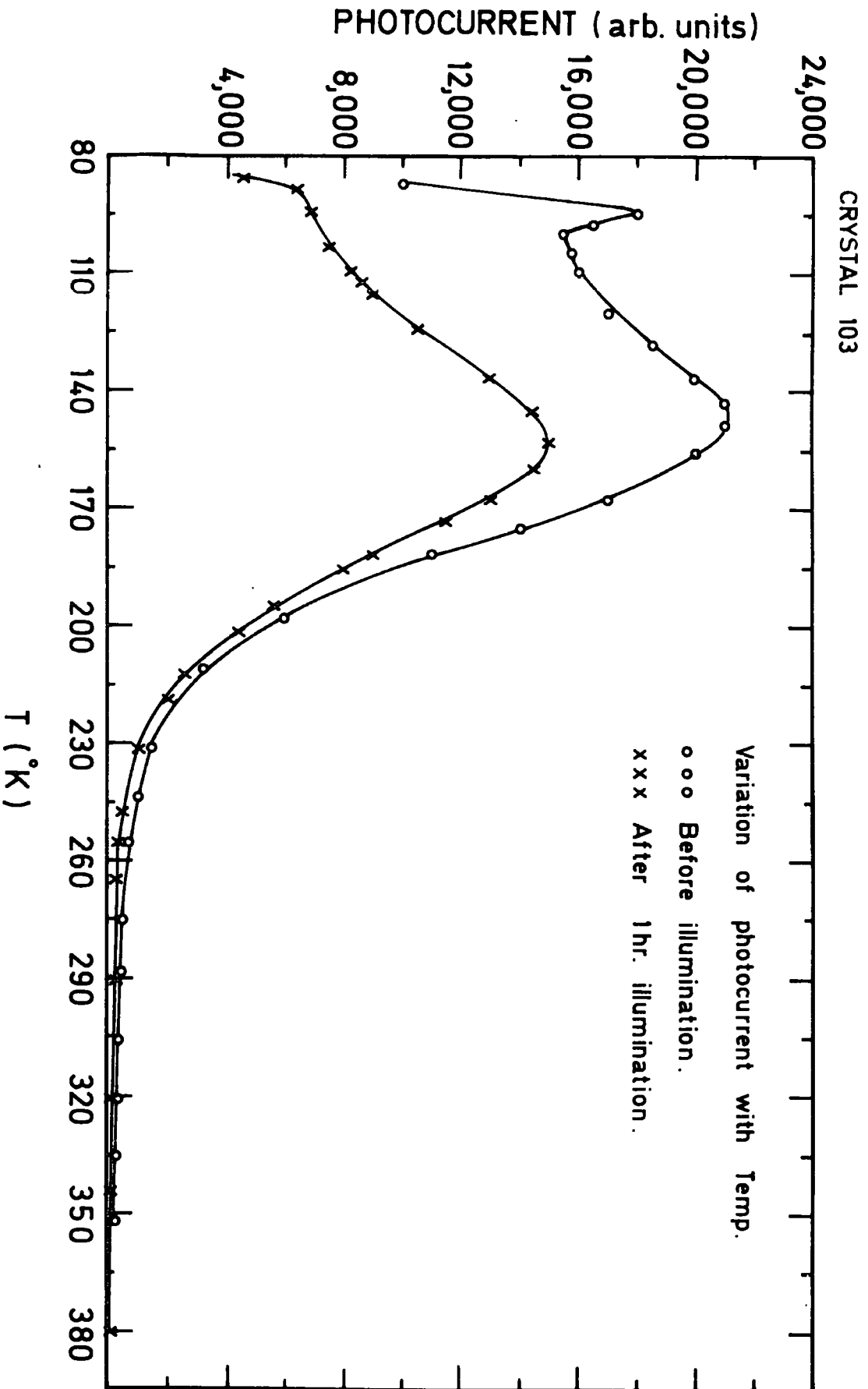


FIG. 5.19

using monochromatic illumination with an intensity some four orders of magnitude less than that provided by the projector lamp which was responsible for the changes in photosensitivity illustrated by the curves in Figures (5.14) and (5.16). With the crystal (105) doped with cuprous ions the photocurrent increased by a factor of three to a broad maximum as the temperature was increased from 85 to 185° K. As the temperature was increased still further to 380° K, the photocurrent decreased steadily. The shape of the curve illustrating the variation of photocurrent with temperature was substantially unchanged following the illumination of the sample with intense light for 6 h. Fig. (5.18). It is possible to conclude therefore that the T.S.C. curves of Fig. (5.17) indicate that the crystal contains two groups of electron traps, i.e. shallow traps with trap depths in the range 0.15 to 0.25 eV which empty over the range 100 to 180 K and deep traps with depths of the order 0.4 to 1.2 eV (see Section 5.14) which empty between 300 and 400° K. The 6 hours illumination produces a threefold increase in the concentration of the shallow traps and a corresponding decrease in the density of deep traps. The photocurrent of the sample (103) doped with cupric ions displayed a broad maximum in the vicinity of 150 K Fig. (5.19). After allowing for the changes in the photosensitivity it is possible to conclude that the high initial concentration of shallow traps in such samples is reduced by at least three orders of magnitude by the one hour illumination. At the same time the concentration of deep traps is greatly increased.

#### 5.14 The Evaluation of the Ionization Energies of the Traps

There are several ways that one can determine the ionization energies of traps. A comparative study of these methods has been made by Nicholas and Woods (1964). To evaluate the trap ionization energies we have used the initial rise method. This method which was first advocated by Garlick and Gibson (1948), is independent of the recombination kinetics. It depends on the fact that when the traps begin to empty as the temperature is raised, the

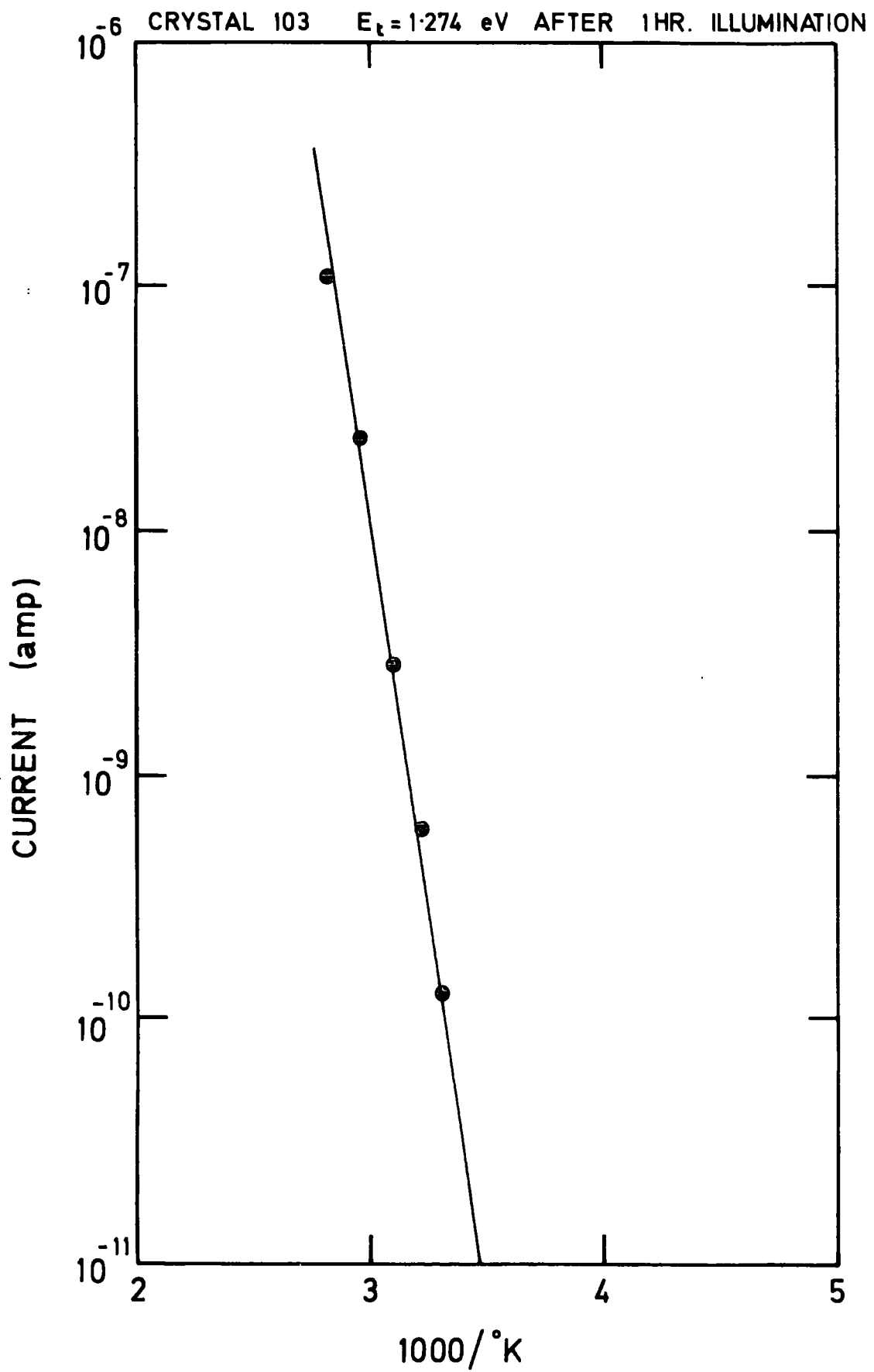


FIG. 5-20

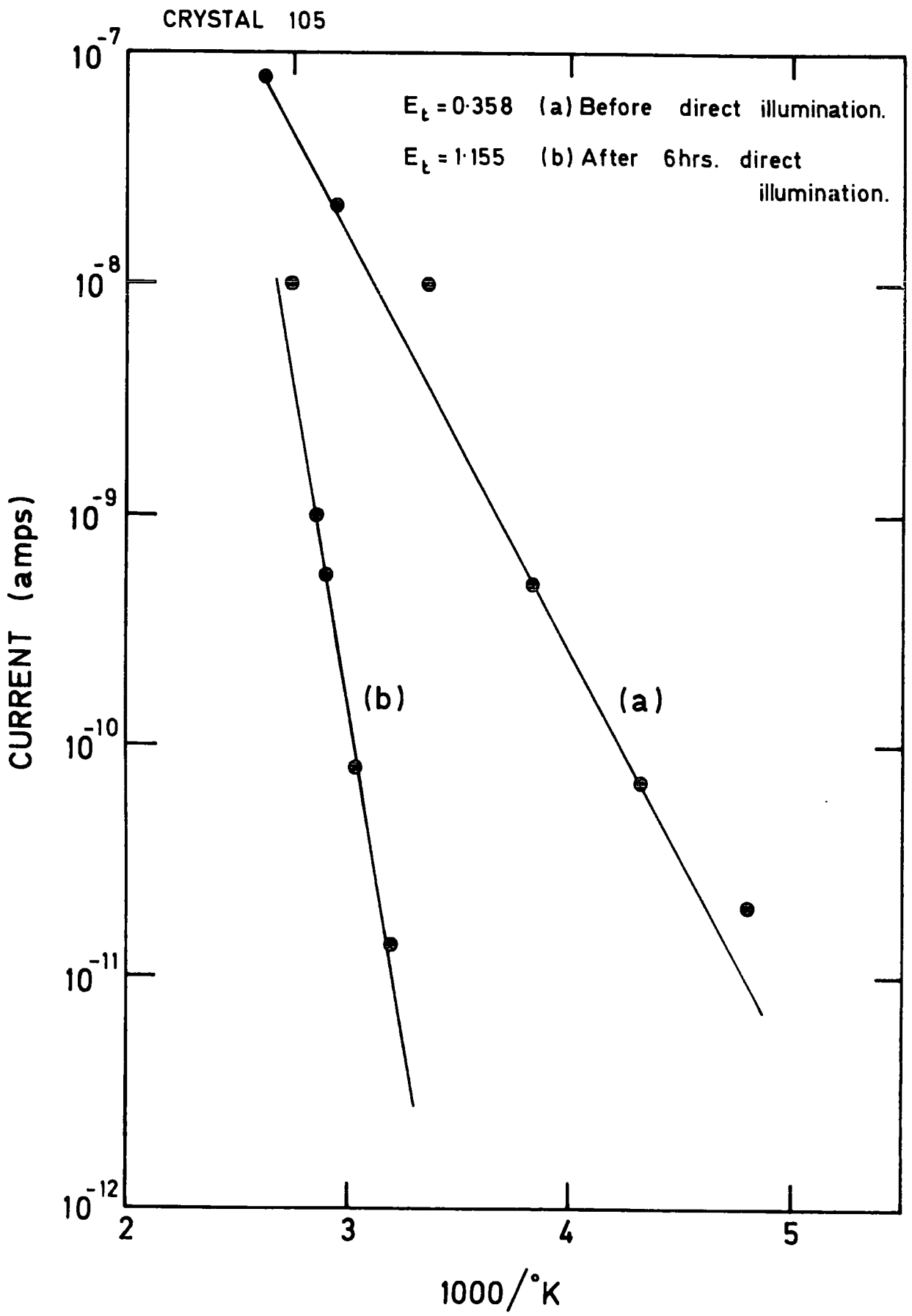


FIG. 5-21

integrals in equations 2.26 and 2.36 are negligibly small and consequently

$$\Delta \sigma = \text{constant} \times \exp \left( \frac{-E_t}{KT} \right) . \quad (5.1)$$

In practice the initial portion of the T.S.C. is measured. A plot of the logarithm of the current flow against  $\frac{1}{T}$  should yield a straight line with a slope of  $-\frac{E_t}{k}$ .

The plots of the logarithm of the initial portion of the T.S.C. versus  $\frac{1}{T}$  of crystal 103 ( $\text{Cu}^{++}$  doped CdS) after 1 hour direct illumination and of crystal 105 ( $\text{Cu}^+$  doped CdS) before and after 6 hours of direct illumination are shown in Figures (5.20) and (5.21). The calculated ionization energies of traps from the slope of the lines indicates that one hour direct illumination of crystal 103 leads to the formation of deep traps with an ionization energy of 1.274 eV and the direct illumination of the crystal 105 for 6 hours causes a change in the ionization energy of the traps from 0.36 eV to 1.155 eV.

### 5.15 Discussion

Photoconductive studies of the CdS:Cl samples counter doped with cupric and cuprous ions show that the incorporation of copper ions with different charge states has a substantial effect on the photoconductive properties, i.e. the photosensitivity of the samples containing bivalent copper ions is unstable and decreases due to the photochemical reaction whereas in samples doped with monovalent copper ions the photosensitivity increases slightly under prolonged illumination. Studies of the T.S.C. curves of these samples reveal that there is a close connection between the distribution of electron traps and the photoconductive performance of the samples. The principal properties of these trapping centres and the characteristic feature of the mechanism of their formation are as follows :-

(1) Illumination of the samples doped with cupric ions results in the formation of deep traps presumably by association of primary simpler defects.

(2) The primary defects are electron-capture centres which exchange carriers with the conduction band and not with the valence band.

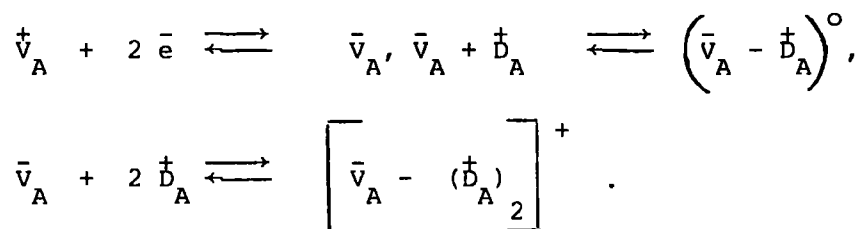
(3) The new trapping centres are formed in the filled state and no additional excitation of crystals at low temperature is required to detect them.

(4) The fact that a decrease in the density of shallow traps is accompanied by a corresponding increase in the density of deep traps suggests that there is a close connection between these two groups of traps.

(5) With the samples doped with cuprous ions, an increase in the density of shallow traps leads to a corresponding decrease in the density of deep traps. This confirms that the charge state of the copper ions has a substantial effect on the type of the photochemical reaction. According to Tscholl (1968), T.S.C. curves with shapes similar to those in Figure 5.15 can be explained in terms of a donor-acceptor pair model. If the separation of the donor and acceptor is large, the energy required for the release of an electron from the trap is relatively small. This corresponds to the T.S.C. peak at  $100^{\circ}$  K. With decreasing separation of the components of the pair, the Coulombic interaction energy becomes larger and more energy is required to eject an electron from the trap to the conduction band in the close presence of a positively charged donor. Thus according to Tscholl, the T.S.C. peak in the vicinity of  $370^{\circ}$  K corresponds to the presence of closely neighbouring donor-acceptor pairs. Considering our experimental results especially the suggestion that there is a close connection between the densities of the shallow and deep trapping centres, we shall assume that the centres under consideration can be described in terms of a model similar to the donor-acceptor pair model in which charged sulphur vacancies are assumed to be a constituent in addition to the copper and chlorine ions. One reason in favour of the choice of a sulphur vacancy as a constituent of the aggregates is that the deep traps were not formed following direct illumination of the samples treated in sulphur vapour at  $700^{\circ}$ C for 2 hours. Comparison of the T.S.C. curves of

CdS (Woods and Nicholas, 1964) and CdSe (Bube and Barton, 1958 ; and Shimizu, 1965) shows that the ionization energy of a common trap (Anion vacancy) is  $E_t = 0.14$  eV. This means that  $\bar{V}_S$  (charged sulphur vacancy) has an energy state near the conduction band. Although it has not yet been proved experimentally that the  $E_t = 0.14$  eV level belongs to the  $\bar{V}_A$  vacancy, this hypothesis has been used successfully by Rezakhanov (1972) in the interpretation of the line spectra of the induced impurity photoconductivity in CdS, CdSe and their solid solutions. According to Rezakhanov, et al (1975) the centres responsible for the photochemical reactions in CdS can be described by dimers like  $(\bar{V}_S - \overset{\dagger}{D}_A)^0$  and Trimers like  $\left[ \bar{V}_S - (\overset{\dagger}{D}_A)_2 \right]^+$  where  $\overset{\dagger}{D}_A$  is the ionized donor at the anion site. They have satisfactorily used the expression  $E_t + \frac{e^2}{\epsilon r_{nm}}$  for dimers and  $E_t + \frac{2e^2}{\epsilon r_{nm}}$  for trimers to describe the position in energy of these centres in the forbidden gap. Here  $r_{nm}$  is the distance between  $V_A$  and  $D_A$  centres.

The mechanism postulated to account for the photochemical reaction is that initially there are  $\overset{\dagger}{V}_A$  and  $\overset{\dagger}{D}_A$  centres. When nonequilibrium carriers (electrons) are generated the vacancies become charged and associates are formed from the  $\overset{\dagger}{V}_A$  and  $\overset{\dagger}{D}_A$  centres under the influence of coulombic attraction. It is also likely that the charging of the vacancies  $V_A$  increases their diffusion coefficient. The reactions which occur can be described as follows :



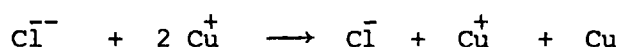
Studies of the effect of photochemical reactions on the photoluminescence spectra of the Cu-doped CdS crystals (Korsunskaya, et al 1973) show that the reduction in photosensitivity of these crystals is accompanied by an increased

intensity of the 1.6 - 2.2  $\mu\text{m}$  luminescence band and by the transformation of the 1.03  $\mu\text{m}$  band into a band at 1.06  $\mu$ . Similar effects, i.e. the increase in the intensity of 1.02, 1.57 and 1.87  $\mu\text{m}$  bands and the corresponding decrease in the intensity of the 0.71 - 0.78 bands accompanying the photochemical reaction have been reported by Patil and Woods (1971). Both groups consider the role of copper for the interpretation of their results. According to Korsunskaya, et al, the change in the luminescence spectrum is due to the formation during the photochemical reaction of two types of recombination centres : fast S centres corresponding to 1.6 - 2.2  $\mu\text{m}$  band and slow r' centres corresponding to 1.06  $\mu\text{m}$  band which both contain copper atoms. While according to (Patil and Woods, 1971) the centre responsible for the 1.02, 1.57 and 1.87  $\mu\text{m}$  emission bands is either a substitutional copper ion or a complex association of copper ions and Cd vacancies. We have already mentioned the reasons in favour of the choice of sulphur vacancies as a constituent of the aggregates. We assume, following earlier work by Woods (1958) and Woods and Wright (1958), that the presence of a high concentration of sulphur vacancies is accompanied by a high rate of degradation of the photoconductive sensitivity under continuous illumination. Thus for example crystals made photoconducting by heating in a low pressure of cadmium vapour contain sulphur vacancies and are unstable. In contrast, crystals doped with chlorine and heated in sulphur vapour to compensate the chlorine donors with cadmium vacancies contain few sulphur vacancies and are stable. In addition, since there is a substantial difference between the T.S.C. curves of the samples doped with monovalent and divalent copper ions, the other components of the aggregates must somehow include the presence of these impurities.

In our experiments to compare the compensating effects of cuprous and cupric ions the inward diffusion process was carried out by heating at 700°C in argon. This constitutes a chemically reducing condition so that sulphur vacancies would be produced as the diffusion proceeded. With cupric

ions the filled chlorine donors  $\text{Cl}^{\bar{\bar{-}}}$  (this is simply a  $\text{Cl}^-$  ion plus an electron bound in a relatively large "orbit" of hydrogen type embracing many of the neighbouring atoms of the crystal) would be compensated by the diffusing  $\text{Cu}^{++}$  leaving empty donors  $\text{Cl}^-$  and filled acceptors  $\text{Cu}^+$ . This, of course, is a good charge compensation situation. The sulphur vacancies would also be compensated by the cupric ions so that the crystal would contain  $\text{Cu}^+$ ,  $\text{Cl}^-$  and  $\bar{V}_A$  centres. As a working hypothesis one might suppose that the isolated  $\text{Cl}^-$  and  $\bar{V}_A$  centres would act as shallow traps. (In the nomenclature used here  $\text{Cl}^-$  and  $\bar{V}_A$  represent filled traps; in the unfilled condition they would be represented as  $\text{Cl}$  and  $V_A$ ). Under illumination the presence of sulphur vacancies leads to a loss of photosensitivity and the formation of deep traps as the point defects tend to aggregate. This argument requires that the acceptor having captured a photoionized hole, i.e.  $\text{Cu}^{++}$ , must have an effective positive charge whereas somewhat similarly the filled electron trap  $\bar{V}_A$  must have an effective negative charge in order that there will be a coulombic attraction between those point defects when the crystal is illuminated.

In the contrasting situation when compensation is effected with two cuprous ions,  $2 \text{Cu}^+$ , the ionizable electron of the filled  $\text{Cl}^{\bar{\bar{-}}}$  donor is compensated by one of the cuprous ions in a reaction which can be written



Since the diffusion of cuprous ion was also carried out under reducing conditions, sulphur vacancies would have been formed. However, experiment shows that the photoconductive sensitivity is maintained under prolonged illumination and deep traps are not formed. Our working hypothesis would require then that the sulphur vacancies were immobilised in some way. This might happen if the  $\text{Cu}^+$  ions in the reaction above were accommodated on substitutional sites while the  $\text{Cu}$  atoms were occupying interstitial sites

immediately adjacent to the sulphur vacancies and locked to them. Such a suggestion requires that the negatively charged Cu atoms are strongly bound to the empty positively charged sulphur vacancies.

## CHAPTER SIX

### SOME ELECTRICAL & OPTICAL PROPERTIES OF

#### Au-CdS DIODES

##### 6.1 Introduction

Electrical and optical properties of CdS diodes made mainly with one gold contact and one ohmic contact have been investigated fairly extensively. The devices were made from CdS single crystals as described in Chapter 4. Those devices which were made primarily from high resistivity material did not show Schottky barrier characteristics. Although the measurement of the short circuit photocurrent of these devices supported the existence of a potential barrier between the metal and the semiconductor, the low donor density of these samples meant that they were not suitable for the measurement of C-V characteristics. With the samples of suitable donor density however, photoresponse measurements have been made and used to determine barrier heights. The uncompensated donor density was determined from the capacitance-voltage measurements. The discrepancy between the values of barrier height obtained from the two different methods (i.e. the short circuit photoresponse and the intercept of the C-V plot) was used to calculate the thickness of the semi-insulating film present between the gold and the CdS. Conductance-voltage characteristics have also been measured on a few samples and the current-voltage characteristics have been investigated in both forward and reverse directions. Finally photocapacitance measurements were carried out for a few samples at room temperature.

##### 6.2 Device Preparation

Most of the devices were prepared by depositing a film of pure gold on to the etched surface of a CdS cube (see Chapter 4). Prior to the deposition of the gold, an indium ohmic contact had been applied to

the sample. In addition to gold, a few devices were made using other suitable metals such as copper and silver. Although the CdS samples which were used for the fabrication of these devices had relatively high resistivities, it was possible to measure their short circuit photocurrent and therefore to determine the photocurrent thresholds corresponding to these metal-semiconductor contacts. The values of photothreshold obtained were generally greater than those made of CdS samples with higher donor densities.

### 6.3 Photoresponse Measurements

Shortcircuit photocurrent measurements were carried out on devices made from CdS samples of various conductivity using different metal contacts. The technique has been described in Chapter 4. (Section 4.2.4). Devices were usually illuminated through the thin layer of the metal contact. (Front illumination) and the shortcircuit photocurrent was measured over the wavelength range from 0.4 to 3  $\mu\text{m}$ . With devices carrying gold contacts, the variation of the wavelength over the range from 0.4 to 2  $\mu\text{m}$  was adequate. The measurements were made both at room and liquid nitrogen temperatures.

### 6.4 Photoresponse of the High Resistivity Samples

Metal-semiconductor devices were prepared by the deposition of gold, silver or copper on to one face of the CdS chips cut from boule No.613. The resistivity of these CdS chips was of the order of  $10^6 \Omega\text{-cm}$ . To test the effect of the different metal contacts the same CdS sample was used for the fabrication of the subsequent devices. Prior to the deposition of a new contact, the device was etched in Conc.HCl in order to remove the old contact for which photoresponse measurements had already been carried out.

A typical curve showing the shortcircuit photoresponse of the device 613 A1 (CdS with gold contact) is shown in Figure 6.1. In addition to the large peak at the band gap of CdS the curve shows a maximum in the

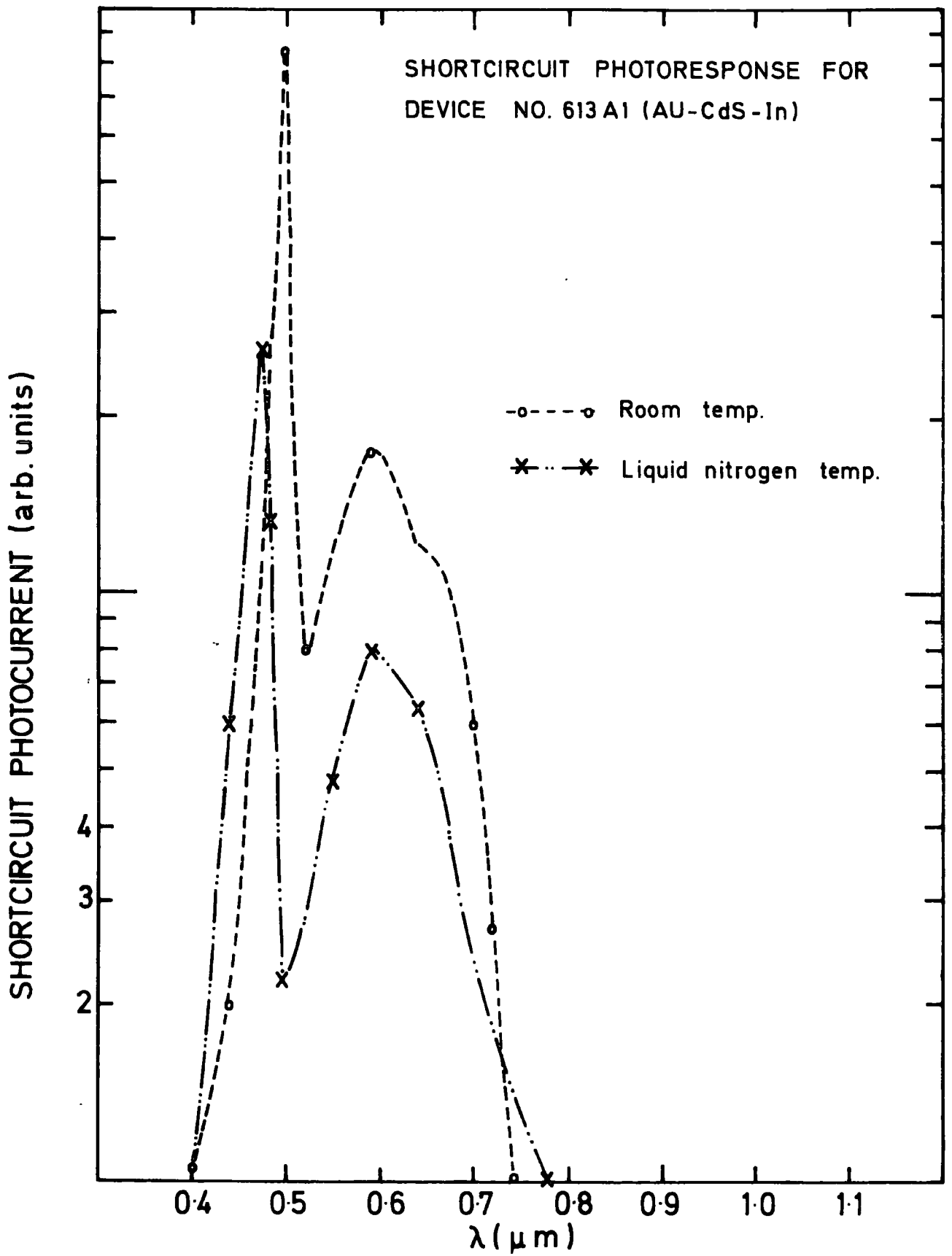


FIG. 6.1

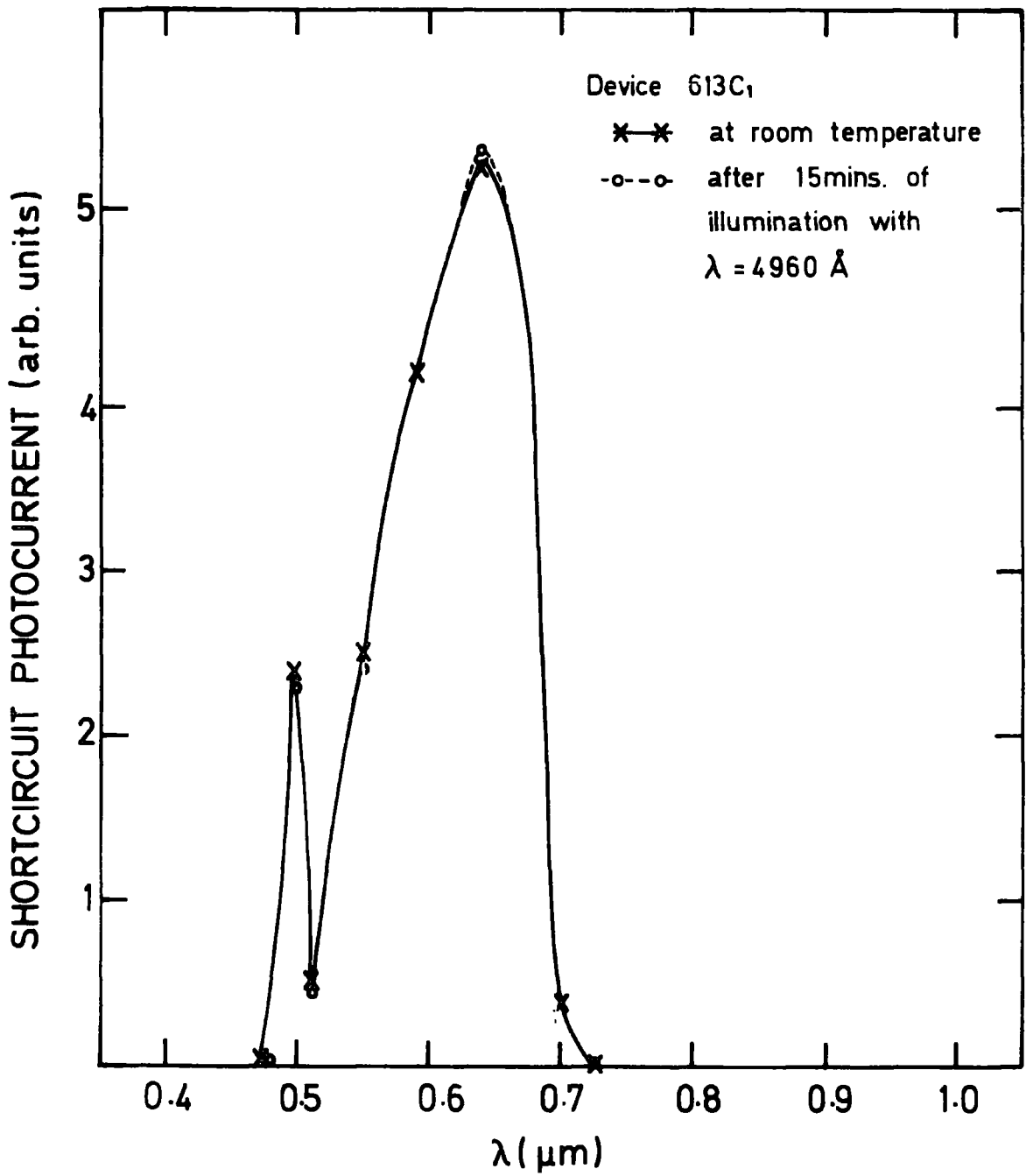
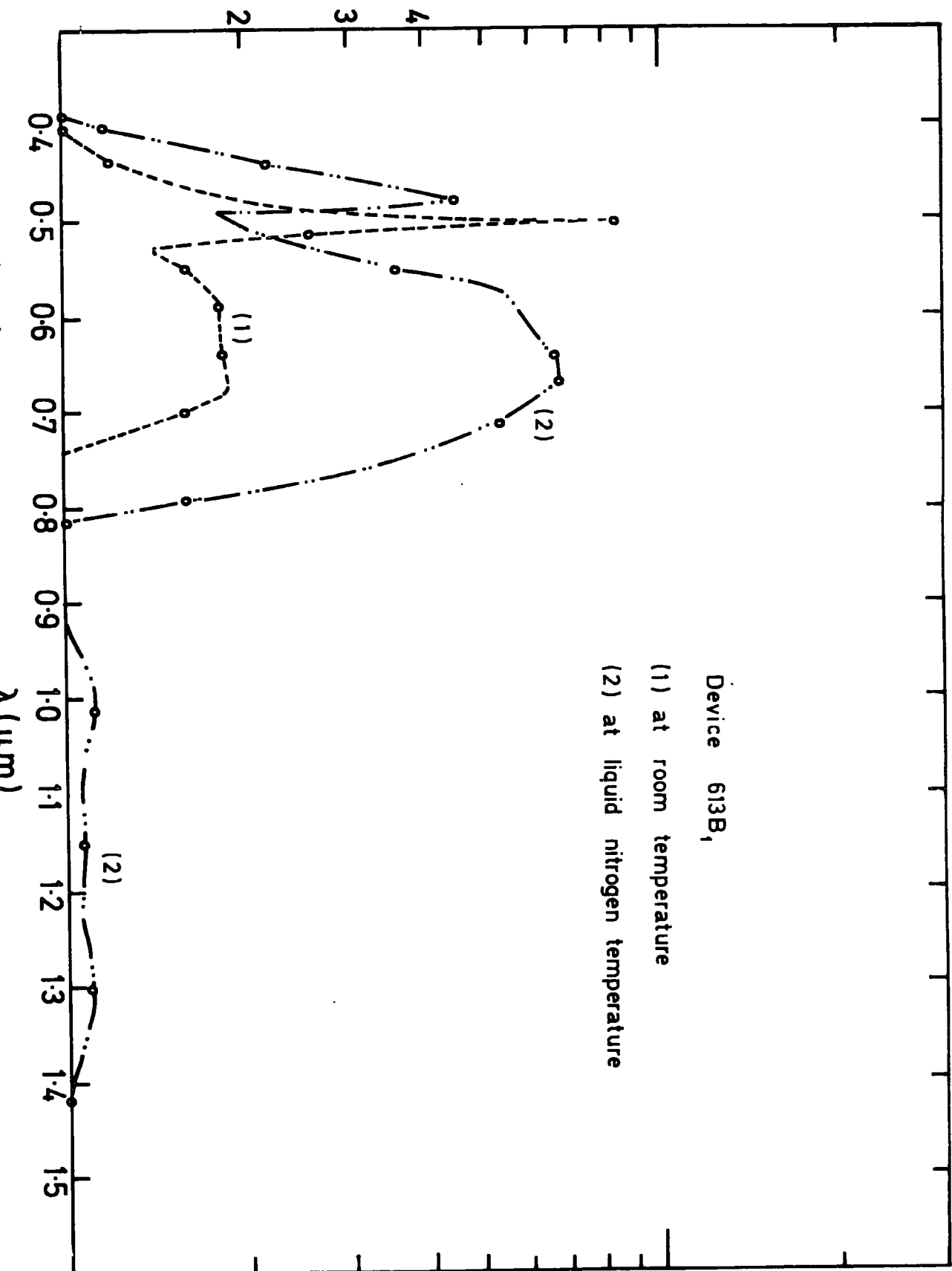


FIG. 6.2

SHORTCIRCUIT PHOTOCURRENT (arb. units)



Device 613B<sub>1</sub>

(1) at room temperature

(2) at liquid nitrogen temperature

extrinsic region at  $\lambda = 5900 \text{ \AA}$  and a shoulder at  $\lambda = 6400 \text{ \AA}$ . With the device 613 C1 (CdS with copper contact) however, the situation in the extrinsic region was reversed with the maximum now at  $\lambda = 6400 \text{ \AA}$  and the shoulder at  $\lambda = 5900 \text{ \AA}$  Figure 6.2. The major difference in the short-circuit photoresponse of device 613 C1 compared with that of 613 A1 and 613 B1 (Figure 6.3, CdS with silver contact) was that with 613 C1; the impurity excitation dominated the band gap excitation whereas the reverse was true for the devices made with gold or silver contacts. The reason is that the diffusion of copper into the semiconductor gives rise to the enhancement of the impurity excitation and suppression of the band gap excitation. This is in agreement with what was observed during the measurement of the photoconductive properties of Cu-doped CdS samples in which copper was introduced by dipping them in copper sulphate solutions with different concentrations (Chapter 5).

#### 6.5 The Effect of Illumination

To test the effect of light on diodes with non-ohmic contacts, the device 613 C1 (CdS with Cu contact) was mounted in a cryostat and cooled to liquid nitrogen temperature ; it was then illuminated with light of wavelength  $\lambda = 4930 \text{ \AA}$  (band gap illumination) for 15 minutes. Figure 6.4 shows the shortcircuit photoresponse of the device before and after illumination. Enhancement of the photocurrent associated with the impurity excitation has resulted from the illumination. For devices made from boule No. 623 in which copper impurity was introduced during the growth, however, the effect of illumination was to reduce the photocurrent associated with the impurity excitation. Figure 6.5 shows the shortcircuit photocurrent response of device 623 A.

#### 6.6 Importance of Sample Resistivity

Measurements of the shortcircuit photocurrent of the devices made

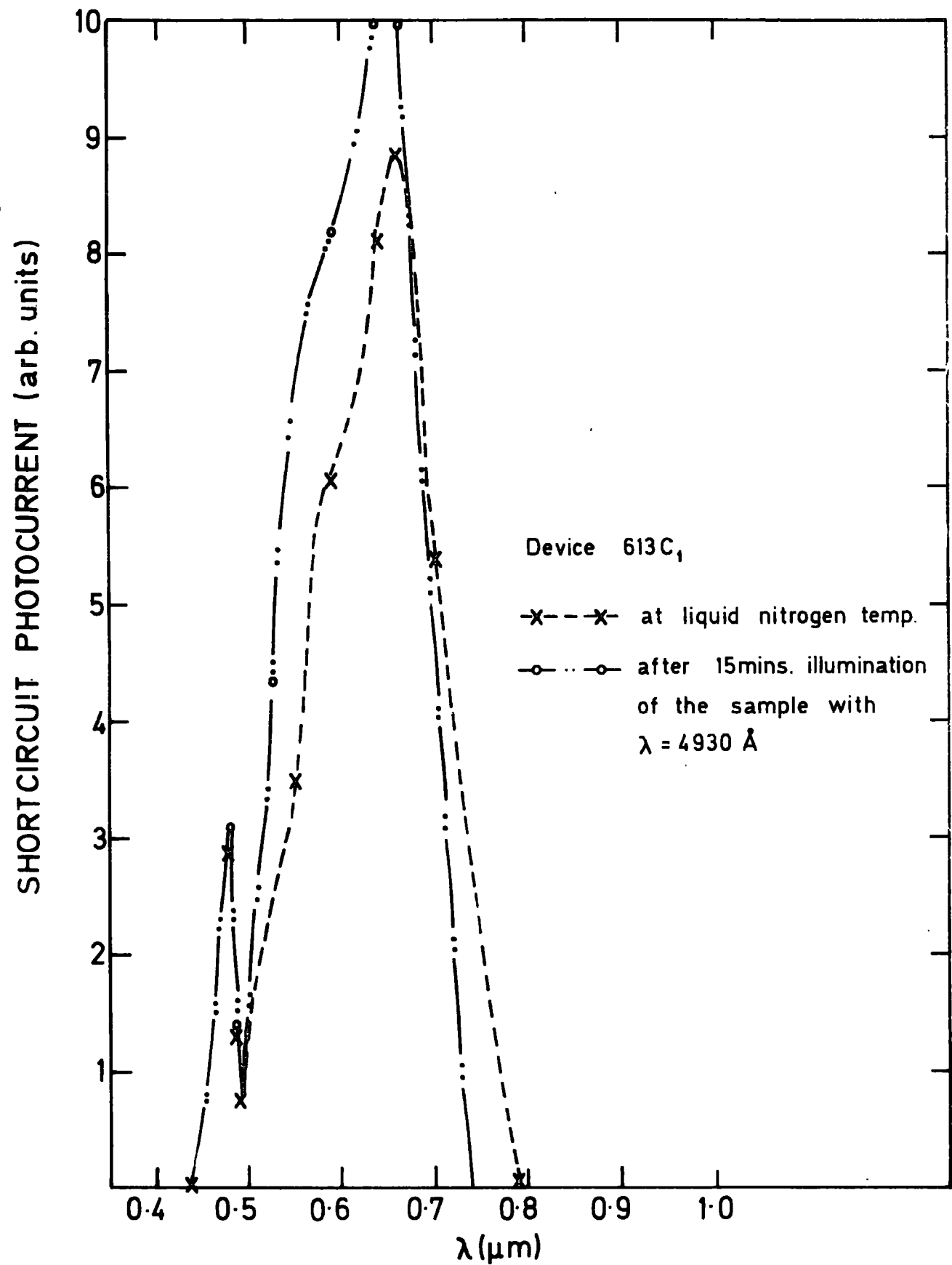


FIG. 6.4.

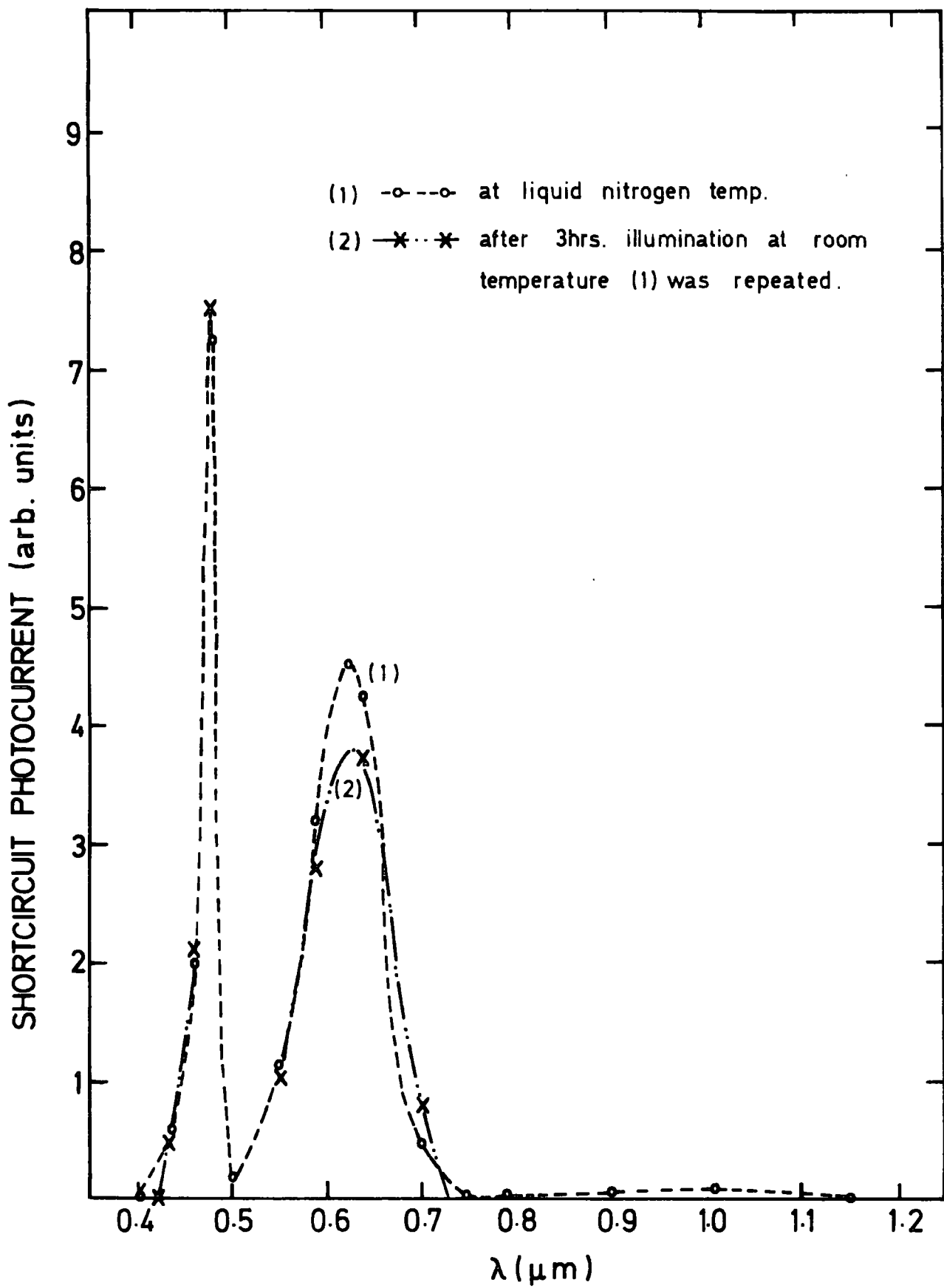


FIG. 6.5

from boules 613 and 623 confirmed that the resistivity of a sample has a great effect on the behaviour of a metal-semiconductor device. For a CdS substrate of resistivity,  $2 \times 10^6 \Omega \text{ cm}$ , the calculation of the depletion width from equation 2.43 gives the value of  $2.69 \times 10^{-2} \text{ cm}$ . For such a low conductivity sample, the image force shifts the maximum of the potential barrier far inside the semiconductor and photoexcited electrons in the metal will thermalize before reaching the potential barrier maximum. It is, therefore, of little surprise to find that the long wavelength threshold of the photocurrent of these devices is not a measure of the barrier height of the corresponding metal contact to the CdS.

In order to make a proper Schottky diode in which electrons can be photoemitted from the metal to the semiconductor, CdS samples of lower resistivity were prepared by diffusing cadmium into samples of high resistivity and sulphur into conductive ones. In addition to heating the conductive samples in an excess pressure of sulphur, sometimes it was found adequate to heat the samples in vacuum at the temperature of  $1000^\circ \text{ C}$  for various periods of 1-72 hours to increase their resistivity.

#### 6.7 Photoresponse of Au-CdS Devices

Bearing in mind the importance of the resistivity of the semiconductor in the fabrication of a metal-semiconductor device, samples from boule 623 were heated in molten cadmium at  $600^\circ \text{ C}$  for 3 days (see Chapter 3). This reduced the resistivity from a value of  $3.8 \times 10^9 \Omega\text{-cm}$  to  $\rho = 0.12 \Omega\text{-cm}$ . Treatments of this kind, even for a period of 3 hours, caused a drastic reduction in the sample's resistivity. To maintain a better control over the resistivity, samples were baked in cadmium vapour for a period of 20 hours, (see Chapter 3).

Device 623A was made from samples treated in this way, by applying an indium contact to one side of the cube and an evaporated gold contact to



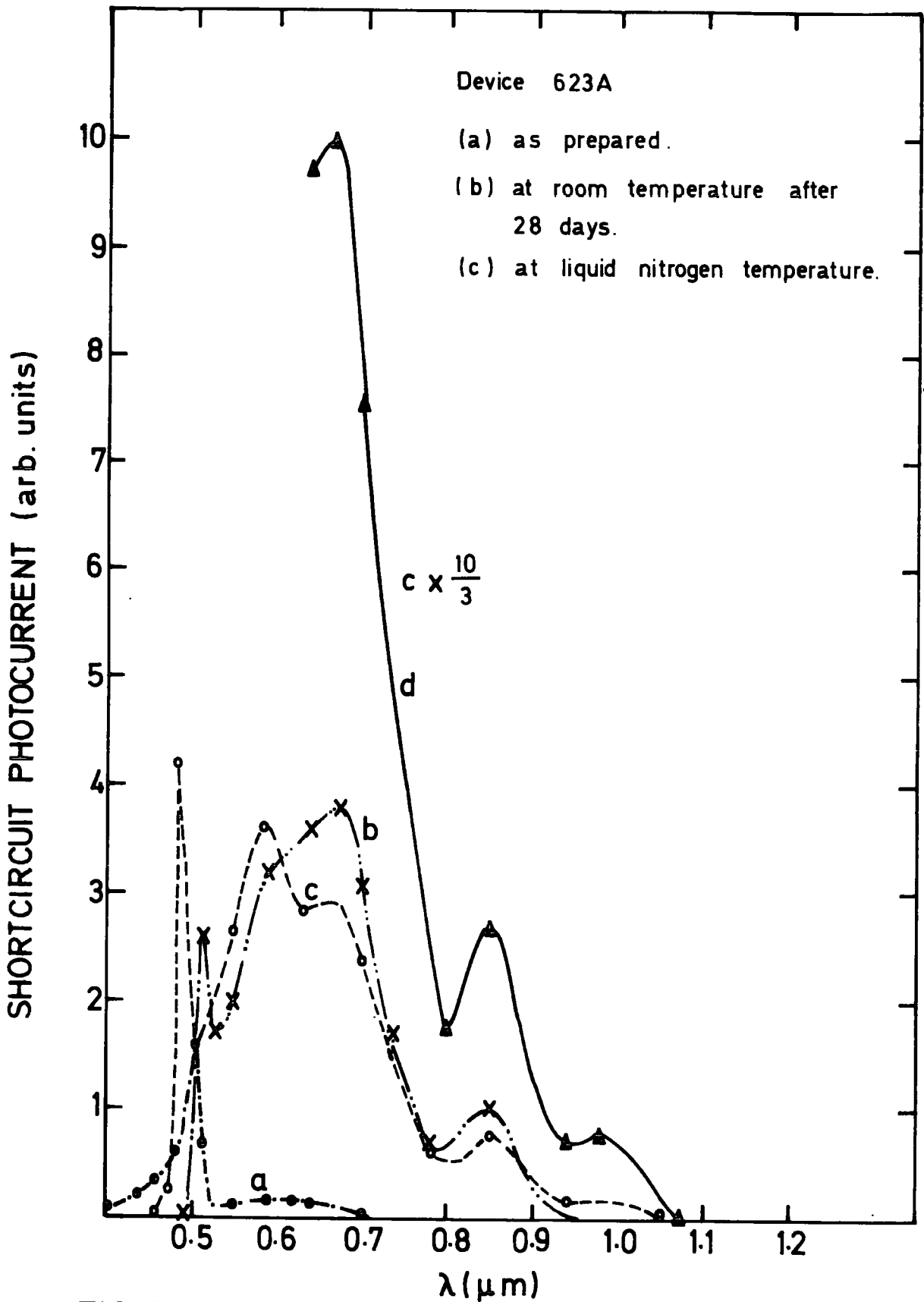


FIG. 6.6

the other. Figure 6.6 (a) displays the shortcircuit photoresponse of the device immediately after it was made. Curves (b) and (c) are the photoresponse of the same device after the lapse of a period of 28 days, at room and liquid nitrogen temperatures respectively. The curve (d) is the same as the curve (c) which has been magnified by a factor of  $\frac{10}{3}$ .

Interesting features of the photoresponse of this device, which was made from a cadmium vapour treated Cds:cu sample, are as follows :

1) The shortcircuit photocurrent response of the device has a long tail in the short wavelength region with the threshold at  $0.396 \mu\text{m}$  equivalent to  $3.13 \text{ eV}$ .

The significance of the short wavelength threshold lies in the fact that it is sensitive to changes in the surface recombination velocity of the device. As the properties of the surface change the surface trap and recombination parameters change and affect the short wavelength photoresponse of the device.

2) Because of the introduction of Cd atoms in the crystal (self diffusion), there is a shift in the band gap excitation of the device towards higher energy values. The band gap excitation peak occurs at  $\lambda = 0.504 \mu\text{m}$  equivalent to  $2.46 \text{ eV}$ , instead of  $2.40 \text{ eV}$  for the untreated samples.

3) Subsequent measurements of photocurrent response, curves (b) and (c), show that the shift of the band gap towards higher energy values is not a stable state. A 20-fold increase in the shortcircuit photocurrent of the device in the extrinsic region and about 2-fold increase in the band gap region are indicative of the presence of a higher electric field established in the device due to ageing. In addition, the shift in the short wavelength threshold of the photocurrent response from  $0.396 \mu\text{m}$

(3.13 eV) to  $0.49 \mu\text{m}$  (2.53 eV) which is associated with the above mentioned increase in the shortcircuit photocurrent of the device supports the idea of the migration to the surface of the diffusion in Cd atoms and the formation of an oxide layer (CdO) between the metal and the semiconductor.

4) Apart from the band gap excitation, curves (b) and (c) display several peaks which occur at  $0.59 \mu\text{m}$  (2.1 eV),  $0.67 \mu\text{m}$  (1.85 eV),  $0.85 \mu\text{m}$  (1.46 eV) and  $0.98 \mu\text{m}$  (1.26 eV) respectively.

The photothreshold energy which is at 1.28 eV ( $0.96 \mu\text{m}$ ) at room temperature reduces to the lower energy of 1.18 eV at liquid nitrogen temperature.

Attempts to prepare devices from CdS chips of suitable resistivity were continued and device 626 B was prepared from the cut samples of boule no. 626 (CdS: Cl : Cu) which had been heated at vacuum at  $1000^{\circ}\text{C}$  for a period of 1.5 hours.

The photoresponse of device 626 B and of the device 611 A are shown in Figures 6.7 and 6.8 respectively. The photocurrent at the lower photon energies is associated with the photoelectric emission from the gold into CdS and the low energy threshold is a measure of the barrier height  $\phi_{\text{BN}}$ . For the accurate determination of the barrier height, however, the square root of the photocurrent was plotted against photon energy in the vicinity of the threshold. Good straight lines were obtained and the barrier heights  $\phi_{\text{BN}}$  could then readily be determined from the intercepts. In this way, the barrier height of gold contact to CdS obtained from device 626 B (CdS: Cl: Cu) is  $\phi_{\text{BN}} \approx 0.742 \pm 0.01$  and from the device 611 A (CdS: Cl) is  $\phi_{\text{BN}} \approx 0.77 \pm 0.01$ . Prior to the gold deposition, both devices were etched in Conc. HCl.

The difference in the shape of the curves of Figures 6.7 and 6.8

626B ROOM TEMPERATURE

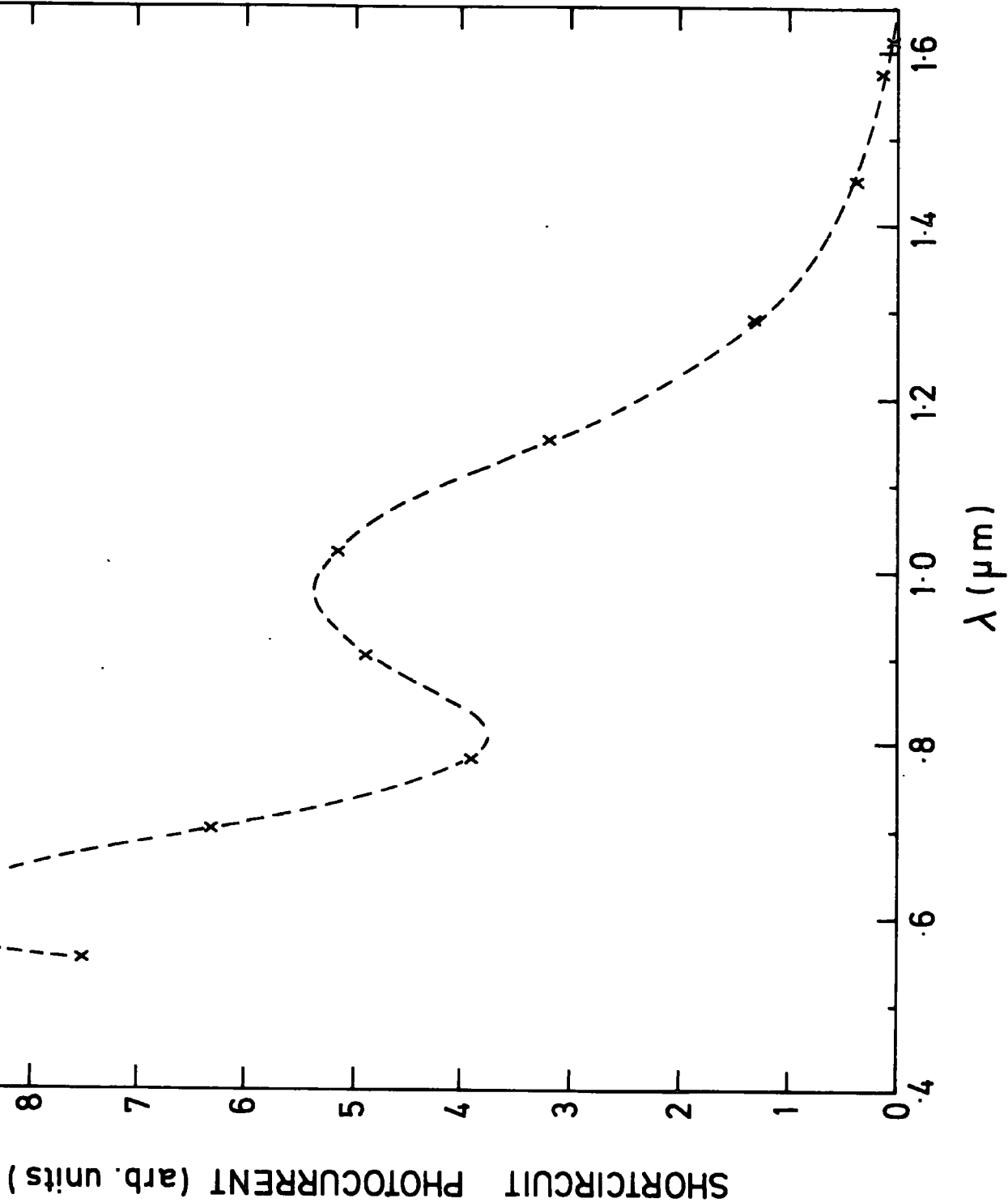
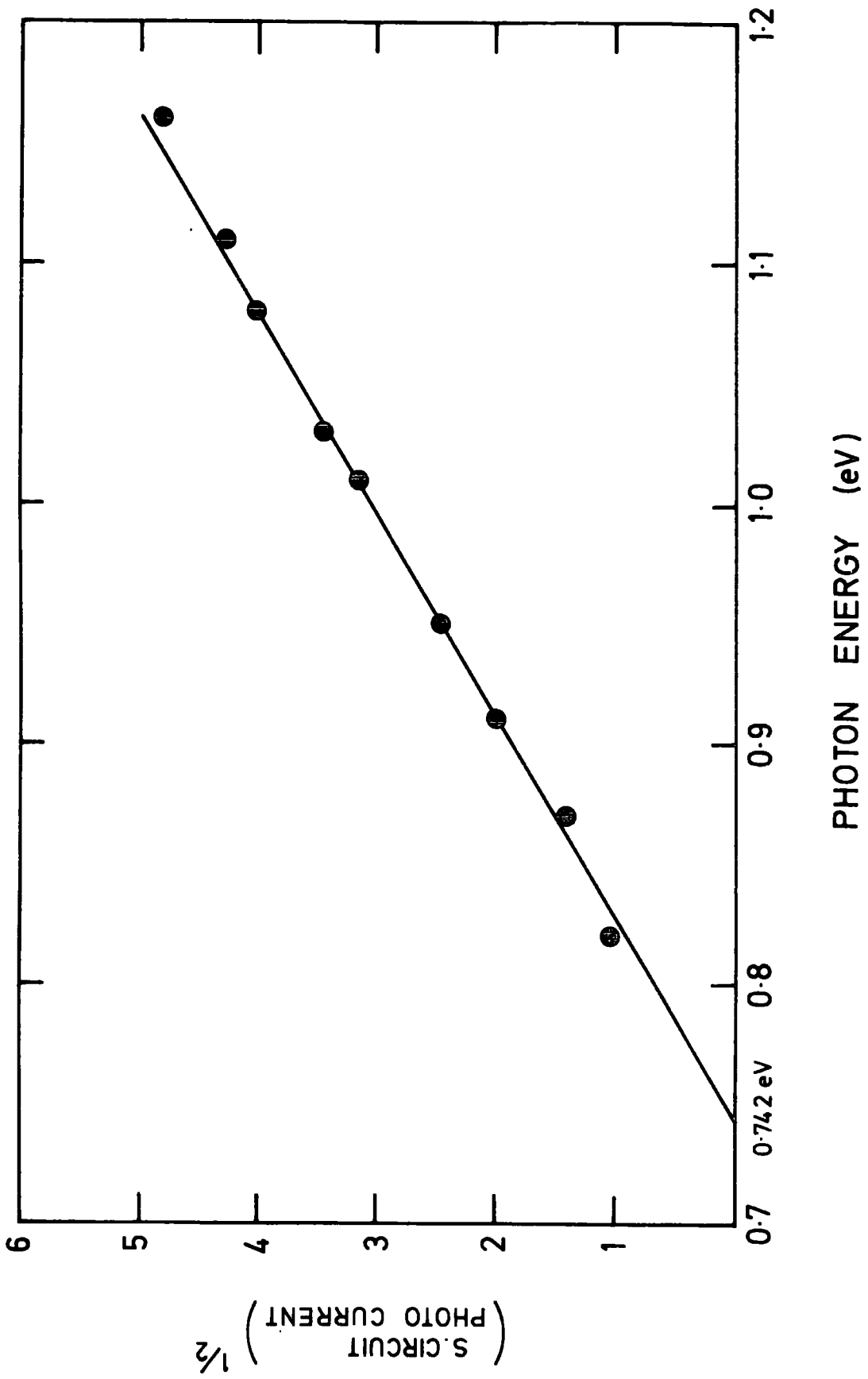


FIG. 6.7

(626 B) BARRIER HEIGHT DETERMINATION FROM SHORTCIRCUIT PHOTOCURRENT MEASUREMENT



SHORTCIRCUIT PHOTOCURRENT (arb.unit)

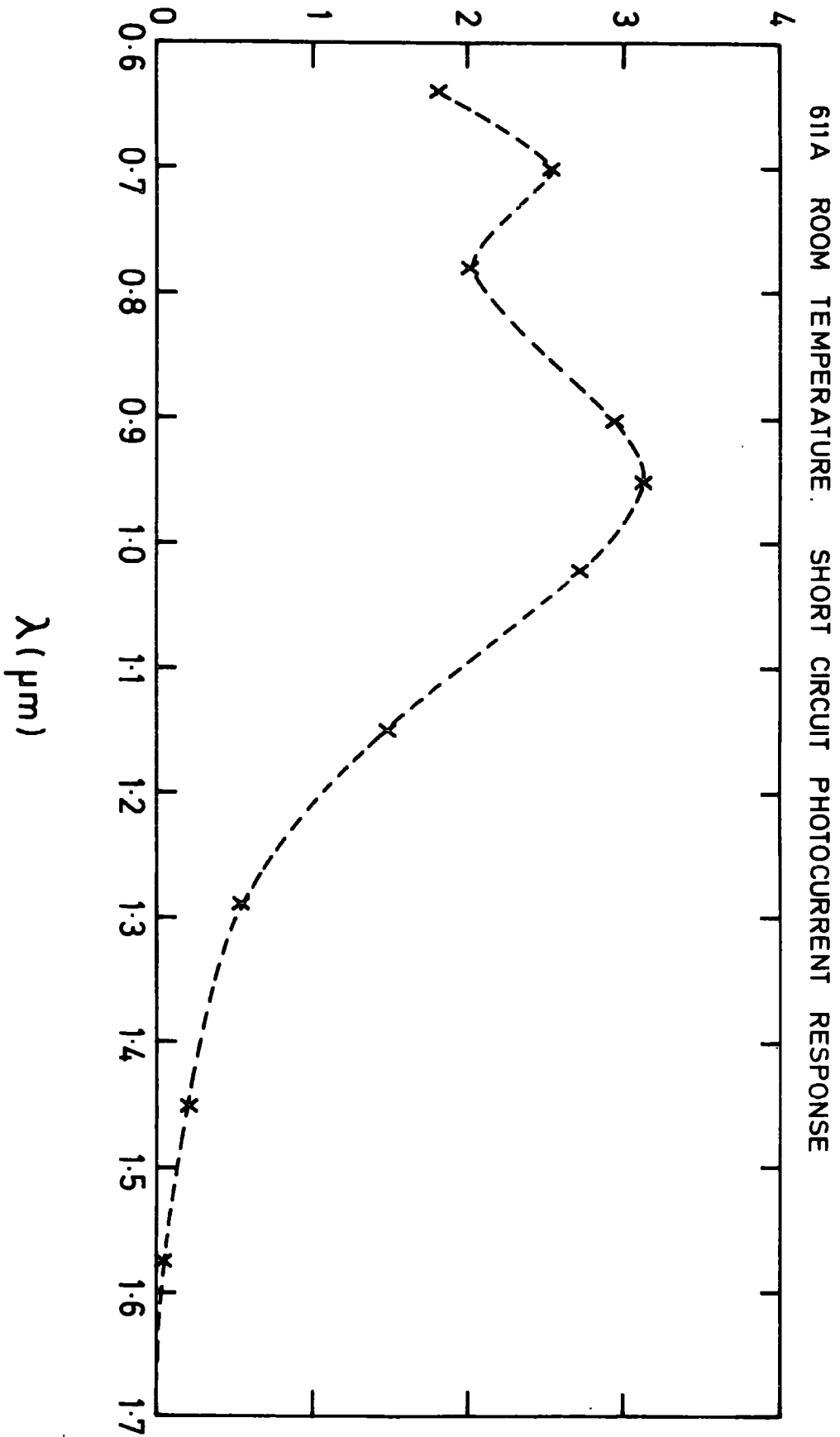
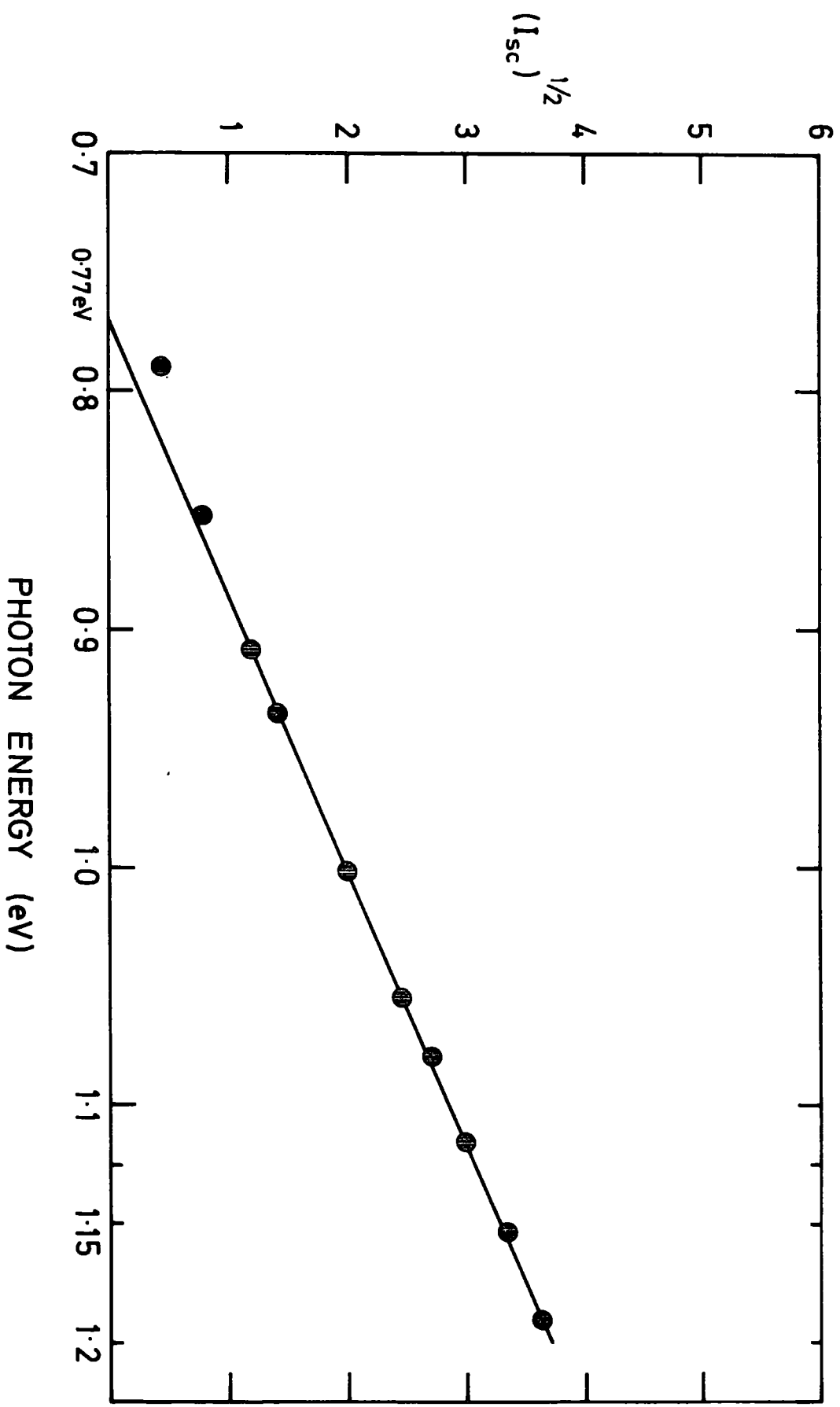


FIG. 6.8

BARRIER HEIGHT DETERMINATION FROM SHORTCIRCUIT PHOTOCURRENT MEASUREMENTS (611A)



can be explained by considering the different processes by which the shortcircuit photocurrent in a metal-semiconductor system is generated. If photons of adequate energy are incident on the surface of the metal, free electrons in the metal are excited and emitted to the semiconductor. In this case the photon energy is equal to or greater than the metal-semiconductor barrier height  $\phi_{BN}$ . Apart from the emission of photoelectrons from the metal to the semiconductor, the excitation of electrons from impurity states to the conduction band also contributes to the measured shortcircuit photocurrent  $I_{sc}$ , provided that the excitation of these electrons takes place in conjunction with the creation of mobile holes. The magnitude of this contribution depends on the position of the impurity levels in the forbidden gap as well as to the density and electron and hole optical emission rates of these centres. The latter process is responsible for the difference in the shape of the curves of Figures 6.7 and 6.8.

#### 6.8 Capacitance-Voltage Measurements

The C-V characteristics of the Au-CdS diodes were measured as described in Chapter 4, 4.2.3. A typical  $\bar{C}^{-2}$ -V plot measured at 10 K Hz of diode 626 B is shown in Figure 6.9. The bias range was usually from 2 volts in the reverse to 0.5 volt in the forward direction. The plots of  $\frac{1}{C^2}$  versus V were found to be linear for the junctions examined. The measurements were made on Au-CdS diodes doped with Cl and also on those doped with Cl and counter doped with Cu. The uncompensated donor density  $N_d$  was found from the slope of the plot  $\frac{1}{C^2}$  versus V using equation 2.47. With the devices examined  $N_d$  was usually in the range of  $10^{16}$  -  $10^{17}$   $\text{cm}^{-3}$  at  $293^{\circ}$  K. The voltage intercept  $V_i$  gave a value greater than the barrier height of gold contact to CdS.

#### 6.9 C-V Measurements on Au-CdS Diodes Containing Dopants

The C-V characteristics of Au-CdS diodes prepared from CdS crystals doped either with chlorine or with chlorine and counter doped

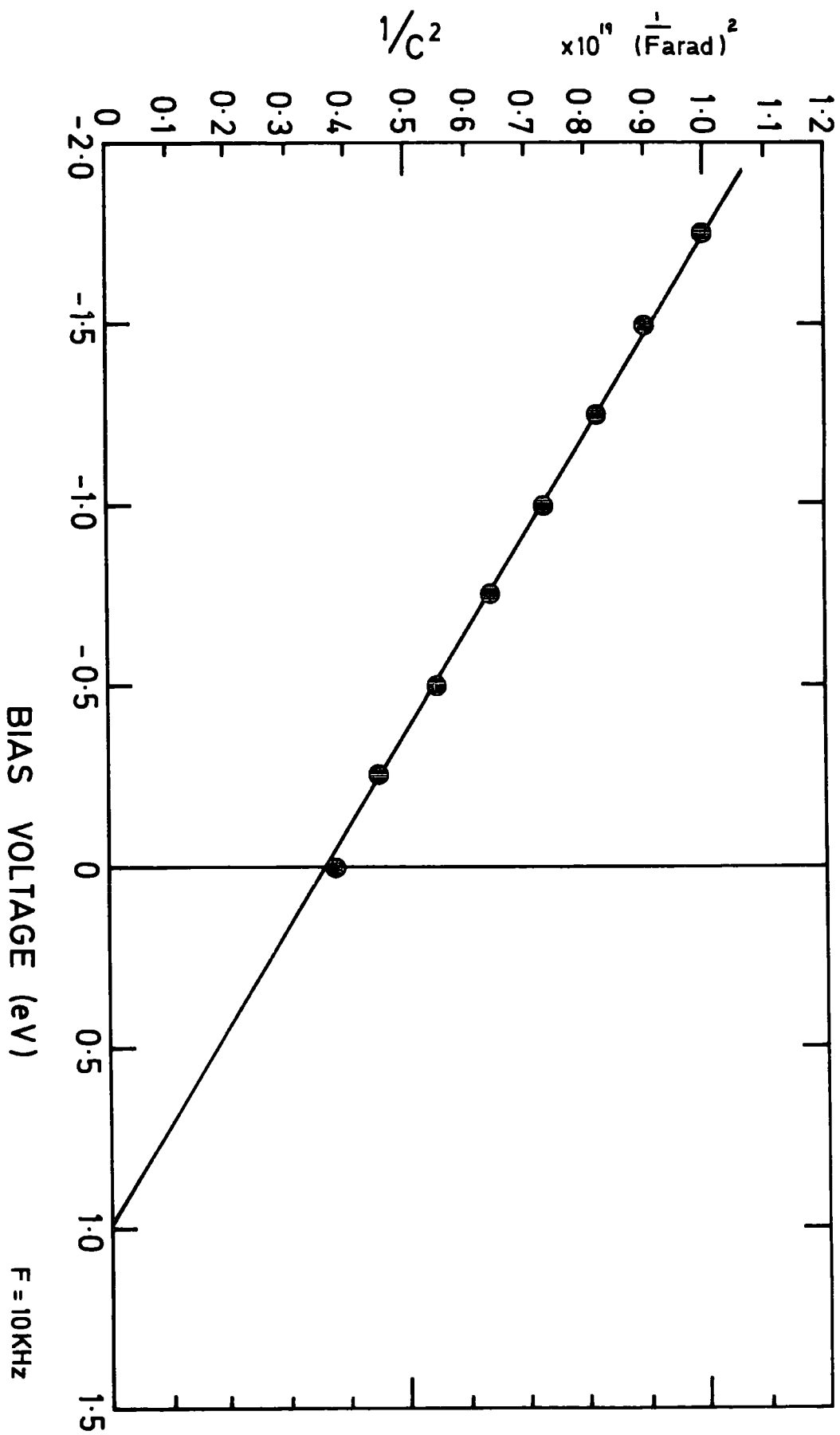


FIG. 6-10

with copper have been studied and some typical  $\bar{C}^2$ -V plots of these devices are shown in Figure 6.10.

An uncompensated donor concentration of  $N_d = 9.1 \times 10^{16} \text{ cm}^{-3}$  and a voltage intercept of  $V_i = 1.475$  volt were found for device 611 A (CdS: Cl). For device 626 B, however, the slope of the  $\bar{C}^2$ -V plot gave a donor concentration of  $N_d = 1.216 \times 10^{16} \text{ cm}^{-3}$  and the voltage intercept  $V_i$  was found to be 0.98 volt.

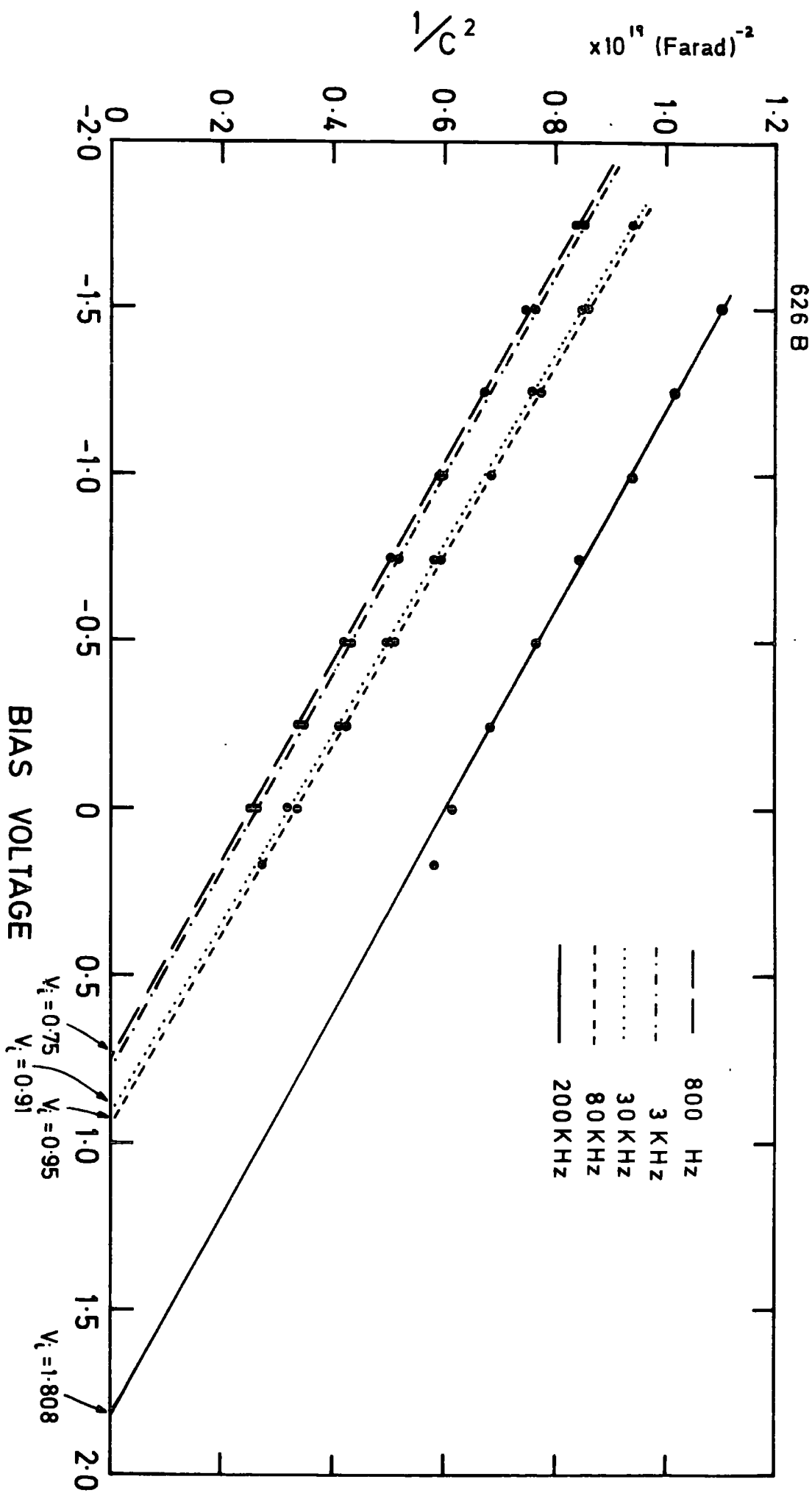
The voltage intercept  $V_i$  is a measure of the barrier height of the metal semiconductor contact, and in a Schottky diode should give barrier height values equal to that found by the photoelectric method. In practice, however, the existence of a thin interfacial layer between the metal and the semiconductor and the dependence of capacitance on frequency have substantial effects on the C-V characteristics of the device and likewise on the value of the voltage intercept.

#### 6.10 Variation of Capacitance in Frequency

As mentioned previously in Chapter 2.6, the reverse bias capacitance of a Schottky barrier depends on the depletion width  $W$  which exists in the semiconductor side of the junction. If this is determined solely by a shallow donor density  $N_d$ , the expression for depletion layer capacitance per unit area is given by Equation (2.46). This equation is valid only if the edge of the depletion region follows the frequency of the applied a.c. voltage. If the junction contains deep impurities whose ionization must change with change of the applied voltage, the response time for the system may not allow the capacitance to follow the applied frequency unless this is very low. The capacitance at a low frequency such as  $10^2$  to  $10^3$  Hz is then greater than that measured at a high frequency such as  $10^5$  to  $10^6$  Hz.

Apart from deep impurities which affect the C-V characteristic of the device especially at low frequencies, the existence of surface

FIG. 6-11



states at the semiconductor-oxide layer interface which are frequency dependent also affects the C-V measurements. The frequency dependence can be observed from the  $\bar{C}^{-2}$  versus V plots shown in Figure 6.11. The slope of the  $\bar{C}^{-2}$ -V lines did not change over the wide range of signal frequencies used, except that at 100 K Hz, the  $\bar{C}^{-2}$ -V plot was not linear at all. The lines in Figure 6.11 also show that there is a sudden increase in the value of voltage intercept from 0.95 volt at the signal frequency of 80 K Hz to 1.808 volt at the frequency of 200 K Hz. It was thought that the greatest change would occur when the surface states responded to the signal frequency and the change could be accounted for if some of the parameters concerning surface states were known.

As mentioned in Chapter 2, 2.12, valuable information about the surface states can be obtained by measuring the equivalent conductance  $G_p$  of the device which is in effect a 'metal insulator-semiconductor' capacitor. The conductance arises from the fact that the process of capture and emission of carriers by the surface states lags behind the applied signal. Since surface states are capable of storing charge, there will be capacitance  $C_s$  associated with them which is proportional to their density. The conductance related to the surface states is  $G_s = \frac{C_s}{\tau}$ , where  $\tau$  is the time constant of the interface states. Both  $\tau$  and  $C_s$  can be extracted directly from the measurement of the equivalent parallel conductance. The equivalent circuit of an M.I.S. capacitor assuming a single level state model, has been represented in Figure 2.4. The measured capacitance  $C_m$  across the terminals of X and Y of this equivalent circuit is :

$$\frac{1}{C_m} = \frac{1}{C_{ox}} + \frac{1}{C_p} \quad (6.1)$$

where  $C_{ox}$  is the capacitance associated with the insulator (oxide) layer and  $C_p$  is the capacitance of the parallel branch of the equivalent circuit.

The conductance and the capacitance of the parallel branch in Figure 2.4 are given by equations 2.81 and 2.82 respectively. These equations can be extended to include the effect of  $C_{ox}$ , i.e. with the measured conductance  $G_m$  and measured capacitance  $C_m$  across the terminals of the equivalent circuit in Figure 2.4, equations 2.81 and 2.82 become :

$$\frac{G_p}{\omega} = \frac{\omega C_{ox}^2 G_m (G_m^2 + \omega^2 C_m^2)}{\omega^2 C_{ox}^2 G_m^2 + \left[ \omega^2 C_m (C_{ox} - C_m) - G_m^2 \right]^2} \quad (6.2)$$

and

$$C_p = \frac{C_{ox} (G_m^2 + \omega^2 C_m^2) \left[ \omega^2 C_m (C_{ox} - C_m) - G_m^2 \right]}{\omega^2 C_{ox}^2 G_m^2 + \left[ \omega^2 C_m (C_{ox} - C_m) - G_m^2 \right]^2} \quad (6.3)$$

It should be noted that the circuit across the terminals X-Y in Figure 2.4 has a shorter time constant than that of the interface state branch of the circuit only because of  $C_{ox}$ .

### 6.11 G-V Measurements

The variation of conductance with voltage has been measured using the G-C-V plotter described in Chapter 4, 4.2.3. Measurements were made in the dark and in the frequency range from 400 Hz to 300 K Hz. The conductance of the Au-CdS diodes was found to rise steeply at forward biases greater than 0.5 volt, therefore measurements were usually made over the range from 2 volts in the reverse to a voltage less than 0.5 volt in the forward direction. The sharp increase in the conductance in forward bias prevented the measurement of the oxide layer capacitance  $C_{ox}$ . The capacitance of an ideal M-I-S (Metal-Insulator-n-type Semiconductor) capacitor should saturate in forward bias and give the capacitance of the oxide layer. In our experiments, because of the non-ideality of devices, the saturation was not detected. An attempt was made, therefore, to measure  $\frac{G_p}{\omega}$  versus  $\omega$  without considering the

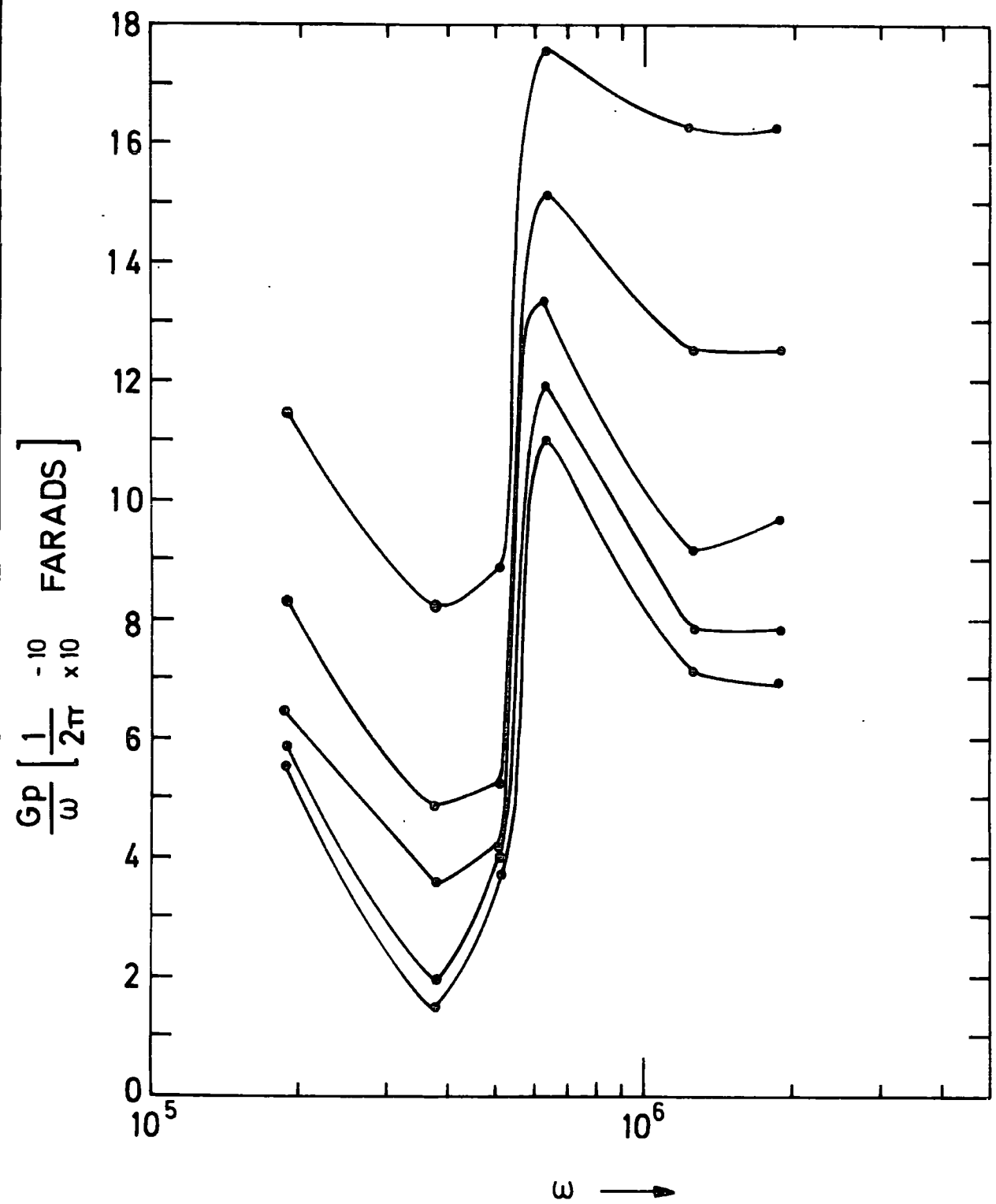


FIG. 6-12

effect of oxide-layer capacitance i.e. the measured conductance  $G_m$  was assumed to be the same as  $G_p$  in equation 2.81.

The  $\frac{G_p}{\omega}$  versus  $\omega$  characteristics of device 626 B at different reverse biases are shown in Figure 6.12.  $\frac{G_p}{\omega}$  goes through a maximum at 100 K Hz. The value of  $(\frac{G_p}{\omega})_{\max.}$  at zero bias is equal to  $2.81 \times 10^{-10}$  Farads. As already described in Chapter 2, 2.12, the value of  $\frac{G_p}{\omega}$  at the maximum, i.e. when  $\omega\tau = 1$  is equal to  $\frac{C_s}{2}$ , where  $C_s$  is the capacitance associated with the surface states and is proportional to their density according to the relation  $C_s = q A N_{ss}$ . From the value of  $(\frac{G_p}{\omega})_{\max.}$  the surface state density  $N_{ss}$  is calculated to be  $1.98 \times 10^{11}$  states/eV/ $C_m^2$  and the frequency associated with the  $(\frac{G_p}{\omega})_{\max.}$  gives a characteristic time constant of 1.59  $\mu$  sec.

The above mentioned parameters have been obtained by ignoring the effect of any oxide layer capacitance. If, however, this effect is included by substituting the value of  $C_{ox} = 1.003 \times 10^{-7} F/C_m^2$  (see Section 6.16) in equation 6.2, the value of  $\frac{G_p}{\omega}$  can be determined for different frequencies. For example, the value of  $\frac{G_p}{\omega}$  at the frequency of 10 K Hz, calculated using equation 6.2, was found to be larger than the measured value by a factor of 2. It follows therefore that the density of surface states determined from equation 2.83 where the effect of  $C_{ox}$  was ignored, can be in error by a factor of 2.

#### 6.12 The Effect of the Interfacial Layer on C-V Measurements

Apart from the effect of the signal frequency on the C-V characteristics of a device, the existence of an interfacial layer between the metal and the semiconductor has substantial effects on the C-V measurements. An increase in the value of voltage intercept,  $\delta V_i$  is one such consequence. Since  $\delta V_i$  depends on the thickness and dielectric properties of the layer, it can be used to determine the thickness of the layer. This requires that some of the device parameters such as the diffusion potential  $V_{bi}$ ,

uncompensated donor density  $N_d$ , the depletion layer width  $W$ , the maximum electric field at the junction  $\epsilon_{\max}$ , the depth of the Fermi level below the conduction band  $V_n$ , the barrier height  $\phi_{Bn}$  and the Schottky barrier lowering  $\Delta\phi_n$  be known.

### 6.13 The Diffusion Potential $V_{bi}$

The diffusion potential  $V_{bi}$ , which is equal to  $(\phi_{Bn} - V_n)$  can be obtained from the photoelectric threshold and  $C^{-2} - V$  plots. The depth of the Fermi level below the conduction band  $V_n$ , is given by

$$qV_n = K T \ln \frac{N_c}{N_d} \quad (6.4)$$

where  $N_d$  is the donor density and  $N_c$  is the effective density of states in the conduction band. For a non-degenerate semiconductor,  $N_c$  is given by

$$N_c = 2 \left( \frac{2\pi m_e^* K T}{h^2} \right)^{3/2} \quad (6.5)$$

where  $m_e^*$  is the electron effective mass,  $K$  is Boltzmann's constant, and  $h$  Planck's constant. The magnitude of the constants in equation 6.5 are :

$$m_e^* = 0.17 m_e \quad \text{where } m_e = 9.108 \times 10^{-31} \text{ Kg.}$$

$$K = 1.38 \times 10^{-23} \text{ joule/}^\circ\text{K}$$

$$h = 6.625 \times 10^{-34} \text{ joule-sec.}$$

By substituting these values in equation 6.5, the effective density of states in the conduction band at  $293^\circ\text{K}$  is found to be :

$$N_c = 1.7019 \times 10^{18} \frac{\text{states}}{\text{cm}^3} . \quad \text{For the device 626 B with a donor density of } N_d = 1.216 \times 10^{16} \text{ cm}^{-3}, \text{ the depth of Fermi level below the conduction band}$$

is then calculated from equation 6.4 to be  $qV_n = 0.125$  eV. With the value of barrier height  $\phi_{Bn} = 0.742$  v, the diffusion potential  $V_{bi}$  then becomes  $V_{bi} = (\phi_{Bn} - V_n) = 0.617$  volt.

#### 6.14 The Depletion Layer Width, W

The width of the depletion layer for a metal-semiconductor junction is given by equation 2.43 and can be determined if the diffusion potential  $V_{bi}$  and the donor density  $N_d$  are known. Using  $\epsilon_s = 9.35 \epsilon_0$  for CdS (Berlincourt, et al, 1963), the depletion layer width at zero bias for device 626 B was found to be about  $2240 \text{ \AA}$ . It is seen from equation 2.43 that the depletion width  $W$ , increases when the diode is reverse biased and decreases when the diode is biased in the forward direction.

#### 6.15 The Image Force Barrier Lowering $\Delta\phi_n$ and the Maximum Electric Field Strength $\epsilon_{max}$ at the Junction

The barrier lowering which is due to the combined effect of the field and the image force at the metal-semiconductor junction is given by

$$\Delta\phi_n = \sqrt{\frac{q \epsilon_{max}}{4\pi \epsilon_s}} \quad (6.6)$$

where  $\epsilon_{max}$  is the maximum electric field strength at the junction given by equation 2.44. Comparing equation 2.44 with equation 2.43,  $\epsilon_{max}$  can also be expressed as

$$\epsilon_{max} = \left( \frac{qN_d}{\epsilon_s} \right) W \quad (6.7)$$

Therefore, if the donor density  $N_d$  and the depletion layer width  $W$  are known,  $\epsilon_{max}$  and  $\Delta\phi$  can be determined easily by equations 6.7 and 6.6. For example, the maximum electric field at zero applied bias for the device 626 B, was found to be :  $0.527 \times 10^5 \frac{\text{volt}}{\text{cm}}$  and the substitution of this value in equation 6.6 for  $\epsilon_{max}$ , gave the value of  $\Delta\phi_n$  as high as 28.5 mV.

As can be seen from equations 6.6 and 6.7,  $\Delta\phi_n$  is proportional to  $(N_d)^{1/4}$  and therefore increases with the semiconductor donor density.

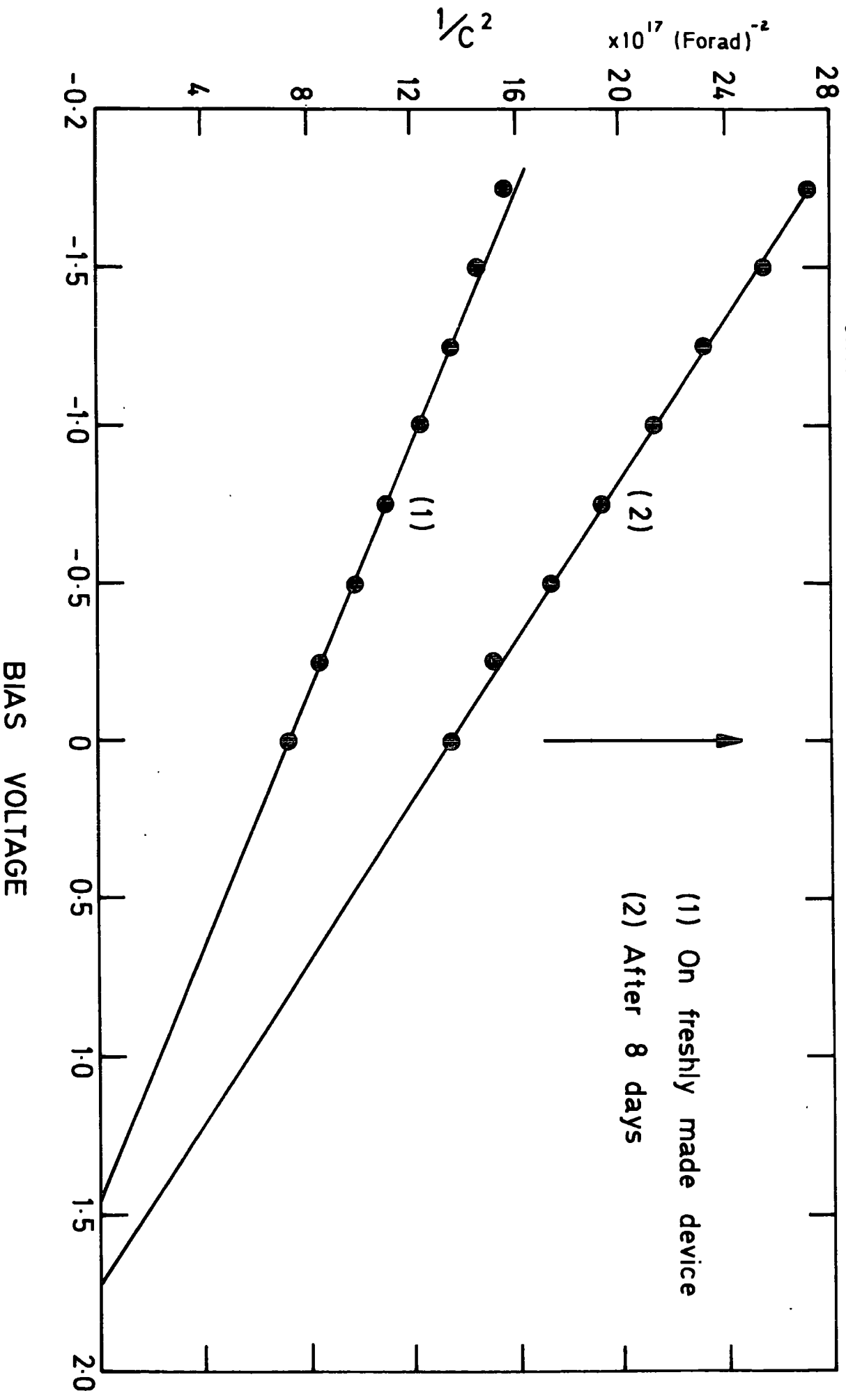
#### 6.16 The Evaluation of the Interfacial Layer Thickness

As mentioned earlier in this chapter, the thickness of any interfacial layer between the metal and the semiconductor affects the magnitude of the intercept in the  $C^{-2}$ -V plot. According to the model proposed by Cowley (1966), for the metal-interfacial layer-semiconductor contact without surface states, the magnitude of the intercept  $V_o$  of the  $\frac{1}{C^2}$  versus V line is given by equation 2.59. If the permittivity of the interfacial layer,  $\epsilon_i$  is known the thickness of the layer  $\lambda_i$  can be determined by substituting the corresponding values of the diffusion potential  $V_{bi}$  and the donor density  $N_d$  in equation 2.59.

No investigation has been made to determine the elemental constituents of the interfacial layer, but it is quite likely that among these cadmium and oxygen will be present in the form of CdO as a result of the oxidation of the surface layer. Cadmium oxide is an n-type semiconductor with a direct band gap of 2.38 eV and two indirect gaps of 1.12 and 1.18 eV. (Koffyberg 1976, Breeze and Perkins, 1973). Its conductivity is caused by the relatively large concentration of native defects (either cadmium interstitials or oxygen vacancies) acting as donors. With these properties, the permittivity of the CdO part of the interfacial layer should be similar or smaller than that of CdS itself. If the following parameters :

$$\begin{array}{ll}
 V_{bi} = 0.617 \text{ V} & N_d = 1.216 \times 10^{16} \text{ Cm}^{-3} \\
 T = 293^\circ \text{ K} & V_2 = 0.02525 \text{ V} \\
 \epsilon_s = 9.35 \epsilon_o & V_o = 0.98 \text{ V} \\
 \epsilon_o = 8.854 \times 10^{-14} \frac{\text{Farad}}{\text{Cm}} & N_{ss} = 1.98 \times 10^{11} \frac{\text{states}}{\text{eV/Cm}^2} \\
 \epsilon_i \approx \epsilon_s & U = 0.152 \text{ volt}
 \end{array}$$

611A cds : cl



for diode 626 B are substituted in equation 2.59, the interfacial layer thickness  $\lambda_i$  is found to be about 630 Å. On the other hand, if use is made of equations 2.61 and 2.67 in which the effect of surface states has been considered, the thickness of the layer is calculated to be about 825 Å. Assuming that the insulating layer behaves as a parallel plate capacitor, i.e.  $C_{ox} = \frac{\epsilon_i}{\lambda_i}$ , the calculated value of  $\lambda_i$  gives the insulating layer capacitance per unit area of  $C_{ox} = 1.003 \times 10^{-7} \frac{\text{Farad}}{\text{Cm}^2}$ .

#### 6.17 Changes in C-V Characteristics of a Diode with Time (Ageing)

It has already been shown in Section 6.7 that in the long term the short circuit photoresponse of a diode is time dependent. The C-V characteristics of a diode do not remain stable and invariant with time. As ageing proceeds the slope and voltage intercept in the  $C^{-2}$ -V plot change. An example of this effect for diode 611 A is shown in Figure 6.13. To eliminate the frequency effect, both C-V measurements were carried out at 20 K Hz. The time interval between the measurements was about 200 hours during which the donor density  $N_d$  of the diode decreased from a value of  $9.1 \times 10^{16}$  to  $5.85 \times 10^{16} \text{ Cm}^{-3}$ . An increase in the voltage intercept  $\delta v_i$  of 0.267 volt was also observed which can be used to calculate the change in the thickness of the interfacial layer. If the following two sets of parameters :

$$\begin{array}{ll}
 \phi_{Bn} = 0.77 \text{ V} & v_n = 0.085 \text{ V} \\
 v_n = 0.074 \text{ V} & N_d = 5.85 \times 10^{16} \text{ Cm}^{-3} \\
 N_d = 9.1 \times 10^{16} \text{ Cm}^{-3} & v_o = 1.717 \text{ V} \\
 v_o = 1.45 \text{ V} & \epsilon_s = 9.35 \epsilon_o \\
 N_c = 1.702 \times 10^{18} \text{ Cm}^{-3} & \epsilon_o = 8.854 \times 10^{-4} \text{ F/Cm} \\
 v_2 = 0.02526 \text{ (T=293}^\circ \text{ K)} & \epsilon_i \approx \epsilon_s
 \end{array}$$

are substituted in equation 2.59, the increase in the thickness of interfacial layer is found to be as high as  $235 \text{ \AA}$  from  $355 \text{ \AA}$  to  $590 \text{ \AA}$ . This increase, which occurs in conjunction with the decrease in the donor density of the diode, is indicative of the basic instability of the device. The decrease in the donor density may be due to the creation of cadmium vacancies which are acceptor imperfections. The process is continued by the out-diffusion of cadmium atoms from the bulk to the surface where oxidation produces a thicker interfacial layer between the metal and the semiconductor.

#### 6.18 Current-Voltage Characteristics

The conduction mechanism in a metal-semiconductor rectifier mainly is determined either by the emission of electrons from the semiconductor to the metal (Thermionic Emission Theory) or by the process of diffusion and drift operating in the space-charge region (Diffusion Theory). It is possible to determine the process according to which the conduction mechanism takes place in a M-S system. According to Bethe (1942) the condition for the validity of the thermionic emission theory is that the electron mean free path  $\lambda$  be greater than the distance  $d$  in which the barrier falls by  $KT$  from its maximum value. This condition leads to the criterion given by equation 2.54. Substituting  $0.17 m_0$  for the effective electron mass in equation 2.54, the average velocity of electrons in CdS at  $T = 293^\circ \text{ K}$  is found to be  $2.58 \times 10^7 \text{ Cm/sec}$ . With the calculated maximum electric field  $\epsilon_{\text{max}}$  of  $5.28 \times 10^4 \text{ volt/Cm}$  and the electron mobility  $\mu_e$  of  $300 \text{ Cm}^2 \text{ V}^{-1} \text{ sec}^{-1}$  (Sze, 1969), the ratio of  $\frac{\mu_e \epsilon_{\text{max}}}{\bar{v}/4}$  for diode 626 B is then found to be 2.45. This indicates that thermionic emission is not the only process which contributes to the transport of electrons in diode 626 B. On the other hand, a ratio of

$\frac{V_R}{V_D} = 0.4$  (see equation 2.52) does not indicate that diffusion is the prevailing

mechanism at the barrier. ( $\bar{V}_R = \frac{A^* T^2}{q N_C}$  is the effective recombination velocity at the top of the barrier and  $V_D$  is the carrier diffusion velocity which approximately equals to  $\mu \epsilon_{\max}$  when  $\mu$  is field-independent).

It would seem, therefore, that the thermionic emission Diffusion theory (Crowell & Sze, 1966) is applicable to this particular diode.

For diodes on dice from boule No. 611, however, the ratio of  $\frac{\mu \epsilon_{\max}}{\bar{V}/4}$  was about 10, which means that the thermionic emission was the dominant conduction mechanism in those devices.

### 6.19 Forward Bias - I-V Characteristics

Measurements of forward bias I-V characteristics of diodes prepared on the chemically etched surfaces of the cubes cut from different boules were made as described in Chapter 4. A typical forward I-V characteristic of diode 626 B is shown in Figure 6.14, curve (b). The tendency for the current to saturate at higher voltages is attributable to the potential drop across the bulk resistance of the diode. As the forward bias voltage increases the semiconductor energy band approaches the flat band situation, and at high enough forward bias voltages the semiconductor bulk resistance can be found from the measured values of current and voltage. Once this has been done the voltage drop across the bulk resistance can be calculated and subtracted from curve (a) to yield curve (b), the barrier-limited characteristic. Curve (b) shows that the plot of logarithm of current versus voltage remains linear over more than two orders of magnitude.

The non-ideality factor  $n$ , which is given by equation 2.72 is found to be as high as 2.5. The large  $n$ -value originates from the shunting effect of the semi-insulating layer left by the etching process on the orthogonal faces of the cube.

If the barrier lowering  $\Delta\phi$  is not taken into account it is seen from equation 2.71 that as the bias voltage tends to zero, the current density approaches a saturation value  $J_s$  from which the barrier height  $\phi_{Bn}$  can be

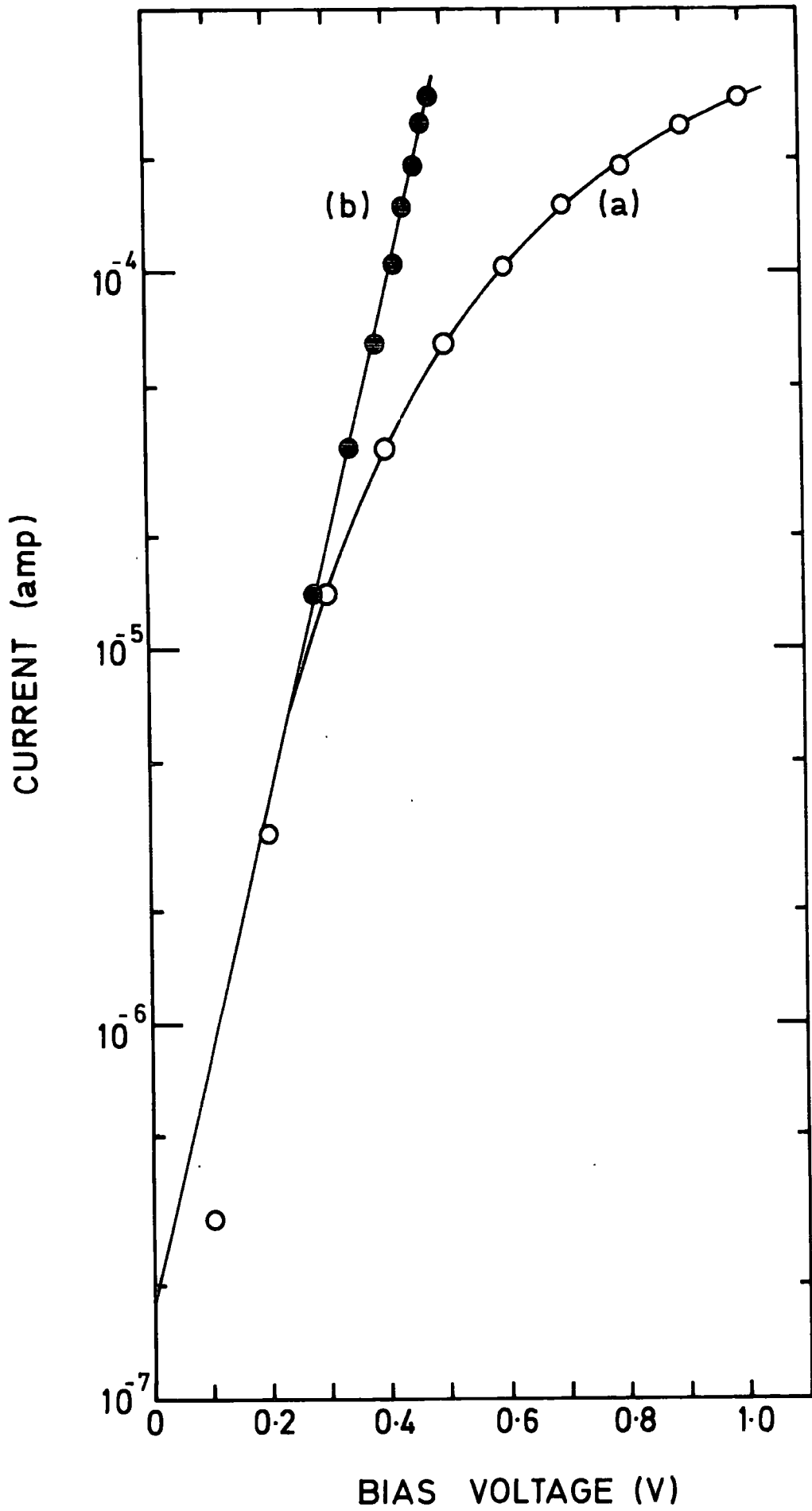


FIG. 6-14

611A I-V CHARACTERISTICS FORWARD BIAS

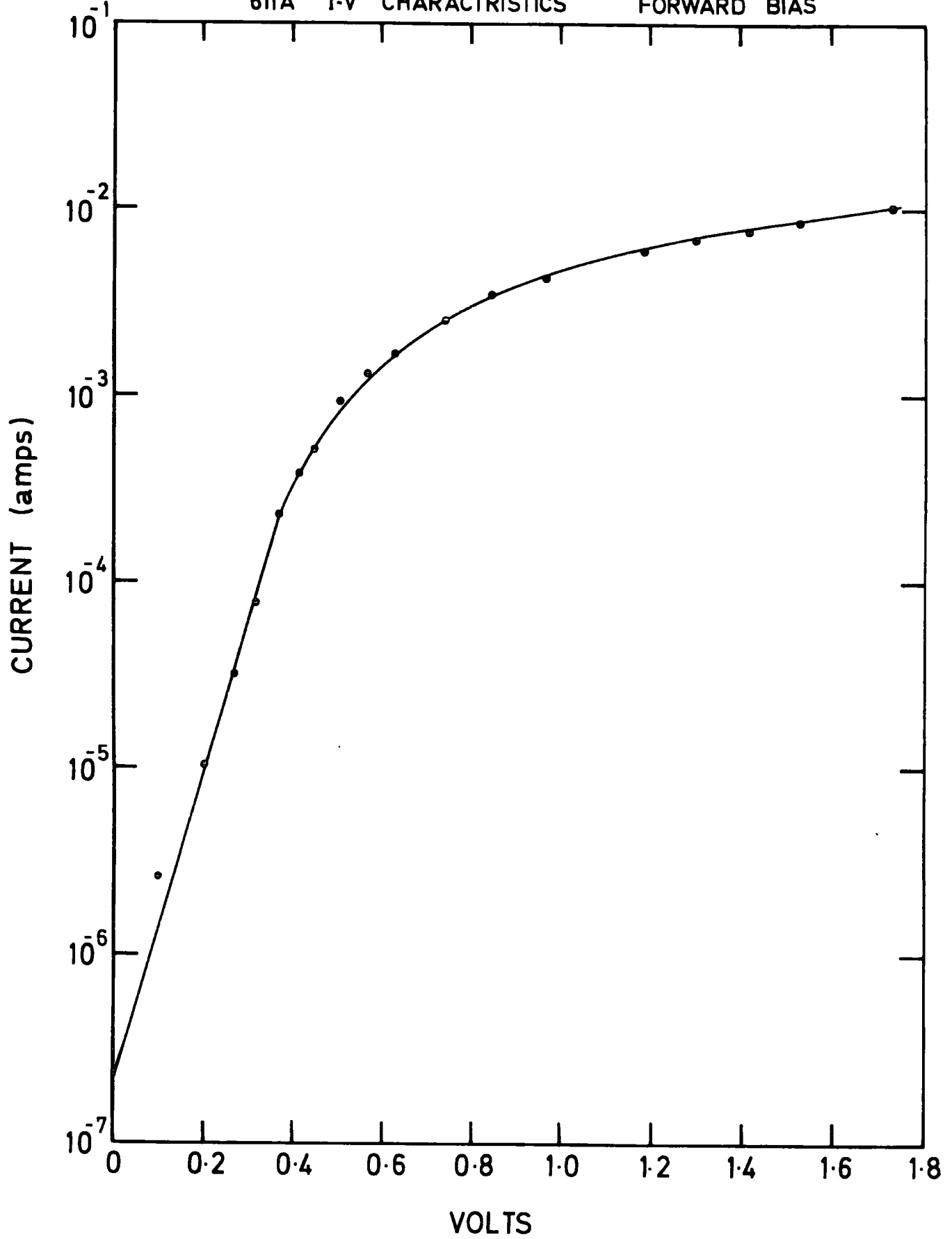


FIG. 6-15

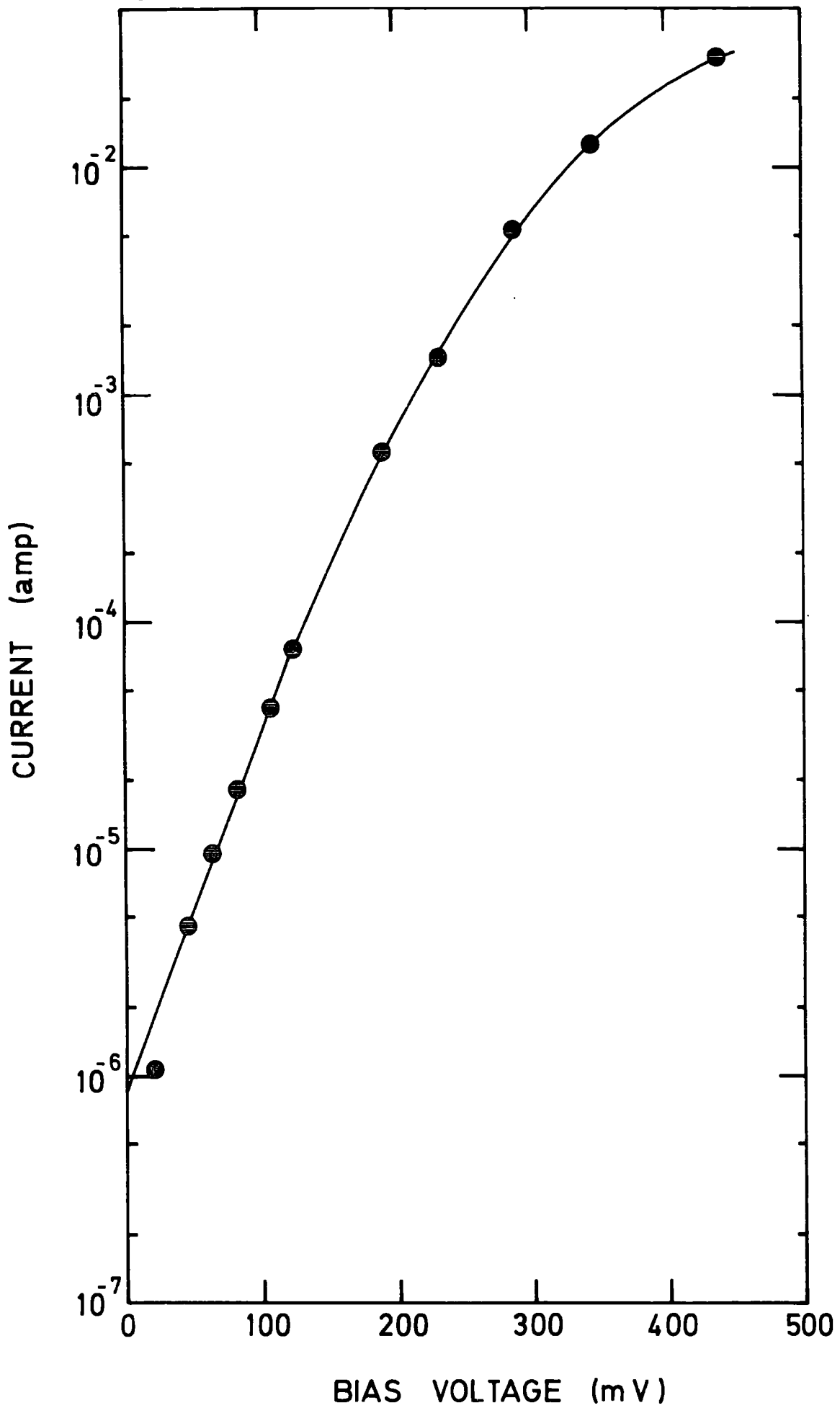


FIG. 6-16

easily calculated. For diode 626 B the saturation current was found by extrapolation of curve (b) in Figure 6.14 to be  $I_s = 1.8 \times 10^{-7}$  amp.

Assuming  $f_p f_Q \approx 1$ , the substitution of  $\frac{V_R}{V_D} = 0.4$  in equation 2.69 leads to a value of  $A^{**}$  and then equation 2.73 yields a value of 0.645 eV for  $\phi_{Bn}$ .

It is worth noting that the value of barrier height  $\phi_{Bn}$  is not very sensitive to the choice of  $A^{**}$ , since the substitution of the effective Richardson constant  $A^*$  for  $A^{**}$  in equation 2.73 produces an increase of only 0.008 volt in  $\phi_{Bn}$ .

The forward characteristics of diodes 611 A and 611 D are shown in Figure 6.15 and 6.16 respectively. It is seen from the I-V characteristics of diodes 626 B, 611 A and 611 D, that for the same bias voltage the corresponding measured current is different. For example, for the bias voltage of 300 mV, the current from diode 626 B is about  $1.4 \times 10^{-5}$  amp., from diode 611 A,  $6 \times 10^{-5}$  amp., and from diode 611 D,  $6 \times 10^{-3}$  amp. These differences may be accounted for if some of the parameters of these diodes are considered. For example, the uncompensated donor densities of the diodes determined by C-V measurements are  $1.216 \times 10^{16} \text{ cm}^{-3}$ ,  $9.1 \times 10^{16} \text{ cm}^{-3}$  and  $3.97 \times 10^{17} \text{ cm}^{-3}$  respectively. Substituting the values of  $N_d$  in equation 2.43, the depletion width is found to be about 2240 Å for diode 626 B, 870 Å for diode 611 A, and 420 Å for diode 611 D. It can be seen from the values of the mentioned parameters that the higher current values correspond to the smaller depletion widths. It seems reasonable, therefore, to assume that as the depletion width is decreased the possibility of the tunnelling of the carriers through the depletion region is increased and as a result there is a contribution to the conduction mechanism at the barrier.

## 6.20 Reverse Bias Characteristics

In the reverse direction the dominant effect is due to Schottky barrier lowering, and for reverse biases greater than  $\frac{3kT}{q}$ , equation 2.70

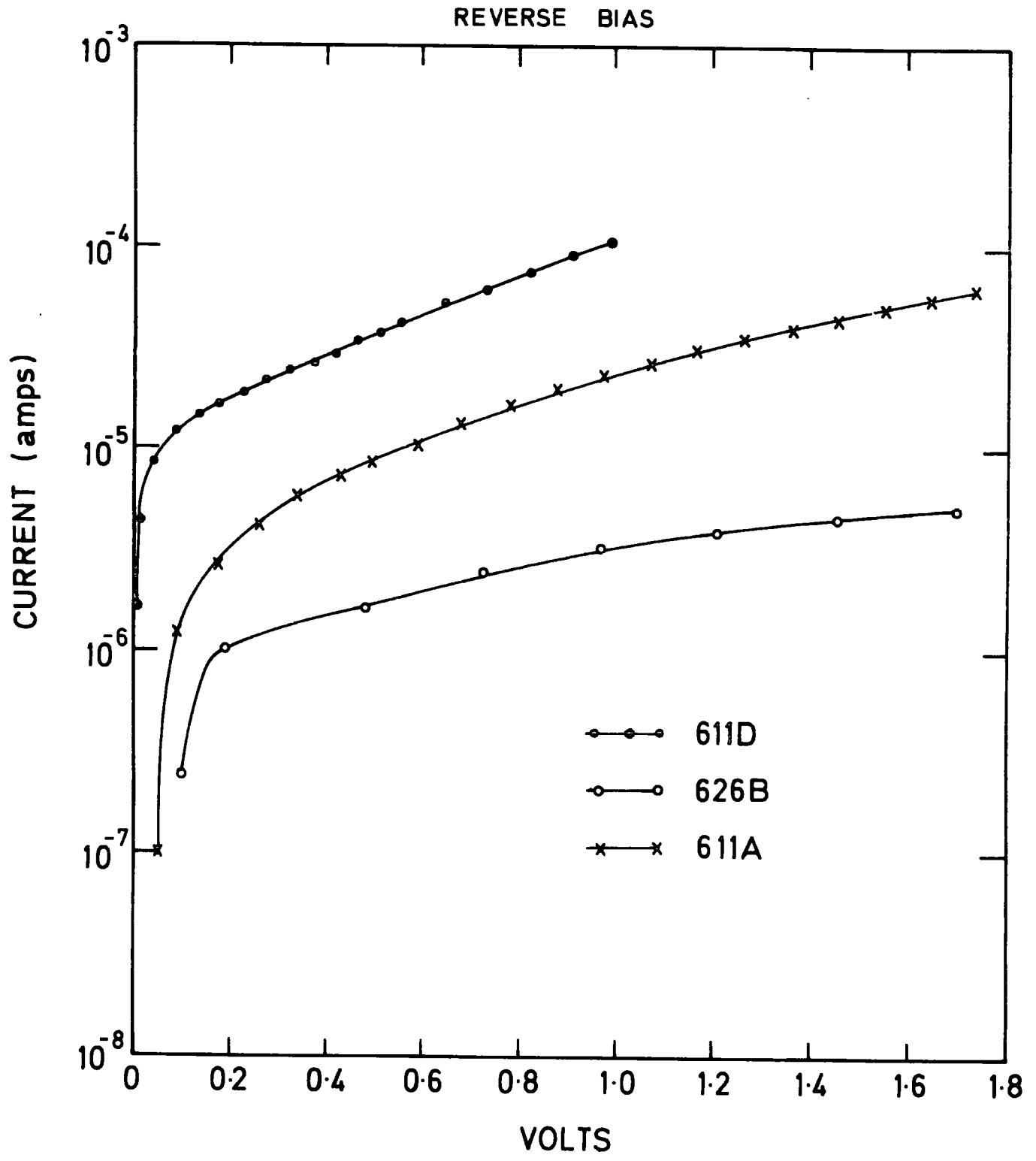


FIG. 6-17

can be written as

$$J_R \approx J_S = A^{**} T^2 \exp\left(\frac{-q \phi_{BO}}{KT}\right) \exp\left(\frac{q \Delta \phi}{KT}\right) \quad (6.8)$$

where

$$\Delta \phi = \sqrt{\frac{q \epsilon}{4 \pi \epsilon_s}}$$

and

$$\epsilon = \sqrt{\frac{2q N_d (V + V_{bi} - \frac{KT}{q})}{\epsilon_s}}$$

As the reverse bias is increased the magnitude of the electric field at the junction increases which leads to a greater value for the Schottky barrier lowering  $\Delta \phi$ . The reverse current density  $J_R$  will then increase gradually as given by equation 6.8.

The reverse bias characteristics of diodes 626 B, 611 A and 611 D, are shown in Figure 6.17. Comparing these characteristics it can be seen that the current values corresponding to the same reverse bias are higher for diodes with greater uncompensated donor densities. This effect can be attributed, as described in the previous section, to the smaller depletion widths of diodes with higher donor densities. The magnitude of the Schottky barrier lowering is also affected by the donor density. For example, with the same reverse bias of 2 volts, the barrier lowering was found to be 0.04 V for diode 626 B, 0.07 V for diode 611 A, and 0.1 volt for diode 611 D.

All the reverse bias characteristics shown in Figure 6.17 show two regions out of three in which a diode can be operated. The first region is characterized by the exponential rise of current with voltage for biases smaller than  $\frac{3KT}{q}$ . In the second region the current increases gradually with the voltage according to equation 6.8. Finally, there is a rapid rise of the current with voltage due to avalanching. The third region, which starts

with voltages greater than 2 volts, is not shown in Figure 6.17.

### 6.21 Effects of Ageing on Current-Voltage Characteristics of AU-CdS Diodes

The effects of ageing on the photoresponse and the C-V characteristics of a diode have been previously described in this chapter. The current-voltage characteristics of a diode also change with time. Although no investigation has been made with regard to the long term ageing, the results presented here show clearly the type of change which occurs in the forward and the reverse characteristics. Curves (a) and (b) of Figure 6.18 are forward bias characteristics of diode 611 D. Curve (a) was measured just after the preparation of the diode, whereas curve (b) shows the result of the same measurement 25 hours later. It can be seen that the current for a given bias was reduced as a result of ageing. This reduction may be due to the growth of the interfacial layer, developed between the metal and the semiconductor. The presence of such a layer also gives rise to n-values greater than unity. According to the theory developed by Card and Rhoderick (1971 a), the value of n is affected by both the presence of surface states and the interfacial layer. If, however, the effect of surface states is ignored, the value of n is given by

$$n = 1 + \frac{\lambda_i \epsilon_s}{\epsilon_i w} \quad (6.9)$$

where  $\lambda_i$  and  $\epsilon_i$  are the thickness and the permittivity of the interfacial layer respectively.  $\epsilon_s$  is the permittivity of the semiconductor and w the thickness of the depletion layer. Assuming that the thickness of the depletion layer does not change, the substitution of the change of n-value of 0.16 in equation 6.9 leads to the calculation of an increase in the thickness of the interfacial layer of about  $65 \text{ \AA}$  as a result of ageing. In the reverse direction the effect of ageing is similar to the forward direction and is

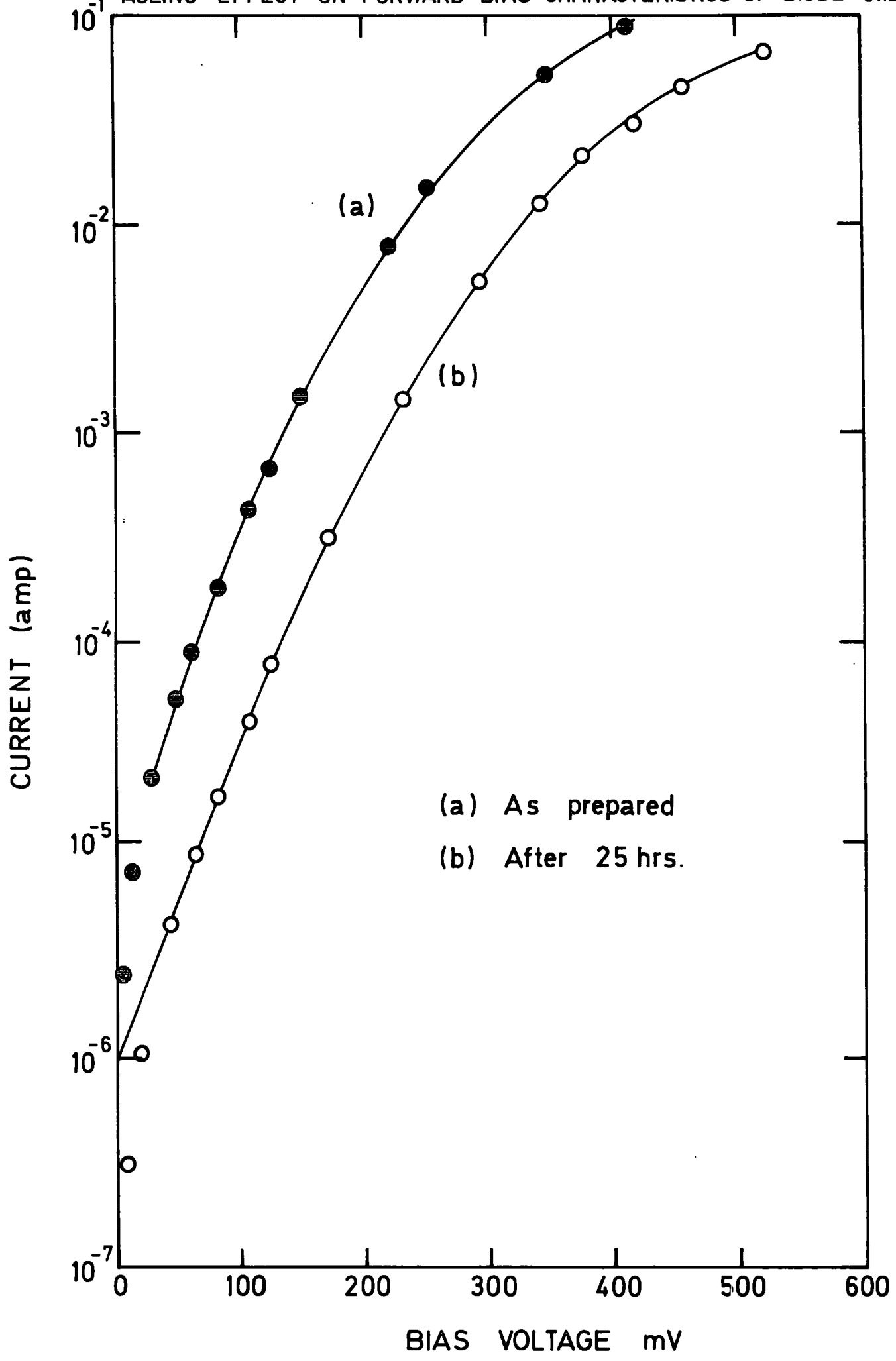


FIG. 6.18

AGEING EFFECT ON REVERSE BIAS  
CHARACTERISTICS OF DIODE 611D

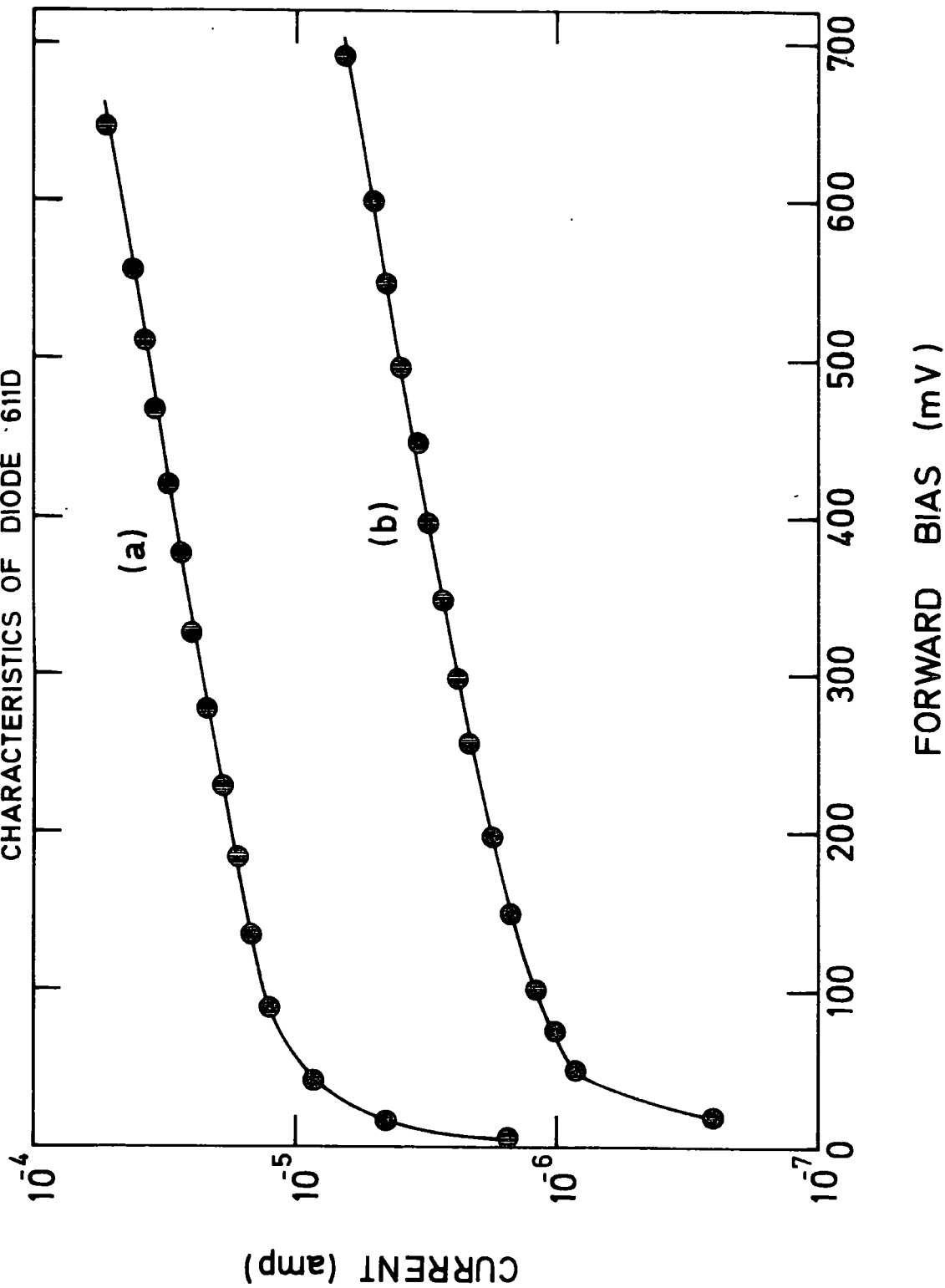


FIG. 6.19

shown in Figure 6.19.

#### 6.22 Photocapacitance Measurements on Au-CdS Diodes

The measurement of photocapacitance provides a method for detecting deep traps in a depletion layer by observing the change in the junction capacitance when the charge state of a trap is changed by the absorption of light. This method is very sensitive and permits a direct measurement of trap concentrations. The photocapacitance technique has recently been applied to the study of Si by Sah, et al (1969, and 1971), to the study of Ge by Kotina, et al (1969), to the study of Cu-doped GaP by Grimmeiss and Olofsson (1969), to the investigation of deep impurity centres in InP by Krushko and Gutkin, 1975, and to the study of  $\text{Cu}_2\text{S}$ -CdS heterojunction by Lindquist and Bube (1972).

In Schottky barrier diodes valuable information can be obtained about impurities in the bulk since the depletion region is of the same composition as the bulk material, unaffected by alloying or diffusion. In this case, an extra complication arises in measuring photocurrent or photovoltage if one works in a spectral region where photoemission from the metal to the semiconductor gives an important contribution to the current. Photocapacitance measurements, however, are not seriously affected by photoemission and can also give information on the sign of changes in the photoinduced charge.

#### 6.23 Photocapacitance Results on Au-CdS Diodes Containing Donors and Acceptors

Photocapacitance measurements were carried out on donor doped CdS crystals (i.e. with Cl) as well as those doped with an acceptor (like Cu), as described in Chapter 4.

Because of the compensating effects of copper in CdS, samples doped only with copper usually have a very high resistivity. As a result, the dark capacitance associated with these samples is nearly zero. When light is

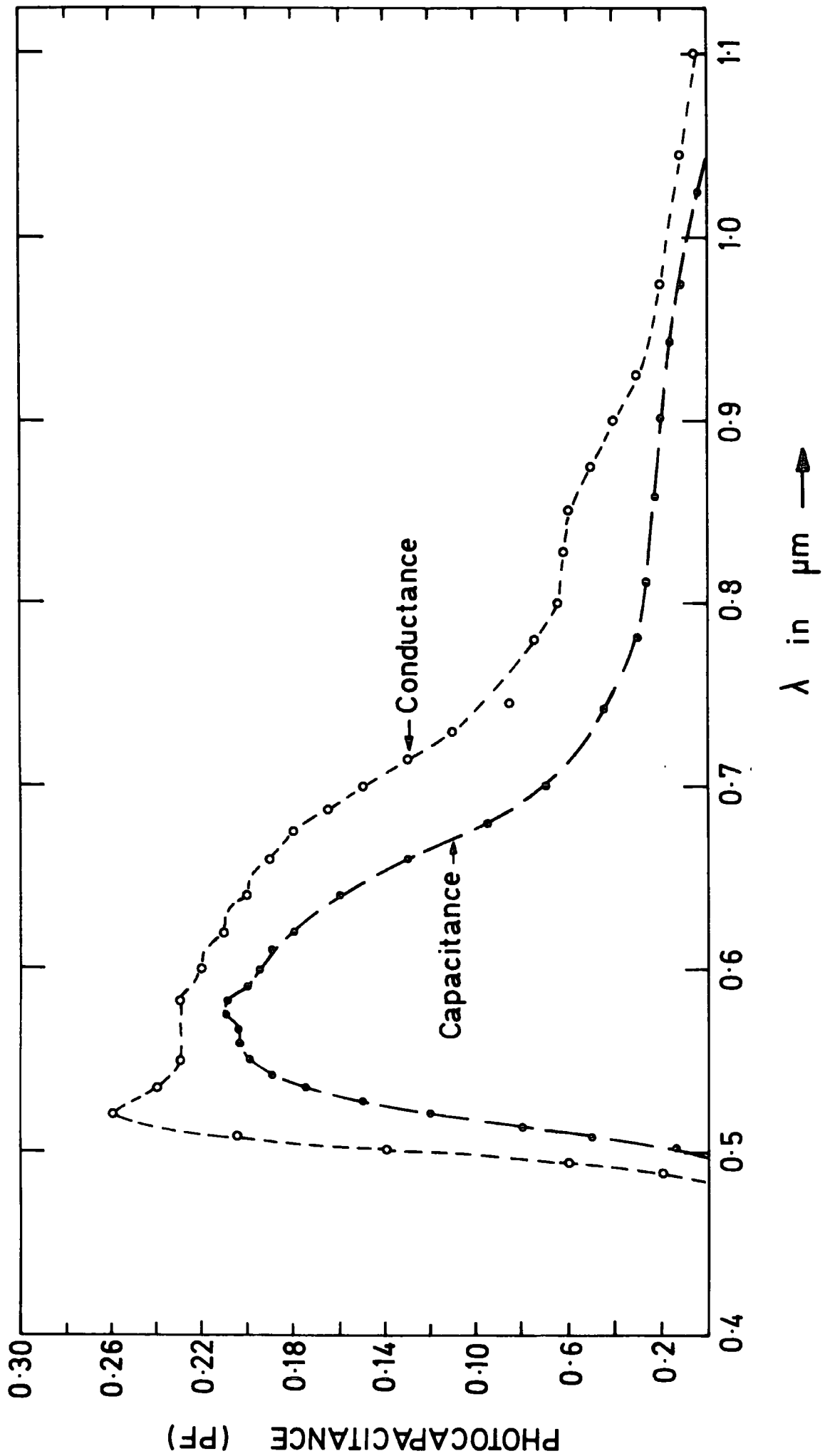


FIG. 6·20

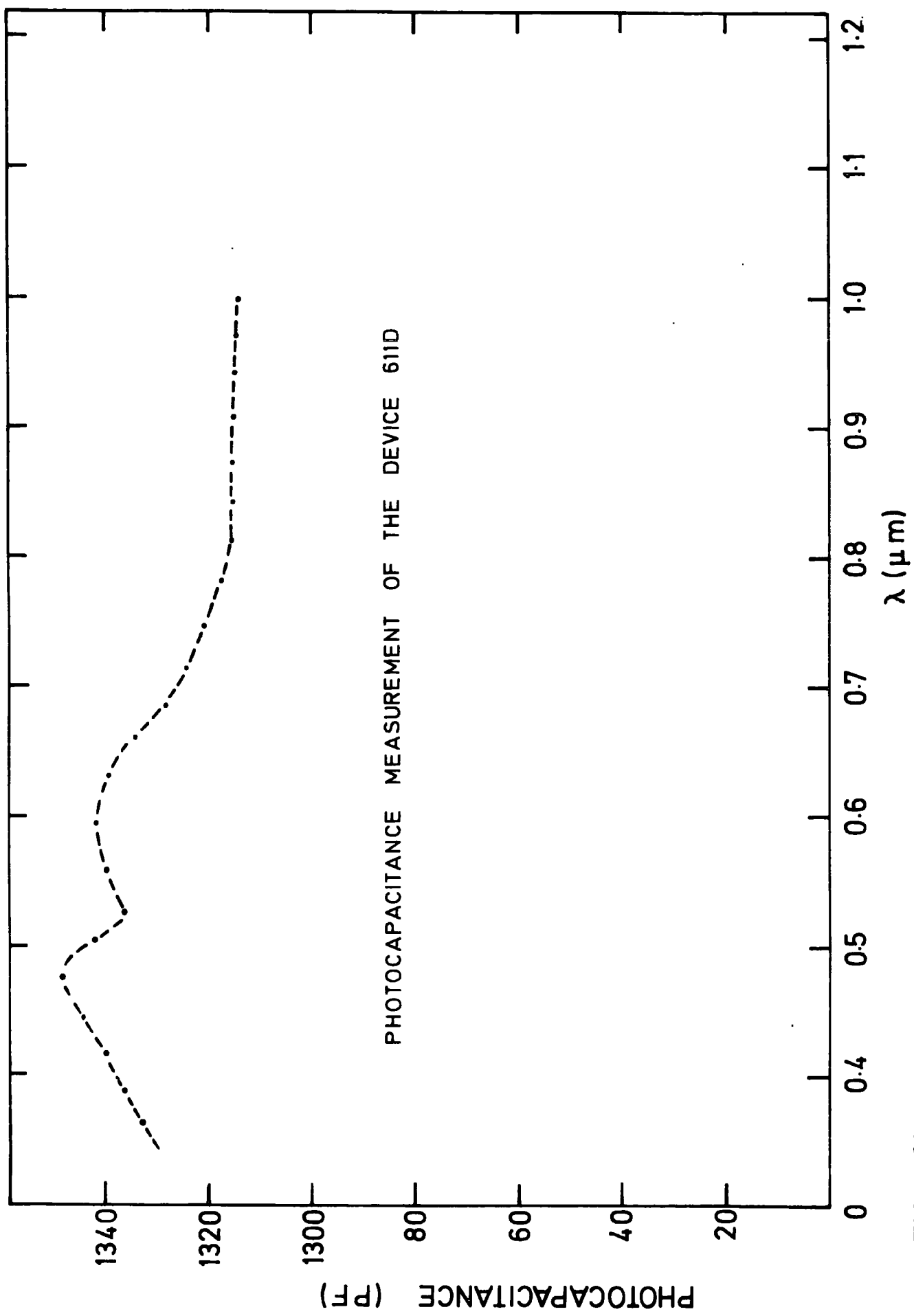


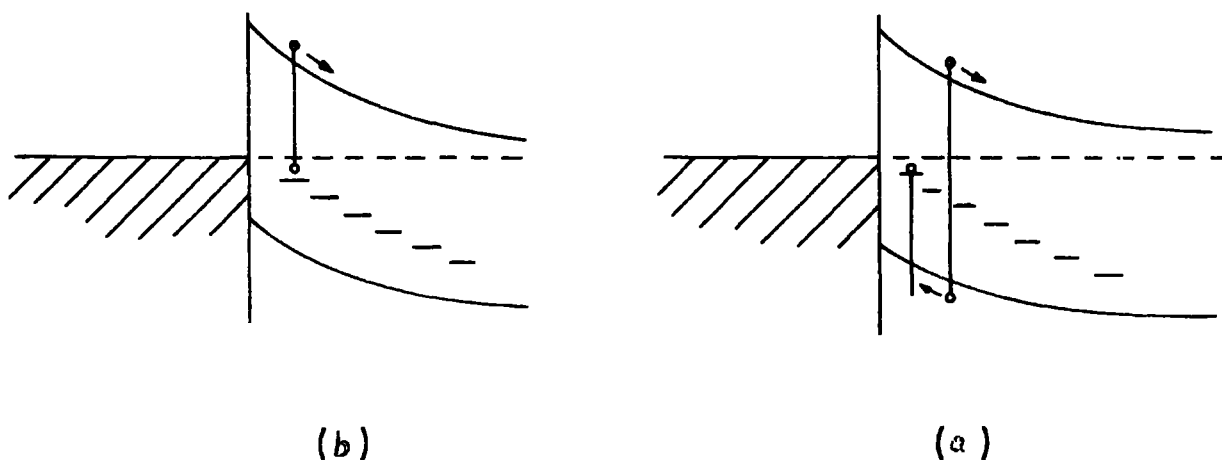
FIG. 6.21.

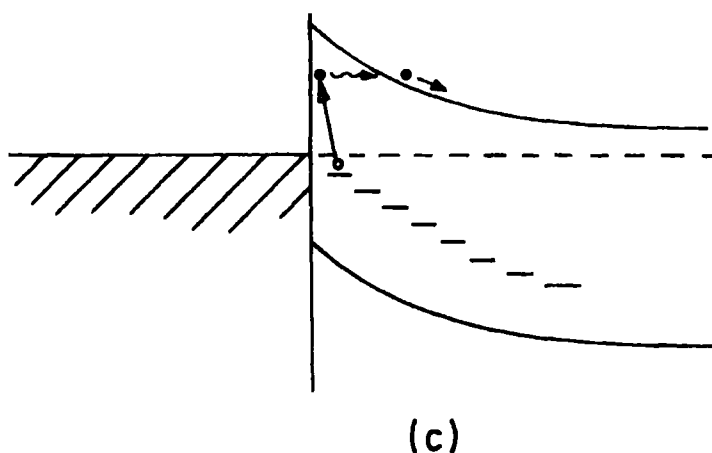
incident on such a device, as a result of the photo-ionization of the traps, the device depletion width reduces and leads to a measurable quantity for the depletion capacitance. As a typical example, the photocapacitance measurement of diode 623 A is shown in Figure 6.20. The long wavelength photocapacitance threshold of the devices occurs at  $\lambda = 1.05 \mu\text{m}$ , i.e. at an energy of 1.18 eV. The photocapacitance increases continuously up to an energy of 2.15 eV below the conduction band with a shoulder around  $\lambda = 0.6 \mu\text{m}$  (2.07 eV). It then starts to fall and with another shoulder around  $\lambda = 0.56 \mu\text{m}$  (2.21 eV), finally reduces to zero at  $\lambda = 0.5 \mu\text{m}$  (2.48 eV).

For diode 611 D with a donor concentration of  $N_d = 3.97 \times 10^{17} \text{ cm}^{-3}$  determined from the slope of  $C^{-2}$  versus  $V$  plot, the photocapacitance is small compared with the large background. The result of photocapacitance measurements on diode 611 D is shown in Figure 6.21. The photocapacitance threshold occurs around  $\lambda = 1 \mu\text{m}$ , i.e. at an energy of 1.24 eV. The photocapacitance then increases and reaches a broad maximum centred at  $\lambda = 0.6 \mu\text{m}$  (2.07 eV). The second maximum occurs around  $\lambda = 0.48 \mu\text{m}$ , i.e. at an energy of 2.58 eV.

#### 6.24 Some Electronic Processes in the Photocapacitance Effect

The electronic processes responsible for the observed photocapacitance can be described in terms of the energy band diagram of a metal-semiconductor junction as in Figure 6.22.





Some of these processes are as follows :

(a) Excitation of photocapacitance by intrinsic radiation.

When an electron-hole pair is created in the vicinity of the junction, the electron drifts further into the CdS and the hole is captured by one of the deep levels in the CdS depletion region. The hole trapped in these levels gives rise to the measured photocapacitance by narrowing the depletion layer in the CdS.

(b) Excitation of photocapacitance by extrinsic radiation,  $0.5 - 1 \mu$ . Direct excitation of an electron out of deep level produces a trapped hole with the same effect of (a).

(c) Excitation of photocapacitance by extrinsic radiation with  $\lambda > 1\mu$ . Excitation of photocapacitance by long wavelength radiation could take place by means of interface states, i.e. by the excitation of an electron out of the deep level to a higher-lying interface level, followed by tunnelling of the electron into the CdS conduction band. This leaves a trapped hole in the deeper level.

Assuming that process (b) is responsible for the observed photocapacitance in device, with photon energies greater than  $E_g/2$ , i.e. that the effect is entirely due to the photo-ionization of the deep levels, then :

$$\frac{\Delta C}{C_0} = \frac{\Delta n}{N_d} \quad (6.10)$$

where  $\Delta n$  is the density of the photo-ionized deep centres at a given light intensity and  $C_0$  is the dark background capacitance.

For diode 611 D the ratio  $\frac{\Delta C}{C_0}$  is found to be  $2.05 \times 10^{-2}$ . Knowing the donor concentration  $N_d = 3.97 \times 10^{17} \text{ cm}^{-3}$  from  $C^{-2}$  versus  $V$  plot,  $\Delta n$  is calculated to be  $8.13 \times 10^{15} \text{ cm}^{-3}$ .  $\Delta n$  is directly proportional to the density of deep level centres  $N_{TT}$ , (lying 2.07 eV below the conduction band) the calculation of which requires further experiments to determine the optical photo-ionization cross-section of electrons and holes from these centres.

## CHAPTER SEVEN

### THE EFFECTS OF HEAT TREATMENT ON Cu-CdS CONTACTS

#### 7.1 Introduction

Devices in which copper contacts are applied to CdS have received considerable attention in the past because of their possible use as photovoltaic cells, (William and Bube, 1960, DUC Cuong and Blair, 1966).

Since the photovoltaic effect in CdS was observed by Reynolds in 1954, many workers have attempted to explain the mechanism of this effect. Williams and Bube (1960) have interpreted the behaviour of CdS cells (made by electroplating copper from copper ion solution on n-type CdS crystals) in terms of a metal semiconductor junction which Grimmeis and Memming (1962) described their cells as a p-n homojunction. Cusano (1963) suggested as a result of his work on CdTe that a heterojunction of  $\text{Cu}_2\text{S}$ -CdS might be formed in the Cu-CdS system.

It has now been established that copper may react with sulphur at the Cu-CdS interface. The report by Singer (1973) contains some evidence of such a chemical reaction taking place at a Cu-CdS interface, which results in the formation of a  $\text{Cu}_{2-x}\text{S}$ -CdS heterojunction. It is, therefore, of little surprise to observe Cu-CdS contacts exhibiting characteristics different from those expected of Schottky barrier. It has been shown by McCarthy & Yee (1973) that a copper contact to CdS may exhibit the same electrical and photoelectric properties as  $\text{Cu}_2\text{S}$ -CdS heterojunctions formed by the CuCl dip method.

In this chapter we present the results of an investigation on the effects of heat treatment on Cu-CdS (metal-semiconductor) contacts.

#### 7.2 Sample Preparation

Oriented CdS cubes with dimensions of  $(2 \times 2 \times 2 \text{ mm}^3)$  cut from boule no. 611 were used for the fabrication of Cu-CdS contacts. The samples had a

low resistivity of  $\rho \approx 0.1 \Omega\text{-cm}$  prior to applying any contact, the sample was etched in Conc. Hcl for a period of between 0.5-1 minute. The ohmic indium contact was then applied to one side of the cube in an argon atmosphere at a temperature between  $200\text{-}220^{\circ}\text{C}$ , (see Chapter 4). The copper contact was deposited using the evaporation system described in Chapter 4. Before the evaporation, the face of the cube opposite to that on which indium contact had been applied was etched again. To protect the indium contact, it was covered with a layer of "lacomit" which the etchant did not affect. The thin protective layer was removed by washing in acetone and distilled water, after ultimately a copper film was deposited on the freshly cleaned surface.

After fabrication, devices were heated in an argon atmosphere at a temperature of  $200^{\circ}\text{C}$  for various periods of time from 15 minutes to 3 hours. After each intervening period of heat treatment some optical and electrical measurements were made on the device, and these are described in the following sections.

### 7.3 Photoresponse Measurements

Photoresponse measurements were made according to the technique described in Chapter 4. The quantity actually determined was short circuit photocurrent  $I_{sc}$ , which was measured as a function of wavelength in the range  $0.35 \mu\text{m} < \lambda < 1.4 \mu\text{m}$ .

Some typical curves of photoresponse for diode 611 $\beta$  are shown in Fig. 7.1. Curve (1) was measured after the device had been heated for 30 minutes in an argon atmosphere at a temperature of  $200^{\circ}\text{C}$ . Curve (2) is the result of the measurement after 1 hour of heat treatment and Curve (3) after 2 hours.

It can be seen from Figure 7.1 that as the period of heat treatment is increased, changes occur in the magnitude and shape of the photoresponse curves. In Curves (1) and (2) the long wavelength threshold of the photo-

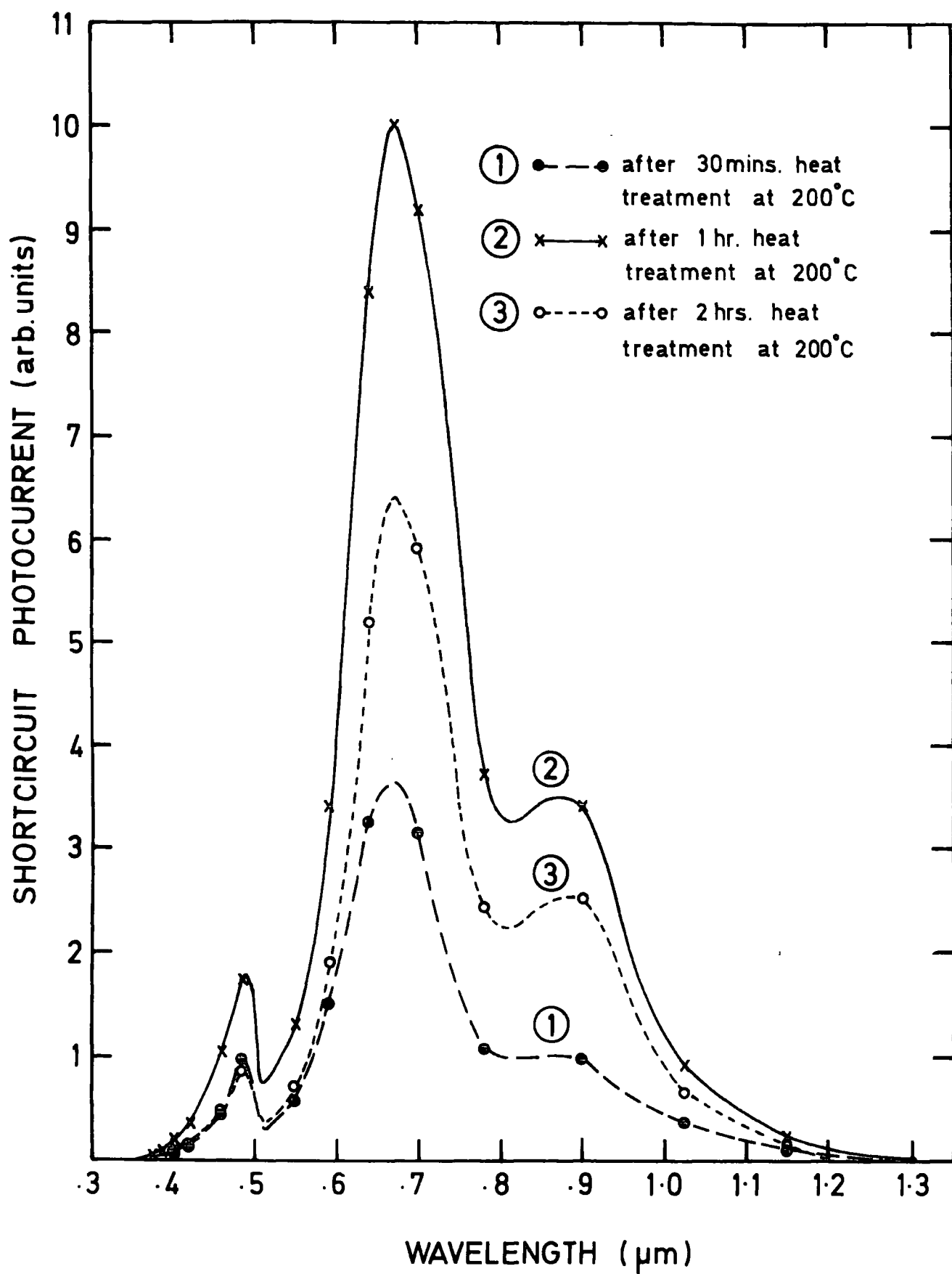


FIG. 7.1

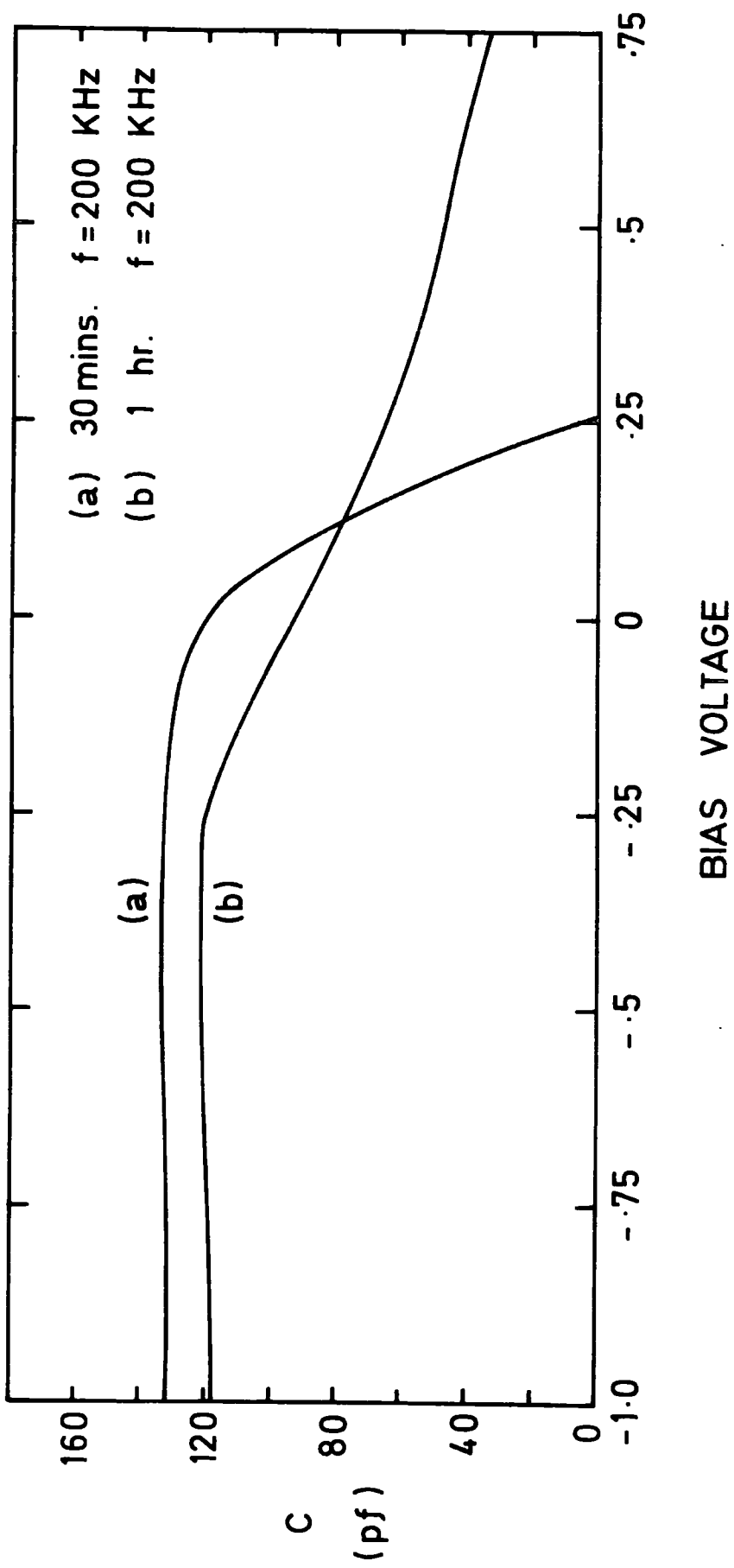


FIG. 7·2

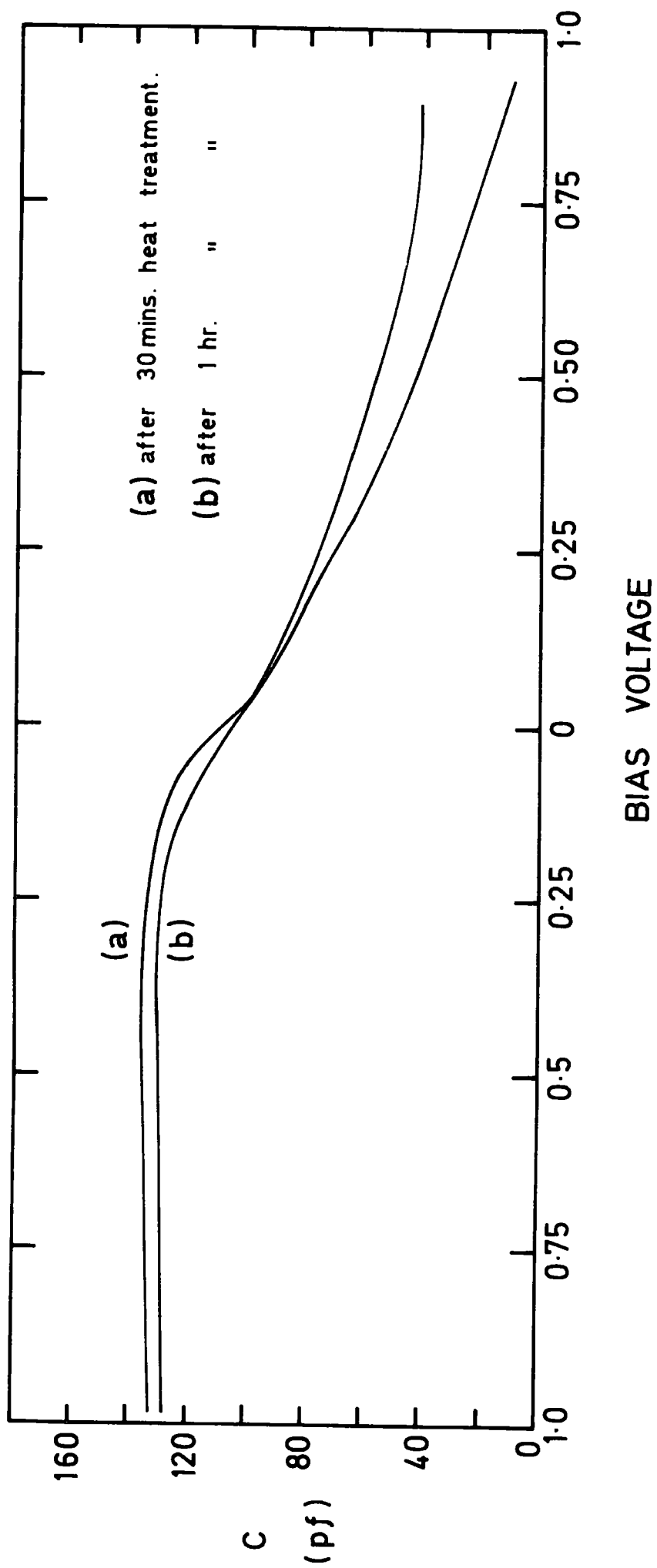


FIG. 7.3

response occurs at the same wavelength of  $\lambda = 1.3 \mu\text{m}$  corresponding to an energy of 0.95 eV. However, a threefold increase is observed in the magnitude of the maxima occurring around  $\lambda = 0.875 \mu\text{m}$  and  $\lambda = 0.67 \mu\text{m}$ . With Curve (3), however, the photothreshold shifts towards shorter wavelengths and occurs at  $\lambda = 1.2 \mu\text{m}$ , which corresponds to an energy of 1.03 eV. Neither of the photothreshold energies of 0.95 and 1.03 eV correspond to the reported barrier height of a copper contact to CdS, i.e. 0.50 eV. However, the comparison of the curves in Figure 7.1 with those obtained by Caswell, et al (1975) from similar measurements on a  $\text{Cu}_2\text{S}$ -CdS heterojunction formed by the CuCl dip method, indicates the possibility of the formation of a layer of copper sulphide containing both chalcocite  $\text{Cu}_2\text{S}$ , and djurleite  $\text{Cu}_{1.95}\text{S}$ , as a result of these heat treatments.

#### 7.4 Capacitance-voltage Measurements

In addition to photoresponse measurements, the C-V characteristics were measured in the dark as described in Chapter 4. Some typical curves showing the C-V characteristics of device 611 $\beta$  are shown in Figures 7.2 and 7.3. The capacitances of the cell, measured at different frequencies of 20 KHz and 200 KHz and at different stages of heat treatment, were found to be almost independent of the reverse voltage. It can be seen that a longer period of heat treatment gives rise to a lower value of the capacitance. For example, the reverse bias capacitance of device 611 $\beta$  was reduced from 134 pf to almost 121 pf following an additional heat treatment of  $\frac{1}{2}$  hour. The reason for this reduction is the in-diffusion of copper and further increase in the thickness of the insulating layer formed as a result of compensation effect of copper in CdS.

#### 7.5 The Effect of Heat Treatment on the Current-voltage Characteristics of Cu-CdS Diodes

I-V characteristics of the diodes with copper contacts were measured as described in Chapter 4. Substantial changes were observed in these

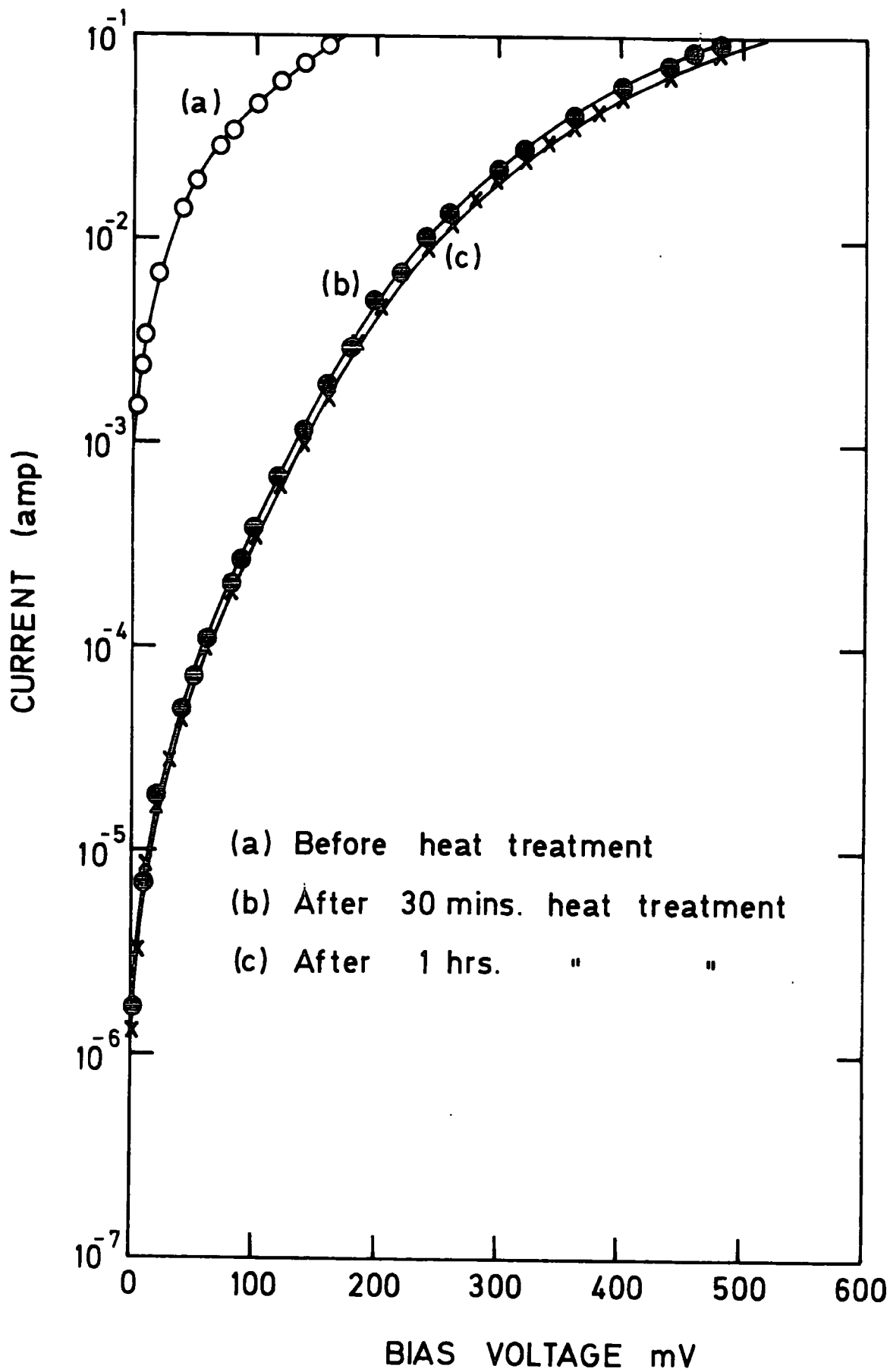


FIG. 7.4

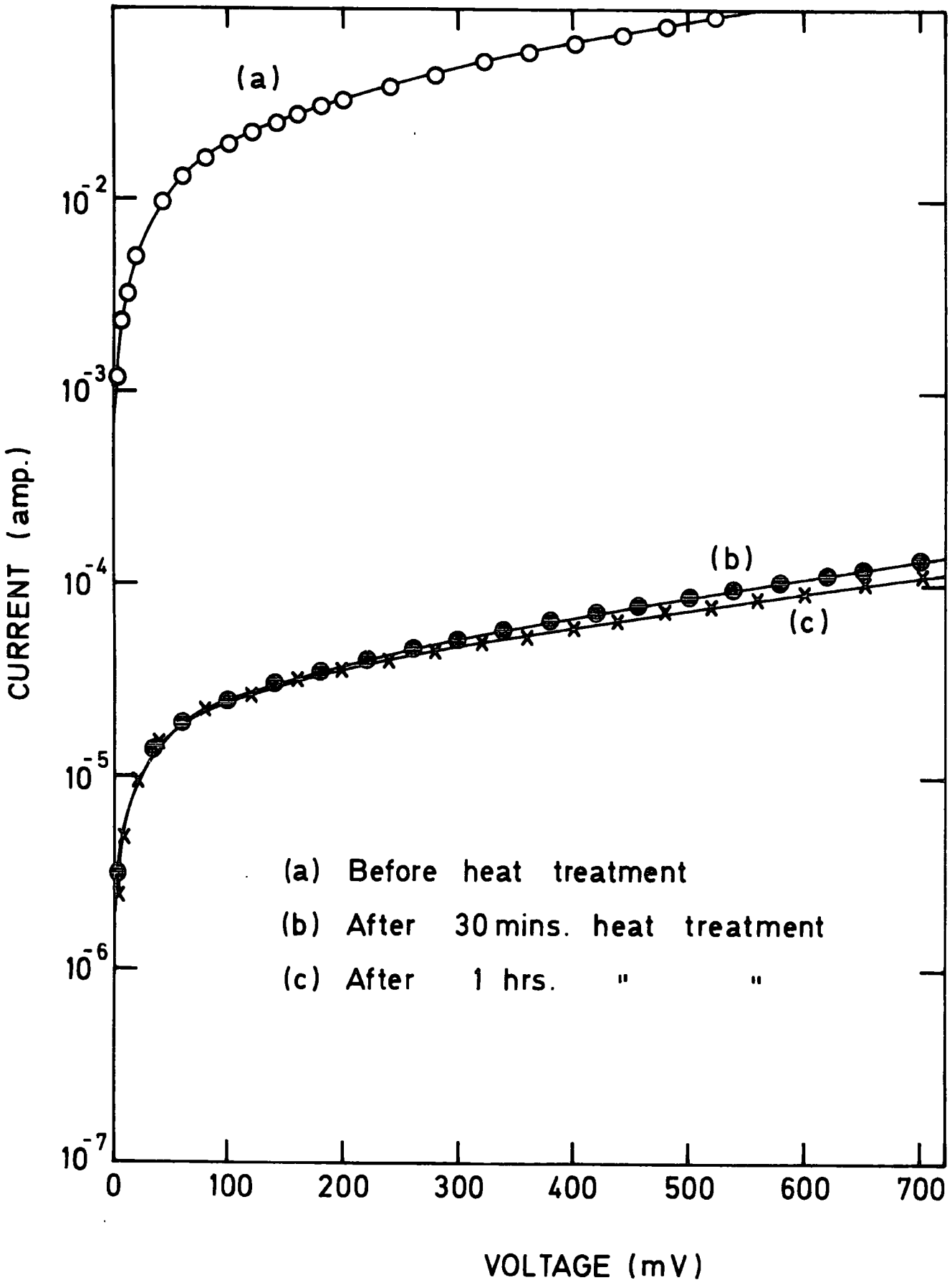


FIG. 7-5

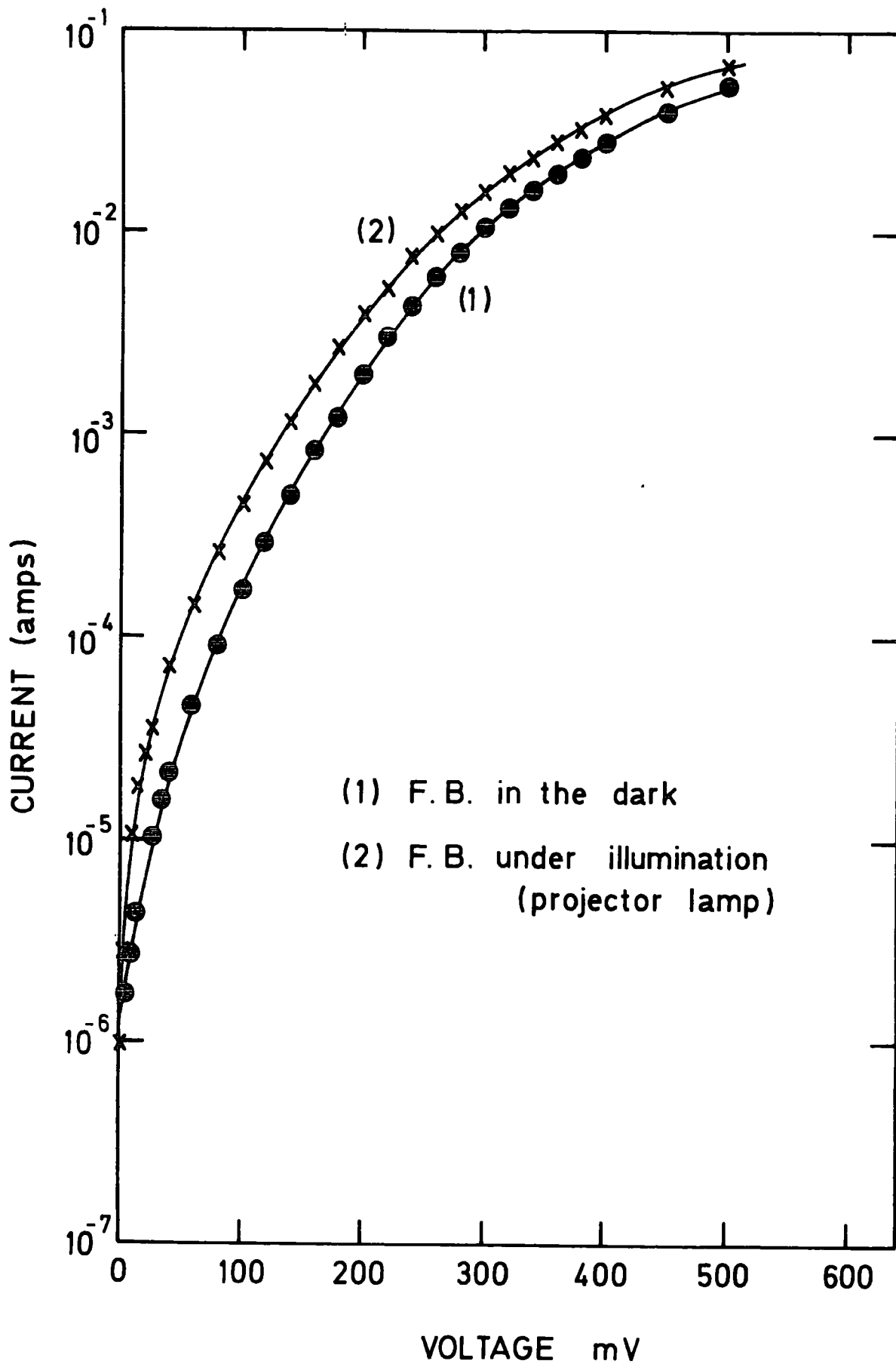


FIG. 7-6

characteristics when devices were heated in an argon atmosphere at  $200^{\circ}$  C for various periods of time. The I-V characteristics of diode 611 $\beta$  are shown in Fig. 7.4. Curve (a) illustrates the forward bias characteristics of diode 611 $\beta$  before the heat treatment, whereas, Curves (b) and (c) were obtained after the diode had been heated for periods of 30 and 60 minutes respectively. A substantial decrease in the value of the current corresponding to the same value of bias voltage is observed between curves (a) and (b) which is due to the reaction of the in-diffused copper with sulphur and the formation of a layer of  $\text{Cu}_{2-x}\text{S}$ .

In the reverse direction the current also decreases substantially as a result of heat treatment and this is shown in Figure 7.5. Curve (a) shows the reverse characteristics of diode 611 $\beta$  before heat treatment and Curves (b) and (c) show the characteristics of the diode after it was heated for periods of 30 and 60 minutes respectively.

We have also measured the effect of light on the I-V characteristics of the diode 611 $\beta$  which is shown in Figure 7.6. Curve (1) represents the dark forward bias characteristics of the device after it had been heated in argon at a temperature of  $200^{\circ}$  C for 3 hours and Curve (2) shows the current in forward bias, measured under illumination from a projector lamp.

## 7.6 Conclusion

According to Palz, et al (1973), the short-circuit current of a CdS solar cell is dependent on the composition of the cuprous sulphide layer, and optimum values of S.C.C. are obtained when the copper sulphide is present as the  $\text{Cu}_2\text{S}$  phase. As the phase of copper sulphide changes from  $\text{Cu}_2\text{S}$  to  $\text{Cu}_{1.96}\text{S}$  as a consequence of oxidation in the room ambient, the magnitude of the S.C.C. decreases and the S.C.C. maximum at  $\lambda = .92 \mu\text{m}$  associated with the chalcocite phase shifts towards higher energies and occurs around  $\lambda = 0.68 \mu\text{m}$  which is characteristic of the djurleite phase. Using the technique of reflection electron diffraction (R.E.D.), Caswell, et al (1977) have shown

that the spectral response of a cell with a layer of chalcocite has a major band of sensitivity at  $0.90 \mu\text{m}$  in contrast with a cell with a layer of djurleite which has a major band of sensitivity at  $0.70 \mu\text{m}$ .

Considering the results presented in this Chapter, and comparing particularly the short circuit photoresponses of Figure 7.1 with those obtained by Palz et al (1973) from cells corresponding to different  $\text{Cu}_{2-x}\text{S}$  compositions and also the results obtained by Caswell, et al (1977), one can conclude that the heat treatment of a Cu-CdS contact leads to the formation of a layer of  $\text{Cu}_{2-x}\text{S}$  which is a mixture of djurleite and chalcocite. The C-V measurements made on devices at different stages of heat treatment indicate that in parallel with the formation of the copper sulphide layer, the diffusion of copper also leads to the formation of a compensated layer of CdS.

## CHAPTER EIGHT

### CONCLUSION

#### 8.1 Summary of the results

The work presented in this thesis was mainly concerned with the optical and electrical properties of three types of device, namely:

- (1) photoconductors with two ohmic contacts,
- (2) Schottky diodes with one ohmic contact, and
- (3) heterojunctions made by the heat treatment of copper deposited on CdS crystals.

Since a high stability in use is essential for successful applications of CdS photoconductors and solar cells, the processes which lead to the degradation of the efficiency of CdS solar cells have attracted considerable attention in recent years. It has been shown by Kanev et al (1971) and Fahrenbruch and Bube (1974) that heat treatment alone does not produce appreciable degradation of the short circuit current in  $\text{Cu}_2\text{S}$ -CdS single crystal heterojunctions. The degradation, which has been commonly observed, is the result of effects induced optically into the heat-treated cell, subsequent to the heat treatment.

Using the technique of thermally stimulated currents we have shown that the effect of direct illumination of CdS:Cl samples doped with  $\text{Cu}^{++}$  ions, is to reduce the density of the shallow traps with the simultaneous formation of deep traps. Subsequent measurement of the photo-response of the samples showed that the degradation of the photocurrent is closely related to the observed changes in the distribution of the traps.

In contrast with the situation mentioned above, optical illumination does not have any deleterious effect on the CdS:Cl samples doped with  $\text{Cu}^+$  ions. In fact under prolonged illumination a reduction in the density

of deep traps with the simultaneous increase in the density of shallow traps causes an increase in the photosensitivity of such devices. A similar stable situation was also observed with CdS:Cl rods treated in sulphur vapour.

To account for the results obtained, we have presented a working hypothesis according to which aggregates are formed from  $\text{Cl}^-$ ,  $\text{Cu}^+$  and charged sulphur vacancies,  $\bar{V}_A$ , under Coulombic attraction. For the CdS:Cl rods doped with  $\text{Cu}^+$  ions, however, the sulphur vacancies are immobilised by the presence of copper atoms in interstitial sites which we suggest leads to a stable situation.

With devices of the second type, i.e. Schottky diodes, the resistivity of the sample was found to play a significant role. Samples with donor density in the range  $10^{16} - 10^{17} \text{ cm}^{-3}$  were obtained by doping the CdS crystals with donor impurities (such as chlorine) during growth or by subsequent treatment of high resistivity samples in cadmium vapour or, conductive ones in sulphur vapour. It was adequate sometimes to heat the conductive samples in vacuum at a temperature of  $1000^\circ\text{C}$  to increase their resistivity.

The shortcircuit photocurrent of device 623 A which had been prepared from CdS:Cu samples heated in Cd vapour, was measured immediately after preparation and after a lapse of 28 days. Interesting features of the photoresponse of such devices were:

- (1) the shortcircuit photocurrent response of as-prepared devices had a long tail in the short wavelength region with the threshold at 3.13 eV.
- (2) Because of the introduction of cadmium atoms in the crystal (self diffusion), there was a shift in the band gap excitation of the device towards higher energy values. The band gap excitation peak

occurred at  $\lambda = 0.504 \mu\text{m}$  equivalent to 2.46 eV instead of 2.40 eV for the untreated samples.

(3) Subsequent measurement of photoresponse after 28 days showed that the shift in the band gap excitation towards higher energy values was not a stable state. A 20-fold increase in the shortcircuit photocurrent of the device in the extrinsic region and a 2-fold increase in the band gap region suggested that a higher electric field had been established in the device due to ageing. The short wavelength threshold of the photoresponse also shifted from 3.13 to 2.53 eV. Since the short wavelength threshold is sensitive to changes in the surface recombination velocity of the device, the shift mentioned above meant that the surface properties, i.e. the surface trap and recombination parameters, had changed. Considering the changes observed in the photoresponse of the device, it was suggested that the diffused-in Cd atoms migrate to the surface and an oxide layer (CdO) is formed between the metal and the semiconductor.

With devices 626B and 611A, the shortcircuit photoresponse measured was used to determine accurately the barrier height of gold on CdS. The square root of the photocurrent was plotted against photon energy in the vicinity of the threshold. Good straight lines were obtained and the barrier heights determined from the intercepts were  $\phi_{\text{Bn}} \approx 0.742 \pm 0.01$  for device 626B and  $\phi_{\text{Bn}} \approx 0.77 \pm 0.01$  for device 611A.

Capacitance-voltage characteristics were measured for various diodes with different donor densities. An uncompensated donor concentration of  $N_{\text{d}} = 9.1 \times 10^{16} \text{ cm}^{-3}$  and a voltage intercept of  $V_{\text{i}} = 1.475$  volts were found for device 611A. For device 626B, however, the slope of the  $C^{-2} - V$  plot gave a donor concentration of  $N_{\text{d}} = 1.216 \times 10^{16} \text{ cm}^{-3}$  and the voltage intercept  $V_{\text{i}}$  was found to be 0.98 volts. The discrepancy observed between the value of barrier height determined from the photo-

electric method and the voltage intercept of the C - V plot was due to the presence of a thin interfacial layer between the metal and the semiconductor. Using equation (2.59) the thickness of the interfacial layer  $\lambda_i$ , was found to be about 630 Å for diode 626B. After measuring the surface state density by the conductance method, use was made of equations (2.61) and (2.67) and the thickness of the layer was re-calculated to be 825 Å.

We have already mentioned that in the long term the shortcircuit photoresponse of a diode was time dependent. The C-V characteristics of a diode did not remain stable and invariant with time. As ageing proceeded the slope and voltage intercept of the  $C^{-2}$ -V plot changed. Successive C-V measurements showed that the donor density of diode 611A had changed from a value of  $9.1 \times 10^{16}$  to  $5.85 \times 10^{16} \text{ cm}^{-3}$  during a time interval of 200 hours. The increase in the thickness of the interfacial layer was found to be as high as 235 Å from 355 to 590 Å. This increase which occurred in conjunction with the decrease in the donor density was indicative of the basic instability of the device. The decrease in the donor density was attributed to the creation of cadmium vacancies which are acceptor imperfections. The process was presumably one of out-diffusion of cadmium atoms from the bulk to the surface where oxidation produced a thicker interfacial layer between the metal and the semiconductor.

The current-voltage characteristics of the fabricated diodes were measured and it was shown that the thermionic emission-diffusion theory was applicable to diode 626B. For diodes made from boule No.611, however, the value of the ratio of  $\frac{\mu \epsilon_{\text{max}}}{\bar{v}/4} \approx 10$  meant that thermionic emission was the dominant conduction mechanism in those devices.

Forward-bias characteristics were measured for diodes with different donor densities. It was observed that for the same bias voltage

the corresponding measured currents were different. Substituting the values of donor density of diodes 626B, 611A and 611D in equation 2.43, the depletion width was found to be about 2240 Å for diode 626B, 870 Å for diode 611A and 420 Å for diode 611D. Since the higher current values corresponded to the smaller depletion widths, it seemed reasonable to assume that as the depletion width decreased the possibility of the tunnelling of the carriers through the depletion region increased and as a result there was a contribution to the conduction mechanism of the barrier.

The effect of ageing on current-voltage characteristics of Au-CdS diodes was also studied. The forward bias characteristics of diode 611D were measured just after the preparation of the diode and again 25 hours later. A reduction in the current for a given bias was attributed to the growth of the interfacial layer between the metal and the semiconductor. The presence of such a layer gave rise to n-values greater than unity. The substitution of the change in the n-value of 0.16 in equation 6.9 led to the calculation of about 65 Å as the increase in thickness of the interfacial layer as a result of ageing.

Devices of the third type, i.e. the p-n heterojunctions, were produced by heating CdS carrying a layer of copper metal. As the period of heat treatment was increased, changes were observed in the magnitude and the shape of the photoresponse curves. C-V and I-V characteristics of the device were also sensitive to these heat treatments. Comparing the short circuit photoresponse measured with those obtained by Palz et al (1973) and also results obtained by Caswell et al (1977), we have concluded that heat treatment of a Cu-CdS contact leads to the formation of a layer of  $\text{Cu}_{2-x}\text{S}$  which is a mixture of djurleite and chalcocite.

## 8.2 Suggestions for Future Work

To extend the work described in this thesis, the following suggestions are made:

- (1) Since the instability of M-S devices was related to the imperfections developed in the bulk of the semiconductor and the growth of an interfacial layer between metal and semiconductor, it should be worthwhile to study the changes in the parameters of the interface states, which may take place during these developments and to examine their effects on the optical and electrical properties of these devices.
- (2) To study the influence of deep traps on the photovoltaic properties of M-S, MIS and CdS-Cu<sub>2</sub>S heterojunctions, the measurement of photo-capacitance on these devices should be continued.
- (3) Since CdS samples treated in sulphur vapour are stable, it is suggested that the Cu<sub>2</sub>S-CdS cells are fabricated on such samples.
- (4) Finally it is suggested that the T.S.C. technique be used on M-S and p-n heterojunction systems so that the characteristics of the traps involved in these devices could be evaluated.

REFERENCES

- Adams W G and Day R E (1976) Proc. Roy. Soc. A25 113
- Adirovich E I et al (1966) Sov. Phys. Solid State 7 2946
- Alferov J I et al (1970) Sob. Phys. Semiconductors 3 1103
- Aven M and Prener J S (1967) Phys. and Chem. of II-VI Compounds  
North-Holland Publishing Co. Amsterdam
- Berlincourt D et al (1963) Phys. Rev. 129 1009
- Berman P A (1972) 9th IEEE Photovoltaic Conf. p.281
- Bethe H A (1942) MIT Radiation Lab. Report 43-12
- Bockemuelh R J et al (1961) J.A.P. 32 1324
- Bogus K and Mattes S (1972) 9th IEEE Photovoltaic Specialists Conf.  
Conf. Record p.106
- Breeze A and Perkins P G (1973) Solid State Commun. 13 1031
- Bube R H and Barton L A (1958) J. Chem. Phys. 28 128
- Bube R H and Barton L A (1959) RCA Rev. 20 564
- Bube R H (1957a) J. Phys. Chem. Solids 1 234
- Bube R H and Cardon F (1964a) J. Appl. Phys. 35 2712
- Bube R H (1973) Electronic Properties of Crystalline Solids, An  
Introduction to Fundamentals, Academic Press
- Bulliard H (1954) Phys. Rev. 94 1564
- Burget C and Lin C (1970) J. Phys. Chem. Sol. 31 1353
- Card H C and Rhoderick E H (1971a) J. Phys. D: Appl. Phys. 4 1589
- Cardon F and Bube R H (1964) J. Appl. Phys. 35 3344
- Carter M A and Woods J (1973) J. Phys. D. Vol.6 p.337
- Caswell B G et al (1975) J. Phys. D: Appl. Phys. 8 1889
- Caswell B G et al (1977) Photovoltaic Energy Conf. record  
Luxembourg p.221

- Chamberlin R R and Skarman J S (1966) Solid State Electron. 9 819
- Chapin D M et al (1954) J. Appl. Phys. 25 676
- Clark L and Woods J (1966) Brit. J.A.P. 17 319
- Clark R L (1959) J. Appl. Phys. 30 957
- Cowell T A T and Woods J (1969) J. Phys. D: Appl. Phys. 18 1045-51
- Cowley A M (1966) J. Appl. Phys. 37 8 3024
- Crowell C R and Sze S M (1966) Solid St. Electron. 9 1035
- Crowell C R et al (1962) Phys. Rev. 127 2006
- Crowell C R et al (1965) J. Appl. Phys. 36 3843
- Crowell C R and Roberts G I (1969) J. Appl. Phys. 40 3726
- Cusano D A (1963) Solid State Electron. 6 217
- Elster J and Geitel H (1895) Wied. Ann. 55 685
- Fahrenbeuch A L and Bube R H (1974) J. Appl. Phys. 45 1264
- Fochs P D et al (1968) J. Crystal Growth 3 4 122-125
- Fowler R H (1931) Phys. Rev. 38 45
- Garlick G F J and Gibson A F (1948) Proc. Roy. Soc. A 60 574
- Gill W D and Bube R H (1970) J. Appl. Phys. 41 3731
- Gobrecht H et al (1971) Phys. Stat. Sol. a4 K19
- Goldstein B and Pensak L (1959) J. Appl. Phys. 30 155
- Goodman A M (1963) J. Appl. Phys. 34 2 p.329
- Goodman A M (1964) J. App. Phys. 35 3 p.573
- Gossick B R (1963) Solid State Electron. 6 445
- Grimmeiss H G and Memming R (1962) (a) J. Appl. Phys. 33 2217
- Grimmeiss H G and Olofsson (1969) J. Apple. Phys. 40 2526
- Grimmeiss H J (1974) Inst. of Phys. Conf. Ser. No.22 p.187
- Grondahl L O and Geiger P H ( ) Trans. Am. Inst. Electr. Engrs.  
46 357
- Gross Weiner L I (1953) J. Appl. Phys. 24 1306

- Grushko N S and Gutkin A A Soviet Phys. Semiconductor (U.S.A.) (1975)  
Vol.9 No.1 37-39
- Haering R R and Adams E N (1960) Phys. Rev. Vol.117 No.2 p.451
- Hallwachs W (1888) Ann. Physik 33 301
- Hertz H (1887) Ann. Physik 31 421 983
- Hill E R and Keramidas B G (1966) Rev. de Phys. Appl. 1 189
- Hill R et al (1972) J. Phys. D. Appl. Phys. Vol.5 p.185-7
- Hovel H J (1975) Semiconductors and Semimetals Vol.11 Solar Cells  
Academic Press
- Kanev S K et al (1971) Appl. Phys. Lett. 19 459
- Keating P N (1965) J. Appl. Phys. 36 564
- Kindleysides L (1969) Electrical and Optical Properties of CdSe.  
Ph.D. Thesis University of Durhan
- Klasens H A (1958) J. Phys. Chem. Solids 7 175
- Koffyberg F P (1976) Phys. Rev. B Vol.13 No.10 4470-6
- Korsunskaya N E et al (1973) Sov. Phys. Semiconductor Vol.7 No.2 196
- Landau L D and Lifshitz E M (1936) Physik Z. Sovient Union 9 477
- Lange B (1930) Physik Z. 31 139 964
- Lashkharev V E and Sheinkman M K (1965) Phys. Stat. Sol. 11 429
- Lindquist P F and Bube R H (1972) J. Electrochem. Soc. 119 936
- Lindquist P F and Bube R H (1972) J. Appl. Phys. Vol.43 No.6 2839
- Loferski J J (1956) J. Appl. Phys. 27 777-784
- Loferski J J (1963) Proc. IEEE 51 667-674
- McCarthy S J and Yee S S (1973) Solid State Electron. 16 115
- Maev R G et al (1973) Sov. Phys. Solid State 15 12
- Many A, Goldstein Y and Grover N B (1965) Semiconductor surfaces,  
North-Holland Publishing Co.
- Mandel G (1964) Phys. Rev. 134 A 1073

- Mertz W J (1958) *Helvetica Physica Acta* 31 625
- Milnes A G (1973) *Deep Impurities in Semiconductors* Wiley-Interscience
- Moss T S et al (1953) *Proc. Phys. Soc.* 66B 743 (1953)
- Mott N F (1938) *Proc. Camb. Phill. Soc.* 34 843
- Mott W F (1939) *Proc. Roy. Soc.* A171 281
- Mytton R J (1968) *Brit. J. Appl. Phys.* 1 721
- Mytton R J et al (1972) 9th IEEE Photovoltaic Specialists Conf. p.133
- Nicolas K H and Woods J (1964) *Brit. J. Appl. Phys.* 15 783-95
- Nicoll F H (1963) *J. Electrochem. Soc.* 110 1165
- Nicollian E H and Goetzberger A (1967) *The Bell. Sys. Tech. J*  
Vol. XLVI 1055
- Ozsán M E (1976) *Electroluminescence in Zinc Selenide* Ph.D. Thesis  
University of Durham
- Palz W et al (1970) *Conf. Record 8th IEEE Photovoltaic Con.* p.16
- Palz W et al (1973) *Conf. Record 10th IEEE Photovoltaic Con.* p.69
- Patil S G and Woods J (1971) *J. of Luminescence* 4 231-43
- Piper W W and Polich S J (1961) *J. Appl. Phys.* 32 1278-9
- Potter A E and Schalla R L (1967) *NASA TND - 3849*
- Queisser H J and Shockley W (1960) *Bull. Am. Phys. Soc. II* 5 160
- Queisser H J and Shockley W (1961) *J. Appl. Phys.* 32 510
- Randall J T and Wilkins M H F (1945) *Proc. Roy. Soc.* A184 366 390
- Ray B (1969) *II-VI Compounds* Pergamon Press
- Reed C E and Scott G G (1965) *Brit. J. Appl. Phys.* 16 471
- Reinberg A et al (1971) *Phys. Rev.* B2 410
- Reynolds D C and Czyzack S J (1950) *Phys. Rev.* 79 543-4
- Reynolds D C et al (1954) *Phys. Rev.* 96 533
- Rhoderick E H (1972) *J. Phys. D: Appl. Phys.* 5 1920
- Rezakanov M A et al (1975) *Sov. Phys. Semicond.* Vol.8 No.8 990

- Rezakhanov M A (1972) JETP Letters 15 508
- Rose A and Lampert M (1959) Phys. Rev. 113 1227
- Rose A (1963) Concepts in Photoconductivity and Allied Problems,  
Interscience Publishers
- Rosenzweig W et al (1963) Bell Syst. Tech. J. 42 399
- Sah C T et al (1969) Appl. Phys. Lett. 15 316
- Sah C T et al (1971) Solid State Commun. 9 917
- Salehi Manshadi M A and Woods J (1976) Phys. Stat. Sol. (a) 40 K43
- Schottky W (1938) Natur Wiss 26 843
- Scott C G and Reed C E (1975) Surface Physics of Phosphors and  
Semiconductors Academic Press
- Shay J L and Wagner S (1976) J. Appl. Phys. 47 2 614-18
- Shitaya T and Sato H (1968) Jap. J. Appl. Phys. 7 1348
- Shiozawa L R et al (1969) Aerospace Research Labs. Report ARL 69-0155
- Shimizu K (1965) Jap. J. Appl. Phys. 4 627
- Shockley W and Read W T (1952) Phys. Rev. 87 835
- Singer J NASA TM X-2073
- Slater R L (1967) IEEE Trans. Electron. Devices ED-14 31
- Smith W (1873) Am. J. Sci. 5 301
- Smith R W (1955) Phys. Rev. 97 1525
- Somorjai G A and Jepsen D W (1964) J. Chem. Phys. 41 1389-99
- Spence E (1958) Electronic Semiconductors (New York : McGraw-Hill)
- Stockmann F (1975) RCA Rev. Vol.36 No.3 p.499-507
- Sullivan G A (1969) Phys. Rev. Vol. 184 No.3 p.796-806
- Sze S M (1969) Physics of Semiconductor Devices Wiley-Interscience
- Szeto W and Somorjai G A (1966) J. Chem. Phys. Vol.44 No.9 3490-6
- Tanke R V and Faraday B J (1967) Proc. IEEE 55 234
- Thompson M J and Cornwall M G (1972) Solid State Electron. Vol.15  
p.861-64

- Tscholl E (1967) Thesis Technical University Eindhoven
- Usami A (1970) Solid State Electron 13 1202-1204
- Van Aerschot A E et al (1968) Proc. Seventh Photovoltaic Specialists  
Conf.
- Van Heerden (1957) Phys. Rev. 196 468
- Wagner C (1931) Phys. Z. 32 641
- Wagner S and Shay J L (1975) Appl. Phys. Lett. 26 229
- Wallmark J T (1957) Proc. I.R.E. 45 474
- Williams R and Bube R H (1960) J. Appl. Phys. 31 968
- Wilson J I B (1971) Thin Film of CdS and the CdS-Cu<sub>2</sub>S Heterojunction  
Ph.D. Thesis University of Durham
- Wolf M (1960) Proc. I.R.E. 48 1246-1263
- Woodbury H H (1964) Phys. Rev. Vol.134 No.2A A492
- Woodbury H H (1965) J. Appl. Phys. 36 2287
- Woods J (1958) J. Electronic. Control 5 417
- Woods J and Champion J A (1959) J. Electron and Control 7 243-253
- Woods J and Nicholas K H (1964) Brit. J. Appl. Phys. 15 1361
- Woods J and Wright D A (1958) Brussels Conf. on Physics of Solid  
State II 880
- Wysocki J J and Rappaport P (1960) J. Appl. Phys. 31 571
- Zold T (1973) Rev. Sci. Instrum. Vol.44 No.9 p.1251

